Allosteric regulation of mammalian fructose-1,6-bisphosphatase

by

Yang Gao

A dissertation submitted to the graduate faculty

in partial fulfillment of the requirements for the degree of

DOCTOR OF PHILOSOPHY

Major: Biochemistry

Program of Study Committee:
Richard Honzatko, Major Professor
Amy Andreotti
Mark Hargrove
Scott Nelson
Guang Song

Iowa State University
Ames, Iowa
2013

TABLE OF CONTENTS

Abbreviations v

Abstract vi

Chapter I. General Introduction 1

Figure 8

Thesis Organization 10

References 11

Chapter II. Mechanism of Displacement of a Catalytically Essential Loop from the Active Site of Mammalian Fructose-1,6-bisphosphatase 16

Abstract 16

Introduction 17

Experimental procedures 18

Results 22

Discussion 27

Table 31

Figure 33

References 42

Chapter III. Water Molecules in the Central Cavity of Mammalian Fructose-1,6-bisphosphatase as a Determinant of the Quaternary State 48

Abstract 48

Introduction 49

Experimental procedures 51

Results 54

Discussion 58

Table 61

Figure 65

References 71

Chapter IV. Linkage of Central Cavity to Synergism in AMP/Fructose 2,6-bisphosphate Inhibition of Fructose-1,6-bisphosphatase 77

Abstract 77

Introduction 78

Experimental procedures 79

Results 82

Discussion 86

Table 90

Figure 93

References 98

Chapter V. Relevance of the Dimer-dimer Interface in Porcine Liver Fructose-1,6-bisphosphatase to AMP Inhibition and Cooperativity 103

Abstract 103

Introduction 104

Experimental procedures 106

Results 109

Discussion 114

Table 118

Figure 122

References 129

Chapter VI. Functional Importance of Subunit-Pair Rotation in the Regulation of Tetrameric Mammalian Fructose-1,6-bisphosphatase 134

Abstract 134

Introduction 135

Experimental procedures 137

Results 139

Discussion 144

Table 149

Figure 152

References 160

Chapter VII. Fructose-1,6-bisphosphatase from *Leptospira interrogans*: a Prediction of Allosteric Regulation Leads to a Possible Evolutionary Precursor of AMP/Fructose-2,6-bisphosphatase Synergism in Eukaryotic Organisms 165

Abstract 165

Introduction 166

Experimental procedures 168

Results 170

Discussion 174

Table 178

Figure 181

References 188

Chapter VIII. General Conclusions 192

Acknowledgements 194

ABBREVIATIONS

FBPase	Fructose-1,6-bisphosphatase
Fru-1,6-P_2	Fructose 1,6-bisphosphate
Fru-2,6-P_2	Fructose 2,6-bisphosphate
Fru-6-P	Fructose 6-phosphate
Glc-6-P	Glucose 6-phosphate
ED	1,2-ethanediol
MPD	2-methyl-2,4-pentanediol
MD	Molecular dynamics
PEP	Phosphoenolpyruvate
PFK-1	Phosphofructokinase or fructose-6-phosphate-1-kinase
P_i	Inorganic phosphate
PD	1,2-propanediol

ABSTRACT

Fructose-1, 6-bisphosphate (D-fructose-1, 6-bisphosphate 1-phosphohydrolase; EC 3. 1. 3; FBPase) is an essential regulatory enzyme in gluconeogenesis and has long been considered as a drug target towards type II diabete. In mammalian, the activity of FBPase is regulated by AMP and fructose 2,6-bisphosphate (Fru-2,6-P_2). AMP is an allosteric inhibitor that binds to FBPase with positive coopertivity, and Fru-2,6-P_2 is an active site inhibitor which is up-regulated by hormone. Despite the 30 Å distance between their binding sites, both of AMP and Fru-2,6-P_2 transform FBPase from active R-state to inactive T-state. Large conformational rearrangements are coupled to the R- to T-state transition: subunit pairs within tetrameric FBPase rotate over ten degree relative to each other and an essential catalytic loop (residue 50-72) is forced away from active site. Mutagenesis, kinetics, crystallography and molecular dynamics simulations are combined here to investigate structure-function relationship of FBPase. Tetramer is a functional unit of FBPase; disturbing the tetrameric packing of FBPase leads to loss of AMP cooperativity. A hydrophobic cavity at the center of FBPase tetramer is populated by well-defined clathrate-like waters. The cavity together with waters in it is shown to be thermodynamic determinant for quaternary states of FBPase. Kinetics and crystallographic studies indicate a negative correlation between subunit pair rotation and relative activity of FBPase. Filling the cavity by point mutations selectively hinges subunit pair rotation induced by Fru-2,6-P_2 and largely reduce the synergism between AMP and Fru-2,6-P_2. Mutation that stops subunit pair rotations causes complete loss of AMP inhibition but retains Fru-2,6-P_2 inhibition; whereas mutation promotes the subunit pair rotation turn off cooperative binding of AMP as well as AMP/Fru-2,6-P_2 synergism. MD simulation together with crystal structures of intermediate states of FBPase reveals correlation between subunit pair rotation and status of loop 50-72. Moreover, knowledge of allosteric regulation of porcine liver FBPase and FBPase from *Escherichia coli* was used predict the regulatory properties of all Type-I FBPases, for which sequence information is available. Subsequent expression of FBPase from a bacterial organism, predicted to have the regulatory properties of a eukaryotic FBPase, proved correct and established a basis for the evolution of regulatory properties for all Type-I FBPases.

CHAPTER I. GENERAL INTRODUCTION

Blood glucose homeostasis is highly controlled in mammals. On one hand, glucose is the main energy source for all mammalian cells and the sole energy source for brain (1). A short period of hypoglycemia will lead to permanent damage to brain (2). On the other hand, chronic hyperglycemia is a hallmark for diabetes mellitus and can cause serious health problems such as kidney damage, neurological damage, and cardiovascular damage and so on (3). Glucose metabolism mainly occurs in liver and kidney. Gluconeogenesis and glucogenolysis produce glucose from either metabolic intermediates (such as pyruvate, lactate, glycerol, and some amino acids) or glycogen; whereas glycolysis degrades glucose to pyruvate for energy and glycogenesis converts glucose to glycogen for storage. These pathways are highly regulated to maintain blood glucose homeostasis.

Fructose-1, 6-bisphosphate (D-fructose-1, 6-bisphosphate 1-phosphohydrolase; EC 3. 1. 3; FBPase) governs a key regulatory step in gluconeogenesis, hydrolyzing fructose-1,6-bisphosphate (Fru-1,6-P_2) to fructose 6-phosphate (F6P) and inorganic phosphate (4,5). FBPase and phosphofructokinase (PFK), the counterpart of FBPase in the glycolysis pathway (6), creates a fultile cycle that consumes ATP. Activity of mammalian FBPase and PFK is under dynamic hormone control. Fructose 2,6-bisphosphate (Fru-2,6-P_2) and AMP are inhibitors for FBPase, while both serve as activators for PFK (6-12). During starvation, glucagon is secreted and a downstream bifunctional enzyme fructose-6-phosphate-2-kinase/fructose-2,6-bisphosphatase (PFK-2/FBPase-2) is phosphorylated, which leads to the degradation of Fru-2,6-P_2; whereas in the fed state, insulin reverses the effect of glucagon and raises the level of Fru-2,6-P_2 (13-16). The increment in Fru-2,6-P_2 level is not enough to inhibit FBPase completely by itself; however, AMP inhibition is enhanced up to 10 fold in the presence of Fru-2,6-P_2, which is named AMP/Fru-2,6-P_2 synergism (8-9). Thus, even though AMP concentration is relatively constant *in vivo*, the fluctuation of Fru-2,6-P_2 levels can dynamically alter FBPase activity (17).

Porcine liver FBPase is a homotetramer, with a molecular weight of 37 kDa for each monomer. The four subunits are arranged in D2 symmetry and named C1 to C4, clockwisely (Figure 1, A) (18). Two distinct subunit interfaces, C1-C2 and C1-C4, are in the FBPase

tetramer and play important roles in the functional properties of FBPase. Investigations of hybrid tetramers of FBPase (subunits of the tetramer have nonequivalent primary structures) indicate subunit exchange among tetramers, dimers (C1-C2 and C3-C4) and monomers (19). At least two quaternary states exist when different effectors bind to FBPase: FBPase complex with products and divalent cations creates the R-state whereas the complex with AMP and/or Fru-2,6-P_2 defines T-state (20-22). R-state and T-state FBPase differ by a 15 degree rotation of the C1-C2 dimer relative to the C3-C4 dimer (Figure 1, A).

The active site of FBPase is near the C1-C2 interface and requires residues from both subunits to recognize the 6-phosphoryl group of the substrate (23). Divalent metal ions (Mg^{2+}, Mn^{2+}, or Zn^{2+}) are required for hydrolysis of Fru-1,6-P_2 (4-5). In product complexes of FBPase, three metals formed coordinate bonds to the 1-phosphoral group of Fru-1,6-P_2 (26). Hydrolysis of Fru-1,6-P_2 requires the presence of all three metals. Metal at Site-I is independent of inhibitor ligations; whereas metal at Site-III only shows up in active forms of FBPase (26-27). The binding of Mg^{2+} to the Site-II and Site-III in the same subunit is cooperative (28). A dynamic loop (residue 50-72) can exist in engaged, disordered or disengaged conformations (29). Metal at Site-III is stabilized only with the engaged dynamic loop (26) (Figure 1, B). When metals at Site-II and Site-III are missing, part of dynamic loop (usually 58-70) becomes disordered (20-25). The cycle between engaged and partially disordered conformation of dynamic loop could be important for substrate binding and product release. Certain monovalent cations such as K^+, NH_4^+ and Tl^+ are activators for FBPase at low concentrations (30-32). However, when at high concentrations, Tl^+ displace active site Mg^{2+}, partially disorder the dynamic loop and inhibit FBPase (33). Ca^{2+} and Cd^{2+} are potent inhibitors for FBPase. Product complex of FBPase with Ca^{2+} reveals only two metal binding and a partially disordered dynamic loop (Gao, Y., and Honzatko, R. B., unpublished data) (Figure 2).

AMP is an allosteric inhibitor for FBPase (5). AMP binding sites are near the C1-C4 interface, some 28 Å away from nearest active site (21) (Figure 1). Hydrogen bonds near or at the C1-C4 interface are disrupted/formed in response to AMP ligation (36). As a consequence, the C1-C2 dimer rotates 15 degrees with respect to C3-C4 dimer and the dynamic loop adopts its disengaged conformation (27) (Figure 1).

Backbone dihedral angles of residues 50-51, which is the N-terminal hinge of the dynamic loop, change dramatically in the transition from an engaged to disengaged dynamic loop (27, 36). Residues that interact with divalent cations on the C-terminal end of dynamic loop shift more than 10 Å from the active site (27). Kinetically, AMP is a non-competitive inhibitor with respect to Fru-1,6-P_2 and a competitive inhibitor with respect to Mg^{2+}. The competitive relationship between AMP and Mg^{2+} is likely mediated by the dynamic loop (37-38). Tryptophan fluorescence confirms the status of dynamic loop with or without AMP in solution (29). Introduction of a proline into the hinge of the dynamic loop eliminates AMP inhibition (36). The mutation Ala^{54}→Leu, which destabilizes disengaged conformation of dynamic loop, decreases AMP inhibition over one thousand fold (39). Crystal structures of Leu^{54} FBPase complexed with AMP and products are in two distinct conformations: T-state with a 15 degree subunit-pair rotation and a disordered dynamic loop, and a near R-state (called the I_R-state) with 3 degree rotation and engaged loop (39). Based on structures of Leu^{54} FBPase, Iancu suspects that dimer-dimer rotation is the direct consequence of AMP binding (39); however, how dimer-dimer rotation is coupled to loop displacement is unclear.

AMP inhibition is cooperative, with a hill coefficient of two (7, 40-41). The positive coopertivity, in principal, forces FBPase into one of two quaternary states, depending on a threshold concentration of AMP (and Fru-2,6-P_2). The binding of at least two AMP molecules drives the R- to T-state transition of FBPase (42). The interaction between the C1-C2 dimer and C3-C4 dimer is essential for AMP cooperativity: AMP cooperativity is not present in hybrid FBPase tetramers with AMP molecules bound only at subunits C1 and C2, but is present in hybrid FBPase tetramers with AMP molecules bound to each dimer of the tetramer (42). Point mutations at the C1-C4 interface, the C1-C2 interface and the dynamic loop eliminate AMP coopertivity (36, 43-48). Among them, the case of Arg^{22}→Met FBPase is most compelling as the resulting mutant enzyme retains wild-type properties in catalysis and regulation save AMP coopertivity (43). Arg^{22} from subunit C1 is near the AMP binding site of that subunit and hydrogen bonds with residues near the AMP binding site of subunit C4. The special location and long polar sidechain of Arg^{22} provides a direct connection between two AMP binding sites; however, how changes at the C1-C2 interface, dynamic

loop and other parts of the C1-C4 interface influence AMP cooperativity need further exploration.

Fru-2,6-P_2 was found in 1981 independently by Pilkis and Van Shaftingen (8-9). The inhibition of Fru-2,6-P_2 towards FBPase is competitive with respect to Fru-1,6-P_2 (8-9). Binding of Fru-2,6-P_2 to active site of FBPase is confirmed by chemical modification (49), NMR (50) and X-ray crystallography (22). Fru-2,6-P_2 can enhance AMP inhibition by several fold. Binding studies by NMR confirms the synergism between AMP and Fru-2,6-P_2. In UV spectroscopy, AMP and Fru-2,6-P_2 induce similar conformational change (51). FBPase complexed with AMP and Fru-2,6-P_2 is in the T-state (22); however, early crystallographic studies failed to reveal conformation changes induced by Fru-2,6-P_2 alone (Fru-2,6-P_2 in crystal soaks caused no change (52) and co-crystallizations revealed degraded Fru-2,6-P_2 (53)). Hines successfully co-crystallized FBPase with Fru-2,6-P_2 (54). FBPase complexed with Fru-2,6-P_2 exhibits a 13 degree of rotation between the C1-C2 dimer and C3-C4 dimer, which is similar to the T-state (54) (Figure 2). Fru-2,6-P_2 binding induces local structural rearrangement which is not favorable for a engaged dynamic loop (54). Two metals sit in the active site and the dynamic loop is in its disengaged conformation (54). The similar end state caused by AMP and Fru-2,6-P_2 separately could explain the AMP/ Fru-2,6-P_2 synergism. The remaining question is how the binding of Fru-2,6-P_2 to C1-C2 interface affects rotations at C1-C4 interface.

FBPase from muscle (mFBPase) shares 80-90% sequence identify to its liver isoform. Same as liver FBPase, mFBPase requires divalent cations for catalysis and AMP and Fru-2,6-P_2 for inhibition (4-5,55-56); however, mFBPase is 50-100 times more sensitive to AMP inhibition, which indicates that mFBPase is inhibited under normal condition (55-56). Aldolase interacts with mFBPase and can partially releive AMP inhibition (57-58). The interaction between liver aldolase and liver FBPase is not observed (57). Gizak shows that N-terminal residues of mFBPase are essential for mFBPase/aldolase interaction (59). In vivo, mFBPase localizes in both sides of z-lines as well as in nuclei (60-63). The exact function of mFBPase is unclear.

FBPase in plant chloroplast (cFBPase) works as part of Calvin cycle in carbon fixation. cFBPase is redox-regulated by light, by a mechanism entirely different from its mammalian homologs (64-66). cFBPase is a homotetramer, with active sites nearly identical to porcine liver FBPase. Unlike porcine FBPase, there are no quaternary structural changes linked to inactivation (67-68). cFBPase tetramer is close to the T-state of porcine FBPase, with a 20 degree dimer-dimer rotation relative to the R-state of porcine FBPase and 5 degree rotation relative to T-state porcine FBPase (Figure 2). A regulatory loop with three conserved cysteine residues is inserted between strands β4 and β5 (69-70). Light induces formation of a disulfide bond between two cysteines in the loop (65-66). When these cysteines are in the reducted state, the enzyme is active; on the other hand, formation of the disulfide bond turns off cFBPase. Disulfide bond formation promotes a shift in strands β1 and β2 and pushes a valine sidechain into cation binding sites (68). The movement of the valine would conflict with the engaged conformation of the dynamic loop (68); however, electron density for the dynamic loop is not observed in any of the cFBPase crystal structures (67-68). Hence, without clear evidence of a cFBPase in an active conformation, the mechanism of inhibition remains speculative.

FBPases in prokaryotic systems are classified to five types according to their sequence similarity (71-73). Type I FBPase is homolog to eukaryotic FBPase. Type I-III FBPases are found in bacteria (71). Type IV FBPase from archaea, though not physiological FBPase in archaea, are structurally similar to Type I FBPase and carries both FBPase activity inositol monophosphatase activity (72). A common sugar phosphatase fold is shared by all type I-IV FBPase as well as eukaryotic FBPase. However, type V FBPase, which is widely found in thermophilic prokaryotes, is completely different from type I-IV in both sequences and structures (73). The regulatory mechanism for type II-V FBPase is largely unknown. In contrast, type I FBPase from E coli (eFBPase) is well studied (54,74-77).

eFBPase shares 41% sequence identity with porcine liver FBPase. In solution, eFBPase exists in equilibrium between dimer and tetramer (76). Dilution of eFBPase leads to slow loss of activity, indicating that dimer form of eFBPase is less active than tetramer. Anion activators, such as phosphoenolpyruvate (PEP) or citrate, bind to an allosteric site at the C1-C4 interface and promotes the formation of tetramers (76). The tetramer complex

with product and PEP/citrate defines the active R-state of eFBPase, which is in the same quaternary state as the porcine R-state. Unlike the porcine enzyme, the dynamic loop is disordered in the complexes of eFBPase loop (76) (Figure 2). SO_4^{2-} is a weak activator for eFBPase, binds to the same allosteric site as PEP/citrate and induces a 3-degree rotation between dimers C1-C2 and C3-C4 (75). The corresponding allosteric activator site in porcine FBPase is filled by a negatively charged side chain (Glu^{192} in porcine FBPase). AMP and glucose 6-phosphate (Glc-6-P) are synergistic inhibitors to eFBPase (77). The AMP binding site is topologically identical to that of as porcine FBPase, whereas the Glc-6-P binding site is at C1-C2 interface (77). The eFBPase complex with product, AMP and Glc-6-P reveals extensive conformational change at both C1-C4 and C1-C2 interfaces. The C1-C2 dimer rotates 9 degree relative to the C3-C4 dimer, which is similar to the effect of AMP effect porcine FBPase (Figure 2). The two subunits that make up the dimer rotate 3 degrees relative to each other, causing significant disruption to the active site. If the AMP inhibitory mechanism is the same in eFBPase and porcine FBPase, rotations at C1-C4 interface would correlate with displacement of dynamic loop. However, in both active and inactive form of eFBPase structures, the dynamic loops are disordered (75-77). The inhibition of Glc-6-P and AMP towards eFBPase is antagonized by PEP and/or citrate. Within different nutritional states, the concentration of metabolism intermediates, PEP, citrate and Glc-6-P changes dramatically, providing the basis for dynamic control of FBPase activity. Fru-2,6-P_2 is not presented in E. coli, but Fru-2,6-P_2 is a potent inhibitor for eFBPase (74). eFBPase stays in the R-state in the presence of Fru-2,6-P_2 (54) (Figure 2), consistent with the absence of Fru-2,6-P_2/AMP synergism in eFBPase (74).

Due to the central regulatory role of FBPase in glucose production, FBPase has been considered a target in the development of drugs for the treatment of Type II diabetes (78-89). The highly hydrophilic nature of active site makes it a less attractive target. Thus, most of drug screening efforts focus on the AMP binding site (78-87). Formycine monophosphate and 3-deoxy-AMP inhibit FBPase with potency similar to AMP (78). Rational modifications based on AMP achieve 10-fold enhancements in binding affinity (79-81). Some chemicals, with entirely different scaffold with respect to AMP, can inhibit FBPase effectively by binding to the AMP site (82-83). A novel series of benzoxazole chemicals occupy the AMP

site and a small cavity in proximity to the AMP site (84-86). Inhibitors with a linker connecting two AMP analogs from adjacent sites gain 10^5 potency in FBPase inhibition (87). Animal experiments shown that some of the predrugs can efficiently reduce gluconeogenesis as well as blood glucose levels (79,81,86).

Recent drug searches also reveal a novel allosteric inhibitory site at the center of FBPase (88-89). OC252, one of these inhibitors, is characterized kinetically and structurally (89). OC252 inhibits FBPase with positive cooperativity. Synergism exists between OC252 and both AMP and Fru-2,6-P_2. FBPase complexed with products and OC252 yields a T-like state, with a 12-degree dimer-dimer rotation and disengaged dynamic loops (Figure 2). The inhibition of OC252 is uncompetitive with respect to Fru-1,6-P_2; effective inhibition of OC252 benefits from high concentrations of substrate not available *in vivo*.

Although current drug screening effort towards FBPase achieves a number of successes, potent, selective and cell penetrable compounds are still in high demand. Understanding the inhibitory mechanism of FBPase would support drug-design efforts at known sites and could lead to the discovery of new inhibitory sites.

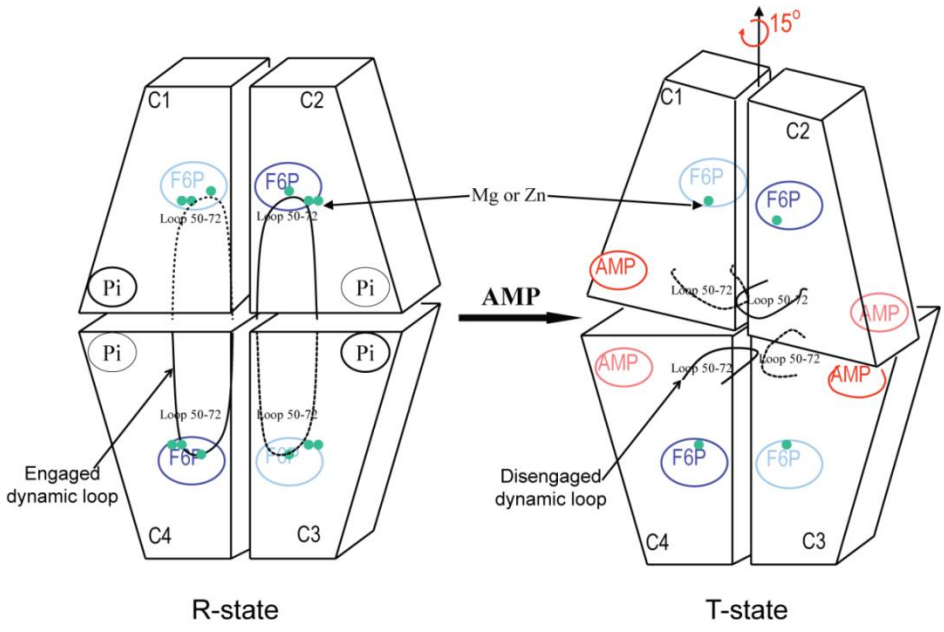

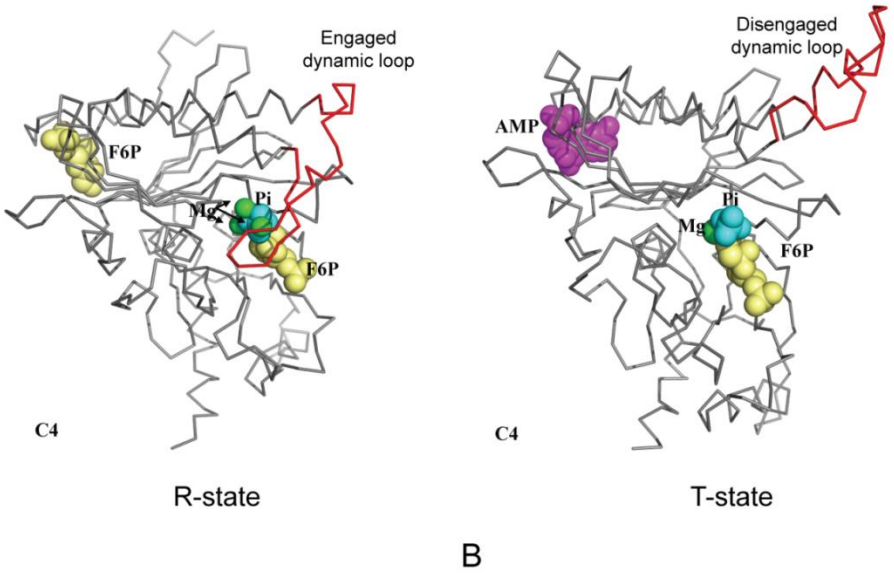

Figure 1. R- to T-state conformational change of FBPase. A. Schemes of FBPase in R- and T-states are drawn with subunits labeled C1-C4 by convention. The relative position of active sites, allosteric sites and dynamic loops are circled. During the R- to T-state transition, the C1-C2 dimer rotates 15 degrees relative to C3-C4 dimer and the dynamic loop moves from engaged to disengaged conformations. B. Cα carbon trace of subunit C4-subunit in R- and T-states. AMP, Mg^{2+}, Fru-6-P (F6P) are shown in spheres. Dynamic loops are red.

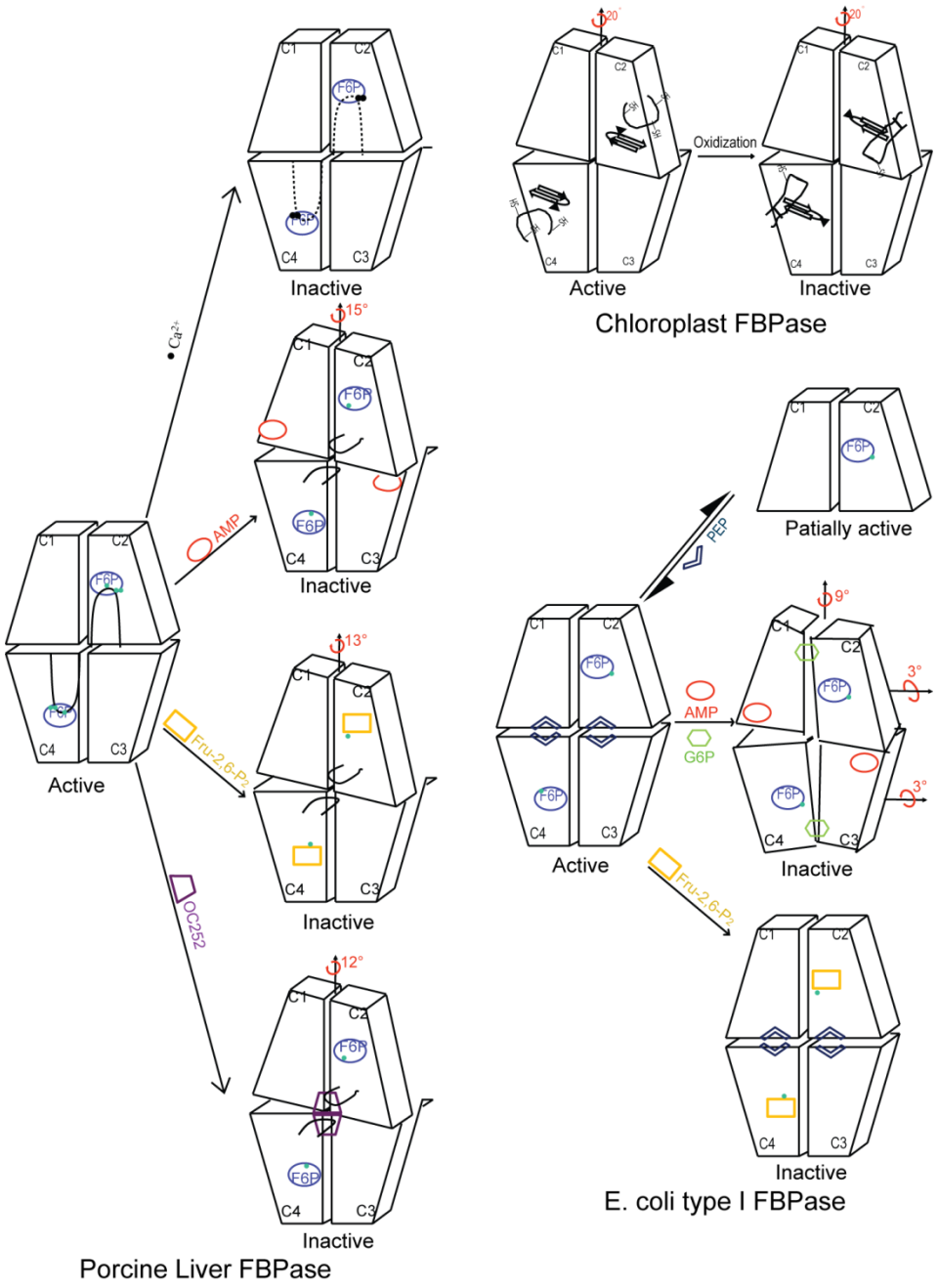

Figure 2. Inhibitory/activation mechanisms of FBPase. Mechanism of mammalian liver FBPase (left), chloroplast FBPase (right top) and bacteria type I FBPase (right bottom) are shown.

Thesis Organization

The dissertation contains eight chapters. Chapter 1 is a general introduction chapter, describes the current status of research on allosteric regulation of FBPase. Chapters 2-7 are the main body of my Ph. D. work on illustrating the inhibitory mechanism of FBPase. Chapter 2 elucidates the conformational transition of FBPase from active R-state to inactive T-state. Chapter 3 characterizes a large hydrophobic cavity at the center of FBPase tetramer, which is populated by ordered water and acts as a thermodynamic determinate for quaternary structure of FBPase. Chapter 4 confirms the essential physiological role of central cavity in allosteric regulation of FBPase, the presence of which determines AMP/Fru-2,6-P_2 synergism. Chapter 5 re-examines the point mutations with reduced AMP cooperativity on dimer-dimer interface and sorts the mutant FBPases to two clusters, some with distablized tetramer and others with T-state-like AMP binding site in the absence of AMP. Chapter 6 verifies subunit pair rotation as structural basis for AMP cooperativity in tetrameric FBPase. Chapter 7 characterized FBPase from *Leptospira interrogans*, and verified it as an evolutionary precursor for eukaryotic FBPases. Final chapter gives a brief summary of the experiments described in previous chapter.

References

1. Berne, R. M., Levy, M. N. (1992) Physiology. Third Edition Mosby Year Book, Chicago
2. Hers, H. G., and Hue, L. (1983) Annu. Rev. Biochem. 52, 617-653
3. Raskin, R. J. (1994) Diabetes Complications. 8, 195-200
4. Benkovic, S. J., and de Maine, M. M. (1982) Mechanism of action of fructose 1,6-bisphosphatase. Adv. Enzymol. Relat. Areas Mol. Biol. 53, 45–82
5. Tejwani, G. A. (1983) Regulation of fructose-bisphosphatase activity. Adv. Enzymol. Relat. Areas Mol. Biol. 54, 121–194
6. Blangy, D., Buc, H. & Monod, J. (1968) J. Mol. Biol. 31, 13-35
7. Taketa, K., and Pogell, B. M. (1965) J. Biol. Chem. 240, 651–662
8. Pilkis, S. J., El-Maghrabi, Pilkis, J., and Claus, T. (1981) J. Biol. Chem. 256, 3619–3622
9. Van Schaftingen, E., and Hers, H.-G. (1981) Proc. Natl. Acad. Sci. U. S. A. 78, 2861–2863
10. Pilkis S. J., El-Maghrabi, Pilkis, J., Claus, T. H., and Cumming D. A. (1981) J. Biol. Chem. 256, 3171–3174
11. Van Schaftingen, E., Jett, M.-F., Hue, L., and Hers, H.-G. (1981) Proc. Natl.Acad. Sci. U. S. A. 78, 3483–3486
12. Uyeda, K., Furuya, E., and Luby, L. J. (1981) J. Biol. Chem. 256, 8394–8399
13. Pilkis, S. J., el-Maghrabi, M. R., and Claus, T. H. (1988) Annu. Rev. Biochem. 57, 755-783
14. Christophe, J. (1995) Biochim. Biophys. Acta. 1241, 45-57
15. Pilkis, S. J., Claus, T. H., Kurland, I. J., and Lange, A. J. (1995) Annu. Rev. Biochem. 64, 799-835
16. Okar, D. A., Manzano, A., Navarro-Sabate, A., Riera, L., Bartrons, R., and Lange, A. J. (2001) Trends Biochem. Sci. 26, 30-35
17. Okar, D. A., and Lange, A. J. (1999) Biofactors 10, 1–14
18. Ke, H., Thorpe, C. M., Seaton, B. A., Marcus, F., and Lipscomb, W. N. (1989) Proc. Natl. Acad. Sci. U.S.A. 86, 1475-1479
19. Nelson, S. W., Honzatko, R. B., and Fromm, H. J. (2001) FEBS. Lett. 492, 254-258
20. Ke, H. M., Liang, J. Y., Zhang, Y. P., and Lipscomb, W. N. (1991) Biochemistry. 30, 4412-4420
21. Ke, H. M., Zhang, Y. P., and Lipscomb, W. N. (1990) Proc. Natl. Acad. Sci. U.S.A. 87, 5243-5247
22. Xue, Y., Huang, S., Liang, J. Y., Zhang, Y., and Lipscomb, W. N. (1994) Proc. Natl. Acad. Sci. U.S.A. 91, 12482-12486

23. Giroux, E., Williams, M. K., and Kantrowitz, E. R. (1994) J. Biol. Chem. 269, 31404-31409

24. Zhang, Y., Liang, J., Huang, S., Ke, H., and Lipscomb, W. N. (1993) Biochemistry 32, 1844-1857

25. Villeret, V., Huang, S., Zhang, Y., and Lipscomb, W. N. (1995) Biochemistry 34, 4307-4315

26. Choe, J. Y., Poland, B. W., Fromm, H. J., and Honzatko, R. B. (1998) Biochemistry 37, 11441-11450

27. Choe, J. Y., Fromm, H. J., and Honzatko, R. B. (2000) Biochemistry 39, 8565-8574

28. Nelson, S. W., Honzatko, R. B., and Fromm, H. J. (2004) J. Biol. Chem. 279, 18481-18487

29. Nelson, S. W., Iancu, C. V., Choe, J. Y., Honzatko, R. B., and Fromm, H. J. (2000) Biochemistry 39, 11100-11106

30. Hubert, E., Villanueva, J., Gonzalez, A. M., and Marcus, F. (1970) Arch. Biochem. Biophys. 138, 590-597

31. Marcus, F., and Hosey, M. M. (1980) J. Biol. Chem. 255, 2481-2486

32. Zhang, R., Villeret, V., Lipscomb, W. N., and Fromm, H. J. (1996) Biochemistry 35, 3038-3043

33. Choe, J. Y., Nelson, S. W., Fromm, H. J., and Honzatko, R. B. (2003) J. Biol. Chem. 278, 16008-16014

34. Gao, Y., and Honzatko, R. B. unpublished data

35. Zhang, Y., Liang, J. Y., Huang, S., and Lipscomb, W. N. (1994) J. Mol. Biol. 244, 609-624

36. Nelson, S. W., Choe, J. Y., Honzatko, R. B., and Fromm, H. J. (2000) J. Biol. Chem. 275, 29986-29992

37. Scheffier, J. E., and Fromm, H. J. (1986) Biochemistry 25, 6659-6665

38. Liu, F., and Fromm, H. J. (1990) J. Biol. Chem. 265, 7401-7408

39. Iancu, C. V., Mukund, S., Fromm, H. J., and Honzatko, R. B. (2005) J. Biol. Chem. 280, 19737-19745

40. Nimmo, H. G., and Tipton, K. F. (1975) Eur. J. Biochem. 58, 567-574

41. Stone, S. R., and Fromm, H. J. (1980) Biochemistry 19, 620-625

42. Nelson, S. W., Honzatko, R. B., and Fromm, H. J. (2002) J. Biol. Chem. 277, 15539-15545

43. Shyur, L. F., Aleshin, A. E., Honzatko, R. B., and Fromm, H. J. (1996) J. Biol. Chem. 271, 3005-3010

44. Shyur, L. F., Aleshin, A. E., Honzatko, R. B., and Fromm, H. J. (1996) J. Biol. Chem. 271, 33301-33307
45. Shyur, L. F., Poland, B. W., Honzatko, R. B., and Fromm, H. J. (1997) J. Biol. Chem. 272, 26295-26299
46. Kurbanov, F. T., Choe, J. Y., Honzatko, R. B., and Fromm, H. J. (1998) J. Biol. Chem. 273, 17511-17516
47. Lu, G., Stec, B., Giroux, E. L., and Kantrowitz, E. R. (1996) Protein Sci. 5, 2333-2342
48. Lu, G., Giroux, E. L., and Kantrowitz, E. R. (1997) J. Biol. Chem. 272, 5076-5081
49. Liu, F., and Fromm, H. J. (1988) J. Biol. Chem. 263, 10035-10039
50. Ganson, N. J., and Fromm, H. J. (1985) J. Biol. Chem. 260, 2837-2843
51. McGrane, M. M., El-Maghrabi, M. R., and Pilkis, S. J. (1983) J. Biol. Chem. 258, 10445-10454
52. Liang, J. Huang, S., and Lipscomb, W. N. (1992) Proc. Natl. Acad. Sci. U.S.A. 89, 2404-2408
53. Ke, H., Thorpe, C. M., Seaton, B. A., and Lipscomb, W. N. (1989) J. Mol. Biol. 212, 513-539
54. Hines, J. K., Chen, X., Nix, J. C., Fromm, H. J., and Honzatko, R. B. (2007) J. Biol. Chem. 282, 36121-36131
55. Dzugaj, A., and Kochman, M. (1980) Biochim. Biophys. Acha 614, 407-412
56. Skalecki, K., Mularczyk, W., and Dzugaj, A. (1995) Biochem. J. 310, 1029-1035
57. Rakus, D., and Dzugaj, A. (2000) Biochem. Biophys. Res. Com. 275, 611-616
58. Rakus, D., Pasek, M., Krotkiewski, H., and Dzugaj, A. (2003) FEBS Lett. 547, 11-14
59. Gizak, A., Maciaszczyk, E., Dzugaj, A., Eschrich, K., and Rakus, D. (2008) Proteins. 72, 209-216
60. Rakus, D., Mamczur, P., Gizak, A., Dus, D., and Dzugaj, A. (2003) Biochem. Biophys. Res. Com. 311, 294-299
61. Gizak, A., Rakus, D., and Dzugaj, A. (2003) Histol Histopathol 18, 135-142
62. Gizak, A., Rakus, D., and Dzugaj, A. (2005) Histol Histopathol 36, 243-248
63. Mamczur, P., Sok, A. J., Rzechonek, A., and Rakus, D. (2012) Histichem Cell Biol. 137, 121-136
64. Pedersen, T. A., Kirk, M., and Bassham, J. (1966) Chlorella. Physiol. Plant. 19, 219-231
65. Buchanan, B. B., and Wolosiuk, R. A. (1976) Nature 264, 669-670
66. Buchanan, B. B. (1980) Annu. Rev. Plant Physiol. 31, 341-374
67. Villeret, V., Huang, S., Zhang, Y., Xue, Y., and Lipscomb, W. N. (1995) Biochemistry 34, 4299-4306

68. Chiadmi, M., Navaza, A., Miginiac-Maslow, M., Jacquot, J.-P., and Cherfils, J. (1999) EMBO J. 18, 6809-6815

69. Marcus, F., Moberly, L., and Latshaw, S. P. (1988) Proc. Natl. Acad. Sci. U.S.A. 85, 5379-5383

70. Raines, C. A., Lloyd, J. C., Longstaff, M., Bradley, D., and Dyer, T. (1988) Nucleic Acids Res. 16, 7931-7942

71. Donahue, J. L., Bownas, J. L., Niehaus, W. G., and Larson, T. J. (2000) J. Bacteriol 182, 5624-5627

72. Stec, B., Yang, H., Johnson, K. A., Chen, L., and Roberts, M. F. (2000) Nature 7, 1046-1050

73. Nishimasu, H., Fushinobu, S., Shoun, H., and Wakagi, T. (2004) Structure 12, 949-959

74. Kelley-Loughnane, N., Biolsi, S. A., Gibson, K. M., Lu, G., Hehir, M. J., Phelan, P., and Kantrowitz, E. R. (2002) Biochim. Biophys. Acta 1594, 6-16

75. Hines, J. K., Fromm, H. J., and Honzatko, R. B. (2006) J. Biol. Chem. 281, 18386–18393

76. Hines, J. K., Fromm, H. J., and Honzatko, R. B. (2007) J. Biol. Chem. 282, 11696–11704

77. Hines, J. K., Kruesel, C. E., Fromm, H. J., and Honzatko, R. B. (2007) J. Biol. Chem. 282, 24697–24706

78. Iversen, L. F., Brzozowski, M., Hastrup, S., Hubbard, R., Kastrup, J. S., Larsen, I. K., Naerum, L., Norskov-Lauridsen, L., Rasmussen, P. B., Thim, L., and Wiberg, F. C. (1997) Protein Sci. 6, 971-982

79. Erion, M. D., van Poelje, P. D., Dang, Q., Kasibhatla, S. R., Potter, S. C., Reddy, M. R., Reddy, K. R., Jiang, T., and Lipscomb, W. N. (2005) Proc. Natl.Acad. Sci. U. S. A. 102, 7970–7975

80. Erion, M. D., Dang, Q., Reddy, M. R., Kasibhatla, S. R., Huang, J., Lipscomb, W. N., and van Poelje, P. D. (2007) J. Am. Chem. Soc. 129, 15480-15490

81. Dang, Q., Kasibhatla, S. R., Reddy, K. R., Jiang, T., Reddy, M. R., Potter, S. C., Fujitaki, J. M., van Poelje, P. D., Huang, J., Lipscomb, W. N., and van Poelje, P. D. (2007) J. Am. Chem. Soc. 129, 15491-15502

82. Heng, S., Harris, K. M., and Kantrowitz, E. R. (2010) Eur. J. Med. Chem. 45, 1478-1484

83. Rudnitskaya, A., Huynh, K., Török, B., and Stieglitz, K. (2009) J. Med. Chem. 52, 878-882

84. von Geldern, T. W., Lai, C., Gum, R. J., Daly, M., Sun, C., Fry, E. H., and Abad-Zapatero, C. (2006) Bioorg. Med. Chem. Lett. 16, 1811-1815

85. Kitas, E., Mohr, P., Kuhn, B., Hebeisen, P., Wessel, H. P., Haap, W., Ruf, A., Benz, J., Joseph, C., Huber, W., Sanchez, R. A., Paehler, A., Benardeau, A., Gubler, M., Schott, B., and Tozzo, E. (2010) Bioorg. Med. Chem. Lett. 20, 594-599

86. Hebeisen, P., Haap, W., Kuhn, B., Mohr, P., Wessel, H. P., Zutter, U., Kirchner, S., Ruf, A., Benz, J., Joseph, C., Alvarez-Sánchez, R., Gubler, M., Schott, B., Benardeau, A., Tozzo, E., and Kitas, E. (2011) Bioorg. Med. Chem. Lett. 21, 3237-3242

87. Hebeisen, P., Kuhn, B., Kohler, P., Gubler, M., Huber, W., Kitas, E., Schott, B., Benz, J., Joseph, C., and Ruf, A. (2008) Bioorg. Med. Chem. Lett. 18, 4708-4712

88. Wright, S. W., Carlo, A. A., Carty, M. D., Danley, D. E., Hageman, D. L., Karam, G. A., Levy, C. B., Mansour, M. N., Mathiowetz, A. M., McClure L. D., Nestor, N. B., McPherson, R. K., Pandit, J., Pustilnik, L. R., Schulte, G. K., Soeller, W. C., Treadway, J. L., Wang, I.-K., and Bauer, P. H. (2002) J. Med. Chem. 45, 3865-3877

89. Choe, J. Y., Nelson, S. W., Arienti, K. L., Axe, F. U., Collins, T. L., Jones, T. K., Kimmich, R. D., Newman, M. J., Norvell, K., Ripka, W. C., Romano, S. J., Short, K. M., Slee, D. H., Fromm, H. J., and Honzatko, R. B. (2003) J. Biol. Chem. 278, 51176-51183

CHAPTER II. MECHANISM OF DISPLACEMENT OF A CARALYTICALLY ESSENTIAL LOOP FROM THE ACTIVE SITE OF MAMMALIAN FRUCTOSE-1,6-BISPHOSPHATASE

A paper submitted to *Biochemistry*

Yang Gao, Cristina V. Iancu, Susmith Mukind, Jun-Yong Choe, and Richard B. Honzatko

Roy J. Carver Department of Biochemistry, Biophysics, and Molecular Biology,

Iowa State University, Ames, IA 50011

Abstract

AMP triggers a 15 ° subunit-pair rotation in fructose-1,6-bisphosphatase (FBPase) from its active R-state to its inactive T-state. During this transition, a catalytically essential loop (residues 50–72) leaves its active (engaged) conformation. Structures of Ile^{10}→Asp FBPase and molecular dynamic simulations here reveal factors responsible for loop displacement. AMP/Mg^{2+} and AMP/Zn^{2+} complexes of Asp^{10} FBPase are in intermediate quaternary conformations (completing 12 ° of subunit-pair rotation), but the complex with Zn^{2+} provides the first instance of an engaged loop in a near-T quaternary state. The 12 ° subunit-pair rotation generates close contacts involving the hinges (residues 50–57) and hairpin turns (residues 58–72) of the engaged loops. Additional subunit-pair rotation toward the T-state would make such contacts unfavorable, presumably causing displacement of the loop. Targeted molecular dynamics simulations reveal no steric barriers to subunit-pair rotations up to 14 °, followed by the displacement of the loop from the active site. Principal component analysis reveals high-amplitude motions that exacerbate steric clashes of engaged loops in the near-T state. The results of simulations and crystal structures are in agreement: subunit-pair rotations just short of the canonical T-state, coupled with high-amplitude modes, sterically displace the dynamic loop from the active site.

Introduction

Fructose-1,6-bisphosphatase (D-fructose -1,6-bisphosphate 1-phosphohydrolase, EC 3.1.3.11; FBPase[1]) catalyzes the hydrolysis of fructose 1,6-bisphosphate (Fru-1,6-P_2) to fructose 6-phosphate (Fru-6-P) and inorganic phosphate (P_i) (1, 2). FBPase controls a tightly regulated step of gluconeogenesis: AMP and fructose 2,6-bisphosphate (Fru-2,6-P_2) bind to allosteric and active sites, respectively, and inhibit FBPase while activating fructose-6-phosphate 1-kinase in glycolysis (3, 4). Physiological levels of Fru-2,6-P_2 are subject to control by glucagon and insulin (4, 5). As Fru-2,6-P_2 enhances the binding of AMP to FBPase by up to an order of magnitude (6), AMP should become a more potent inhibitor of FBPase *in vivo* as concentrations of Fru-2,6-P_2 increase. AMP binds 28 Å away from the nearest active site, inhibiting catalysis noncompetitively with respect to Fru-1,6-P_2. Yet, AMP is a competitive inhibitor of catalysis with respect to essential divalent cations (Mg^{2+}, Mn^{2+}, or Zn^{2+}), all of which probably bind with the 1-phosphoryl group of Fru-1,6-P_2 (7–10).

FBPase is a homotetramer [subunit M_r of 37,000 (11)] and exists in at least two distinct quaternary states called R and T (12–13), as well as intermediate conformations that are R-like (I_R-state) (14) and T-like (I_T-state) (15). For the wild-type enzyme, the binding of AMP alone can drive the R- to T-state transition, in which the upper subunit-pair rotates 15 ° relative to the bottom subunit-pair of the FBPase tetramer. Substrates or products in combination with metal cations stabilize the R-state conformation.

A dynamic loop (residues 50–72), essential for activity, has been observed in three conformations called engaged, disengaged, and disordered (16). AMP alone or with Fru-2,6-P_2 stabilizes a disengaged loop (16, 17), whereas metals with products stabilize an engaged loop (10, 18–20). In active forms of the enzyme, loop 50–72 probably cycles between its engaged and disordered conformations (16, 18). Fluorescence from a tryptophan reporter group at position 57 is consistent with the conformational states for loop 50–72 observed in crystal structures (21, 22). Thus far, the engaged conformation of loop 50–72 has appeared only in R-state crystal structures, and the disengaged conformer only in T-state structures; however, disordered conformations of the dynamic loop have appeared in both the R- and T-states (14, 18, 19, 23, 24). Although the engaged conformation of the dynamic loop

correlates with the R-state, and the disengaged conformer with the T-state, the mechanism of loop displacement in the R- to T-state transition has yet to be defined.

Here, we present results from molecular dynamics simulations and crystal structures that identify factors responsible for loop-displacement in the R- to T-state transition. Targeted molecular dynamics (TMD) simulations of the R- to T-transition reveal unhindered subunit-pair rotations (dynamic loop engaged) until just short of the T-state. Consistent with TMD simulations is the crystal structure of the AMP•Zn^{2+} complex of Ile^{10}→Asp FBPase, presented here, which reveals an engaged dynamic loop in a near-T quaternary state with tight contacts involving the hinge and hairpin turn of the loop. Principal component analysis (PCA) of MD trajectories of this near-T state identifies large-amplitude motions that exacerbate steric clashes of the engaged loop. Hence, the quaternary transition to the T-state harnesses large-amplitude modes to sterically eject the loop from the active site.

Experimental procedures

Materials— Fru-1,6-P_2, Fru-2,6-P_2, and AMP were purchased from Sigma. DNA-modifying and restriction enzymes, T4 polynucleotide kinase and ligase were from Promega. Glucose-6-phophate dehydrogenase and phosphoglucose isomerase came from Roche. Other chemicals were of reagent grade or equivalent. *Escherichia coli* strains BMH 71-18 mutS and XL1-Blue came from Clontech and Stratagene, respectively. The FBPase-deficient *E. coli* strain DF 657 came from the Genetic Stock Center at Yale University.

Mutagenesis of wild-type FBPase— The mutation of Ile^{10} to aspartate was accomplished as described previously (16). The mutation and the integrity of the construct were confirmed by sequencing the promoter region and the entire open reading frame. The Iowa State University sequencing facility provided DNA sequences, using the fluorescent dye-dideoxy terminator method.

Expression and Purification of Asp^{10} FBPase— Cell-free extracts of wild-type and Asp^{10} FBPase were subjected to heat treatment (63 ℃ for 7 minutes), followed by centrifugation.

The supernatant solution was loaded onto a Cibracon Blue sepharose column, previously equilibrated with 20 mM Tris-HCl, pH 7.5. The column was washed first with 20 mM Tris-HCl, pH 7.5. Enzyme was eluted with a solution of 500 mM NaCl and 20 mM Tris-HCl of the same pH. After pressure concentration (Amicon PM-30 membrane) and dialysis against 10 mM Tris-HCl, pH 8.0, the protein sample was loaded onto a DEAE sepharose column equilibrated with 10 mM Tris-HCl, pH 8.0. Purified enzyme was eluted with a NaCl gradient (0–0.5 M) in 10 mM Tris-HCl, pH 8.0, and then dialyzed extensively against 50 mM Hepes, pH 7.4. Purity and protein concentrations of FBPase preparations were confirmed by SDS-polyacrylamide gel electrophoresis (25) and the Bradford assay (26), respectively.

Crystallization of the product complex— Crystals of Asp^{10} FBPase were grown by the method of hanging drops. Equal parts of a protein solution and a precipitant solution were combined in a droplet of 4 μL total volume. Wells contained 500 μL of the precipitant solution. R-state crystals grew from a protein solution [Asp^{10} FBPase (10 mg/ml), Hepes (25 mM, pH 7.4), $MgCl_2$ (5 mM), and Fru-1,6-P_2 (5 mM)] combined with a precipitant solution [Hepes (100 mM, pH 7.4), polyethylene glycol 3350 (8% (w/v)), glycerol (27% (v/v)), and t-butanol (5% (v/v))]. Crystals of the T-like AMP complex grew from a protein solution [Asp^{10} FBPase (10 mg/ml), Hepes (25 mM, pH 7.4), $ZnCl_2$ (5 mM), Fru-1,6-P_2 (5 mM), and AMP (5mM)] combined with a precipitant solution [Hepes (100 mM, pH 7.4), polyethylene glycol 3350 (12% (w/v)), glycerol (23% (v/v)), and t-butanol (5% (v/v))]. Crystals of the T-state AMP complex grew from a protein solution [Asp^{10} FBPase (10 mg/ml), Hepes (25 mM, pH 7.4), $MgCl_2$ (5 mM), Fru-1,6-P_2 (5 mM), and AMP (5 mM)] combined with a precipitant solution [Hepes (100 mM, pH 7.4), polyethylene glycol 3350 (14% (w/v)), 2-methyl-2,4-pentanediol (21% (v/v)), and t-butanol (5% (v/v))]. Crystals were of equal dimensions (0.2–0.4 mm), growing in approximately three days at 20 °C. Conditions of crystallization include cryoprotectants, allowing crystals to be transferred directly from droplet to liquid nitrogen.

Data collection— Data were collected at Brookhaven National Laboratory on beamlines X4A (R- and I_T-state structures) and X12C (T-state structure) at a temperature of 110 K. Data were reduced with the program HKL (27).

Structure determination, model building and refinement— Crystals of Asp^{10} FBPase are isomorphous to either the AMP•Zn^{2+}•product complex (18) or the Zn^{2+}•product complex (10). Phase angles, used in the generation of initial electron density maps, were based on model 1EYJ or 1CNQ of the PDB, from which water molecules, metal cations, small-molecule ligands, and residues 50–72 had been omitted. Residues 50–72 were built into the electron density of omit maps, using the program XTALVIEW (28). Ligands were added to account for omit electron density at the active site and/or the AMP site. The resulting models underwent refinement, using CNS (29) with force constants and parameters of stereochemistry from Engh & Huber (30). A cycle of refinement consisted of slow cooling from 1000–300 K in steps of 25 K, followed by 120 cycles of conjugate gradient minimization, and concluded by the refinement of individual thermal parameters. Thermal parameter refinement employed restraints of 1.5 $Å^2$ on nearest neighbor and next-to-nearest neighbor main chain atoms, 2.0 $Å^2$ on nearest neighbor side chain atoms, and 2.5 $Å^2$ on next-to-nearest neighbor side chain atoms.

In subsequent cycles of refinement, water molecules were fit to difference electron density of 2.5σ or better and were added until no significant decrease was evident in the R_{free} value. Water molecules in the final models make suitable donor-acceptor distances to each other and the protein and have thermal parameters under 60 $Å^2$. Stereochemistry of the models was examined by the use of PROCHECK (31).

Measurement of the rotation angle— Hines et al. (32) defined the rotation angle by alignment to the R-state structure. This method is intractable in determining subunit-pair rotations of thousands of structures from MD trajectories. Subunit-pair rotations from MD simulations are determined as follows: Firstly, Cα atoms of residues 33–49, 75–265 and 272–330 define the center of mass of each subunit. Secondly, the acute angle defined by the line segments connecting mass centers within the subunit pair (C1 and C2 or C3 and C4) is taken as the subunit-pair rotation angle. Subunit-pair rotation angles for R-, I_R-, I_T- and T-states become 15.1, 18.2, 24.6 and 28.6 °, respectively, corresponding to 0, 3, 12, 15 ° as determined by superpositions of crystal structures.

MD simulations— MD simulations here employed NAMD (33) with the CHARMM 27 force field (34). The initial coordinates for R- I_R-, and I_T- and T-states were RCSB database entries 1CNQ, 1YYZ, 2F3D, and 1EYJ, respectively (10). The system included an entire tetramer of FBPase and approximately 30,000 TIP3P water molecules (35) in a rectangular water box with a buffering distance of 15 Å. Sodium and chloride ions were added to neutralize the net charge of system. Periodic boundary conditions were applied and the Particle mesh Ewald algorithm (36) was used for the calculation of long-range electrostatic interactions. The cutoff was set to 12 Å for non-bonded Van der Waals interactions and the integration time step was 2.0 fs. All models were energy-minimized for 10 ps and gradually heated to 310 K to relax unfavorable contacts (if any), followed by another 10 ps simulation to equilibrate the system. Finally, simulations of 15 ns were carried out with constant pressure and temperature (1.01325 bar at 310 K). Results from simulation were analyzed with VMD (37) and user-written programs described in the next section.

Principal component analysis (PCA)— Motions from MD simulations can be recast into an orthogonal set of principal components, each of which corresponds to a specific motion and amplitude. Principle components with large amplitudes correspond to collective motions in protein, which can be important functionally (38, 39). Principle components were calculated as follows: A covariance matrix C was calculated from the MD trajectory as:

$$C_{ij} = \left\langle \left(r_i - \left\langle r_i \right\rangle\right) \bullet \left(r_j - \left\langle r_j \right\rangle\right) \right\rangle, \quad \text{Eqn. 1}$$

where i,j = 1,...3N, N is the total number of Cα atoms in the structure, r is the Cartesian coordinates of i^{th} Cα atom, and the angle brackets denote an average over the entire MD trajectory. Rigid-body translations and rotations of the tertramer were removed before PCA by aligning trajectory structures onto the starting structure. 3N eigenvectors and associated eigenvalues were obtained by diagonalization of the matrix C. Each eigenvector corresponds to a principal component of motion and the associated eigenvalue reflects its contribution to the collective motion. The root-mean-square inner product (RMSIP, 40) was used to compare PCA results from different trajectories:

$$RMSIP = \left(\frac{1}{10} \sum_{1}^{10} \sum_{1}^{10} (\nu_i \bullet \nu_j)^2 \right)^{1/2}$$, Eqn. 2

where ν_i and ν_j are the i^{th} and j^{th} eigenvectors of the two sets having the ten largest associated eigenvalues.

Targeted molecular dynamics simulations (TMD)— Details of the TMD procedure are in the original paper (41) and early applications (42, 43). TMD employs an artificial energy constraint to force a conformational change toward a target structure, and can be a powerful tool in the exploration of transition pathways (42-45). The energy constraint is as follows:

$$U_{TMD} = \frac{1}{2} \frac{k}{N} \left[RMS(t) - RMS^*(t) \right]^2$$, Eqn. 3

where *k* is the force constant, *N* is the total number of atoms, *RMS(t)* is the root-mean-squared deviation (RMSD) between a given trajectory structure and the target structure at transition time *t* while the *RMS*(t)* is the expected RMSD, assuming a linear decrease in RMSD proportional to time. TMD simulations here employed NAMD under the CHARMM 27 force-field with an integration time step of 1 fs. As the starting and target structures should have the same atoms, residues 6-9 and two Mg^{2+} in the R-state structure and AMP in T-state structure were removed. The simulation system included 10659 TIP3P water molecules and 20364 protein atoms (the value of *N* in Eqn. 3). The initial and target structures were energy-minimized and equilibrated, followed by the TMD simulations at constant temperature (310 K). TMD simulations were performed with different time steps and force constants to determine the sensitivity of the observed transition pathways to parameters of the simulation.

Results

Rationale for the Ile^{10}→Asp mutation— The side chain of Ile^{10} packs against hydrophobic residues from loop 190 in the R-state, and against hydrophobic residues of the disengaged

dynamic loop in the T-state. (Figures of Ile^{10} and nearby residues are in references 14 and 16). The Ile^{10}→Asp mutation then introduces an electrostatic charge that destabilizes the R- and T-states. The R-state hydrophobic cluster is not present in the R-like AMP complex (14), and hence, Ile^{10}→Asp should have little or no effect on the stability of intermediate quaternary states with engaged dynamic loops. Moreover, as Zn^{2+} (relative to Mg^{2+}) stabilizes the engaged conformation of the dynamic loop by fully occupying metal site-3 of the active site (10, 18), the AMP•Zn^{2+}•product complex of Asp^{10} FBPase offers a reasonable opportunity to capture an intermediate quaternary state of FBPase with bound AMP and an engaged dynamic loop.

Product complex of Asp^{10} FBPase (PDB identifier 2F3B)— Preparations of Asp^{10} FBPase used here are at least 95% pure, as judged by SDS-polyacryamide gel electrophoresis (data not shown). Gels indicated no proteolysis of the purified enzyme.

Crystals (space group I222, a=52.94, b=82.50 and c=165.0 Å) are isomorphous to those of wild-type FBPase in its R-state, containing one subunit of the tetramer in the asymmetric unit of the crystal (10, 18–20). The model begins at residue 10 (electron density for residues 1–9 is weak or absent) and continues to the last residue of the sequence. Thermal parameters vary from 11 to 55 $Å^2$. This and all other models presented here have stereochemistry comparable to that of structures of equivalent resolution (31). Statistics for data collection and refinement are in Table 1.

The product complex of Asp^{10} FBPase has one molecule each of Fru-6-P and P_i bound to the active site with three atoms of Zn^{2+}. The dynamic loop (residues 50–72) is in its engaged conformation. We refer the reader to other descriptions of R-state product complexes (10, 18–20) for more detailed descriptions of active site interactions.

Superposition reveals a close match to the wild-type R-state; however, deviations in the relative positions of Cα atoms in excess of 0.5 Å are evident for residues 10–19 (Fig. 1). Asp^{10} has dissociated from the hydrophobic surface against which Ile^{10} packs in the R-state of the wild-type tetramer. Helix H1 shifts essentially as a rigid body, and its movement perturbs the connecting element between helices H1 and H2 that contains residues critical to

the recognition of AMP. The mutation of Ile^{10} to aspartate and the binding of AMP to Leu^{54} FBPase (14) have comparable effects on helix H1 and the conformation of its N-terminal segment.

AMP•product T-like complex of Asp^{10} FBPase (PDB identifier 2F3D)— Crystals (space group I222, *a*=55.84, *b*=82.50 and *c*=165.0 Å) contain one subunit in the asymmetric unit and are nearly isomorphous to those of wild-type FBPase R-state crystals (10, 18–20). The model begins at residue 10 (electron density absent for residues 1–9) and continues to the last residue of the sequence. Thermal parameters vary from 9 to 59 $Å^2$.

The subunit of the AMP/product complex of Asp^{10} FBPase has one molecule each of Fru-6-P and P_i with three atoms of Zn^{2+} at the active site (Fig. 2). In addition, strong electron density for bound AMP is present in the allosteric inhibitor pocket. The dynamic loop (residues 50–72) adopts the engaged conformation. Superposition of the Asp^{10} tetramer onto canonical wild-type R- and T-states reveals an intermediate quaternary state in which subunit-pair C1–C2 has rotated approximately 12 ° relative to subunit pair C3–C4. The subunit-pair rotation is near that of the wild-type enzyme in its complex with the allosteric inhibitor OC252 (15).

The superposition of the I_R-state subunit (AMP complex of Leu^{54} FBPase) onto subunits of the I_T-state tetramer of the AMP complex of Asp^{10} FBPase reveals tertiary conformational changes that accompany the 9 ºsubunit-pair rotation from the I_R- to I_T-states. For the most part, changes in the relative positions of Cα atoms are less that 0.2 Å; however, shifts in Cα atoms of 0.5–4.0 Å define four symmetry-related bands, connecting the AMP binding sites of subunits C1, C2, C3, and C4 to the active sites of subunits C2, C1, C4, and C3, respectively (Fig. 2). Shifts extend from the AMP molecule to helix H1, from helix H1 to loop 190, and then across subunit boundaries to the dynamic loop.

AMP and helix H1 move through comparable displacements of 0.5–1.0 Å during the I_R- to I_T-state transition (Fig. 3, *top*). In the I_T-state structure, Thr^{39} hydrogen bonds with Glu^{192} of a neighboring subunit (C1–C4 contact); this hydrogen bond was disrupted in the AMP complex of Leu^{54} FBPase (14). The movement in helix H1 carries over to residues

194–197, and from there to residues 53–55 of the dynamic loop (Figure 3, *middle*). The entire dynamic loop shifts toward Arg^{313} by approximately 0.5 Å. In contrast, residues 264–274 move in opposition to the general thrust of the dynamic loop, generating tight contacts (Figure 3, *bottom*). In the I_R-state, the side chain of Arg^{313} hydrogen bonds with the backbone carbonyls of residues 66 and 274 (donor-acceptor distances of 2.8–2.9 Å), and is in contact with the Cβ atom of Thr^{66} (distance of 3.6 Å). In the I_T-state, however, the donor-acceptor contacts diminish to 2.5 Å, and the contact involving the Cβ atom of Thr^{66} becomes 2.9 Å. In short, the transition from the I_R- to I_T-state lessens the space for the engaged conformation of the dynamic loop.

The movement in loop 264–274 is relatively large (up to 4 Å), and results in the elimination of a tight internal contact between the backbone carbonyl group of residue 272 and the backbone amide group of residue 314. In the I_R-state (as well as the R-state), the contact distance is approximately 2.8 Å. Although the contact distance is reasonable for a donor-acceptor pair, the axis of the backbone carbonyl 272 is perpendicular to the plane of the peptide link between residues 313 and 314. Hence, an unfavorable contact exits between residues 272 and 314 in the I_R-state, and a small rotation of the carbonyl group of residue 272 relieves this tight contact in the I_T-state (contact distance becomes 3.1 Å), and drives the observed motion of loop 264–274 in the I_R- to I_T-state transition.

AMP/product T-state complex of Asp^{10} FBPase (PDB identifier 2F3H)— Crystals (space group $P2_12_12$, a=60.28, b=167.0 and c=79.06) are isomorphous to those of AMP complexes of FBPase (16, 17). The subunit pair C1–C2 is in the asymmetric unit of this crystal form. The model begins at residue 10 and continues to the last residue of the sequence, but segment 55–72 is unreliable, as evidenced by thermal parameters as high as 100 $Å^2$. The enzyme in this crystal form is in the T-state (quaternary transition angle of 15°); however, unlike loop-disengaged AMP complexes of the wild-type enzyme, the dynamic loop in T-state Asp^{10} FBPase is disordered. The active site retains Fru-6-P and Mg^{2+} bound to site 1. Conditions of crystallization of the T-state and I_T-state AMP complexes of Asp^{10} FBPase differ only in the type of metal ion, Mg^{2+} for the former and Zn^{2+} for the latter. As anticipated, the Ile^{10}→Asp mutation has destabilized the disengaged conformation of the dynamic loop.

MD simulations of FBPases— Structures were stable over simulations of 15 ns as indicated by the time evolution of the energy function and root-mean-squared displacements in Cα atoms. Hydrogen and coordinate bonds involving protein residues and active-site ligands were stable. Although Asp^{68} and Arg^{276} remained bonded to the Mg^{2+} at site 3 and to P_i, respectively, the hydrogen bond between Asp^{68} and Arg^{276} observed in crystal structures was disrupted early in all simulations without noticeable secondary responses. Subunit-pair rotations for the R-, I_R-, I_T- and T-states averaged to 15, 19, 29 and 29 °, respectively, with standard deviations of approximately 1 ° and extremes of ±3 °. The average values remain close to the starting crystallographic angles (15.1, 18.2, 24.6 and 28.6 °, respectively) except for the I_T-state, which drifted toward the canonical T-state. Dynamic loops remained in engaged conformations during the R-state simulation; however, in the I_R- and I_T-state simulations, residues 59–70 and loop 264–274 of one subunit exhibited substantial transitory movements readily seen as high fluctuations (Fig. 4). Residues 59–70 (hairpin turn of the engaged loop) exit the active site as observed in first stage of loop displacement in targeted molecular dynamics (see next section).

PCA of residues 50–72 and 264–274 in each subunit of the R-, I_R- and I_T-state simulations reveal relatively simple motions for the first 10 eigenvectors representing collectively 50% of the total motion. Root-mean-squared inner products (RMSIP, 40) between the first 10 eigenvectors from each subunit exceed 0.5, indicating similar motions for all subunits in all states. Segments 59–72 and 264–274 have correlated and anti-correlated motions (Fig. 5). Correlated motions between these segments preserve contact distances, whereas anti-correlated motions periodically increase and decrease contact distances. Anti-correlated motions involving segments 59–72 and 264–274 cause significant steric clashes, which tend to force the dynamic loop out of its engaged conformation. Both correlated and anti-correlated motions have similar magnitudes in the R-, I_R- and I_T-states; however, in the T-state the amplitude decreases by 50% (Fig. 6A). In subunit C3 of the I_R-state and subunit C4 of the I_T-state, the amplitude of the anti-correlated motions exceeds that of the correlated motions (Fig. 6B). These are subunits in which engaged loops become transiently displaced from the active site during the simulation.

TMD simulation of the R- to T-state transition— R- and T-state FBPase define the extremes of TMD simulations with force constants (k) of 10, 100, 1000, 10000 kcal•mol^{-1}•Å^{-2} distributed over 20364 atoms. The highest force constant represents a force per atom substantially less than that of a hydrogen bond. The RMSD for k=10 kcal•mol^{-1}•Å^{-2} drops from 6.3 to 5.7 Å over the simulation largely due to an increase of 5 ° in the subunit-pair rotation (Fig. 7A). The dynamic loop, however, remains in place (RMSD declines from 7.4 to 7.0 Å). Force constants of 100 and 1000 kcal•mol^{-1}•Å^{-2} drive the subunit-pair rotation to completion, with final RMSD values of 3.5 and 1.2 Å, respectively. For k=100 kcal•mol^{-1}•Å^{-2}, residues 59–72 dissociate from the active site while residues 50–58 remain in the engaged conformation. For k=1000 kcal•mol^{-1}•Å^{-2}, the entire dynamic loop dissociates from the active site, and with a force constant of 10000 kcal•mol^{-1}•Å^{-2}), the structure goes to the T-state (final RMSD <0.5 Å). For the latter simulation, subunit-pairs first rotate through ~15 °, and then loops move out of their engaged conformation to the disengaged conformation.

Simulations with transition times from 200–2000 ps with k=10000 kcal•mol^{-1}•Å^{-2} are similar in appearance (Fig. 7B). The simulation with a transition time of 2000 ps (final RMSD 0.36 Å relative to T-state) reveals four stages: (i) subunit-pair rotation of ~15 °, dynamic loops remains engaged, (ii) hairpin turn of the dynamic loop (residues 59-72) exits the active site, (iii) residues 56 and 57 leave hydrophobic pockets of the engaged conformer followed by loss of helical conformation for residues 50–53, and (iv) residues 54–58 become coiled followed by a rapid acquisition of the disengaged conformation (Fig. 8).

Discussion

Studies here and elsewhere are consistent with the following sequence of events in the R- to T-state transition: two AMP molecules bind to the R-state, disrupting hydrogen bonds (Thr^{39} to Glu^{192}) across the C1–C4 interface (14). The disrupted hydrogen bonds reform after a sterically unhindered subunit-pair rotation of 12–14 °. Movements in structural elements across the C1–C2 interface (Fig. 2) attend the subunit-pair rotation, creating tight

contacts at the hinges and hairpin turns of engaged loops (Fig. 3). High-amplitude modes (Fig. 5&6) exacerbate these contacts, displacing loops from the active site. The displaced dynamic loop undergoes conformational change (Fig. 8), leading to the formation of a cluster of hydrophobic residues in the canonical T-state. The R- to T-state transition pathway from TMD simulation agrees well with observed crystals structures (Fig. 9), passing through the I_R- and I_T- states to the T-state before the engaged dynamic loop undergoes its transition to the disengaged conformation.

The reduction of space for the engaged loop comes by direct action of AMP moving helix H1 into residues 194–197 and indirectly through subunit-pair rotation. Loops 190 from subunits C1 and C4 are in contact, and subunit-pair rotation mutually pushes each loop toward the hinge of the dynamic loop. The entire dynamic loop translates toward loop 264–274, causing a conformational change in that loop. That change was noted previously in a comparison of R- and T-state structures, but dismissed as an artifact of different packing environments in crystal forms of FBPase (10). Crystals of the R-, I_R-, and I_T-states of FBPase, however, are nearly isomorphous with a maximum change of 5% in the *b* parameter of the unit cell. Hence, conformational changes in loop 264–274 are an integral part of the quaternary transition.

Molecular dynamics simulations indicate little steric hindrance in subunit-pair rotations at any point in the R- to T-state transition. During simulations of the R-, I_R-, I_T- and T-states, subunit-pair rotations wander over a range of 6°. Even with minimal force constants employed in targeted molecular dynamics, the change in the subunit-pair rotation proceeds smoothly (Fig. 7). As the binding of AMP to the R-state causes a loss of hydrogen bonds across the C1–C4 interface (14), AMP could facilitate subunit-pair rotation by weakening interactions between the C1-C4 interfaces.

The stepwise displacement of the loop from its engaged conformation in targeted molecular dynamics simulations has support from crystallography. Residues 59–72 (hairpin turn of the engaged loop) are the first to exit the engaged conformation in simulations, an event that requires the disruption of the coordinate bond between Asp^{68} and the metal at site 3. Residues 59–70 are disordered in a crystal structure at high ionic strength (19), consistent

with the partial dislocation of the dynamic loop. The second step of loop displacement is the release of Tyr^{57} from its hydrophobic pocket, after which the RMSD decays exponentially. In several crystal structures the entire loop is disordered (14, 18, 19, 23, 24). Such disorder could be due to inter-conversion between conformers as the loop relaxes toward its disengaged conformation. The final step is a formation of residues 54–58 into a short helix and the rapid acquisition of the disengaged conformation (crystallographic T-state).

As the catalytic loop remains engaged over 12–14 ° of subunit-pair rotation, the enzyme is likely active in quaternary states of intermediate rotation (such as the I_T-state). The observation (16) of potent but partial AMP inhibition of Asp^{10} FBPase is probably due to an active AMP-bound I_T-state, which accommodates the engaged dynamic loop, albeit with elevated steric stress. Other mutations of FBPase have resulted in partial inhibition at saturating levels of AMP (48, 50–51). For these, investigators have suggested an active T-state (52), but as demonstrated here by the AMP complex of Asp^{10} FBPase, the inability to form the disengaged conformation of the loop could leave the tetramer in an intermediate quaternary state. Leu^{54} FBPase may be an extreme case in which the AMP-bound enzyme remains in a near R-state.

High-amplitude modes are a characteristic in the functional transitions of other systems (39, 53-57). Such modes play roles in the extraction cycle of myosin (53), allosteric activation of epidermal growth factor receptor (56), substrate specificity of α-lytic protease (39) and substrate induced conformational changes (55, 55, 57). There are two perspectives regarding the coupling of motion to macromolecular function. Specific motions can facilitate ligand-induced conformational change, such as for the myosin motor (53). Alternatively, molecular motion can establish a pre-existing equilibrium of conformational states, some subset of which is recognized by the ligand (58). In the case of mammalian FBPase, the apo-enzyme could exist in a variety of quaternary states. But under physiological conditions (substrate and metals present), the enzyme favors the R-state, and AMP-inhibition is necessarily an induced process. AMP binds to the R-state as demonstrated by hybrid tetramers with a single functional AMP site (49) and by crystallographic investigations of

Leu^{54} FBPase (14). The role of dynamics then for mammalian FBPase comes in the displacement of the engaged dynamic loop and relaxation to the inactive state.

Table 1. Statistics of data collection and refinement for Asp[10] FBPase.

Crystalline complex[a]	R-state	I_T-state	T-state
Resolution limit (Å)	1.80	1.83	2.7
Number of measurements	784,010	707,677	380,196
Number of unique reflections	31,968	40,278	31,820
Completeness of data (%):			
Overall	93.7	94.7	93.1
Last shell/resolution-range (Å)	74.3/1.86-1.80	93.6/1.91-1.83	95.7/2.85-2.7
R_{sym}[b]			
Overall	0.062	0.055	0.167
Last shell/resolution-range (Å)	0.095/1.86-1.80	0.118/1.91-1.83	0.332/2.85-2.7
Number of reflections in refinement	30,433	32,827	18,448
Number of atoms	2,672	2,736	5,307
Number of solvent sites	179	186	201
R_{factor}[c]	0.226	0.214	0.198
R_{free}[d]	0.25	0.243	0.284
Mean B ($Å^2$) overall/protein	23/22	25/24	40/40
Mean B ($Å^2$) for AMP	-	36	37/31
Root mean square deviations (deg):			
Bond lengths (Å)	0.005	0.005	0.006
Bond angles	1.4	1.3	1.3
Dihedral angles	22.9	22.7	23.1
Improper angles	0.76	0.76	0.77

[a] Unit cell lengths (a, b, c) in Å for the R-, I_T- and T-state complexes are (52.94, 82.50, 164.96), (55.84, 82.50, 165.02), and (60.28, 167.00, 79.06), respectively. Unit cell angles (α, β, γ) are 90° for space groups *I222* and $P2_12_12$.

[b] $R_{sym} = \Sigma_j\Sigma_i \mid I_{ij} - \langle I_j \rangle \mid / \Sigma_i\Sigma_j I_{ij}$, where i runs over multiple observations of the same intensity, and j runs over all crystallographically unique intensities.

[c] $R_{factor} = \Sigma \parallel F_{obs} \mid - \mid F_{calc} \parallel / \Sigma \mid F_{obs} \mid$, where $\mid F_{obs} \mid > 0$.

[d] R_{free} based upon 10% of the data randomly culled and not used in the refinement.

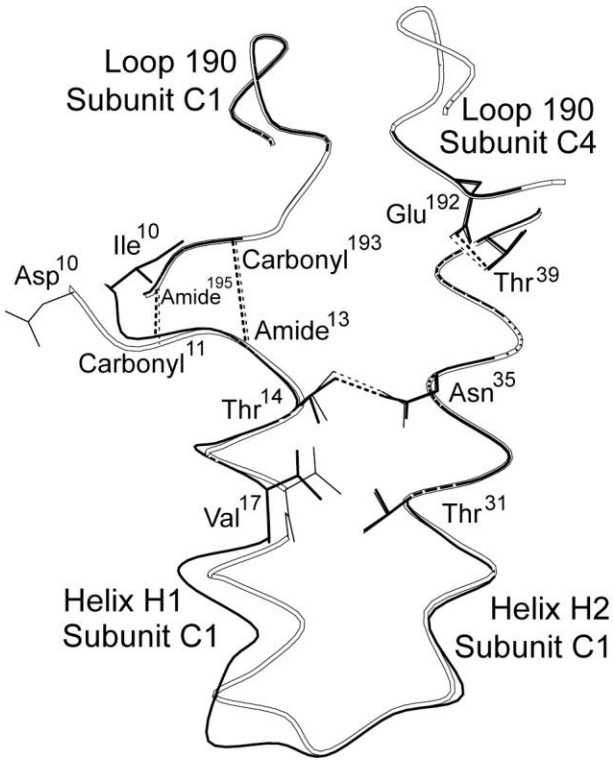

Figure 1. Conformational changes in the R-state structure of Asp[10] FBPase. The side chain of Asp[10] projects into the solvent, away from the hydrophobic surface against which Ile[10] packs in the wild-type enzyme. Conformational differences are limited to those shown (helix H1 and the connecting element between helices H1 and H2). Black lines represent the R-state of the wild-type enzyme (RCSB 1CNQ) and open lines represent R-state Asp[10] FBPase. This drawing was prepared with MOLSCIRPT (59).

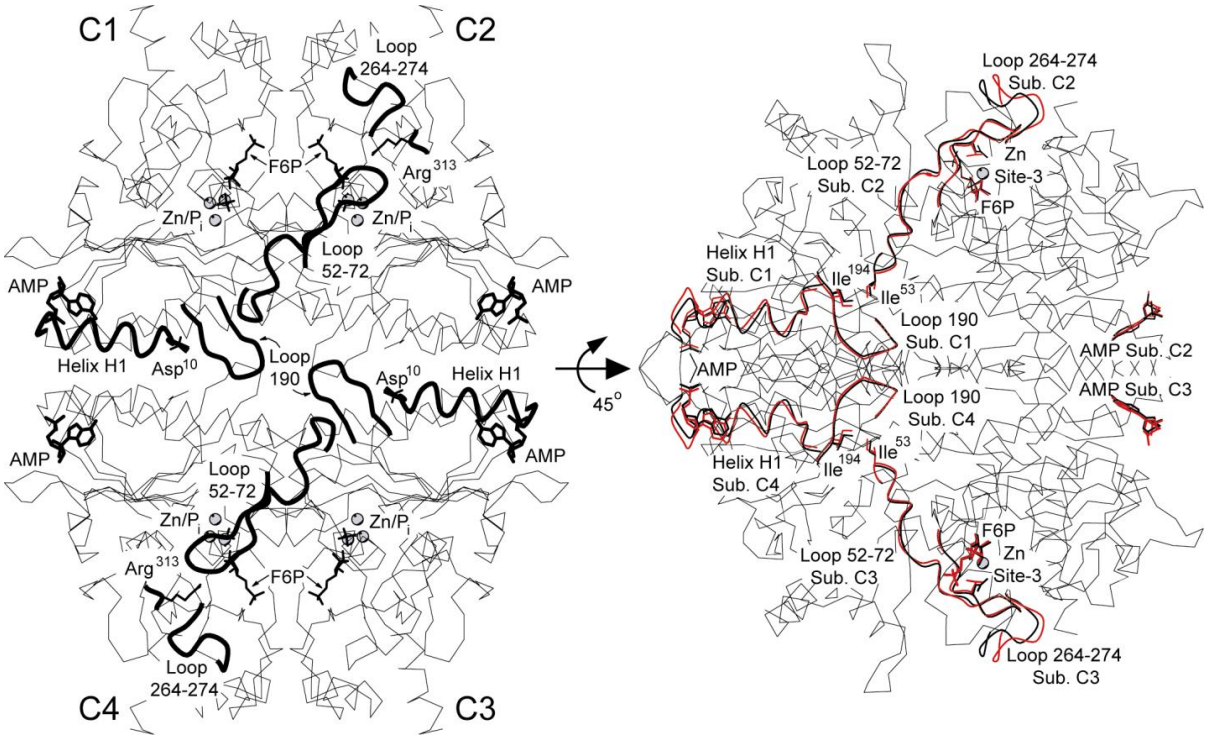

Figure 2. AMP/product complex of Asp^{10} FBPase. Overview of the complex (left). Subunits of the tetramer, labeled C1 through C4, have each one molecule of bound AMP, Fru-6-P (labeled F6P) and P_i, and three atoms of Zn^{2+}. Side chains of Asp^{10} from subunits C1 and C3 are omitted for clarity. Residues 10–25 (helix H1, subunits C1 and C3), 187–195 (loop 190, subunits C1 and C3), 50–72 (dynamic loop, subunits C2 and C4), and 264–274 (subunits C2 and C4) are in bold lines. Rotation of the tetramer by 45 ° about the horizontal twofold axis (right). I_R-state subunits from Leu^{54} FBPase (red lines) are superimposed on the subunits of the I_T-state Asp^{10} tetramer (black lines). Shown only are Cα-atoms of the I_R subunit that deviate from those of the I_T structure by more than 0.5 Å. This drawing was prepared with MOLSCIRPT (59).

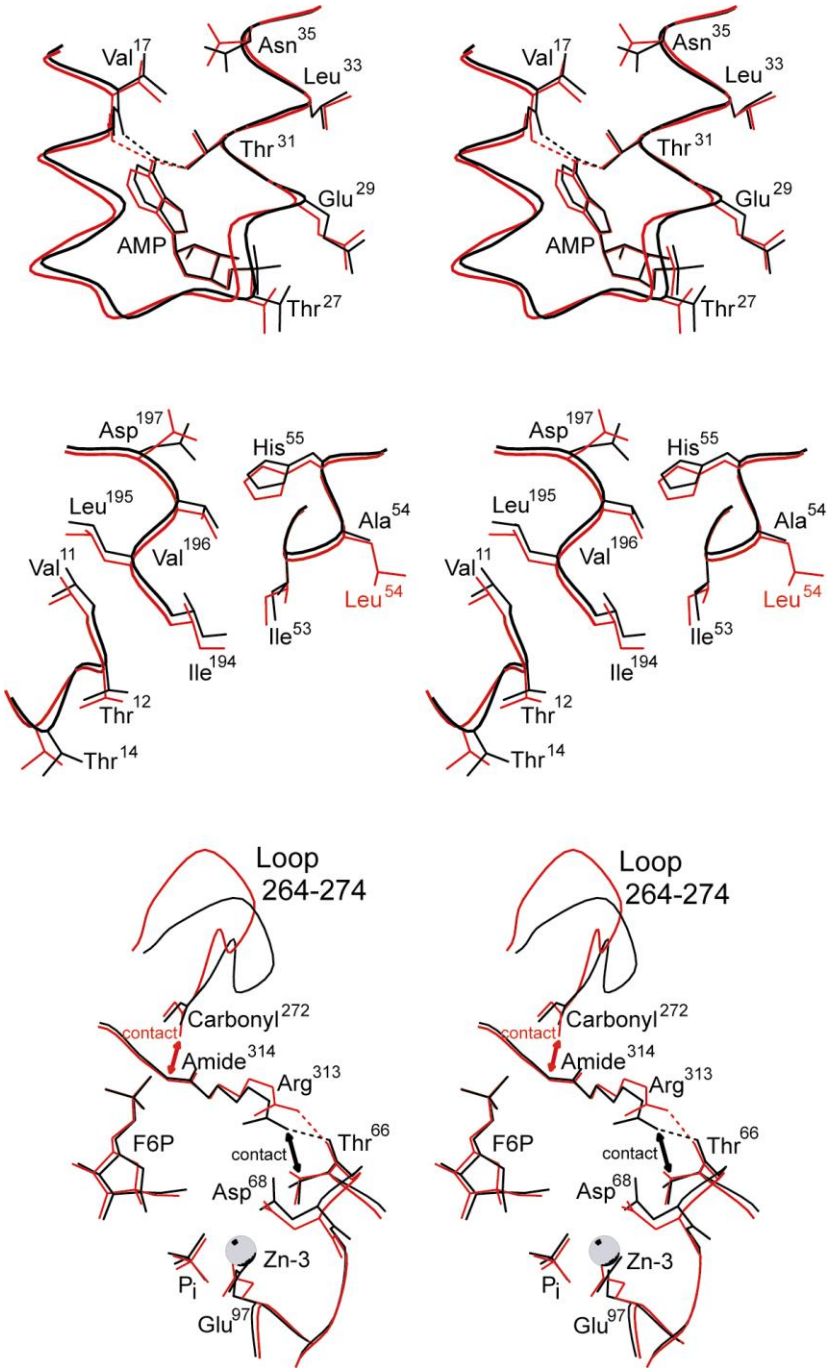

Figure 3. Stereoviews of tertiary conformational changes between the I_R- and I_T-states. Dotted lines represent selected donor-acceptor interactions of 3.2 Å or less. Double-headed arrows represent tight contacts less than 3 Å. Superposition of the I_R-state subunit from the AMP complex of Leu^{54} FBPase (red) onto each subunit of the AMP complex of Asp^{10} FBPase (black) reveals conformational change induced by a 9 ° subunit-pair rotation. Conformational changes at the AMP binding site (top), conformational changes from helix H1 to loop 190 and then across a subunit interface to hinge residues of the dynamic loop (middle), and conformational changes in the hairpin turn of the dynamic loop, loop 264–274 and Arg^{313} (bottom) are shown. This drawing was prepared with MOLSCIRPT (59).

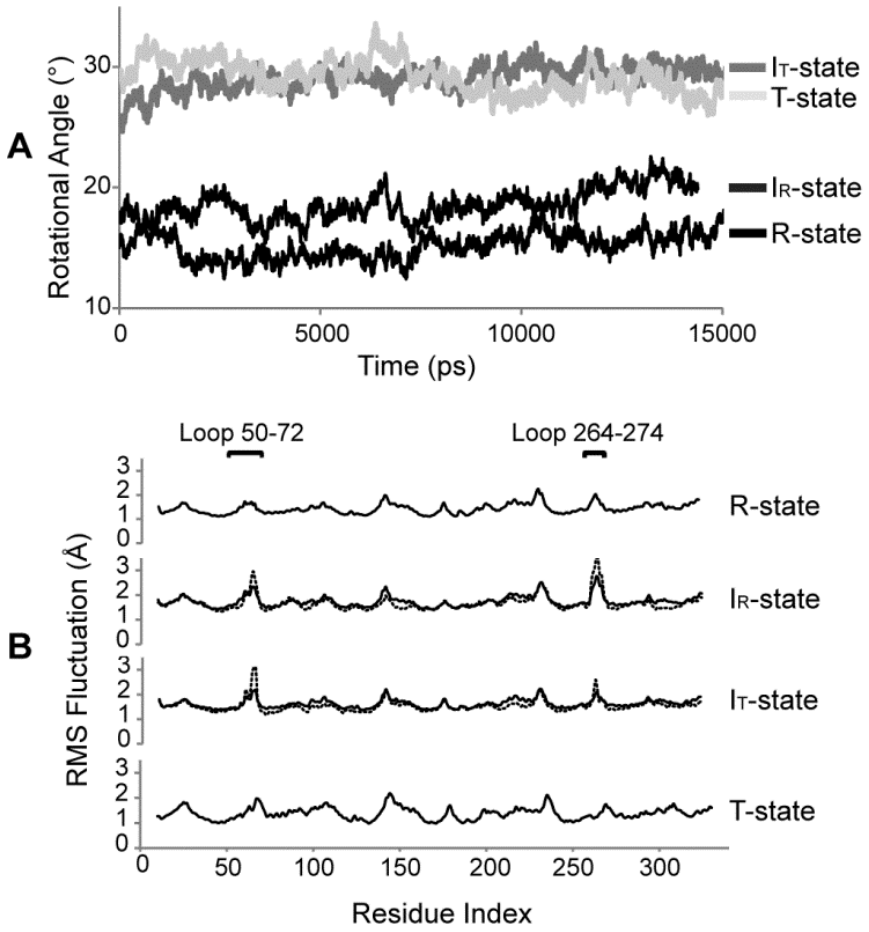

Figure 4. Molecular dynamic simulations of FBPase. Time evolution of subunit-pair rotation angles (panel A) and root-mean-square (RMS) fluctuation as a function of residue index (panel B) from 15 ns simulations of the R-, I_R-, I_T- and T-state of FBPase. Solid lines in panel B represent fluctuations averaged over all four subunits, whereas dashed curves for the I_R- and I_T-states are RMS fluctuations for subunits C3 and C4, respectively.

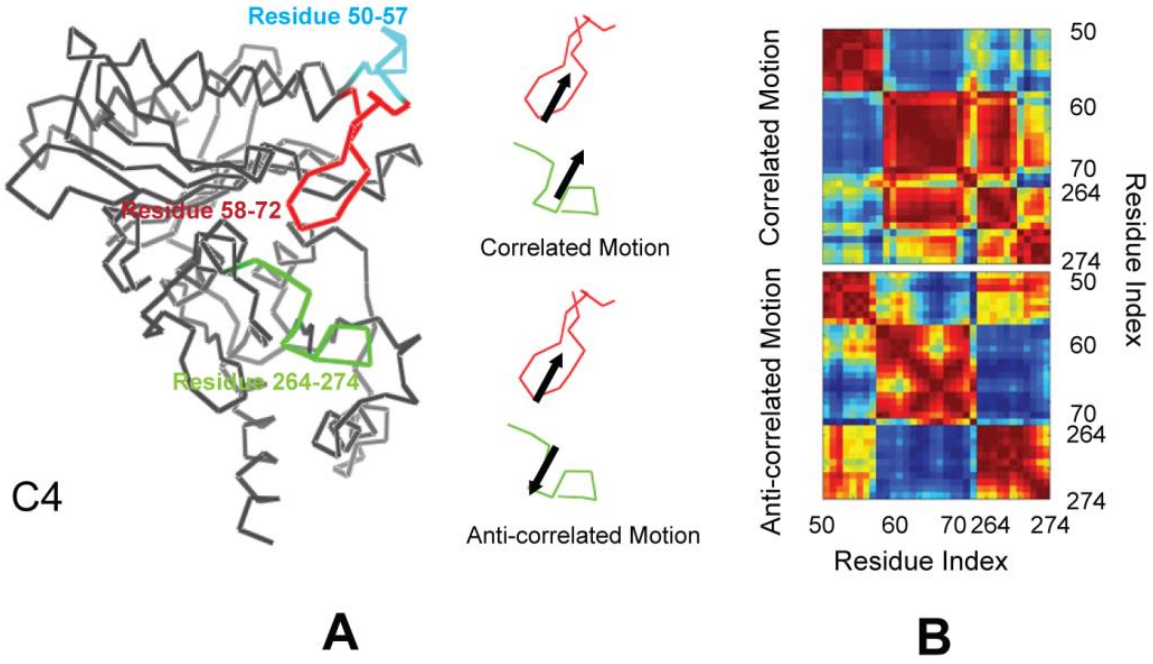

Figure 5. PCA analysis of the dynamic loop. A. Locations of segments 68-72 (red) and 264-274 (green) in the tertiary structure of the subunit along with correlated and anti-correlated motions of each segment shown by arrows. Images are prepared with PYMOL (60). B. Examples of high-amplitude correlated (upper) anti-correlated (lower) modes from PCA analysis. Blue off-diagonal elements represent strong anti-correlated motions between pairs of residues, whereas red off-diagonal elements represent correlated motions.

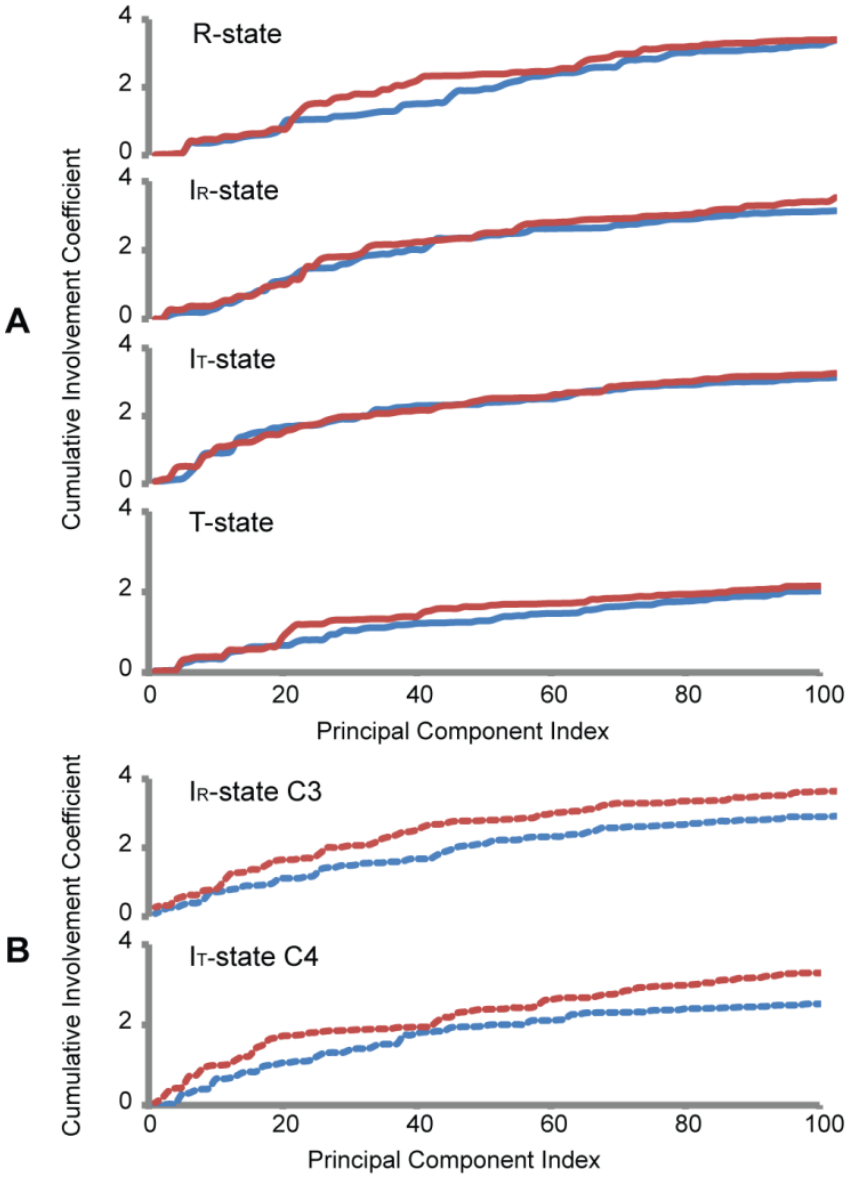

Figure 6. Cumulative involvement coefficients of anti-correlated and correlated motions. Cumulative involvement coefficients of R-, I_R-, I_T- and T-state of FBPase were plotted against the principal component index (A). Red lines indicate correlated motions between loop 58-72 and loop 264-274 and blue lines indicate the anti-correlated motions. The cumulative involvement coefficients of subunit C3 in the I_R-state and subunit C4 in I_T-state are drawn in dotted lines (B). In instances of loop displacement, the anti-correlated motions dominate the correlated motions.

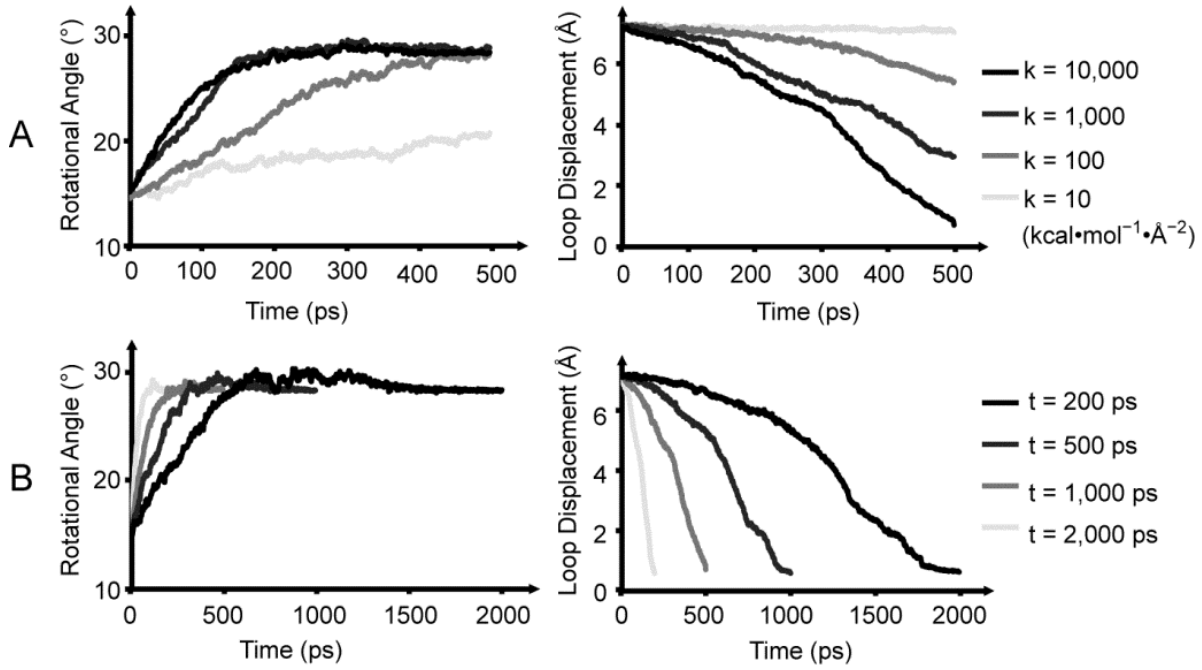

Figure 7. TMD simulation of the R- to T-state transition. A. TMD simulations with different force constants. Lines go from light grey to black with increasing force constant corresponding to k = 10, 100, 1000 and 10000 kcal/mol/Å^2. B. TMD simulations with different time steps (light grey, 200 ps; grey, 500 ps; dark grey, 1000 ps; black, 2000 ps). Panels on the left in A and B show subunit-pair rotation angle versus simulation time. Those on the right show RMSD change for residues of the dynamic loops versus simulation time.

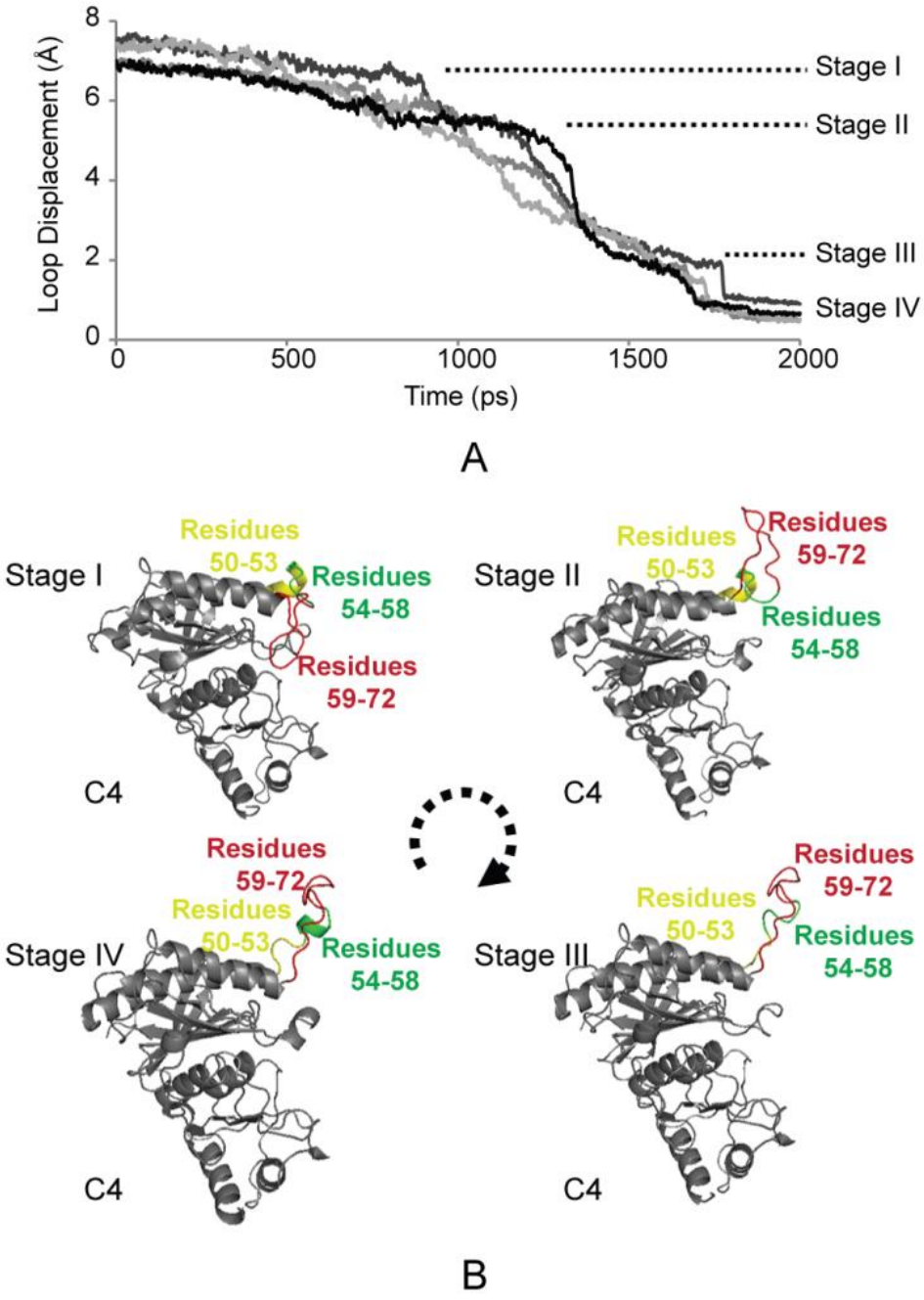

Figure 8. Displacement of the dynamic loop. A. TMD simulation (2000 ps) with force constant *k*=10000 kcal/mol/Å^2 reveals distinct steps in loop displacement (Stages I-IV). Each curve tracks the RMSD of the loop for each subunit of the tetramer. B. Illustration of the dynamic loop at the onset of each stage. This illustration was prepared with PYMOL (60).

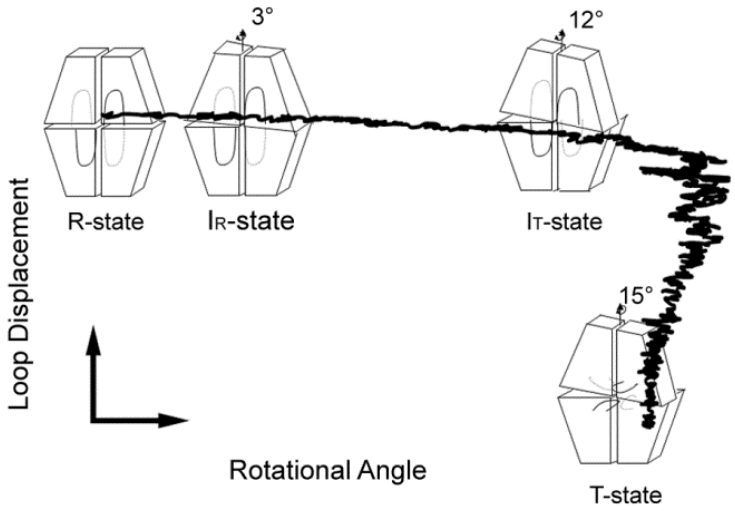

Figure 9. R- to T-state transition from TMD simulation. The TMD trajectories of the R- to T- transition are projected onto a two dimensional plane determined by the loop displacement (y-axis) and subunit-pair rotation angle (x-axis). Data points provided by crystal structures are represented by tetramer icons. The simulation indicates subunit-pair rotation beyond 15 ° followed by loop displacement and relaxation to the canonical T-state.

Reference

1. Benkovic, S. T., and de Maine, M. M. (1982) Mechanism of action of fructose 1,6-bisphosphatase. Adv. Enzymol. Relat. Areas Mol. Biol. 53, 45-82

2. Tejwani, G. A. (1983) Regulation of fructose-bisphosphatase activity. Adv. Enzymol. Relat. Areas Mol. Biol. 54, 121-194

3. Van Schaftingen, E. (1987) Fructose 2,6-bisphosphate. Adv. Enzymol. Relat. Areas Mol Biol. 59, 45-82

4. Pilkis, S. J., El-Maghrabi, M. R., and Claus, T. H. (1988) Hormonal regulation of hepatic gluconeogenesis and glycolysis. Ann. Rev. Biochem. 57, 755-783

5. Okar, D. A., and Lange, A. J. (1999)Fructose-2,6-bisphosphate and control of carbohydrate metabolism in eukaryotes. Biofactors 10, 1-14

6. Pilkis, S. J., El-Maghrabi, R. M, McGrane, M. M., Pilkis, J., and Claus, T. H. (1981) Inhibition of fructose-1,6-bisphosphatase by fructose 2,6-bisphosphate. J. Biol. Chem. 256, 3619-3622

7. Liu, F., and Fromm, H. J. (1991) 31P nuclear magnetic resonance spectroscopy studies of substrat and product binding to fructose-1,6-bisphosphatase. J. Biol. Chem. 266, 11774-11778

8. Liu, F., and Fromm, H. J. (1988) Interaction of fructose 2,6-bisphosphate and AMP with fructose-1,6-bisphosphatase as studied by nuclear magnetic resonance spectroscopy. J. Biol. Chem. 263, 9122-9128

9. Scheffler, J. E., and Fromm, H. J. (1986) Regulation of rabbit liver fructose-1,6-bisphosphatase by metals, nucleotides, and fructose 2,6-bisphosphate as determined from fluorescence studies. Biochemistry 25, 6659-6665

10. Choe J-Y., Poland B. W., Fromm H. J., and Honzatko R. B. (1998) Role of a dynamic loop in cation activation and allosteric regulation of recombinant porcine fructose-1,6-bisphosphatase. Biochemistry 33, 11441-11450

11. Stone, S. R., and Fromm, H. J. (1980) Studies on the mechanism of adenosine 5'-monophosphate inhibition of bovine liver fructose 1,6-bisphosphatase. Biochemistry 19, 620-625

12. Ke, H., Zhang, Y. Liang, J-Y., and Lipscomb, W. N. (1991)Crystal structure of the neutral form of fructose-1,6-bisphosphatase complexed with the product fructose 6-phosphate at 2.1-Å resolution. Proc. Natl. Acad. Sci. U.S.A. 88, 2989-2993

13. Zhang, Y., Liang, J-Y., Huang, S., and Lipscomb, W. M. (1994) Toward a mechanism for the allosteric transition of pig kidney fructose-1,6-bisphosphatase. J. Mol. Biol. 244, 609-624

14. Iancu, C. V., Mukund, S., Fromm, H. J., and Honzatko, R. B. (2005) R-state AMP complex reveals initial steps of the quaternary transition of fructose-1,6-bisphosphatase. J. Biol. Chem. 280, 19737–19745

15. Choe, J-Y., Nelson, S. W, Arienti, K. L., Axe, F. U., Collins, T. L., Jones, T. K., Kimmich, R. D. A., Newman, M. J., Norvell, K., Ripka, W. C., Romano, S. J., Short, K. M., Slee, D. H., Fromm, H. J., and Honzatko, R. B. (2003) Inhibition of fructose-1,6-bisphosphatase by a new class of allosteric effectors. J. Biol. Chem. 278, 51175-51183

16. Nelson, S. W., Kurbanov, F., Honzatko, R. B. and Fromm, H, J. (2001) The N-terminal segment of recombinant porcine fructose-1,6-bisphosphatase participates in the allosteric regulation of catalysis. J. Biol. Chem. 276, 6119-6124

17. Xue, Y., Huang, S., Liang, J-Y. Zhang, Y., and Lipscomb, W. N. (1994) Crystal structure of fructose-1,6-bisphosphatase complexed with fructose 2,6-bisphosphate, AMP, and Zn2+ at 2.0-Å resolution: aspects of synergism between inhibitors. Proc. Natl. Acad. Sci. USA 91, 12482-12486

18. Choe, J-Y., Fromm, H. J., and Honzatko, R. B. (2000) Crystal structures of fructose 1,6-bisphosphatase: mechanism of catalysis and allosteric inhibition revealed in product complexes. Biochemistry 39, 8565-8574

19. Choe, J-Y., Nelson, S. W., Fromm, H. J., and Honzatko, R. B. (2003) Interaction of Tl+ with product complexes of fructose-1,6-bisphosphatase. J. Biol. Chem. 278, 16008-16014

20. Choe, J-Y., Iancu, C. V., Fromm, H. J., and Honzatko, R. B. (2003) Metaphosphate in the active site of fructose-1,6-bisphosphatase. J. Biol. Chem. 278, 16015-16020

21. Nelson, S. W., Choe, J-Y., Iancu, C. V., Honzatko, R. B., and Fromm, H. J. (2000) Tryptophan fluorescence reveals the conformational state of a dynamic loop in recombinant porcine fructose-1,6-bisphosphatase. Biochemistry. 39, 11100-11106

22. Wen, J., Nelson, S. W., Honzatko, R. B., Fromm, H. J., and Petrich, J. W. (2001) Environment of tryptophan 57 in porcine fructose-1,6-bisphosphatase studied by time-resolved flurescence and site-directed mutagenesis. Photochem. Photobiol. 74, 679-685

23. Ke, H. M., Thorpe, C. M., Seaton, B., Lipscomb, W. N., and Marcus F. (1990) Structure refinement of fructose-1,6-bisphosphatase and its fructose 2,6-bisphosphate complex at 2.8 Å resolution. J. Mol. Biol. 212, 513-539

24. Lu, G., Stec, B., Giroux, E. L., Kantrowitz, E. R. (1996) Evidence for an active T-state pig kidney fructose 1,6-bisphosphatase: interface residue Lys-42 is important for allosteric inhibition and AMP cooperativity. Protein Science 5, 2333-2342

25. Laemmli, U. K. (1970) Cleavage of structural proteins during the assembly of the head of bacteriophage T4. Nature 227, 680-685

26. Bradford, M. M. (1976) A rapid and sensitive method for the quantitation of microgram quantities of protein utilizing the principle of protein-dye binding. Anal. Biochem. 72, 248-252

27. Otwinoski, Z., and Minor, W. (1997) Processing of X-ray diffraction data collected in oscillation mode. Methods Enzymol. 276, 307-326

28. McRee, D. E. (1992) A visual protein crystallographic software system for X11/Xview. J. Mol. Graph. 10, 44-46

29. Brünger, A. T., Adams, P. D., Clore, G. M., DeLano, W. L., Gros, P., Grosse-Kunstleve, R. W., Jiang, J.-S., Kuszewski, J., Nilges, M., Pannu, M. S., Read, R. J., Rice, L. M., Simonson, T., Warren, G. L. (1998) Crystallography & NMR system: a new software suite for macromolecular structure determination. Acta Crystallogr. D 54, 905-921

30. Engh, R. A., and Huber, R. (1991) Accurate bond and angle parameters for X-ray protein structure refinement. Acta Crystallog. A 47, 392-400

31. Laskowski, R. A., Mac Arthur, M. W., Moss, D. S., and Thornton, J. M. (1993) PROCHECK: a program to check the stereochemical quality of protein structures. J. Appl. Crystallogr. 26, 283-291

32. Hines, J. K., Kruesel, C. E., Fromm, H. J., and Honzatko, R. B. (2007) Structure of inhibited fructose-1,6-bisphosphatase from Escherichia coli: distinct allosteric inhibition sites for AMP and glucose 6-phosphate and the characterization of a gluconeogenic switch. J. Biol. Chem. 282, 24697-24706

33. Phillips, J. C., Braun, R., Wang, W., Gumbart, J., Tajkhorshid, E., Villa, E., Chipot, C., Skeel, R. D., Kale, L., Schulten, K. (2005) Scalable molecular dynamics with NAMD J. Comput. Chem. 26, 1781-1802

34. Jr. MacKerell, A. D., Banavali, N., Foloppe, N. (2001) Development and current status of the CHARMM force field for nucleic acids. Biopolymers. 56, 257-265

35. Jorgensen, W. L., Chandrasekhar, J., Madura, J. D., Impey, R. W. and Klein, M. L. (1983) Comparison of simple potential functions for simulating liquid water. J. Chem. Phys. 79, 926-935

36. Essmann, U., Perera, L., Berkowitz, M. L., Darden, T., Lee, H., Pedersen, L. G. (1995) A smooth particle mesh Ewald method. J. Chem. Phys. 103, 8577-8593

37. Humphrey, W., Dalke, A. and Schulten, K. J. (1996) VMD – Visual Molecular Dynamics. Molec. Graphics. 14.1, 33-38

38. Tournier, A. L., and Smith, J. C. (2003) Principal components of the protein dynamical transition. Phys, Rev. Lett. 91, 208106-4

39. Ota, N. and Agard, D. A. (2001) Enzyme specificity under dynamic control II: principal component analysis of alpha-lytic protease using global and local solvent boundary conditions. Protein Sci. 10, 1403-1414

40. Amadei, A., Ceruso, M. A. and Nola, A. D. (1999) On the convergence of the conformational coordinates basis set obtained by the essential dynamics analysis of protein's molecular dynamics simulations. Proteins 36, 419-424

41. Schlitter, J., Engels, M., Kruger, P., Jacoby, E. and Wollmer, A. (1993) Targeted molecular dynamics simulation of conformational change – application to the T to R-transition in insulin. Mol. Sim. 10, 291-308

42. Ma, J. and Karplus, M. (1997) The structural basis for the transition from Ras-GTP to Ras-GDP. Proc. Natl. Acad. Sci. USA. 94, 11905-11910

43. Ma, J., Sigler, P. B., Xu, Z. and Karplus, M. (2000) A dynamic model for the allosteric mechanism of GroEL. J. Mol. Biol. 302, 303-313

44. Kong, Y., Shen, Y., Warth, T. E. and Ma, J. (2002) Conformational pathways in the gating of Escherichia coli mechanosensitive channel. Proc. Natl. Acad. Sci. USA. 99, 5999-6004

45. Zhang, J., Li, C., Chen, K., Zhu, W., Shen, X. and Jiang, H. (2006) Conformational transition pathway in the allosteric process of human glucokinase. Proc. Natl. Acad. Sci. USA. 103, 13368-13373

46. Shyur, L.-F., Aleshin, A. E., Honzatko, R. B. and Fromm, H. J. (1996) Site-directed mutagenesis of residues at subunit interfaces of porcine fructose-1,6-bisphosphatase. J. Biol. Chem. 271, 3005-3010

47. Shyur, L.-F., Aleshin, A. E., Honzatko, R. B. and Fromm, H. J. (1996) Biochemical properties of mutant and wild-type fructose-1,6-bisphosphatases are consistent with the coupling of intra- and intersubunit conformational changes in the T- and R-state transition. J. Biol. Chem. 271, 33301-33307

48. Lu, G., Giroux, E. L. and Kantrowitz, E. R. (1997) Importance of the dimer-dimer interface for allosteric signal transduction and AMP cooperativity of pig kidney fructose-1,6-bisphosphatase. Site-specific mutagenesis studies of Glu-192 and Asp-187 residues on the 190's loop. J. Biol. Chem. 297, 5076-5087

49. Nelson, S. W, Honzatko, R. B., and Fromm, H. J. (2002) Hybrid tetramers of porcine liver fructose-1,6-bisphosphatase reveal multiple pathways of allosteric inhibition. J. Biol. Chem. 277, 15539-15545

50. Cárcamo, J. G., Yañez, A. J., Ludwig, H. C., León, O., Pinto, R. O., Reyes, A. M., and Slebe, J. C. (2000) The C1-C2 interface residue lysine 50 of pig kidney fructose-1,6-bisphosphatase has a crucial role in the cooperative signal transmission of the AMP inhibition. Eur. J. Biochem. 267, 2242-2251

51. Nelson, S. W., Choe, J. Y., Iancu, C. V., Honzatko, R. B., and Fromm, H. J. (2000) Mutations in the hinge of a dynamic loop broadly influence functional properties of fructose-1,6-bisphosphatase. J. Biol. Chem. 275, 29986-29992

52. Lu, G., Stec, B., Giroux, E. L., and Kantrowitz, E. R. (1996) Evidence for an active T-state pig kidney fructose 1,6-bisphosphatase: interface residue Lys-42 is important for allosteric inhibition and AMP cooperativity. Protein Sci. 5, 2333-2342

53. Mesentean, S., Koppole, S., Smith, J. C., and Fischer S. (2007) The principal motions involved in the coupling mechanism of the recovery stroke of the myosin motor. J. Mol. Biol. 367, 591-602

54. Kitao, A., and Loeffler, H. H. (2009) Collective dynamics of periplasmic glutamine binding protein upon domain closure. Biophysical J. 97, 2541-2549

55. Cardone, A., Hassan, S. A., Albers, R. W., Sriram R. D., and Pant H. C. (2010) Structural and dynamic determinants of ligand binding and regulation of cyclin-dependent kinase 5 by pathological activator p25 and inhibitory peptide CIP. J. Mol. Biol. 401, 478-492

56. Mustafa, M., Mirza, A., and Kannan, N. (2011) Conformational regulation of the EGFR kinase core by the juxtamembrane and C-terminal tail: a molecular dynamics study. Proteins 79, 99-114

57. Fujiwara, S., and Amisaki T. (2006) Molecular dynamics study of conformational changes in human serum albumin by binding of fatty acids. Proteins 64, 730-739

58. Grant, B. J., McCammon, J. A., and Gorfe, A. A. (2010) Conformational selection in G-proteins: lessons from Ras and Rho. Biophys. J. 99, L87-89

59. Kraulis, P. J. (1991) MOLSCIPT: a program to produce both detailed and schematic plots of protein structures. J. Appl. Cryst. 24, 946-950

60. The PyMOL Molecular Graphics System, Version 1.5.0.4 Schrödinger, LLC.

CHAPTER III. WATER MOLECULES IN THE CENTRAL CAVITY OF MAMMALIAN FRUCTOSE-1,6-BISPHOSPHATASE AS A DETERMINANT OF THE QUATERNARY STATE

A paper to be submitted to *Biochemistry*

Yang Gao, Nathaniel D. Ginder and Richard B. Honzatko

Roy J. Carver Department of Biochemistry, Biophysics, and Molecular Biology,

Iowa State University, Ames, IA 50011

Abstract

AMP transforms porcine fructose-1,6-bisphosphatase (FBPase) from an active R- to an inactive T-state. Intermediate quaternary states (I_R, I_T and T_F) lie on the transition pathway between the R- and T-state extremes, as revealed by crystal structures. As many as 48 ordered water molecules occupy the cavity at the center of the FBPase tetramer, and in the I_R-state, water molecules define ordered clathrate-like structures. Molecular dynamics simulations here of FBPase tetramers in R-, T- and intermediate quaternary states reveal water structures in the central cavity comparable to those observed in crystal structures. The water structure has optimal stability in the cavities of intermediate quaternary states, and is a single stable cluster in the I_R-state. In order to determine whether water molecules of the central cavity influence functional properties and the quaternary state, aqueous/organic solvents were employed in kinetics and crystallization experiments. In the presence of 1,2-ethanediol, 1,2-propanediol, glycerol, xylitol, or sorbitol, Asp^{10} FBPase became progressively more active in the presence of saturating levels of AMP. Under the same solvent conditions, crystal structures of Leu^{54} FBPase exhibited decreasing amounts of subunit-pair rotation relative to the R-state. These results establish a correlation between AMP inhibition and the quaternary state of FBPase, and moreover implicate solvent organization in the central cavity as a determinant of FBPase function and conformation.

Introduction

Fructose-1,6-bisphosphate (D-fructose-1,6-bisphosphate 1-phosphohydrolase; EC 3. 1. 3; FBPase[1]) catalyzes a regulated step in gluconeogenesis, the degradation of fructose 1,6-bisphosphate (Fru-1,6-P_2) to fructose 6-phosphate (Fru-6-P) and phosphate (P_i) (1, 2). Divalent cations (Mg^{2+}, Mn^{2+}, or Zn^{2+}) are essential for phosphatase activity. Fructose 2,6-bisphosphate (Fru-2,6-P_2) and AMP are physiological inhibitors of eukaryotic FBPases. The same effectors activate fructose-6-phosphate-1-kinase (the counterpart of FBPase in glycolysis) in the phosphorylation of Fru-6-P by ATP (3-8). Fru-2,6-P_2 binds to the active site of FBPase, competing with Fru-1,6-P_2 (4, 5). AMP is a non-competitive inhibitor with respect to substrate, and inhibits FBPase with positive cooperativity (3). Fru-2,6-P_2 enhances AMP inhibition in eukaryotic FBPases, a phenomenon called AMP/Fru-2,6-P_2 synergism (4,5). The concentration of AMP *in vivo* is relatively constant while that of Fru-2,6-P_2 is dynamic and under hormone control (9,10). Given the important regulatory role of FBPase in glucose metabolism, FBPase is a drug target for the treatment of type II diabetes (11-18). Understanding regulatory mechanisms of FBPase should facilitate the rational design of drugs.

FBPase has been a subject of extensive structural studies (19-26). Porcine FBPase, taken as a model for eukaryotic FBPases, is a homotetramer of 37 kDa subunits in a near square-planar arrangement. Complexes of enzyme with products (Fru-6-P and P_i) and three divalent cations define the active R-state (20, 22). In several complexes, the metal ion at site 1 coordinates to the 1-OH group of Fru-6-P, whereas metals at sites 2 and 3 coordinate P_i and a loop (loop 50-72) essential for catalysis. Such R-state complexes define the engaged conformation of loop 50-72 (22). AMP binds to sites at least 30 Å from the nearest active site and transforms the tetramer into an inactive T-state (19, 23).

T-state FBPase differs from the R-state by a 15 ° subunit-pair rotation and a disengaged conformation for loop 50-72 (23). Competitive inhibition of AMP with respect to Mg^{2+} in kinetics is consistent with the absence of metals at sites 2 and 3 in AMP/product complexes (23). Fru-2,6-P_2 is a competitive inhibitor with respect to Fru-1,6-P_2 (4, 5), and binds at the active site in crystallographic complexes causing a subunit-pair rotation (13 °)

similar to that caused by AMP (24). Moreover, loop 50-72 is in its disengaged conformation in Fru-2,6-P_2 complexes of porcine FBPase, which is defined here as the T_F-state. The similar end-states induced by AMP and Fru-2,6-P_2 is the likely basis of AMP/Fru-2,6-P_2 synergism (24).

Intermediate states have been trapped by crystallizing mutant FBPases (Ala^{54}→Leu or Ile^{10}→Asp) that destabilize the disengaged conformation of loop 50-72 under conditions that favor the canonical T-state (25, 26). Asp^{10} FBPase is subject to biphasic inhibition by AMP. AMP causes maximal partial inhibition up to concentrations of 100 μM, but no additional inhibition until concentrations exceed 1 mM (27). Biphasic inhibition indicates the presence of an intermediate quaternary state, and consistent with this hypothesis, the AMP complex of Asp^{10} FBPase is in a T-like quaternary state (I_T, 12 ° subunit-pair rotation, engaged loop 50-72). In contrast, Leu^{54} FBPase is relatively insensitive to AMP inhibition, and its AMP complexes define an R-like state (I_R, 3 ° subunit-pair rotation, engaged loop 50-72). The tertiary conformations and quaternary states together define a transition pathway from R- to T-state, in which subunit-pair rotation precedes displacement of loop 50-72 (26).

In all conformers of porcine FBPase there exists a water-filled cavity at the center of the tetramer. The protein surface of the central cavity is largely hydrophobic. The Type I FBPase from *Escherichia coli* has a 41% sequence identity to porcine FBPase; however, the regulatory mechanism of *E coli* FBPase is distinct from its mammalian counterparts (28, 29), lacking AMP coopertivity and AMP/Fru-2,6-P_2 synergism (24, 28). Hydrophilic side chains fill the central cavity in *E coli* FBPase. Many examples are in the literature of essential roles for buried waters molecules in protein folding, stability, flexibility, catalysis and ligand binding (30-34); however, a role for water molecules in the central cavity of mammalian FBPase is undetermined.

Presented here is an analysis of the stability of water molecules in the central cavity of porcine FBPase and the potential structural and functional roles of such water molecules. Molecular dynamics (MD) simulations reveal sites of water localization and stability that are in agreement with crystallographic investigations. Water stability is greatest in intermediate quaternary states with the dynamic loops in the engaged conformation, suggesting that the

formation of highly-ordered water structures in the central cavity may be linked to the quaternary state of FBPase. Different aqueous/organic solvents were introduced to FBPase kinetics and crystallization experiments in order to modulate the structure of water in the central cavity. The activity of FBPase in the presence of saturating AMP varies with the solvent system as does the quaternary state of FBPase crystallized from the same solvent system. The level of inhibition by saturating AMP correlates well with the quaternary state observed in crystal structures, suggesting that changes in water structure within the central cavity could influence FBPase conformation and function.

Experimental procedures

Materials— Fru-1,6-P_2, NADP, AMP, 1,2-ethandiol (ED), 1,2-propanediol (PD), xylitol and sorbitol were purchased from Sigma. Glucose-6-phophate dehydrogenase and phosphoglucose isomerase were from Roche Applied Sciences. FBPase-deficient *E. coli* strain DF 657 came from the Genetic Stock Center at Yale University. Other chemicals were of reagent grade or equivalent.

Expression and purification of FBPase— Asp^{10} and Leu^{54} mutations were the results of previous work (25, 27). DNA sequencing done by Iowa State University sequencing facility, using the fluorescent dye-dideoxy terminator method, confirmed the constructs. *E. coli* DF 657 was used for the expression of FBPase. After cell breakage and centrifugation, the supernatant was loaded onto a Cibracon Blue-Sepharose column equilibrated with 5 mM MgCl and 20 mM Tris-HCl, pH 7.5. Enzyme was eluted with 5 mM AMP and 20 mM Tris-HCl, pH 7.5. The eluted protein sample was then loaded onto a DEAE-Sepharose column equilibrated with 20 mM Tris-HCl, pH 8.3. Purified enzyme was eluted with a NaCl gradient (0–0.5 M) in 20 mM Tris-HCl, pH 8.3. Enzyme was subjected to extensive dialysis against 50 mM Hepes, pH 7.5, before kinetics or crystallization experiments. Purity and protein concentrations of FBPase were confirmed by SDS-polyacrylamide gel electrophoresis (35) and the Bradford assay (36), respectively.

Kinetics— AMP inhibition assays employed the coupling enzymes, phosphoglucose isomerase, and glucose-6-phosphate dehydrogenase (1). The reduction of NADP to NADPH was monitored by absorbance at 340 nm. Assays were performed at 22 ℃ in 50 mM Hepes, pH 7.5. Assay solutions contained EDTA and KCl at concentrations of 10 μM and 150 mM, respectively, and saturating levels of Fru-1,6-P_2 (20 μM) and $MgCl_2$ (5 mM).

Crystallization of product complexes— Crystals of Leu^{54} FBPase in ED or PD were grown by the hanging drop method. 2 μl of protein solution and 2 μl of precipitant solution were combined in a droplet. Wells contained 500 μl of the precipitant solution. Crystals grew from a protein solution with Leu^{54} FBPase (10 mg/ml), Hepes (50 mM, pH 7.5), $MnCl_2$ (5 mM), Fru-1,6-P_2 (5 mM), and AMP (5 mM) combined with a precipitant solution with Hepes (100 mM, pH 7.5), polyethylene glycol 3350 (12%, w/v), *t*-butyl alcohol (5%, v/v) and ED (25%, v/v) or PD (25%. v/v). Crystals were of equal dimensions (0.2–0.4 mm), growing in approximately 3 days at 20 ℃. Crystals can be transferred directly from droplet to liquid nitrogen as conditions of crystallization include cryo-protectants.

X-ray data collection, structure determination, and refinement— Data were collected at Iowa State University from single crystals on a Rigaku R-AXIS IV++ rotating anode/image plate system using CuK_α radiation from an Osmic confocal optics system and a temperature of 110 K. Data were reduced with the program package d*trek (37).

I_R-state FBPase (PDBID: 1YYZ) was used in generating the initial structures by molecular replacement and electron density maps. The resulting models underwent refinement using CNS (38) with force constants and parameters of stereochemistry from Engh and Huber (39). A cycle of refinement consisted of slow cooling from 1000 to 300 K in steps of 25 K followed by 120 cycles of conjugate gradient minimization and concluded by the refinement of individual thermal parameters. Restraints of 1.5 $Å^2$ on nearest neighbor and next-to-nearest neighbor main chain atoms, 2.0 $Å^2$ on nearest neighbor side chain atoms, and 2.5 $Å^2$ on next-to-nearest neighbor side chain atoms were employed in thermal parameter refinement. Water molecules were added to difference electron density of 2.5σ or better until no significant decrease was evident in the R_{free} value. Water molecules in the final models

fell within the allowed range for donor-acceptor distances and have thermal parameters under 60 $Å^2$. Stereochemistry of the models was examined by the program PROCHECK (40).

Analysis of central cavity— Surface area was measured by the rolling probe method with a probe radius of 1.4 Å (41). Hydrophobicity of the central cavity was calculated as the fraction of total surface area of the cavity associated with carbon and sulfur atoms. The volume of the central cavity was estimated by the summation of 0.1 Å cells contained within the cavity.

Molecular dynamics (MD) simulations— MD simulations employed NAMD (42) with the CHARMM 27 force field (43). The initial coordinates for R- I_R-, and I_T-, T_F- and T-states came from RCSB database entries 1NUY, 1YYZ, 2F3D, 2QVV and 1EYK, respectively. The system included an entire tetramer of FBPase and approximately 30,000 TIP3P water molecules (44) in a rectangular water box with a buffering distance of 15 Å. Sodium and chloride ions were added to neutralize the net charge of system. Periodic boundary conditions were applied and the particle mesh Ewald algorithm (45) was used for the calculation of long-range electrostatic interactions. The cutoff was set to 12 Å for non-bonded Van der Waals interactions, and the integration time step was 2.0 fs. All models were energy-minimized for 10 ps and gradually heated to 310 K to relax unfavorable contacts (if any), followed by another 10 ps simulation to equilibrate the system. Protein backbone atoms were fixed in simulations to retain starting quaternary states and facilitate the analysis of the solvent structure. Finally, simulations of 10 ns were carried out with constant pressure and temperature (1.01325 bar at 310 K).

Structural clustering analysis— Fixed backbone atoms eliminated rigid-body motions over the simulation, allowing the direct comparison of water structure by structural clustering analysis. Coordinates of water molecules within the cavity were recorded at 5 ps intervals during the last 5 ns of simulations (a total of 1000 sets). Root mean square deviations (RMSD) between all pair wise combinations of coordinate sets were determined through an iterative process that began with the closest pair of water molecules, one molecule from each set. The distance between matched water molecules separated by 3 Å or less contributed directly to the calculation of RMSD. Otherwise a limiting value of 3 Å was used, reflecting a

match to a dummy water molecule. The process resulted in the one-to-one mapping of water molecules from any given set onto water molecules or dummy water molecules of all other sets. A 1000 by 1000 matrix, in which each element is a RMSD, resulted from the mappings. The structural clustering analysis followed the procedure described in ref 46. The coordinate set which gave the most RMSD values below an arbitrary threshold of 1 Å was taken as the representative of the most prevalent water cluster.

Results

Central cavity of FBPase— The quaternary state of the protein largely defines the boundaries of central cavities; however, two channels connect the cavity to the bulk solvent. These cavity openings, as well as the entire cavity, obey mutually intersecting twofold axes of symmetry of the tetramer. The channels are roughly parallel to the symmetry axis extending from square-planar face of the tetramer (the ±*x*-direction of Fig. 1), and *x*-coordinates of minimum cavity surface (±6 Å) marks the boundaries between cavity and bulk solvent. Measured from its center, the cavity has dimensions of approximately 6, 10, and 12 Å on x, y, and z axes, respectively.

Residues 44-49 from the C-terminus of helix H2, loop 186-192, and the beginning of loop 50-72 define the largely hydrophobic surface of the central cavity, with 70% of the surface formed by atoms of carbon and sulfur (Table 1). Water molecules occupy the cavity, approximately 30 of which are ordered in crystal structures of the R- and T-states and 48 in the I_R-state. All water molecules in the central cavity of I_R-state are within hydrogen bonding distance with at least one other water molecule in the cavity (Fig. 1, C). The hydrogen bond network expands throughout the cavity, defining a clathrate-like structure.

The AMP induced subunit-pair rotation from the R- to the I_T-state reduces the size of cavity and increases the hydrophobicity of the cavity surface (Table 1). When loop 50-72 is in its disengaged conformation, however, further rotation from the T_F- to T-state enlarges the cavity. As residues 49-51, (the N-terminal hinge of loop 50-72) are part of the cavity surface, the movement of loop 50-72 from engaged to disengaged conformation (I_T- to T_F-) induces

extensive conformational change in the protein (47), enlarges the cavity volume, but decreases the cavity surface area.

Molecular dynamics simulations— Water molecules can diffuse into or out of the central cavity through the channels during simulations. The number of water molecules in the central cavity stabilizes within the first 2 ns. (The number of water molecules in the central cavity and hydrogen bonds between them were recorded every 2 ps over the simulation). The I_R-state has the maximum number of water molecules in the central cavity, whereas the T_F-state has the fewest (Table 2). R- and T-states contain similar numbers of water molecules. Water molecules in the I_R- and I_T-states pack more densely than in other states. Water molecules interchange positions during the simulations. The average dwell time for a water molecule at a cavity site is longest in the I_R- and I_T-states, and shortest in the T_F-state.

The sites for water molecules defined by simulations are consistent with those determined by crystallography. Indeed, agreement between simulations and crystal structure is optimal for the I_R-state where the water structure is large and maximally stable (Fig. 2). A single dominant cluster of water molecules in the I_R-state appears in over 90% of frames from the simulation. The water organization in the cavity of the I_T-state is also relatively stable, with 50% of frames contributing to one cluster; however, the I_T-state from simulation identifies more water molecules than does the crystallographic structure (Table 1 *versus* Table 2). For the R-, T_F- and T-states, no cluster of water molecules dominates.

AMP inhibition of Asp^{10} FBPase in different co-solvents— For each of Leu^{54} and Asp^{10} FBPases, three crystal structures have been reported (25, 26). R-state crystals grow in the absence of AMP and I- and T-states both appear in the presence of AMP. The appearance of different quaternary states in the presence of AMP is a result of different cyro-protectants (glycerol for I-state versus 2-methyl-2,4-pentanediol (MPD) for T-state). Changes in quaternary state in response to cyro-protectant suggest the possibility of the systematic manipulation of the quaternary state of FBPase by variations in the solvent system.

The biphasic inhibition of Asp^{10} FBPase by AMP (27) offers the possibility of activity assays as a means of probing the effects of solvent systems on the quaternary state.

The partially active state of Asp^{10} FBPase observed in the presence of saturating AMP is due presumably to an intermediate quaternary state that lies between the fully active R-state and the inactive T-state. (The latter is made energetically inaccessible by the mutation). Indeed, crystallographic studies have identified an intermediate quaternary state in the presence of AMP that can have an engaged loop 50-72 (the I_T-state) (26).

Glycerol reduces Asp^{10} FBPase activity (the enzyme in 25% glycerol has 40% of the specific activity in water), but also significantly reduces partial AMP inhibition (Table 3). In order to focus on the effect of different solvent systems on AMP inhibition, results are presented as velocities relative to that of Asp^{10} FBPase in a particular solvent system in the absence of AMP. Biphasic inhibition curves employ the following empirical relationship in data fitting:

$$V=\frac{1-V_{plateau}}{1+\left(\frac{I}{IC_{high}}\right)^{n_{high}}}+\frac{V_{plateau}}{1+\left(\frac{I}{IC_{low}}\right)^{n_{low}}}$$

where V, $V_{plateau}$, I, IC_{high}, n_{high}, IC_{low} and n_{low} indicate relative velocity, relative velocity at the plateau, AMP concentration, IC_{50} for the high affinity binding site, Hill coefficient for the high affinity binding site, IC_{50} for low affinity binding site, and Hill coefficient for the low affinity binding site, respectively. Activity assays using different concentrations of AMP in different glycerol/water solvent systems reveal a systematic increase in the relative activity of Asp^{10} FBPase as glycerol concentrations increase (Fig. 3). IC_{50} values for the high and low affinity interactions increase 3- and 5-fold, respectively, as glycerol concentrations increase (Table 3). Under all conditions, the Hill coefficient for the high affinity site is near 2, whereas that for low affinity site is approximately unity. Most notably, the effect of glycerol in diminishing AMP inhibition reaches a maximum at 30% (v/v) glycerol, and that the dependence of plateau velocity on glycerol concentration is sigmoidal (Fig. 3).

Other solvents systems have similar effects to that of glycerol (Fig. 4; Table 3). Asp^{10} FBPase is inactive in 25% (v/v) ethanol, 1-propanol, 2-propanol or MPD, and in 25% (v/v) 1,3-propanediol, the enzyme retains less than 10% of its activity. Asp^{10} FBPase,

however, is active in solvent systems with ED, PD, xylitol or sorbitol. Relative velocities as a function of AMP concentration in 25% (v/v or w/v) ED, PD, xylitol and sorbitol (Fig. 4) define plateau relative velocities below (as for xylitol and sorbitol), equal to (ED) and above (as for PD) those determined in the presence of 25% v/v glycerol. In PD, the enzyme is barely inhibited by millimolar levels of AMP, retaining a plateau activity of 80%. The high affinity AMP site exhibits cooperativity in all solvent systems, whereas the low affinity site has a Hill coefficient of unity (Table 3).

Crystal structures of Leu^{54} FBPase in different co-solvents (Protein Data Bank code 4GBV in ED and 4GBW in PD)— Leu^{54} FBPase crystallized under a great variety of solvent systems, and hence served as a surrogate for Asp^{10} FBPase in probing quaternary states of FBPase. Crystals grown in the presence 10 mM AMP and 5 mM of substrate diffract to a resolution equal to or higher than 3 Å in ED and PD solvent systems. Mn^{2+} is used as a divalent cation, which stabilizes engaged loop more than does Mg^{2+} and does not precipitate at high concentrations at neutral pH as does Zn^{2+} (48). Crystals from ED and PD systems are in space group *I222*, isomorphous with R- and I_R-state crystals of Leu^{54} FBPase in glycerol. Space group parameters for crystals grown from ED (a = 53.69, b = 82.51, c = 166.28 Å) are essentially identical to those grown from PD (a = 53.38, b = 82.72, c = 165.17 Å). The statistics of data collection and refinement are in Table 4. Both models begin with residue 10. Electron density for AMP molecules in both models is weak, reflecting weak binding of AMP.

Comparison of the ED and PD structures to the R-, I_R- and T-structures of Leu^{54} FBPase reveals no significant differences at the level of the C1-C2 subunit pair; however, whole-tetramer alignments reveal distinct differences in subunit-pair rotations. The rotation angles for Leu^{54} FBPase in PD, glycerol, ED, and MPD (T-state) in the presence of AMP are 1, 3, 4, and 15 °, respectively (Fig. 5).

Correlation of FBPase activity and subunit-pair rotation— PD exhibits the strongest stabilization effect on the I-state of Asp^{10} FBPase, whereas xylitol and sorbitol show the least effects. Leu^{54} FBPase show different levels of conformational change in different co-solvent

systems. A plot of plateau velocity of Asp^{10} FBPase against subunit-pair rotation (Fig. 6) reveals a correlation between activity and subunit-pair rotation toward the R-state.

Discussion

MD simulations of water molecules in protein cavities are in the literature (49-52). The investigation here identified approximately 45-50 well-ordered water molecules in the central cavity of the I_R-state, on the basis of simulations and crystal structures. To our knowledge, waters in the FBPase central cavity represent the largest cluster of water molecules found inside a protein. Water molecules in the central cavity are well-ordered and resist exchange with the bulk solvent. In both crystal structure and simulation, similar hydrogen bond networks interconnect all water molecules in the cavity. Rings of five water molecules are a clear feature of the hydrogen bond network. Cluster analysis, indicates a stable structure that persists throughout 10 ns of simulation (Fig. 2).

Hydrophilic surfaces directly provide hydrogen bonding sites for water molecules, whereas hydrophobic surfaces enhance water-water interactions (53). Small apolar cavities, therefore, usually remain dehydrated due to the dearth of water-water interactions (54). Nonetheless, hydration of sufficiently large apolar cavities can be favorable energetically (55). Clathrate-like arrangements of water molecules cover hydrophobic surfaces of crambin in crystal structures (56). The cavity in FBPase is large but not entirely hydrophobic. Hydrophilic surfaces may provide hydrogen bonds to water molecules, which in turn become seeds for extended networks of hydrogen-bonded water molecules that span the entire cavity. The hydrophobic surface of the cavity would enhance water-water interactions and stabilize water networks.

The central cavity of FBPase undergoes changes in volume, shape and surface structure due to the subunit-pair rotation and conformational changes in loop 50-72 (Table 1). In the transition from R- to I_T-state, the cavity becomes smaller and more hydrophobic; however, in the transition from I_T- to T-state, the cavity increases in size and becomes less hydrophobic. On the basis of simulations, water clusters are more stable and extensive in the

in I_R- and I_T-states and least stable in the T_F-state (Fig. 2; Table 2). The extra stability of water in I_R- and I_T-state may be due due to elevated hydrophobicity and/or to a more complementary fit of the water network to the central cavity.

The thermodynamic contribution of the water structure could be a significant factor in a conformational transition from the I_T- to T_F-state (movement of the dynamic loop from an engaged to disengaged conformation). The movement of loop 50-72 has been linked to dynamic modes that exacerbate unfavorable steric contacts involving the loop in its engaged conformation (26). The order-to-disorder transition of water structure in the cavity could be a significant free-energy factor in support of conformational change of the dynamic loop to its disengaged conformation.

Polyols like glycerol are chemical chaperones that stabilize proteins from unfolding or aggregation (57). Glycerol may enhance protein stability through the ordering of water molecules on the protein surface (58-60). The correlation between subunit-pair rotation and activity (Fig. 6) may be linked to the ordering of water molecules in the central cavity. If in the absence of glycerol the AMP/FBPase complex is in the I_T-state, then as the concentration of glycerol increases, so too does the order of water structure in the central cavity. Enhanced order of the water structure in turn favors the more active I_R-state of the tetramer. The plot of plateau activity against glycerol concentration (Fig. 3) is sigmoidal, implying a cooperative phenomenon, as would be anticipated for the ordering of water molecules in a symmetric cavity.

The effects of chemical chaperones on FBPase activity suggest that the crowded environment within the cell would favor the ordering of water molecules in the central cavity. Although such an effect may occur, its impact on wild-type FBPase likely would not offset the influence of AMP. A significant chaperone effect occurs only in mutant forms of FBPase which cannot stabilize a disengaged conformation of loop 50-72. The T- and T_F-states of these mutant FBPases are energetically unfavorable and hence these systems exist primarily in energy accessible R-states and/or intermediate quaternary states.

Human FBPase is a drug target for the treatment of Type II diabetes (11-18). Screening efforts usually identify molecules that bind to the AMP pocket (13-18), but at least two different classes of inhibitor bind to the center of FBPase (11-12). OC252 binds to the outside surface of the central cavity channel, and induces a conformational change from R-state to a state that we call here T_F (subunit-pair rotation of 11-13 ° with a disengaged loop 50-72) (12). OC252 inhibits synergistically with AMP and uncompetitively with respect to substrate. The uncompetitive mechanism indicates that OC252 binds to the R-state in the presence of substrate with loop 50-72 in its engaged conformation. Indeed, loop 50-72 in the disengaged conformation of the OC252 complex, wraps over the bound OC252 molecule, consistent with an OC252 binding event that precedes the loop conformational change.

The basis for synergism between AMP and OC252 may in fact be linked to structural modulation of water molecules in the central cavity. An engaged loop 50-72 persists up to at least the I_T-state (11-13 ° subunit-pair rotation). AMP binding energy would go in part toward the generation of ordered water molecules in the central cavity as the tetramer transitions from the R- to the I_T-state. The ordered solvent represents a source of "stored" energy, and any mechanism that releases that energy would act synergistically with AMP in the inhibition of FBPase. By binding to the center of FBPase in its I_R- and/or I_T-state, OC252 could eliminate solvent ordering. Fru-2,6-P_2 displaces loop 50-72 from the active site, and also causes the loss of order water structure in the central cavity. Binding synergism between OC252 and AMP, as well as Fru-2,6-P_2 and AMP then could arise through ligand induced order-to-disorder transition of water molecules in the central cavity.

Water molecules are also important in allosteric effects in mammalian hemoglobin (61-65). Hemoglobin is a hetero-tetramer. Oxygen binds to hemoglobin cooperatively and induces global structural reorganization from T- to R-state. Global conformational change in hemoglobin is coupled to protein hydration (61-62). Oxygen affinity towards hemoglobin can be enhanced by mixed solvent systems (61, 63-65). Effectors such as Cl^- and 2,3-bisphosphoglyceric acid reduce the hydration level of hemoglobin, favoring the T-state (64). The effects of water organization in allosteric transition in both tetrameric FBPase and hemoglobin may imply a general design principle in regulation of oligomeric proteins.

Table 1. Central cavities from crystal structures of FBPase.

Quaternary state	Subunit-pair rotation (°)	Loop 50-72	Volume (Å^3)	Surface area (Å^2)	Surface fraction as C and S	Number of water molecules
R	0	Engaged	316	932	0.70	27
I_R	3	Engaged	259	877	0.73	48
I_T	12	Engaged	235	831	0.74	28
T_F	13	Disengaged	291	765	0.71	35
T	15	Disengaged	385	793	0.72	33

Table 2. Water molecule populations of central cavities from MD simulations.

Quaternary state	Average number of water molecules	Average number of hydrogen bonds	Density ($Å^{-3}$)	Average dwell time (ps)
R	42.3	67.0	0.133	20.5
I_R	45.4	74.7	0.175	33.7
I_T	42.3	68.1	0.180	26.0
T_F	37.7	60.0	0.130	18.1
T	43.6	68.0	0.113	20.8

Table 3. **AMP inhibition of Asp^{10} FBPase in mixed solvent systems.**
Uncertainty in the last significant digit is given parenthetically.

Solvent system	IC_{50} (high-affinity site) (μM)	Hill coefficient (high-affinity site)	IC_{50} (low-affinity site) (mM)	Hill coefficient (low-affinity site)	Relative plateau velocity
Water	4.3(2)	2.1 (1)	3.5 (5)	0.9 (1)	0.28 (1)
Glycerol (5% v/v)	5.8 (3)	2.4 (2)	5.7 (9)	1.1 (1)	0.32 (1)
Glycerol (10% v/v)	7.0 (3)	2.3 (2)	7.5 (7)	1.2 (1)	0.394 (9)
Glycerol (15% v/v)	7.5 (4)	2.2 (2)	9.2 (8)	0.98 (8)	0.46 (1)
Glycerol (20% v/v)	7.4 (6)	2.0 (3)	12 (1)	1.3 (2)	0.52 (1)
Glycerol (25% v/v)	10.6 (9)	2.4 (4)	14 (1)	1.2 (1)	0.55 (1)
Glycerol (30% v/v)	11.3 (4)	1.9 (1)	18.1 (7)	1.04 (5)	0.567 (8)
ED (25% v/v)	8.1 (3)	1.8 (1)	13.6 (6)	1.10 (5)	0.518 (9)
PD (25% v/v)	7.2 (9)	3.2 (9)	21 (1)	1.03 (7)	0.820 (8)
Xilitol (25% v/v)	9.1 (3)	1.8 (1)	11 (1)	1.2 (1)	0.352 (7)
Sorbitol (25% v/v)	9.9 (1)	2.0 (1)	13.1 (2)	1.22 (2)	0.41 (1)

Table 4. Statistics of data collection and refinement for Leu^{54} FBPase.

Crystalline complex[a]	ED	PD
Resolution limit (Å)	2.90	2.00
Number of measurements	23,686	74,692
Number of unique reflections	8,010	20,855
Completeness of data (%):		
Overall	93.7	82.8
Last shell/resolution-range (Å)	96.8/3.00-2.90	56.5/2.07-2.00
R_{sym}[b]		
Overall	0.122	0.065
Last shell/resolution-range (Å)	0.295/3.00-2.90	0.277/2.07-2.00
Number of reflections in refinement	7,635	19,759
Number of atoms	2,601	2,767
Number of solvent sites	103	228
R_{factor}[c]	0.180	0.195
R_{free}[d]	0.243	0.241
Mean B (Å^2) overall/protein	36/35	31/32
Mean B (Å^2) for AMP	67	97
Root mean square deviations (deg):		
Bond lengths (Å)	0.012	0.024
Bond angles	1.5	2.0

[a]Unit cell lengths (*a*, *b*, *c*) in Å for the FBPase AMP complexes in ED and PD are (53.69, 82.51, 166.28), and (53.38, 82.72, 165.17), respectively. Unit cell angles (α, β, γ) are 90° for space groups I222.

[b]$R_{sym} = \Sigma_j\Sigma_i \mid I_{ij} - \langle I_j \rangle \mid / \Sigma_i\Sigma_j I_{ij}$, where *i* runs over multiple observations of the same intensity, and *j* runs over all crystallographically unique intensities.

[c]$R_{factor} = \Sigma \parallel F_{obs} \mid - \mid F_{calc} \parallel / \Sigma \mid F_{obs} \mid$, where $\mid F_{obs} \mid > 0$.

[d] R_{free} based upon 10% of the data randomly culled and not used in the refinement.

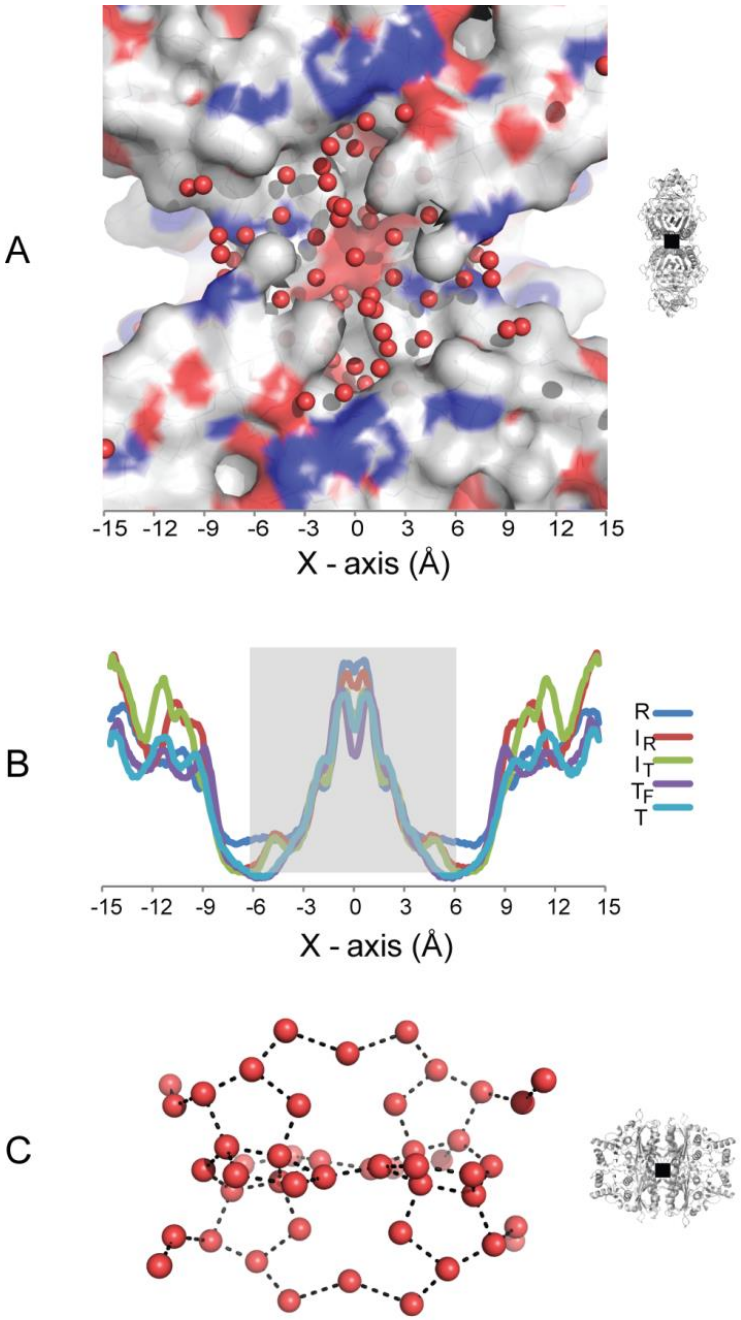

Figure 1. FBPase central cavity and water molecules. A. Central cavity of FBPase in the I_R-state as viewed down the symmetry axis that separates the C1-C2 subunit pair from the C3-C4 subunit pair. Carbon, nitrogen and oxygen atoms are in white, blue and red, respectively. Interior water molecules are represented by red spheres. B. Surface area of the central cavity plotted along the symmetry axis directed from the square-planar face of the tetramer (x-direction). Surface areas from R-, I_R- I_T-, T_F- and T-state cavities are represented by dark blue, purple, green, magenta, and light blue, respectively. Central cavity is defined as shaded region. C. Water molecules from central cavity of I_R-state FBPase are plotted as red spheres connected by possible hydrogen bonds. Figures were prepared with pymol (66).

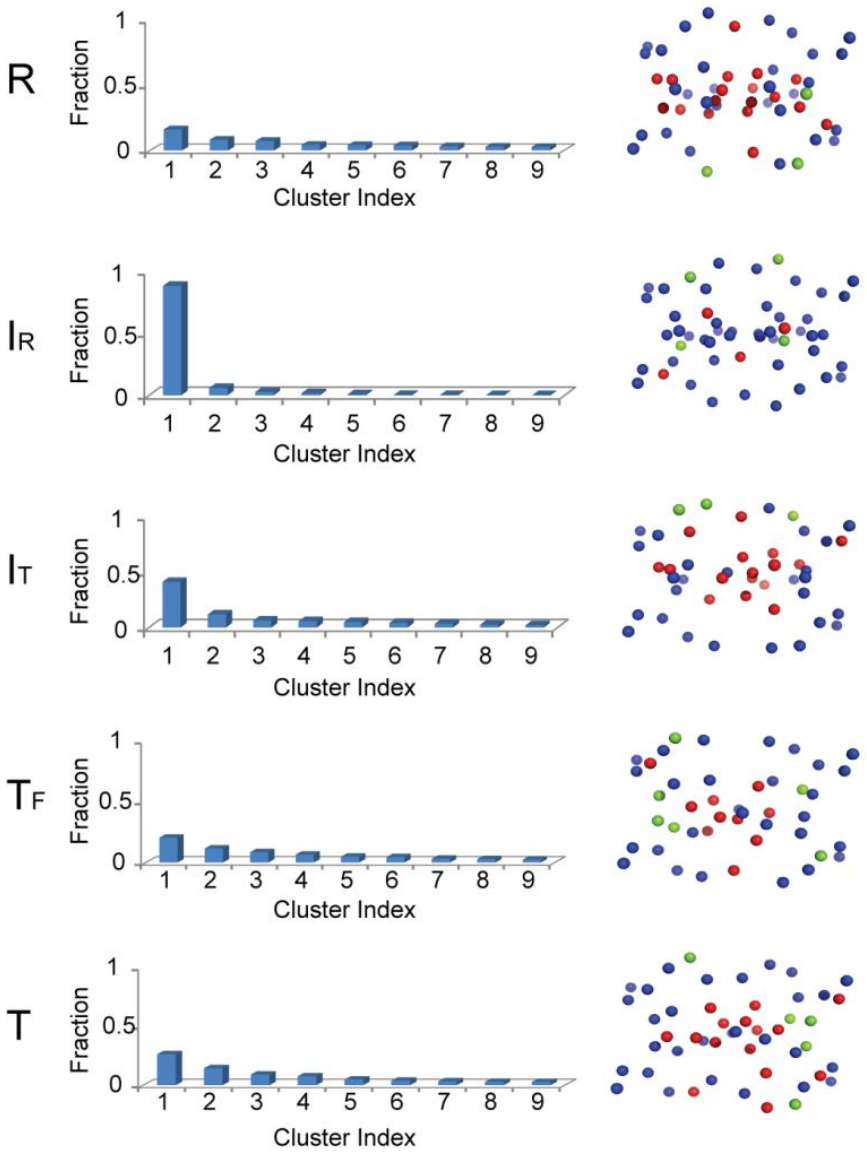

Figure 2. Structural clustering of waters in FBPase central cavity. Fractions of the ten most prevalent clusters are indicated by bars on the left side of the figure for the R, I_R-, I_T-, T_F, and T-states. On the right side is the dominant cluster for each quaternary state aligned with water sites from crystal structures. Blue spheres indicates shared positions from simulation and crystal structure, and red spheres represent sites observed only from structural clustering analysis and green spheres only from crystallographic studies.

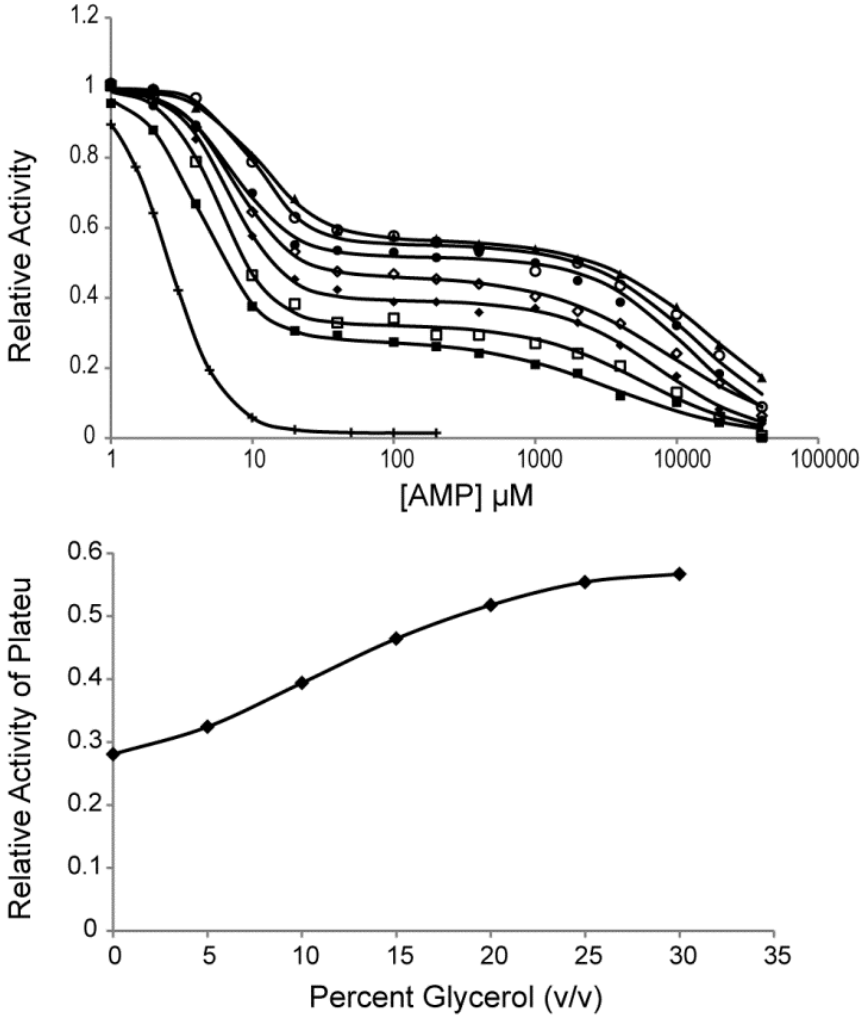

Figure 3. AMP inhibition of Asp^{10} FBPase in the presence of glycerol. Relative velocities (velocities relative to those in the absence of AMP under the specified solvent systems) are plotted against AMP concentration ranging from 1 µM to 40 mM (*top panel*). Percent (v/v) glycerol-aqueous buffer systems for assays of Asp^{10} FBPase are as follows: 0 (■), 5 (□), 10 (◆), 15 (◊), 20 (●), 25 (○) and 30 (Δ). The relative velocity of wild type FBPase in aqueous buffer (+) is presented as a reference curve using a fitting relationship with only high-affinity parameters. Relative activity at the plateau ($V_{plateau}$) as a function of percent (v/v) glycerol is plotted (*bottom panel*).

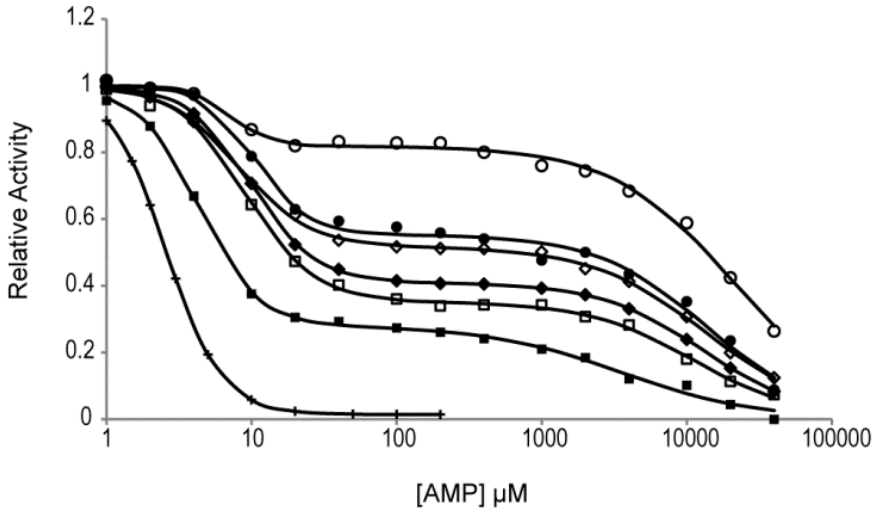

Figure 4. AMP inhibition of Asp[10] FBPase in the presence of different co-solvent systems. Relative activities are plotted against AMP concentrations ranging from 1 µM to 40 mM. Organic-aqueous buffer systems (the organic component at 25% (v/v)) for assays of Asp[10] FBPase are as follows: no organic component (■) xylitol, (□) sorbitol, (◆) ED, (◊) glycerol (●) and PD (○). The relative velocity of wild type FBPase in aqueous buffer (+) is presented as a reference curve using a fitting relationship with only high-affinity parameters.

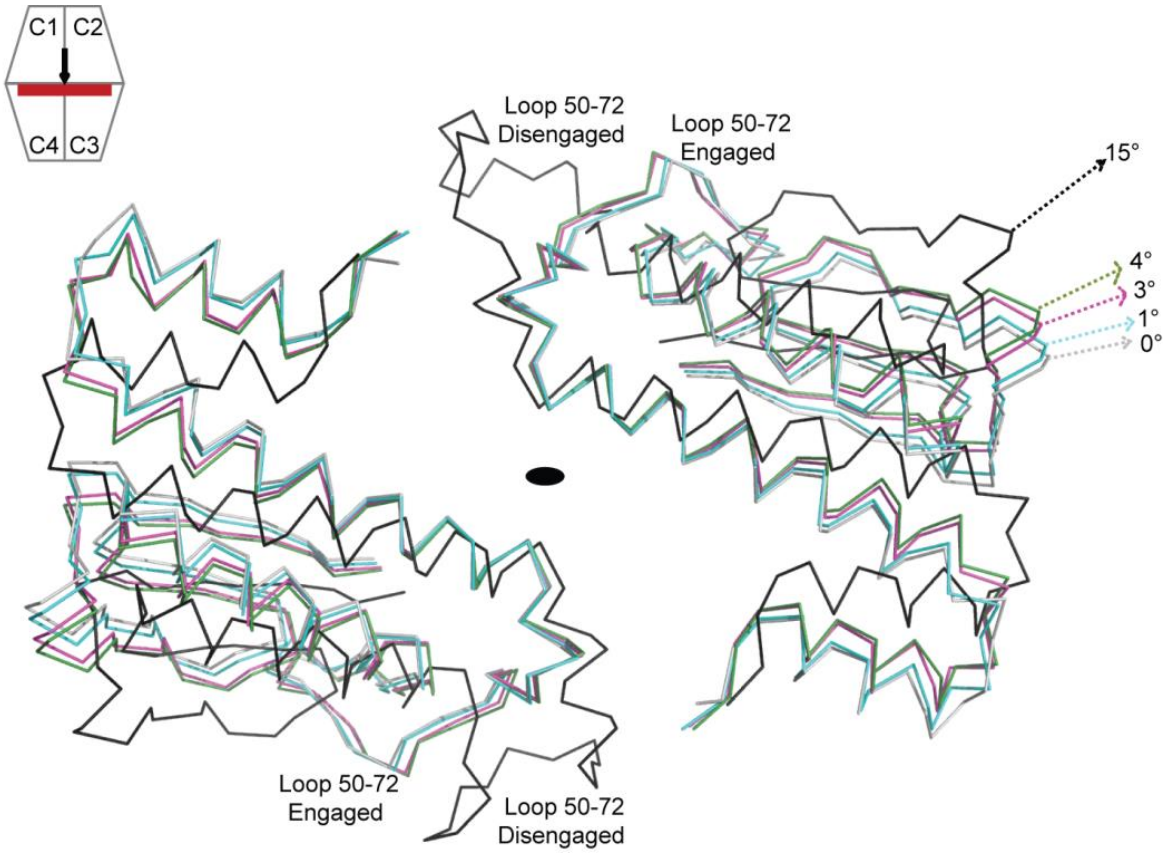

Figure 5. Crystal structures of AMP complexes of Leu^{54} FBPase. AMP complexes of Leu^{54} FBPase in PD (cyan), glycerol (magenta), ED (green) and MPD (black) are aligned to R-state Leu^{54} FBPase (grey). The viewing direction and region of the tetramer shown is indicated by the FBPase icon. C1-C2 subunit-pairs of all structures are aligned, and different subunit-pair rotations are represented by residues 10-120 of the C3-C4 subunit-pair. The rotational angles and the conformation of loop 50-72 are indicated. Figures were prepared with pymol (66).

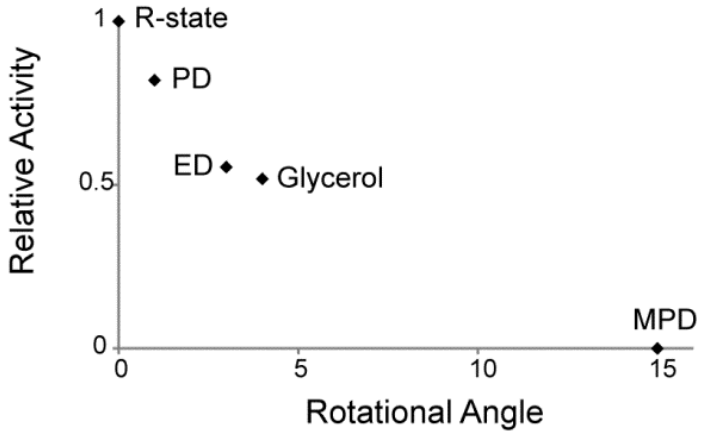

Figure 6. Correlation between subunit-pair rotation and plateau velocity. Subunit-pair rotation angles come from structure of Leu[54] FBPase crystallized in different solvent systems (see methods section and reference 25). The R-state represents 0 ° subunit-pair rotation and the T-state a 15 º subunit-pair rotation. Plateau activities are from activity assays of Asp[10] FBPase taken under solvent conditions used in the crystallization of Leu[54] FBPase. The subunit-pair rotational, relative plateau velocity in PD, glycerol, ED and MPD are as follows: (1 °, 0.82), (3 °, 0.55), (4 °, 0.52) and (15 °, 0.00), respectively.

Reference

1. Benkovic, S. J., and de Maine, M. M. (1982) Mechanism of action of fructose 1,6-bisphosphatase. Adv. Enzymol. Relat. Areas Mol. Biol. 53, 45–82

2. Tejwani, G. A. (1983) Regulation of fructose-bisphosphatase activity. Adv. Enzymol. Relat. Areas Mol. Biol. 54, 121–194

3. Taketa, K., and Pogell, B. M. (1965) Allosteric inhibition of rat liver fructose 1,6-bisphosphatase by adenosine 5'-monophosphate. J. Biol. Chem. 240, 651–662

4. Pilkis, S. J., El-Maghrabi, Pilkis, J., and Claus, T. (1981) Inhibition of fructose-1,6-bisphosphatase by fructose 2,6-bisphosphate. J. Biol. Chem. 256, 3619–3622

5. Van Schaftingen, E., and Hers, H.-G. (1981) Inhibition of fructose-1,6-bisphosphatase by fructose 2,6-biphosphate. Proc. Natl. Acad. Sci. U. S. A. 78, 2861–2863

6. Pilkis S. J., El-Maghrabi, Pilkis, J., Claus, T. H., and Cumming D. A. (1981) Fructose 2,6-bisphosphate. A new activator of phosphofructokinase. J. Biol. Chem. 256, 3171–3174

7. Van Schaftingen, E., Jett, M.-F., Hue, L., and Hers, H.-G. (1981) Control of liver 6-phosphofructokinase by fructose 2,6-bisphosphate and other effectors. Proc. Natl.Acad. Sci. U. S. A. 78, 3483–3486

8. Uyeda, K., Furuya, E., and Luby, L. J. (1981) The effect of natural and synthetic D-fructose 2,6-bisphosphate on the regulatory kinetic properties of liver and muscle phosphofructokinase. J. Biol. Chem. 256, 8394–8399

9. Guynn, R. W., Velose, D., and Veech, R. L. (1972) The concentration of malonyl-coenzyme A and the control of fatty acid synthesis in vivo. J. Biol. Chem. 247, 7325-7331

10. Okar, D. A., and Lange, A. J. (1999) Fructose-2,6-bisphosphate and control of carbohydrate metabolism in eukaryotes. Biofactors 10, 1–14

11. Wright, S. W., Carlo, A. A., Carty, M. D., Danley, D. E., Hageman, D. L., Karam, G. A., Levy, C. B., Mansour, M. N., Mathiowetz, A. M., McClure L. D., Nestor, N. B., McPherson, R. K., Pandit, J., Pustilnik, L. R., Schulte, G. K., Soeller, W. C., Treadway, J. L., Wang, I.-K., and Bauer, P. H. (2002) Anilinoquizoline inhibitors of fructose 1,6-bisphosphatase bind at a novel allosteric site: synthesis, in vitro characterization, and X-ray crystallography. J. Med. Chem. 45, 3865-3877

12. Choe, J. Y., Nelson, S. W., Arienti, K. L., Axe, F. U., Collins, T. L., Jones, T. K., Kimmich, R. D., Newman, M. J., Norvell, K., Ripka, W. C., Romano, S. J., Short, K. M., Slee, D. H., Fromm, H. J., and Honzatko, R. B. (2003) Inhibition of fructose-1,6-bisphosphatase by a new class of allosteric effectors. J. Biol. Chem. 278, 51176-51183

13. Erion, M. D., van Poelje, P. D., Dang, Q., Kasibhatla, S. R., Potter, S. C., Reddy, M. R., Reddy, K. R., Jiang, T., and Lipscomb, W. N. (2005) MB06322 (CS-917): A potent and selective inhibitor of fructose 1,6-bisphosphatase for controlling gluconeogenesis in type 2 diabetes. Proc. Natl.Acad. Sci. U. S. A. 102, 7970–7975

14. von Geldern, T. W., Lai, C., Gum, R. J., Daly, M., Sun, C., Fry, E. H., and Abad-Zapatero, C. (2006) Benzoxazole benzenesulfonamides are novel allosteric inhibitors of fructose-1,6-bisphosphatase with a distinct binding mode. Bioorg. Med. Chem. Lett. 16, 1811-1815

15. Hebeisen, P., Kuhn, B., Kohler, P., Gubler, M., Huber, W., Kitas, E., Schott, B., Benz, J., Joseph, C., and Ruf, A. (2008) Allosteric FBPase inhibitors gain 105 times in potency when simultaneously binding two neighboring AMP sites. Bioorg. Med. Chem. Lett. 18, 4708-4712

16. Rudnitskaya, A., Huynh, K., Török, B., and Stieglitz, K. (2009) Novel heteroaromatic organofluorine inhibitors of fructose-1,6-bisphosphatase. J. Med. Chem. 52, 878-882

17. Kitas, E., Mohr, P., Kuhn, B., Hebeisen, P., Wessel, H. P., Haap, W., Ruf, A., Benz, J., Joseph, C., Huber, W., Sanchez, R. A., Paehler, A., Benardeau, A., Gubler, M., Schott, B., and Tozzo, E. (2010) Sulfonylureido thiazoles as fructose-1,6-bisphosphatase inhibitors for the treatment of type-2 diabete. Bioorg. Med. Chem. Lett. 20, 594-599

18. Hebeisen, P., Haap, W., Kuhn, B., Mohr, P., Wessel, H. P., Zutter, U., Kirchner, S., Ruf, A., Benz, J., Joseph, C., Alvarez-Sánchez, R., Gubler, M., Schott, B., Benardeau, A., Tozzo, E., and Kitas, E. (2011) Orally active aminopyridines as inhibitors of tetrameric fructose-1,6-bisphosphatase. Bioorg. Med. Chem. Lett. 21, 3237-3242

19. Ke, H., Zhang, Y., and Lipscomb, W. N. (1990) Crystal structure of fructose-1,6-bisphosphatase complexed with fructose 6-phosphate, AMP and magnesium. Proc Natl. Acad. Sci. U.S.A. 87, 5243-5247

20. Ke, H., Zhang, Y., Liang, J. and Lipscomb, W. N. (1991) Crystal structure of the neutral form of fructose-1,6-bisphosphatase complexed with the product fructose 6-phosphate at 2.1-Å resolution. Proc Natl. Acad. Sci. U.S.A. 88, 2989-2993

21. Xue, Y., Huang, S., Liang, J., Zhang, Y., and Lipscomb, W. N. (1994) Crystal structure of fructose-1,6-bisphosphatase complexed with fructose 2,6-bisphosphate, AMP, and

Zn2+ at 2.0-Å resolution: aspects of synergism between inhibitors. Proc Natl. Acad. Sci. U.S.A. 91, 12482-12486

22. Choe, J. Y., Poland B. W., Fromm, H. J. and Honzatko, R. B. (1998) Role of a dynamic loop in cation activation and allosteric regulation of recombinant porcine fructose-1,6-bisphosphatase. Biochemistry. 37, 11441-11450

23. Choe, J. Y., Fromm, H. J. and Honzatko, R. B. (2000) Crystal structures of fructose 1,6-bisphosphatase: mechanism of catalysis and allosteric inhibition revealed in product complexes. Biochemistry. 39, 8565-8574

24. Hines, J. K., Chen, X., Nix, J. C., Fromm, H. J., and Honzatko, R. B. (2007) Structures of mammalian and bacterial fructose-1,6-bisphosphatase reveal the basis for synergism in AMP/fructose 2,6-bisphosphate inhibition. J. Biol. Chem. 282, 36121–36131

25. Iancu, C. V., Mukund, S., Fromm, H. J., and Honzatko, R. B. (2005) R-state AMP complex reveals initial steps of the quaternary transition of fructose-1,6-bisphosphatase. J. Biol. Chem. 280, 19737–19745

26. Gao, Y., Iancu, C. V., Mukund, S., Choe, J. Y., and Honzatko, R. B. Mechanism of displacement of catalytically essential loop from the active site of fructose-1,6-bisphosphatase. Submitted, Biochemistry.

27. Nelson, S. W., Kurbanov, F. T., Honzatko, R. B., and Fromm, H. J. (2001) The N-terminal segment of recombinant porcine fructose-1,6-bisphosphatase participates in the allosteric regulation of catalysis. J. Biol. Chem. 276, 6119–6124

28. Kelley-Loughnane, N., Biolsi, S. A., Gibson, K. M., Lu, G., Hehir, M. J., Phelan, P., and Kantrowitz, E. R. (2002) Purification, kinetic studies, and homology model of Escherichia coli fructose-1,6-bisphosphatase. Biochim. Biophys. Acta. 1594, 6-16

29. Hines, J. K., Fromm, H. J., and Honzatko, R. B. (2006) Novel allosteric activation site in Escherichia coli fructose-1,6-bisphosphatase. J. Biol. Chem. 281, 18386–18393

30. Cheung, M. S., Garc á, A. E. and Onuchic, J. N. (2002) Protein folding mediated by solvation: water expelling and formation of the hydrophobic core occur after the structural collapse. Proc Natl. Acad. Sci. U.S.A. 99, 685-690

31. Takano, K., Funahashi, J., Yamagata, Y., Fujii, S., and Yutani, K. (1997) Contribution water molecules in the interior of a protein to the conformational stability. J. Mol. Biol. 274, 132-142

32. Fischer, S., and Verma, C. S. (1999) Binding of buried structural water increases the flexibility of proteins. Proc Natl. Acad. Sci. U.S.A. 96, 9613-9615

33. Meyer, E. (1992) Internal water molecules and H-bonding in biological macro-molecules: a review of structural features with functional implications. Protein Sci. 1, 1543-1562

34. Petrone, P. M., and Garcia, A. E. (2004) MHC-peptide binding is assisted by bound water molecules. J. Mol. Biol. 338, 419-435

35. Laemmli, U. K. (1970) Cleavage of structural proteins during the assembly of the head of bacteriophage T4. Nature 227, 680-685

36. Bradford, M. M. (1976) A rapid sensitive method for the quantitation of microgram quantities of protein utilizing the principle of protein-dye binding. Anal. Biochem. 72, 248-252

37. Pflugraph, J. W. (1999) The finer things in X-ray diffraction data collection. Acta Crystallogr. D. 55, 1718-1725

38. Brünger, A. T., Adams, P. D., Clore, G. M., DeLano, W. L., Gros, P., Grosse-Kunstleve, R. W., Jiang, J.-S., Kuszewski, J., Nilges, M., Pannu, M. S., Read, R. J., Rice, L. M., Simonson, T., Warren, G. L. (1998) Crystallography & NMR system: A new software suite for macromolecular structure determination. Acta Crystallogr. D 54, 905-921

39. Engh, R. A., and Huber, R. (1991) Accurate bond and angle parameters for X-ray protein structure refinement. Acta Crystallogr. A. 47, 392-400

40. Laskowski, R. A., Mac Arthur, M. W., Moss, D. S., and Thornton, J. M. (1993) PROCHECK: a program to check the stereochemical quality of protein structures. J. Appl. Cryst. 26, 283-291

41. Shrake, A., and Rupley, J. A. (1973) Environment and exposure to solvent of protein atoms. Lysozyme and insulin. J. Mol. Biol. 79, 351-364

42. Phillips, J. C., Braun, R., Wang, W., Gumbart, J., Tajkhorshid, E., Villa, E., Chipot, C., Skeel, R. D., Kale, L., Schulten, K. (2005) Scalable molecular dynamics with NAMD. J. Comput. Chem. 26, 1781-1802

43. Jr. MacKerell, A. D., Banavali, N., Foloppe, N. (2001) Development and current status of the CHARMM force field for nucleic acids. Biopolymers. 56, 257-265

44. Jorgensen, W. L., Chandrasekhar, J., Madura, J. D., Impey, R. W. and Klein, M. L. (1983) Comparison of simple potential functions for simulating liquid water. J. Chem. Phys. 79, 926-935

45. Essmann, U., Perera, L., Berkowitz, M. L., Darden, T., Lee, H., and Pedersen, L. G. (1995) A smooth particle mesh Ewald method. J. Chem. Phys. 103, 8577-8593

46. Shortle, D., Simons, K. T., and Baker, D. (1998) Clustering of low-energy conformations near the native structures of small proteins. Proc Natl. Acad. Sci. U.S.A. 95, 11158-11162

47. Nelson, S. W., Choe, J. Y., Honzatko, R. B., and Fromm, H. J. (2000) Mutations in the hinge of dynamic loop broadly influence functional properties of fructose-1,6-bisphosphatase. J. Biol. Chem. 275, 29986-29992

48. Nelson, S. W., Iancu, C. V., Choe, J. Y., Honzatko, R. B., and Fromm, H. J. (2000) Tryptophan flurescence reveals the conformational state of a dynamic loop in recombinant porcine fructose-1,6-bisphosphatase. Biochemistry. 39, 11100-11106

49. Helms, V., and Wade, R. C. (1998) Hydration energy landscape of the active site cavity in cytochrome P450cam. Proteins. 32, 381-396

50. Likić, V. A., and Prendergast, F. G. (2001) Dynamics of internal water in fatty acid binding protein: Computer simulations and comparison with experiments. Proteins. 43, 65-72

51. Henchman, R. H., Tai, K., Shen, T., and McCammon, J. A. (2002) Properties of water molecules in the active site gorge of acetylcholinesterase from computer simulations. Biophys J. 82, 2671-2682

52. Huang, H. C., Jupter, D., Qiu, M., Briggs, J. M., and Vanburen V. (2008) Cluster analysis of hydration waters around the active site of bacterial alanine racemase using a 2-ns MD simulations. Biopolymers. 89, 210-219

53. Raschke, T. M. (2006) Water structure and interactions with protein surfaces. Curr. Opin. Struct. Biol. 16, 152-159

54. Matthews, B. W., and Liu, L. (2009) A review about nothing: are apolar cavities in protein really empty. Protein Sci. 18, 494-502

55. Vaitheeswaran, S., Yin, H., Rasaiah, J. C., and Hummer, G. (2004) Water clusters in nonpolar cavities. Proc Natl. Acad. Sci. U.S.A. 101, 17002-17005

56. Teeter, M. M. (1984) Water structure of a hydrophobic protein at atomic resolution: Pentagon rings of water molecules in crystals of crambin. Proc Natl. Acad. Sci. U.S.A. 81, 6014-6018

57. Davis-Searles, P. R., Saunders, A. J., Erie, D. A., Winzor, D. J., and Pielak, G. J. (2001) Interpreting the effects of small uncharged solutes on protein-folding equilibria. Annua. Rev. Biophys. Biomol. Struct. 30, 271-306

58. Back, J. F., Oakenfull, D., Smith, M. B. (1979) Increased thermal stability of proteins in the presence of sugars and polyols. Biochemistry. 18, 5191-5196

59. Kaushik, J. K., and Bhat, R. (1998) Thermal stability of proteins in aqueous polyol solutions: Role of surface tension of water in the stabilizing effect of polyols. J. Phys. Chem. B. 102, 7058-7066

60. Liu, F. F., Ji, L., Zhang, L., Dong, X. Y., and Sun, Y. (2010) Molecular basis for polyol-induced protein stability revealed by molecular dynamics simulations. J. Chem. Phys. 132, 225103

61. Colombo, M. F., Rau, D. C., and Parsegian, V. A. (1992) Protein solvation in allosteric regulation: a water effect on hemoglobin. Science. 256, 655-659

62. Goldbeck, R. A., Paquette, J. S., and Kliger, D. S. (2001) The effect of water on the rate of conformational change in protein allostery. Biophys J. 81, 2919-2934

63. Colombo, M. F., and Bonilla-Rodriguez, G. O. (1996) The water effect on allosteric regulation of hemoglobin probed in water/glucose and water/glycine solutions. J. Biol. Chem. 271, 4895-4899

64. Colombo, M. F., and Seixas, F. A. (1999) Novel allosteric conformation of human HB revealed by the hydration and anion effect on O(2) binding. Biochemistry. 38, 11741-11748

65. Arosio, D., Kwansa, H. E., Gering, H., Piszczek, G., and Bucci, E. (2002) Static and dynamic light scattering approach to the hydration of hemoglobin and its supertetramers in the presence of osmolites. Biopolymers. 63, 1-11

66. The PyMOL Molecular Graphics System, Version 1.5.0.4 Schrödinger, LLC.

CHAPTER IV. LINKAGE OF CENTRAL CAVITY TO SYNERGISM IN AMP/FRUCTOSE 2,6-BISPHOSPHATE INHIBITION OF FRUCTOSE-1,6-BISPHOSPHATASE

A paper to be submitted to *Biochemistry*

Yang Gao, Lu Shen and Richard B. Honzatko

Roy J. Carver Department of Biochemistry, Biophysics, and Molecular Biology,

Iowa State University, Ames, IA 50011

Abstract

AMP and fructose 2,6-bisphosphate (Fru-2,6-P_2) synergistically inhibit porcine fructose-1,6-bisphosphatase (pFBPase); whereas for *Escherichia coli* FBPase (eFBPase) synergism is absent even though AMP and Fru-2,6-P_2 are potent inhibitors. AMP and Fru-2,6-P_2 induce 15 ° and 13 ° subunit-pair rotations, respectively, in porcine FBPase; however, the corresponding values in eFBPase are 9 ° and 0 °, respectively. A hydrophobic central cavity in pFBPase, populated by water molecules, is filled with hydrophilic side chains in eFBPase. Explored here is the linkage of AMP/Fru-2,6-P_2 synergism to the central cavity in FBPases. The single mutation Ser^{45}→His substantially fills the central cavity of pFBPase, and the triple mutation, Ser^{45}→His, Thr^{46}→Arg and Leu^{186}→Tyr, replaces porcine with *E. coli*-type side chains. Both single and triple mutations significantly reduce synergism, while retaining other wild-type kinetic properties. Similar to the effect of Fru-2,6-P_2 on eFBPase, the triple mutant of pFBPase with bound Fru-2,6-P_2 exhibits only a 2 ° subunit-pair rotation as opposed to the 13 ° rotation exhibited by the Fru-2,6-P_2 complex of wild-type pFBPase. The side chain at position 45 is small in all available eukaryotic FBPases, but large and hydrophilic in bacterial FBPases similar to eFBPase. Analysis of signature residues indicates the likelihood of FBPases in specific bacterial organisms that exhibit AMP/Fru-2,6-P_2 synergism. These FBPases may be models for an evolutionary precursor of eukaryotic FBPase.

Introduction

Fructose-1,6-bisphosphatase (D-fructose-1,6-bisphosphate 1-phosphohydrolase; EC 3. 1. 3; FBPase[1]) catalyzes the penultimate step in gluconeogenesis, hydrolyzing fructose 1,6-bisphosphate (Fru-1,6-P_2) to fructose 6-phosphate (Fru-6-P) and phosphate (P_i) (1, 2). Frutose-6-phosphate-1-kinase (PFK-1) in glycolysis opposes the action of FBPase by the ATP-dependent phosphorylation of Fru-6-P (3). The coordinated regulation of FBPase and PFK-1 limits futile cycling *in vivo*. In mammals and presumably other eukaryotes, fructose 2,6-bisphosphate (Fru-2,6-P_2) and AMP inhibit FBPase while activating PFK-1 (3-10). *In vivo* AMP concentrations are nearly constant due to the action of adenylate kinase (11), whereas the level of Fru-2,6-P_2 varies in response to changing nutritional states (10). AMP/Fru-2,6-P_2 synergism in the inhibition of eukaryotic FBPases (5, 6, 12, 13), however, lowers the apparent K_i of AMP as concentrations of Fru-2,6-P_2 increase, making both AMP and Fru-2,6-P_2 dynamic physiological regulators.

Porcine liver FBPase (hereafter pFBPase) is a model for eukaryotic FBPases (14). Four identical subunits (molecular weight of 37 kDa) form an approximate square-planar arrangement with D2 symmetry. AMP, which binds 28 Å away from the active site (15, 16), is a non-competitive inhibitor with respect to Fru-1,6-P_2, but a competitive inhibitor with respect to catalytically essential divalent cations (Mg^{2+}, Mn^{2+}, or Zn^{2+}) (13, 17, 18). Binding of AMP induces a conformational transition from active R-state to inactive T-state (16, 19). The R- and T-states differ principally by a 15 ° rotation of upper relative to the lower subunit pair of the tetramer, and by the displacement of loop 50-72 from an active-site engaged conformation to disengaged conformation (16). At least two AMP molecules are required for the R- to T-state transition (20). The dimer-dimer interface is the origin of AMP cooperativity (20). Mutations that disrupt interactions between subunit pairs eliminate the cooperative binding of AMP (21, 22). Two AMP-bound intermediate states (I_R-state and I_T-state) have been identified, both of which have engaged loop 50-72 and subunit-pair rotations of 3 ° and 11 °, respectively (23, 24).

Fru-2,6-P_2 is a competitive inhibitor with respect to Fru-1,6-P_2 (5, 6). Chemical modification, NMR, mutagenesis and crystallographic studies consistently indicate Fru-2,6-

P_2 binding to the active site (14, 25-28). In the presence of Fru-2,6-P_2, the K_i for AMP falls 10 fold (AMP/Fru-2,6-P_2 synergism) (5, 6, 29). Hines *et al.* (14) suggest AMP/Fru-2,6-P_2 synergism arises from a similar end-state induced independently by AMP and Fru-2,6-P_2, and indeed, Fru-2,6-P_2 and AMP cause comparable subunit-pair rotations in pFBPase. Moreover, the crystallographic work is in harmony with similar UV spectra of FBPase in complexes with Fru-2,6-P_2 and AMP (14).

Esherichia coli FBPase (eFBPase) has 41% sequence identity with pFBPase, but a fundamentally different mechanism of regulation (30-32). eFBPase is subject to feed-forward activation by phosphoenolpyruvate, the binding of which favors an active tetramer over an inactive or less active dimer (30-31). AMP and glucose 6-phosphate (Glc-6-P) are synergistic inhibitors that together drive the enzyme to a T-like state (32). Fru-2,6-P_2, although not present in *E. coli*, is a potent inhibitor of eFBPase (14). Unlike pFBPase, there is no Fru-2,6-P_2/AMP synergism for eFBPase and, consistent with the hypothesis of Hines *et al.* (14), eFBPase remains in the R-state in the presence of Fru-2,6-P_2.

The foregoing begs the question: If subunit-pair rotation in response to Fru-2,6-P_2 is necessary for synergism, then why do subunit pairs rotate in pFBPase and not eFBPase? A large cavity is present at the center of the pFBPase tetramer. The cavity has ordered water molecules, which collectively influence the quaternary conformation of the porcine enzyme (33). In eFBPase, however, hydrophilic side chains fill the corresponding region. Shown here by directed mutation, kinetics and structure determinations, the central cavity of pFBPase enables the subunit-pair rotation of the tetramer in response to Fru-2,6-P_2. Moreover, analysis of sequences infers the existence of bacterial FBPases that likely exhibit AMP/Fru-2,6-P_2 synergism, even though these organisms are unlikely to produce Fru-2,6-P_2. Hence, the evolution of Fru-2,6-P_2 as a dynamic regulator of FBPase in eukaryotic systems probably evolved from a primordial FBPase possessing a stable tetrameric assembly with a water-filled central cavity.

Experimental procedures

Materials—Fru-1,6-P_2, $NADP^+$ and AMP came from Sigma. Fru-2,6-P_2 was prepared according to ref 34. Glucose-6-phophate dehydrogenase and phosphoglucose isomerase were purchased from Roche Applied Sciences. The FBPase-deficient *E. coli* strain DF 657 was from the Genetic Stock Center at Yale University. Other chemicals were of reagent grade or equivalent.

Directed mutations of pFBPase— Mutations were accomplished by specific base changes utilizing the Transformer^{TM} site-directed mutagenesis kit (Clontech). The mutagenic primers were as follows: Ser^{45}→His, 5'-CAAGGCCATC**CA**CACCGCAGTC-3'; Thr^{46}→Arg, 5'-CAAGGCCATCTCC**CG**CGCAGTCCGCAAG-3'; Leu^{186}→Tyr, TGCTTCATG**TAT**GA CCCGGCCATC; Ser^{45}→His/Thr^{46}→Arg, 5'-CAAGGCCATC**CA**C**CG**CGCAGTCCGCAA G-3' (codons for point mutations are underlined in bold typeface). The constructs were confirmed by sequencing the promoter region and the entire open reading frame. The Iowa State University sequencing facility provided DNA sequences using the fluorescent dye-dideoxy terminator method.

Expression and purification of wild-type and mutant pFBPases— The supernatant solution of a cell free extract was loaded onto a Cibracon Blue-Sepharose column previously equilibrated with 20 mM Tris-HCl, pH 7.5, 5 mM $MgCl_2$. The column was washed with 20 mM Tris-HCl, pH 7.5. Enzyme was eluted with 5 mM AMP and 20 mM Tris-HCl, pH 7.5. The pH of eluted protein solution was adjusted to 8.5 before loading onto a DEAE-Sepharose column equilibrated with 20 mM Tris-HCl, pH 8.3. Purified enzyme was eluted with a NaCl gradient (0–0.5 M) in 10 mM Tris-HCl, pH 8.3, and then dialyzed extensively against 50 mM Hepes, pH 7.4, for kinetic investigations and for crystallization experiments. Purity and protein concentrations of FBPase preparations were confirmed by SDS-polyacrylamide gel electrophoresis (35) and the Bradford assay (36), respectively.

Kinetics— Phosphoglucose isomerase, and glucose-6-phosphate dehydrogenase were used as coupling enzymes in assays for FBPase (1). For specific activity measurements, reduction of NADP to NADPH was monitored by absorbance at 340 nm. Other assays used the same coupling enzymes but monitored the formation of NADPH by its fluorescence emission at 470 nm using an excitation wavelength of 340 nm. Assays were performed at 22 ℃ in 50

mM Hepes, pH 7.5. Assay solutions contained EDTA and KCl at concentrations of 10 μM and 150 mM, respectively. Data for AMP inhibition with respect to Mg^{2+} and Fru-2,6-P_2 inhibition with respect to Fru-1,6-P_2 were fit to several models using Grafit (37), with best fits of data to model reported here.

Crystallization cavity-filled pFBPase— The method of hanging drops was used in crystallizing Ser^{45}→His/Thr^{46}→Arg/Leu^{186}→Tyr pFBPase (hereafter Cav^- FBPase). 2 μl of protein solution was mixed with 2 μl of precipitant solution. Wells contained 500 μl of the precipitant solution. Crystals of the Fru-2,6-P_2 complex grew from a protein solution (10 mg/ml Cav^- FBPase, 25 mM Hepes, pH 7.4, 5 mM $MgCl_2$, and 5 mM Fru-2,6-P_2) combined with a precipitant solution (100 mM Hepes, pH 7.4, 8% (w/v) polyethylene glycol 3350, 27% (v/v) glycerol, and 5% (v/v) *t*-butyl alcohol). Crystals of AMP complex grew from a protein solution (10 mg/ml Cav^- FBPase, 25 mM Hepes, pH 7.4, 5 mM $MgCl_2$, and 5 mM AMP) combined with a precipitant solution (100 mM Hepes, pH 7.4, 12% (w/v) polyethylene glycol 3350, 23% (v/v) glycerol, and 5% (v/v) *t*-butyl alcohol). Crystals were of equal dimensions (0.2–0.4 mm), growing in approximately 3 days at 20 ℃, and were transferred directly from droplet to liquid nitrogen as cryo-protectants were included in the conditions of crystallization.

X-ray data collection, structure determination, and refinement— Data were collected at Iowa State University from single crystals on a Rigaku R-AXIS IV++ rotating anode/image plate system using CuK_α radiation from an Osmic confocal optics system and a temperature of 110 K. Program d*trek (38) was used in reducing data.

Cav^- FBPase with Fru-2,6-P_2 and AMP are isomorphous to R- and T-state FBPase complexes, respectively. R-state FBPase (PDBID: 1CNQ) and T-state FBPase (PDBID:1EYJ) were used as initial models for molecular replacement. The resulting models underwent refinement using CNS (39) with force constants and parameters of stereochemistry from Engh and Huber (40). A cycle of refinement consisted of slow cooling from 1000 to 300 K in steps of 25 K followed by 100 cycles of conjugate gradient minimization and concluded by the refinement of individual thermal parameters. Restraints of 1.5 $Å^2$ on nearest neighbor and next-to-nearest neighbor main chain atoms, 2.0 $Å^2$ on

nearest neighbor side chain atoms, and 2.5 $Å^2$ on next-to-nearest neighbor side chain atoms were employed in thermal parameter refinement. Water molecules were added to difference electron density of 2.5σ or better until no significant decrease was evident in the R_{free} value. Water molecules in the final models were within acceptable donor-acceptor distances to each other and/or a polar group of the protein. Stereochemistry of the models was analyzed by use of PROCHECK (41).

Results

Rationale for directed mutations— Directed mutations have identified residues essential for AMP binding (20, 42), regulation (43-45), and cooperativity (21-22, 46), and Fru-2,6-P_2 binding (47); however, no mutation eliminates AMP/Fru-2,6-P_2 synergism while retaining potent AMP and Fru-2,6-P_2 inhibition. As eFBPase shares 41% identity with pFBPase but lacks AMP/Fru-2,6-P_2 synergism, some subset of residues that differ must be responsible. The water-filled central cavity of pFBPase, absent in eFBPase, can influence the quaternary state of specific mutants of pFBPase (33). Gao *et al.* (33) have hypothesized that the central cavity enables AMP/inhibitor synergism through water structure reorganization (33). Only three positions in or near the central cavity differ in residue type between eFBPase and pFBPase. Ser^{45}, Thr^{46} and Leu^{186} in the porcine enzyme are large hydrophilic residues, His^{37}, Arg^{38} and Tyr^{180}, respectively, in eFBPase (Fig. 1). Side chains of Ser^{45}/His^{37} point into the central cavity, whereas side chains of Thr^{46}/Arg^{38} and Leu^{186}/Tyr^{180} are at the edge of the cavity. If the central cavity is essential to synergism, then mutations that replace residues of pFBPase with those of eFBPase should significantly reduce AMP/Fru-2,6-P_2 synergism.

Expression and purification of wild-type and mutant pFBPase— Wild type and mutant pFBPases were at least 95% pure on the basis of sodium dodecylsulfate-polyacrylamide gel electrophoresis (data not shown). Gels indicated no proteolysis of the purified enzymes.

Kinetics— His^{45}, Arg^{46} and Cav^{-} FBPase have substantial activity (50%) relative to wild type enzyme (Table 1). The K_m for substrate for Tyr^{186} FBPase is 2-fold greater that for wild-type enzyme. Mutations cause only minor changes in the K_a for Mg^{2+}. AMP is a competitive

inhibitor with respect to Mg^{2+} for all mutants. Hill coefficients of approximately 2 indicate positive coopertivity in AMP binding. The K_i of AMP for Arg^{46} FBPase deceases 6-fold, whereas for other mutants, the K_i for AMP inhibition is comparable to that of wild-type enzyme. Fru-2,6-P_2 is a potent inhibitor, competitive with respect to Fru-1,6-P_2 for all mutants. The K_i for Fru-2,6-P_2 ranges from 0.05 μM for His^{45} FBPase to 0.27 μM for Arg^{46} FBPase. Mutantions here evidently have relatively minor effects on activity and binding affinities of inhibitors.

Saturating concentration of Mg^{2+} (10 mM) and Fru-1,6-P_2 (20 μM) were employed in the measurement of Fru-2,6-P_2/AMP synergism. AMP titrations were done at six concentrations of Fru-2,6-P_2 (0, 0.1, 0.3, 1, 3, and 10 μM) (Fig. 2). Each titration curve is fit to Eqn 1:

$$v = \frac{V_M}{1+(\frac{I}{I_{0.5}})^n} \qquad \text{(Eqn 1)}$$

where v, V_M, I, $I_{0.5}$ and n are velocity, maximum velocity, AMP concentration, AMP concentration that gives 50% inhibition and the Hill coefficient for AMP, respectively. For wild-type, Arg^{46} and Tyr^{186} pFBPase, $I_{0.5}$ of AMP inhibition decreases significantly as Fru-2,6-P_2 concentration increases (indicative of Fru-2,6-P_2/AMP synergism). On the other hand, His^{45} and Cav^- pFBPase show little change. For all enzymes, AMP cooperativity decreases as Fru-2,6-P_2 concentrations increase. Hill coefficients for AMP binding are close to 2 at low Fru-2,6-P_2 concentration but fall to unity at high Fru-2,6-P_2 concentration. $I_{0.5}$ at different Fru-2,6-P_2 concentrations can be fit to Eqn 2 (14):

$$I_{0.5} = I_{0.5}^{high} + \frac{I_{0.5}^{low} - I_{0.5}^{high}}{1+\frac{I_b}{\alpha_b}} \qquad \text{(Eqn 2)}$$

where $I_{0.5}$ is the AMP concentration that causes 50% inhibition, $I_{0.5}^{high}$ is the AMP concentration that causes 50% inhibition in the presence of an infinite concentration of Fru-2,6-P_2, $I_{0.5}^{low}$ is the AMP concentration that causes 50% inhibition in the absence of Fru-2,6-P_2, I_b is the concentration of Fru-2,6-P_2, α_b is the concentration of Fru-2,6-P_2 that produces a 50% synergistic effect. The value of ($I_{0.5}^{low}/I_{0.5}^{high}$) is a measure of Fru-2,6-P_2/AMP synergism.

Fitted values for Fru-2,6-P_2/AMP synergism are in Table 2. For wild-type pFBPase, Fru-2,6-P_2 enhances AMP inhibition by ~8-fold, whereas for His^{45} and Cav^{-} pFBPase $I_{0.5}^{low}/I_{0.5}^{high}$ values are approximately 3 and 2, respectively.

AMP complex of Cav^{-} FBPase (Protein Data Bank code 4GWS)— Crystals of the AMP complex of Cav^{-} pFBPase are in space group $P2_12_12$ (*a*=60.78 Å, *b*=166.54 Å and *c*=79.21 Å), isomorphous to crystals of canonical T-state pFBPase. A C1-C2 dimer exists in the asymmetric unit. Both monomers in the model start from residue 9. Electron density for residues 60-72 in the dynamic loop is weak, and associated with high B-parameters. Statistics for data collection and refinement are in Table 3.

The AMP complex of Cav^{-} pFBPase is T-state, with a 15 ° subunit-pair rotation and a disengaged loop 50-72. The root-mean-squared deviation (RMSD) in Cα carbons between AMP complexes of Cav^{-} and wild-type pFBPase (both in the T-state) is 0.3 Å. One molecule each of Fru-6-P, Mg^{2+}, P_i, and AMP binds to each subunit. Side chains of His^{45} and Tyr^{186} in Cav^{-} pFBPase are clear in the electron density map; however, the side chain of Arg^{46} is disordered. Further details regarding the structure of the AMP complex of pFBPase is in the literature (16).

Fru-2,6-P_2 Complex of Cav^{-} FBPase (Protein Data Bank code 4GWU)— Crystals of Fru-2,6-P_2 complexes of Cav^{-} pFBPase belong to space group *I222* (*a*=54.00 Å, *b*=81.22 Å, and *c*=165.06 Å) and are isomorphous to crystals of wild-type pFBPase in its R-state (PDB code 1CNQ). The asymmetric unit is a monomer. Electron density for residues 1-6 and 50-70 is absent. Electron density for residues 22-27 at the AMP binding site is weak and with high B values, consistent with previously reported R-state structures (48). Side chains of His^{45} and Tyr^{186} are clear in electron density maps whereas the side chain of Arg^{46} is disordered (Fig. 1). Electron density confirms the presence of bound Fru-2,6-P_2. Mg^{2+} at metal site-1 is in contact with the 1-hydroxyl group and 2-phosphoryl group of Fru-2,6-P_2.

Superposition of the entire tetramer of the Fru-2,6-P_2 complex of Cav^{-} pFBPase onto the wild-type R-state, wild-type Fru-2,6-P_2 complex and wild-type T-state yields root-mean-square deviations in C_α coordinates of 0.75, 2.3 and 2.5 Å, respectively. The Fru-2,6-P_2

complex of Cav$^-$ pFBPase is near the canonical R-state, exhibiting a 2 ° subunit-pair rotation as opposed to the 13 ° rotation of the Fru-2,6-P_2 complex of wild-type pFBPase (14). The 2 ° rotation in Fru-2,6-P_2 complex of Cav$^-$ pFBPase is similar to the 3 ° rotation of the I_R-state induced by AMP in Leu^{54} pFBPase (23). The shearing of helices H1 and H2 observed in the AMP complex of Leu^{54} pFBPase is evident in the Fru-2,6-P_2 complex of Cav$^-$ pFBPase, as is the loss of the hydrogen bond between Asn^{35} and Thr^{14} and the movement of Ile^{10} moves from its hydrophobic pocket (Fig. 3).

Fru-2,6-P_2 induces local conformational change in Cav$^-$ pFBPase similar to that induced in wild-type pFBPase (14). Loop 121-126 moves towards Fru-2,6-P_2 probably in response to hydrogen bonds formed between backbone amide groups of Ser^{123} and Ser^{124} and the 2-phosphoryl group of Fru-2,6-P_2. α-Carbons of Glu^{97} and Glu^{98} move toward the Mg^{2+} at site-1, most likely a consequence of altered metal coordination due to the absence of metal at site-2. Movements in residues 97-98 and 121-126 may block Asp^{74} from forming a functionally essential hydrogen bond with the C-terminal end of loop 50-72. Loop 50-72 itself is disordered, and metal cations are absent from sites 2 and 3. The conformation of loop 264-274 in the Fru-2,6-P_2 complex of Cav$^-$ pFBPase is nearly identical to that of the product complex of wild-type pFBPase (R-state), having not undergone the conformational change observed in the R- to T-state transition.

Sequence Analysis of Type-I FBPases— The alignment and hierarchical clustering of 307 Type I FBPase sequences from the uniprot database (49) employed the ClustalW web server (*www.genome.jp/tools/clustalw*). Comparison of sequence positions occupied by signature residues responsible for AMP inhibition, tetramer stability, Glc-6-P inhibition, phosphoenolpyruvate activation, and cavity formation segregate FBPases into groups with mutually exclusive regulatory mechanisms. Position 45, for instance, is a small side-chain residue in eukaryotic FBPases, but large and hydrophilic in *E. coli*-like FBPases (Fig. 5). Residue 112 is critical for AMP inhibition (42) and is lysine in the vast majority of eukaryotic and *E. coli*-like FBPases. The salt link between Lys^{42} and Glu^{192} is essential to tetramer stability, and position 192 is glutamate in eukaryotic FBPase, but a non-charged residue type in *E. coli*-like FBPases (30, 31). Positive charges at positions 228 and 38 are

important for Glu-6-P inhibition and anion activation in eFBPase, respectively, both of which are absent in eukaryotic FBPases (30-32).

Signature residue information applied to sequences of 307 Type I FBPase leads to predictions of regulatory properties (Fig. 6). Sequences of eukaryotic FBPases fall into blocks of relatively high similarity corresponding to fungi, mammalian muscle, mammalian liver, and plants. The eukaryotic FBPases should be stable tetramers subject to synergistic inhibition by AMP and Fru-2,6-P_2 (signature residues for the AMP site, tetramer stability and central cavity are present). Plant chloroplasts have a distinct AMP-independent regulatory mechanism (52, 53), and define a block separate from eukaryotic FBPases. A block with 64 sequences in the middle of the similarity matrix includes *E. coli* FBPase. These E. coli-like FBPases have residue types associated with phosphoenolpyruvate activation, a dynamic equilibrium between dimer and tetramer forms, AMP inhibition, no central cavity and hence, no AMP/Fru-2,6-P_2 synergism. More than half of all similarity blocks have scant or no experimental data regarding regulatory properties. FBPases in the large block at the top right of the similarity matrix, for instance, should lack all known mechanisms of FBPase inhibition (AMP and/or Glc-6-P inhibition or reversible disulfide bond formation) and yet be stable tetramers.

Discussion

Ser^{45}→His and Cav^- mutations of pFBPase represent first instances of mutant pFBPases that retain potent AMP and Fru-2,6-P_2 inhibition with greatly reduced AMP/Fru-2,6-P_2 synergism. Kinetic parameters for catalysis, Mg^{2+} activation, AMP inhibition and Fru-2,6-P_2 inhibition of all cavity mutants of pFBPase investigated here are similar to those of the wild-type enzyme. Reduced Fru-2,6-P_2/AMP synergism in Cav^- pFBPase is not due to the disruption of the active or allosteric binding sites, but rather to an impaired quaternary response: Cav^- pFBPase exhibits only a 2 °subunit-pair rotation and disordered loop 50-72 in its Fru-2,6-P_2 complex, in contrast to the 13 °subunit-pair rotation and disengaged loop 50-72 for wild-type pFBPase. Reduced synergism in Cav^- pFBPase arises arguably from the failure

of loop 50-72 to achieve its disengaged conformation in response to bound Fru-2,6-P_2 and the loss of water molecules at the center of the tetramer.

The effect of AMP on Leu^{54} pFBPase provides insights as to how mechanical processes of the protein contribute to Fru-2,6-P_2/AMP synergism. The binding of AMP to Leu^{54} pFBPase shears helices H1 and H2, disrupting hydrogen bonds at the C1-C4 interface (23). Subunit-pair rotation to the T-state re-establishes disrupted hydrogen bonds and also squeezes the loop 50-72 out of its engaged conformation (24). Once displaced from the active site loop 50-72 acquires its disengaged conformation in the case of wild-type pFBPase, but the Ala^{54}→Leu mutation blocks the disengaged conformation of loop 50-72.

Now the binding of Fru-2,6-P_2 to Cav^- pFBPase displaces the engaged loop directly, and helices H1 and H2 exhibit a shear virtually identical to that caused by AMP in its complex with Leu^{54} pFBPase (Fig. 3). Cav^- pFBPase simply traps the Fru-2,6-P_2-bound tetramer early in the R- to T-state transition much like the Leu^{54} pFPBase traps an AMP-bound tetramer (23); however, Cav^- pFBPase differs in that a disengaged conformation for loop 50-72 (and a canonical T-state) is still possible. (Note, the AMP complex of Cav^- pFBPase is in the canconical T-state). The Fru-2,6-P_2 complex of Cav^- pFBPase does not form the disengaged conformation of loop 50-72 because of structural changes to the center or the tetramer. Those changes impact solvent structure (Fig. 1). The side chain of His^{45} does not cause steric conflict in eFBPase or Cav^- pFBPase. Ser^{45}→His does not interfere directly with the R- to T-state transition. On the other hand, His^{45} may disrupt the hydrogen bonding network associated with ordered water molecules at the central cavity of pFBPase. The *Van der Waals* volume is 137 $Å^3$ for His and 89 $Å^3$ for Ser (50). Replacement of Ser by His disrupts the clathrate-like structures of 48 water molecules in the central cavity, observed in I_R-state.

Order/disorder phenomena involving water molecules of the central cavity of wild-type pFBPase are factors in the quaternary transition (33). The binding of AMP to wild-type pFBPase pushes the tetramer into an intermediate quaternary state, which on the basis of crystal structures and molecular dynamics simulations enhances the structure and stability of water in the central cavity (33). The movement of the loop 50-72 from the engaged to

disengaged conformation, causes an order-to-disorder transition in water molecules of the central cavity and contributes a favorable contribution to the overall free energy change of the R- to T-state transition. In the absence of a hydrated central cavity (as is the case for Cav^- pFBPase) this favorable contribution to the overall free energy balance disappears, and hence, the binding of Fru-2,6-P_2, which displaces the engaged conformation of loop 50-72, has a diminished effect on AMP binding.

Fru-2,6-P_2/AMP synergism, although reduced, is still present in His^{45} and Cav^- pFBPase. The 2 ° subunit-pair rotation caused by Fru-2,6-P_2 in Cav^- pFBPase is similar to changes induced by AMP in Leu^{54} pFBPase (I_R-state, 3 ° subunit-pair rotation). Structural changes at C1-C4 interface due to small subunit-pair rotations could be the structural basis for the weak synergism that remains in Cav^- pFBPase. Indeed, wild-type and pFBPase mutant enzymes here exhibit reduced AMP cooperativity in the presence of Fru-2,6-P_2, which may come from conformational changes at the C1-C4 interface (such as the weakening of the hydrogen bond between Glu^{192} and Thr^{39}) within the first few degrees of subunit-pair rotation. The model above predicts that an engaged dynamic loop in the presence of bound Fru-2,6-P_2 would eliminate Fru-2,6-P_2/AMP synergism altogether, and in fact, such is the case for eFBPase: no Fru-2,6-P_2/AMP synergism and the complex of Fru-2,6-P_2 with wild-type eFBPase reveals a dynamic loop in its engaged conformation (14).

The failure of the loop 50-72 to achieve a disengaged conformation in its Fru-2,6-P_2 complex of Cav^- pFBPase is also consistent with the results of targeted molecular dynamics simulations which indicate the transition of loop 50-72 from an engaged to disengaged conformation comes late in the R- to T-state transition (24). Moreover, previous work ties the conformational change in loop 264-274 to subunit-pair rotation from the I_R- to I_T-state (from 3 ° to 12 °, respectively) (23). A comparison of the Fru-2,6-P_2 complexes of Cav^- and wild-type pFBPases reaffirms the correlation between movement of loop 264-274 and a subunit-pair rotation from a near R-state to a near T-state tetramer.

On the basis of molecular dynamics simulations, the stability of waters in the central cavity is related to quaternary changes in FBPase (33). Indeed, for specific mutant forms of pFBPase, water molecules adopt stable and well ordered clusters. Moreover, FBPase activity

in the presence of AMP is dependent on organic solvents that cause change in the properties of bulk water, suggesting the structure of water molecules in the central cavity is on par with the effects caused by AMP or Fru-2,6-P_2 on the quaternary state of FBPase.

AMP and Fru-2,6-P_2 work synergistically in inhibiting mammalian FBPases. Observations here suggest that any tetrameric FBPase with a signature residues of a central cavity should exhibit AMP/Fru-2,6-P_2 synergism. Hence, all eukaryotic organisms for which sequences of FBPase are known should exhibit AMP/Fru-2,6-P_2 synergism, and to the best of our, knowledge all eukaryotic organisms make Fru-2,6-P_2.

Fru-2,6-P_2, however, is not present in bacteria systems (51). Instead, *E. coli* employs Glc-6-P as a synergistic inhibitor with respect to AMP (32). Unlike Fru-2,6-P_2, Glc-6-P is an allosteric non-competitive inhibitor with respect to substrate. Vastly different kinetic properties and a distinct allosteric binding site for Glc-6-P in eFBPase makes Glc-6-P an unlikely direct precursor of Fru-2,6-P_2 through evolution. In our predictions (Fig. 6), FBPases from *Leptospira*, which lies between eukaryotic FBPases and E. coli-like FBPases in the similarity matrix, are most similar to eukaryotic FBPases, having key residues for AMP inhibition, tetramer formation and AMP/Fru-2,6-P_2 synergism. Characterization of one of the *Leptospira* FBPases may extend our understanding of evolution of AMP/Fru-2,6-P_2 synergism in eukaryotic FBPases. Moreover, the sequence analysis also indicates a large block of FBPases (top right corner of the similarity matrix) that have neither AMP nor Glu-6-P inhibition. A novel inhibitory mechanism may be present in this group of FBPases.

TABLE 1. Parameters from the kinetics of wild type and mutant forms of pFBPase.

Assay conditions are 50 mM Hepes, pH 7.5, 150 mM KCl and 10 μM EDTA. Values in parenthesis are standard deviations in the last significant digit.

pFBPase	Specific activity ($\mu mol\ s^{-1}mg^{-1}$)[a]	K_M Fru-1,6-P_2 (μM)[b]	Hill coef. Mg^{2+} [c]	K_a Mg^{2+} (mM)^2 [d]	Hill coef. AMP [e]	K_i AMP (μM)^2 [f]	K_i Fru-2,6-P_2 (μM) [g]
WT	25 (1)	1.47 (7)	1.7 (1)	0.70 (5)	2.2 (1)	0.76 (8)	0.14 (1)
S45H	11.9 (7)	1.07 (7)	1.6 (1)	1.0 (1)	1.8 (1)	0.35 (5)	0.053 (9)
T46R	12.3 (9)	0.68 (8)	1.8 (2)	0.93 (9)	2.4 (2)	4.8 (2)	0.27 (5)
L186Y	21.0 (7)	1.1 (1)	1.6 (1)	0.68 (4)	1.7 (2)	0.58 (9)	0.16 (1)
Cav^-	15.2 (9)	1.1 (2)	1.8 (1)	0.82 (6)	2.2 (2)	0.56 (4)	0.14 (1)

[a]Determined at saturating Fru-1,6-P_2 (20 μM) and Mg^{2+} (5 mM for wild-type and 10 mM for mutant FBPases). Reported values come from five repetitions.

[b]Determined at saturating Mg^{2+} (5 mM for wild-type and 10 mM for mutant FBPases). The concentrations of Fru-1,6-P_2 varies from 0.3 to 20 μM.

[c]Hill coefficient for Mg^{2+} employed 0.2 to 20 mM Mg^{2+} and saturating Fru-1,6-P_2 (20 μM).

[d]Determined by using concentrations in Mg^{2+} from 0.5–5 mM and Fru-1,6-P_2 from 0.5–10 μM.

[e]Determined by using concentrations in AMP from 0.1–100 μM and saturating Fru-1,6-P_2 (20 μM) and Mg^{2+} (10 mM).

[f]Determined by using concentrations in Mg^{2+} from 0.5–5 mM with saturating Fru-1,6-P_2 (20 μM). AMP concentrations range from 0–5 μM for wild-type FBPase, 0–3 μM for His^{45} FBPase, 0–20 μM for Arg^{46} FBPase, 0–5 μM for Tyr^{186} and Cav^- FBPases.

[g]Determined by using Mg^{2+} (5 mM for wild-type and 10 mM for mutant FBPases) and Fru-1,6-P_2 concentrations from 0.5–10 μM. Concentrations of Fru-2,6-P_2 range from 0–1 μM for wild-type FBPase, 0–0.5 μM for His^{45} FBPase, 0–1 μM for Arg^{46} FBPase, and 0–1 μM for Tyr^{186} FBPase and Cav^- FBPases.

TABLE 2. Fru-2,6-P_2/AMP synergism for wild type and mutant forms of pFBPase.

Quantities $I_{0.5}^{high}$ and $I_{0.5}^{low}$ are defined in the results section.

Value in parentheses are uncertainties in the last significant digit.

	Wild-type	Ser^{45}→His	Thr^{46}→Arg	Leu^{186}→Tyr	Cav^{-}
$\boldsymbol{I_{0.5}^{high}}$ [a](μM)	0.6 (1)	0.6 (1)	1.9 ±0.4	0.53 (9)	0.8 (1)
$\boldsymbol{I_{0.5}^{low}}$ [a](μM)	4.4 (2)	1.87 (6)	11.6 ±0.5	2.77 (9)	2.0 (1)
$\boldsymbol{I_{0.5}^{low}/I_{0.5}^{high}}$	7 (2)	3.1 (7)	6 (2)	5 (1)	2.5 (5)

TABLE 3. Statistics of data collection and refinement for Cav⁻ FBPase.

	Fru-2,6-P_2 complex[a]	AMP complex[a]
Resolution limit (Å)	3.00	2.75
Number of measurements	26,045	50,125
Number of unique reflections	7,478	17,334
Completeness of data (%):		
Overall	98.4	82.0
Last shell/resolution-range (Å)	99.9/3.11-3.00	85.5/2.85-2.75
R_{sym}[b]		
Overall	0.163	0.100
Last shell/resolution-range (Å)	0.516/3.11-3.00	0.272/2.85-2.75
Number of reflections in refinement	7,104	16,412
Number of atoms	2,489	5,399
Number of solvent sites	88	281
R_{factor}[c]	0.211	0.198
R_{free}[d]	0.283	0.247
Mean B ($Å^2$) overall/protein	55/55	24/24
Mean B ($Å^2$) for Fru-2,6-P_2	49	—
Mean B ($Å^2$) for AMP	—	29
Root mean square deviations:		
Bond lengths (Å)	0.014	0.012
Bond angles (deg.)	1.6	1.7

[a]Unit cell lengths (*a*, *b*, *c*) in Å for the Fru-2,6-P_2 and AMP complexes are (54.00, 81.22, 165.06), and (60.24, 164.28, 79.14), respectively. Unit cell angles (α, β, γ) are 90° for space groups I222 and $P2_12_12$.

[b]$R_{sym} = \Sigma_j\Sigma_i \mid I_{ij} - \langle I_j \rangle \mid / \Sigma_i\Sigma_j I_{ij}$, where *i* runs over multiple observations of the same intensity, and *j* runs over all crystallographically unique intensities.

[c]$R_{factor} = \Sigma \parallel F_{obs} \mid - \mid F_{calc} \parallel / \Sigma \mid F_{obs} \mid$, where $\mid F_{obs} \mid > 0$.

[d]R_{free} based upon 10% of the data randomly culled and not used in the refinement.

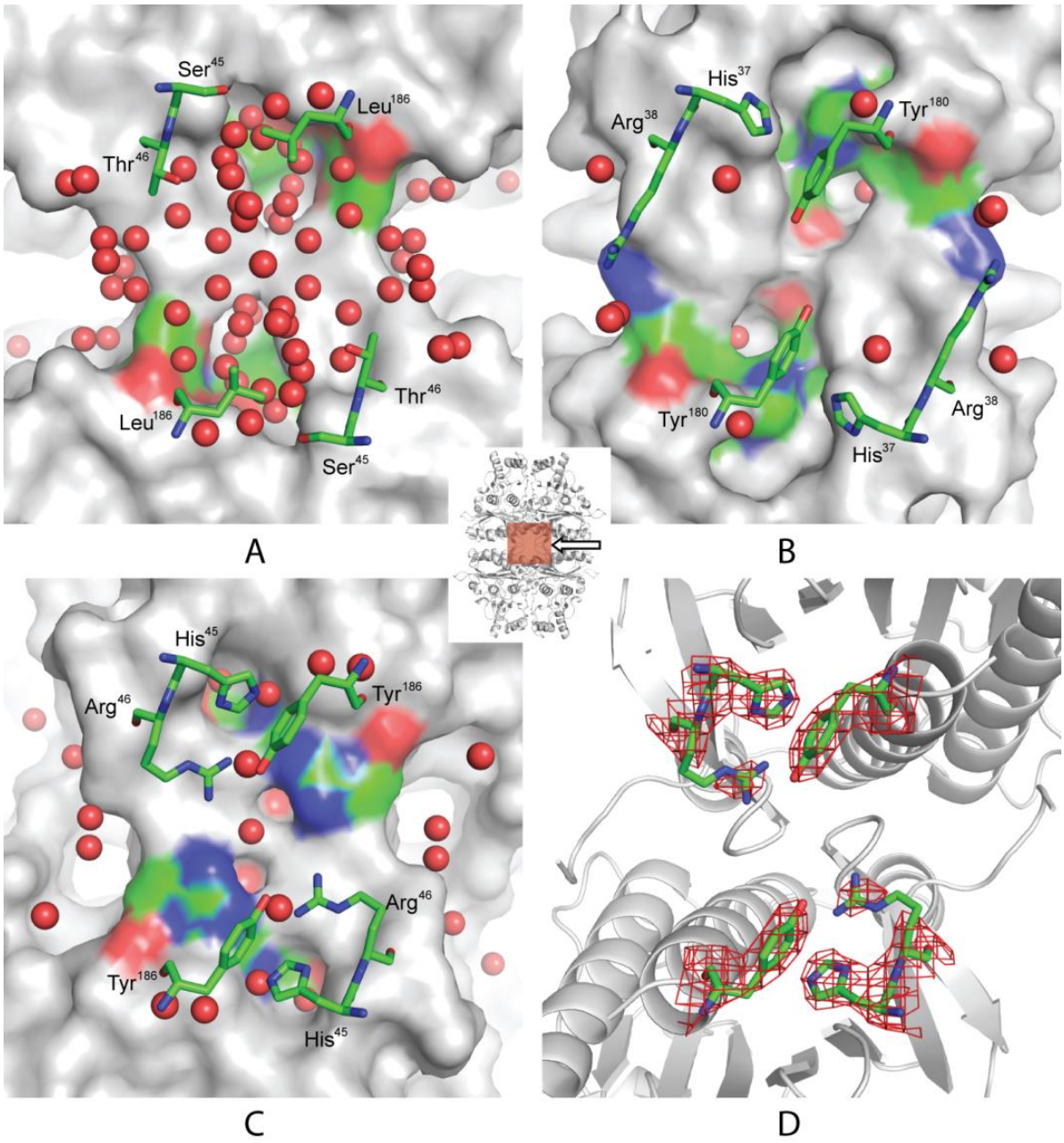

Figure 1. Central cavity regions of FBPases. Leu^{54} pFBPase (I_R-state, AMP complex, *panel A*) and eFBPase (R-state, phosphoenolpyruvate complex, *panel B*) exhibit significant differences in hydration levels at the center of the tetramer. Mutation of positions 45, 46 and 186 to *E. coli* type residues (Cav$^-$ FBPase) has hydration levels comparable to eFBPase (Fru-2,6-P_2 complex of Cav$^-$ pFBPase, near R-state, *panel C*). Electron density covering positions 45, 46 and 186 (Fru-2,6-P_2 complex of Cav$^-$ pFBPase, *panel D*). The surface renderings are of subunits C1 and C4 of the tetramer, with ball-and-stick models representing selected residues from subunits C2 and C3 and water molecules (red spheres). The icon at the center with associated arrow indicates the region viewed and viewing direction, respectively. Image generated with Pymol (54).

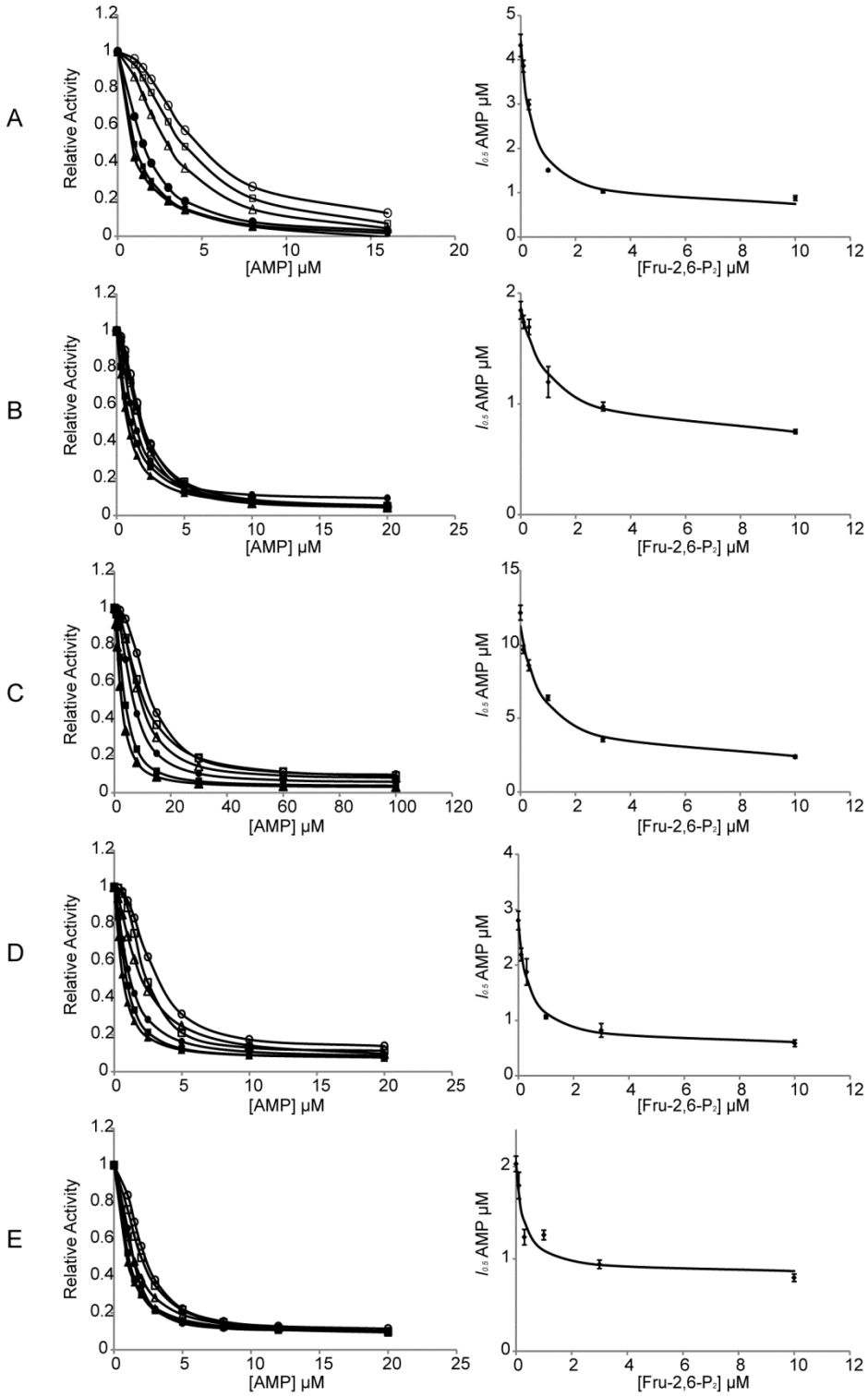

Figure 2. AMP/Fru-2,6-P_2 synergism for wild-type and mutant FBPases. Panels A-E come from assays using wild-type, His^{45}, Arg^{46}, Tyr^{186} and Cav^{-} pFBPases, respectively. Reaction velocities as a function of AMP concentration (*left*) are taken at 0 (○), 0.1 (□), 0.3 (△), 1 (●), 3 (■), and 10 μM (▲) Fru-2,6-P_2. $I_{0.5}$ values from the curves on the left are plotted against Fru-2,6-P_2 concentrations (*right*).

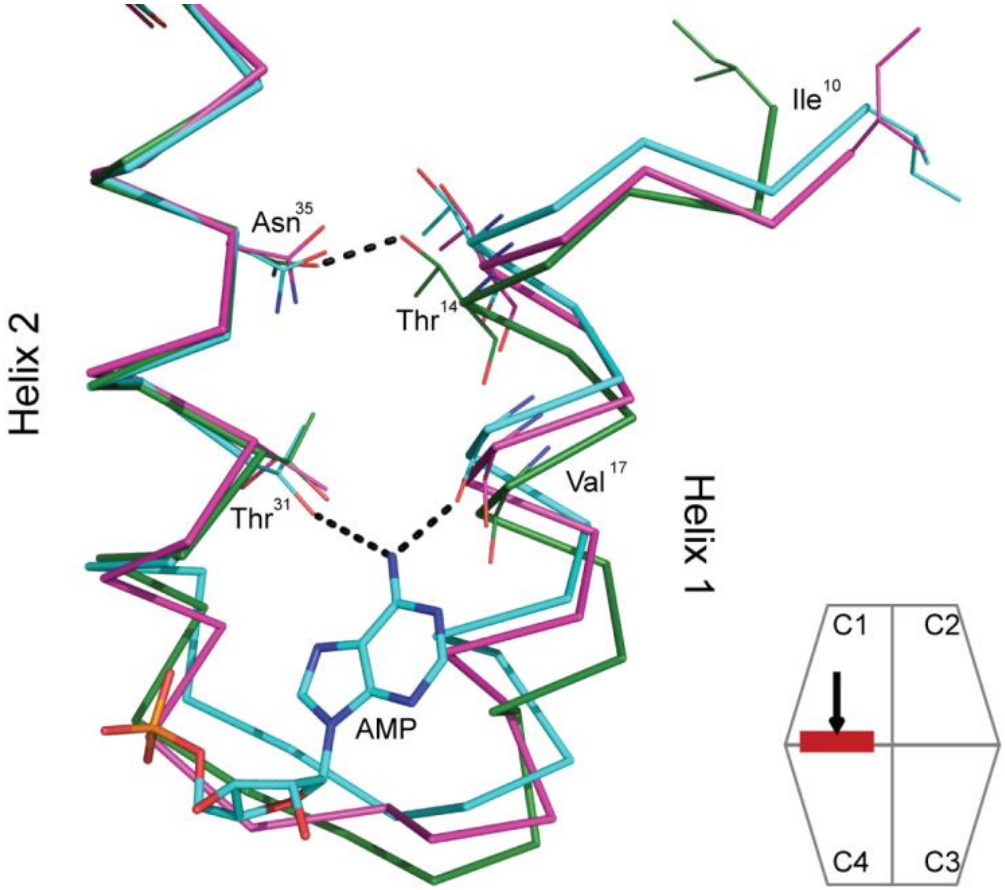

Figure 3. Conformation changes at the C1-C4 interface. Subunits are aligned for the Fru-2,6-P_2 complex of Cav^- pFBPase (*magenta*), the AMP complex of Leu^{54} pFBPase (*cyan*) and the product complex of wild-type pFBPase (*green*). Dotted lines indicate hydrogen bonds. The relative positions of helices H1 and H2 are similar in the Fru-2,6-P_2 complex of Cav^- pFBPase and AMP complex of Leu^{54} pFBPase, which have subunit-pair rotations of 2 °and 3 °, respectively, relative to the R-state product complex of wild-type pFBPase.

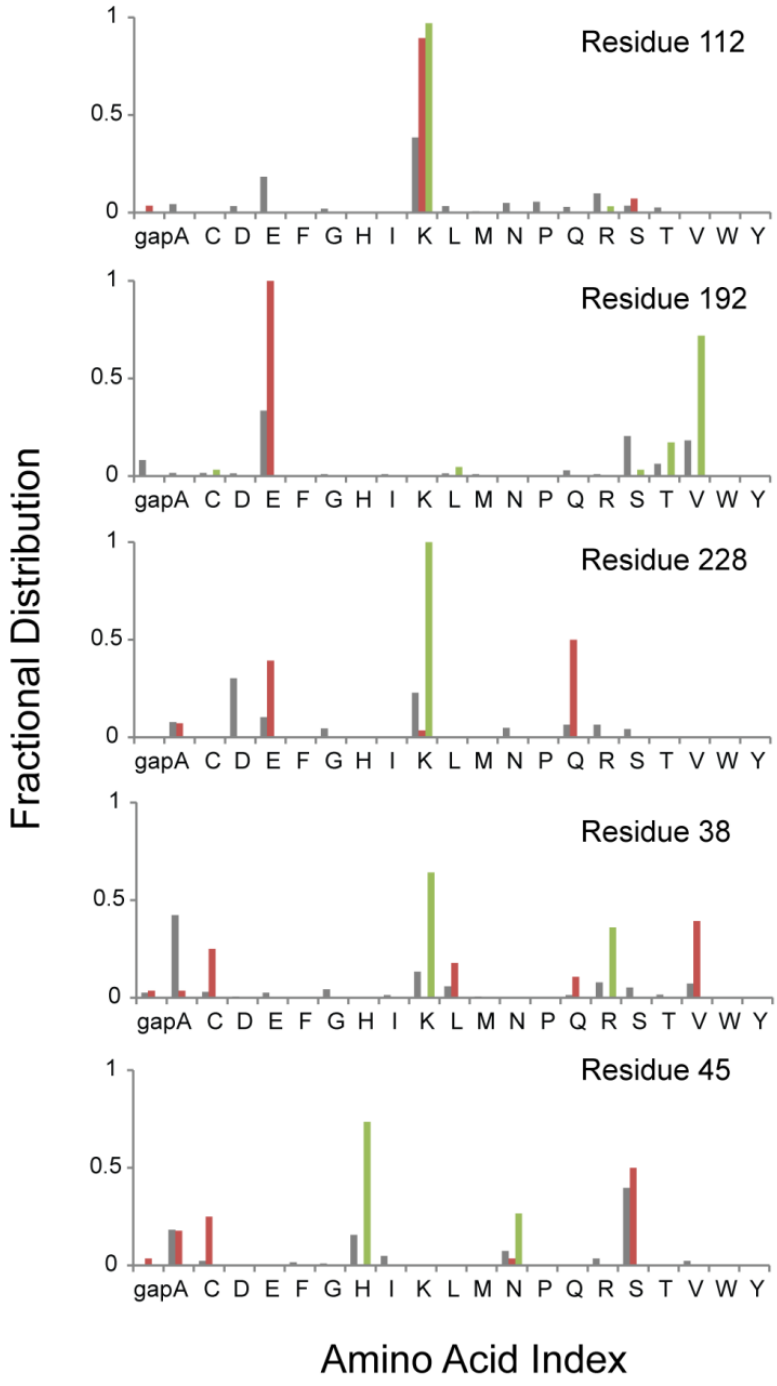

Figure 4. Conservation of selected signature residues associate with regulatory mechanisms of FBPase. Amino acid types associated with sequence positions essential for AMP inhibition (residue 112), tetramer formation (residue 192), Glc-6-P inhibition (residue 228), anion activation (residue 38), and central cavity formation (residue 45) are presented from top to bottom. Grey, red and green columns represent the amino acid type for all FBPases, eukaryotic FBPases and *E. coli*-like FBPases, respectively.

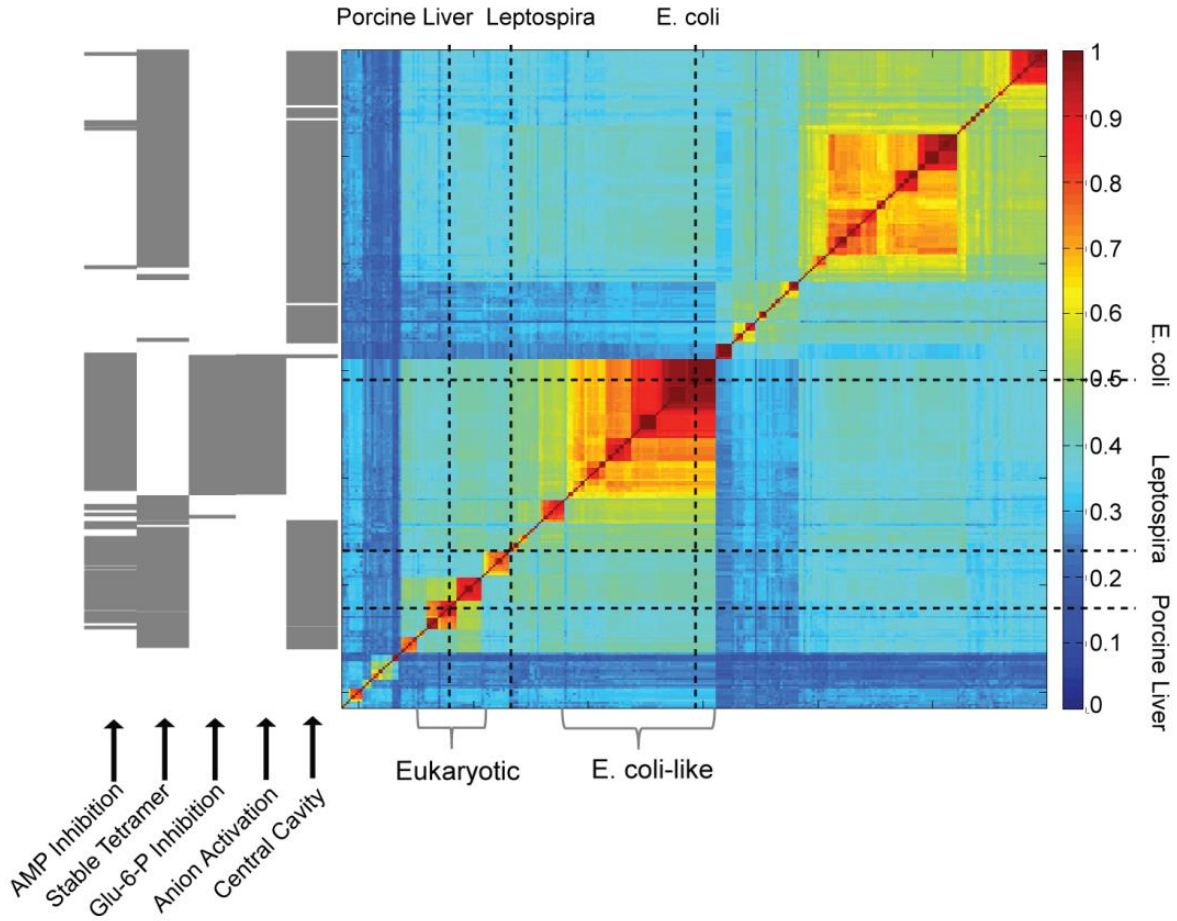

Figure 5. Similarity matrix of Type-I FBPase sequences and the prediction of structural and regulatory properties. The fraction of identical residues in sequence pairs are represented by color according to the scale on the right-hand side of the similarity matrix. The positions of eFBPase, pFBPase and the FBPase from *Leptospira interogans* are marked by vertical and horizontal dotted lines. FBPases from eukaryotic systems and *E. coli*-like are indicated by brackets. Regulatory properties are predicted (gray bar) according to residue types associated with key positions in the amino acid sequence. AMP inhibition, requires serine or threonine for residue 31, lysine or arginine for residue 112, and tyrosine for residue 113. Tetramer stability requires lysine or arginine for residue 42, and glutamate for residue 192. Glc-6-P inhibition requires tyrosine for residue 216, lysine or arginine for residue 228, and glutamine for residue 231. Anion activation requires glycine for residue 14, lysine or arginine for residue 38, lysine or arginine for residue 88, and not glutamate for residue 192. Presence of a central cavity (AMP/Fru-2,6-P_2 synergism) requires small side chains (glycine, alanine, cysteine, serine, or gap) for residue 45.

Reference

1. Benkovic, S. J., and de Maine, M. M. (1982) Mechanism of action of fructose 1,6-bisphosphatase. Adv. Enzymol. Relat. Areas Mol. Biol. 53, 45–82

2. Tejwani, G. A. (1983) Regulation of fructose-bisphosphatase activity. Adv. Enzymol. Relat. Areas Mol. Biol. 54, 121–194

3. Blangy, D., Buc, H. & Monod, J. (1968) Kinetics of the allosteric interactions of phosphofructokinase from Escherichia coli. J. Mol. Biol. 31, 13-35.

4. Taketa, K., and Pogell, B. M. (1965) Allosteric inhibition of rat liver fructose 1,6-bisphosphatase by adenosine 5'-monophosphate. J. Biol. Chem. 240, 651–662

5. Pilkis, S. J., El-Maghrabi, Pilkis, J., and Claus, T. (1981) Inhibition of fructose-1,6-bisphosphatase by fructose 2,6-bisphosphate. J. Biol. Chem. 256, 3619–3622

6. Van Schaftingen, E., and Hers, H.-G. (1981) Inhibition of fructose-1,6-bisphosphatase by fructose 2,6-biphosphate. Proc. Natl. Acad. Sci. U. S. A. 78, 2861–2863

7. Pilkis S. J., El-Maghrabi, Pilkis, J., Claus, T. H., and Cumming D. A. (1981) Fructose 2,6-bisphosphate. A new activator of phosphofructokinase. J. Biol. Chem. 256, 3171–3174

8. Van Schaftingen, E., Jett, M.-F., Hue, L., and Hers, H.-G. (1981) Control of liver 6-phosphofructokinase by fructose 2,6-bisphosphate and other effectors. Proc. Natl.Acad. Sci. U. S. A. 78, 3483–3486

9. Uyeda, K., Furuya, E., and Luby, L. J. (1981) The effect of natural and synthetic D-fructose 2,6-bisphosphate on the regulatory kinetic properties of liver and muscle phosphofructokinase. J. Biol. Chem. 256, 8394–8399

10. Okar, D. A., and Lange, A. J. (1999) Fructose-2,6-bisphosphate and control of carbohydrate metabolism in eukaryotes. Biofactors 10, 1–14

11. Derr, R.F. and Zieve, L. (1972) Adenylate energy charge: relation to guanylate energy charge and the adenylate kinase equilibrium constant. Biochem. Biophys. Res. Commun. 49, 1385-1390

12. Stone, S. R., and Fromm, H. J. (1980) Studies on the mechanism of adenosine 5'-monophosphate inhibition of borvine liver fructose 1,6-bisphosphatase. Biochemistry 19, 620–625

13. Nimmo, H. G., and Tipton, K. F. (1975) The effect of pH on the kinetics of beef-liver fructose bisphosphatase. Eur. J. Biochem. 58, 567–574

14. Hines, J. K., Chen, X., Nix, J. C., Fromm, H. J., and Honzatko, R. B. (2007) Structures of mammalian and bacterial fructose-1,6-bisphosphatase reveal the basis for synergism in AMP/fructose 2,6-bisphosphate inhibition. J. Biol. Chem. 282, 36121–36131

15. Ke, H., Zhang, Y., and Lipscomb, W. N. (1990) Crystal structure of fructose-1,6-bisphosphatase complexed with fructose 6-phosphate, AMP and magnesium. Proc Natl. Acad. Sci. U.S.A. 87, 5243-5247

16. Choe, J. Y., Fromm, H. J. and Honzatko, R. B. (2000) Crystal structures of fructose 1,6-bisphosphatase: mechanism of catalysis and allosteric inhibition revealed in product complexes. Biochemistry. 39, 8565-8574

17. Scheffler, J. E., and Fromm, H. J. (1986) Regulation of rabbit liver fructose-1,6-bisphosphatase by metals, nucleotides, and fructose 2,6-bisphosphate as determined from flurescence studies. Biochemistry 25, 6659–6665

18. Liu, F. and Fromm, H.J. (1988) Purification and characterization of fructose-1,6-bisphosphatase from bovine brain. Arch. Biochem. Biophys. 260, 609-615

19. Zhang, Y., Liang, J. Y., Huang, S., and Lipscomb, W. N. (1994) Toward a mechanism for the allosteric transition of pig kidney fructose-1,6-bisphosphatase. J. Mol. Biol. 244, 609

20. Nelson, S. W, Honzatko, R. B., and Fromm, H. J. (2002) Hybrid tetramers of porcine liver fructose-1,6-bisphosphatase reveal multiple pathways of allosteric inhibition. J. Biol. Chem. 277, 15539-15545

21. Shyur, L.-F., Aleshin, A. E., Honzatko, R. B. and Fromm, H. J. (1996) Site-directed mutagenesis of residues at subunit interfaces of porcine fructose-1,6-bisphosphatase. J. Biol. Chem. 271, 3005-3010

22. Shyur, L.-F., Aleshin, A. E., Honzatko, R. B. and Fromm, H. J. (1996) Biochemical properties of mutant and wild-type fructose-1,6-bisphosphatases are consistent with the coupling of intra- and intersubunit conformational changes in the T- and R-state transition. J. Biol. Chem. 271, 33301-33307

23. Iancu, C. V., Mukund, S., Fromm, H. J., and Honzatko, R. B. (2005) R-state AMP complex reveals initial steps of the quaternary transition of fructose-1,6-bisphosphatase. J. Biol. Chem. 280, 19737–19745

24. Gao, Y., Iancu, C. V., Mukund, S., Choe, J. Y., and Honzatko, R. B. Mechanism of displacement of catalytically essential loop from the active site of fructose-1,6-bisphosphatase. In preparation.

25. Ganson, N.J., and Fromm, H.J. (1985) Nuclear magnetic resonance studies of fructose 2,6-bisphosphate and adenosine 5'-monophosphate interaction with bovine liver fructose-1,6-bisphosphatase. J. Biol. Chem. 260, 2837-2843

26. Liu, F., and Fromm, H. J. (1988) Interaction of fructose 2,6-bisphosphate and AMP with fructose-1,6-bisphosphatase as studied by nuclear magnetic resonance spectroscopy. J. Biol. Chem. 263, 9122–9128

27. Liu, F. and Fromm, H.J. (1988) Relationship between thiol group modification and the binding site for fructose 2,6-bisphosphate on rat liver fructose-1,6-bisphosphatase. J. Biol. Chem. 263, 10035-10039

28. Xue, Y., Huang, S., Liang, J.-Y., and Lipscomb, W.N. (1994) Crystal structure of fructose-1,6-bisphosphatase complexed with fructose 2,6-bisphosphate, AMP and Zn2+ at 2.0-Å resolution: aspects of synergism between inhibitors. Proc. Natl. Acad. Sci. 91, 12482-12486

29. McGrane, M.M., El-Maghrabi, M.R. and Pilkis, S.J. (1983) The interaction of fructose 2,6-bisphosphate and AMP with rat hepatic fructose 1,6-bisphosphatase. J. Biol. Chem. 258, 10445-10454

30. Hines, J. K., Fromm, H. J., and Honzatko, R. B. (2006) Novel allosteric activation site in Escherichia coli fructose-1,6-bisphosphatase. J. Biol. Chem. 281, 18386–18393

31. Hines, J. K., Fromm, H. J., and Honzatko, R. B. (2007) Structures of activated fructose-1,6-bisphosphatase from Escherichia coli. Coordinate regulation of bacterial metabolism and the conservation of the R-state. J. Biol. Chem. 282, 11696–11704

32. Hines, J. K., Kruesel, C. E., Fromm, H. J., and Honzatko, R. B. (2007) Structures of inhibited fructose-1,6-bisphosphatase from Escherichia coli: distinct allosteric inhibition sites for AMP and glucose 6-phosphate and the characterization of a gluconeogenic switch. J. Biol. Chem. 282, 24697–24706

33. Gao, Y., and Honzatko, R. H. Water Molecules in the Central Cavity of Mammalian Fructose-1,6-bisphosphatase as a Determinant of the Quaternary State. Submitted to the J. Biol. Chem.

34. Van Schaftingen, E., and Hers, H-G. (1981) Formation of fructose 2,6-bisphosphate from fructose 1,6-bisphosphate by intramolecular cyclisation followed by alkaline hydrolysis. Eur. J. Biochem. 117, 319-323

35. Laemmli, U. K. (1970) Cleavage of structural proteins during the assembly of the head of bacteriophage T4. Nature 227, 680-685

36. Bradford, M. M. (1976) A rapid sensitive method for the quantitation of microgram quantities of protein utilizing the principle of protein-dye binding. Anal. Biochem. 72, 248-252

37. Leatherbarrow, R.J. (2009) GraFit Version 7, Erithacus Software Ltd., Horley, U.K.

38. Pflugraph, J. W. (1999) The finer things in X-ray diffraction data collection. Acta Crystallogr. D. 55, 1718-1725

39. Brünger, A. T., Adams, P. D., Clore, G. M., DeLano, W. L., Gros, P., Grosse-Kunstleve, R. W., Jiang, J.-S., Kuszewski, J., Nilges, M., Pannu, M. S., Read, R. J., Rice, L. M., Simonson, T., Warren, G. L. (1998) Crystallography & NMR system: A new software suite for macromolecular structure determination. Acta Crystallogr. D 54, 905-921

40. Engh, R. A., and Huber, R. (1991) Accurate bond and angle parameters for X-ray protein structure refinement. Acta Crystallogr. A. 47, 392-400

41. Laskowski, R. A., Mac Arthur, M. W., Moss, D. S., and Thornton, J. M. (1993) PROCHECK: a program to check the stereochemical quality of protein structures. J. Appl. Cryst. 26, 283-291

42. Kelley-Loughnane, N., and Kantrowitz, E. R. (2001) AMP inhibition of pig kidney fructose-1,6-bisphosphatase. Biochim. Biophys. Acta. 1548, 66-71

43. Nelson, S. W., Choe, J. Y., Iancu, C. V., Honzatko, R. B., and Fromm, H. J. (2000) Mutations in the hinge of a dynamic loop broadly influence functional properties of fructose-1,6-bisphosphatase. J. Biol. Chem. 275, 29986-29992

44. Nelson, S. W., Kurbanov, F., Honzatko, R. B. and Fromm, H, J. (2001) The N-terminal segment of recombinant porcine fructose-1,6-bisphosphatase participates in the allosteric regulation of catalysis. J. Biol. Chem. 276, 6119-6124

45. Kurbanov, F. T., Choe, J. Y., Honzatko, R. B., and Fromm, H. J. (1998) Directed mutations in the poorly defined region of porcine liver fructose-1,6-bisphosphatase significantly affect catalysis and the mechanism of AMP inhibition. J. Biol. Chem. 273, 17511-17516

46. Shyur, L. F., Poland, B. W., Honzatko, R. B., and Fromm, H. J. (1997) Major changes in the kinetic mechanism of AMP inhibition and AMP cooperativity attend the mutation of Arg49 in fructose-1,6-bisphosphatase. J. Biol. Chem. 272, 26295-26299

47. El-Maghrabi, M. R., Austin, L. R., Correia, J. J., and Pilkis, S. J. (1992) Lysine 274 is essential for fructose 2,6-bisphosphate inhibition of fructose-1,6-bisphosphatase. J. Biol. Chem. 267, 6526-6530

48. Choe, J. Y., Poland B. W., Fromm, H. J. and Honzatko, R. B. (1998) Role of a dynamic loop in cation activation and allosteric regulation of recombinant porcine fructose-1,6-bisphosphatase. Biochemistry. 37, 11441-11450

49. UniProt Consortium. (2012) Reorganizing the protein space at the Universal Protein Resource (UniProt). Nucleic Acids Res. 40, D71-D75

50. Zamyatnin, A. A. (1972) Protein volume in solution. Prog. Biophys. Mol. Biol. 24, 107-123

51. Michels, P. A., and Rigden, D. J. Evolutionary analysis of fructose 2,6-bisphosphate metabolism. IUBMB Life. 58, 133-141

52. Buchanan, B. B., and Wolosiuk, R. A. (1976) Photosynthetic regulatory protein found in animal and bacterial cells. Nature 264, 669-670

53. Buchanan, B. B. (1980) Role of light in the regulation of chloroplast enzymes. Annu. Rev. Plant Physiol. 31, 341-374

54. The PyMOL Molecular Graphics System, Version 1.5.0.4 Schrödinger, LLC

CHAPTER V. RELEVANCE OF THE DIMER-DIMER INTERFACE IN PORCINE LIVER FRUCTOSE-1,6-BISPHOSPHATASE TO AMP INHIBITION AND COOPERATIVITY

A paper to be submitted to *Biochemistry*

Yang Gao and Richard B. Honzatko

Roy J. Carver Department of Biochemistry, Biophysics, and Molecular Biology,

Iowa State University, Ames, IA 50011

Abstract

The hydrolysis of fructose 1,6-bisphosphate by fructose-1,6-bisphosphatase (FBPase) is a highly regulated reaction in most organisms. In mammals, FBPase is stable tetramer subject to cooperative allosteric inhibition by AMP coupled with synergistic inhibition by fructose-2,6-bisphosphate. Positive cooperativity in AMP binding arises from the interaction of allosteric sites across a specific dimer-dimer interface of the mammalian tetramer. Point mutations at that interface (targeting Arg^{22}, Thr^{39}, Lys^{42}, Ile^{190}, Gly^{191} and Glu^{192}) exhibit a range of effects on AMP cooperativity and tetramer stability; however, functional changes due to mutations have not been correlated with conformational changes because of insufficient structural information. Point mutations at positions 39, 42, 190, 191 and 192 resulted in the formation of FBPase dimmers on the basis of significant shifts in mobility in nondenaturing gel electrophoresis and determinations of mass by equilibrium analytical sedimentation. Met^{22} FBPase, however, has mass determinations identical to the wild-type tetramer. Met^{22} and Gln^{192} FBPases were crystallized in the absence/presence of AMP, as well as products and divalent cations. Crystal structures with AMP are similar to that of the wild-type enzyme, exhibiting a 15 ° dimer-dimer rotation relative to the wild-type structure in the absence of AMP (R-state). Crystal structures of Gln^{192} and Met^{22} FBPases with no AMP, however, exhibit 2 and 14 ° dimer-dimer rotations, respectively. Moreover, AMP binding sites in the absence of AMP assume conformations similar to AMP-bound conformations of the wild-type enzyme. Loss of cooperativity in AMP inhibition then arises from two

mechanisms: dissociation of tetramers into stable dimers and the dominance of a T-like quaternary state in the absence of bound AMP.

Introduction

Fructose-1,6-bisphosphate (D-fructose-1, 6-bisphosphate 1-phosphohydrolase; EC 3. 1. 3; FBPase) governs a key step in gluconeogenesis. In the presence of divalent cations (Mg^{2+}, Mn^{2+}, or Zn^{2+}), FBPase hydrolyzes fructose 1,6-bisphosphate (Fru-1,6-P_2) to fructose 6-phosphate (Fru-6-P) and inorganic phosphate (P_i) (1-2). FBPase and fructose-6-phosphate-1-kinase (PFK-1) define a futile cycle, which in mammalian systems is coordinately regulated by adenine nucleotides and fructose 2,6-bisphosphate (Fru-2,6-P_2) (3-8). AMP allosterically inhibits FBPase with positive cooperativity (9-10) and Fru-2,6-P_2 is a potent active-site inhibitor that enhances AMP inhibition, a phenomenon called AMP/Fru-2,6-P_2 synergism (4-5). Levels of Fru-2,6-P_2 are under hormonal control, ensuring regulation of FBPase in response to the nutritional status of the organism.

In eukaryotic systems, FBPase is a homotetramer of 37 kDa monomers. The four subunits are arranged in D2 symmetry and named clockwise from C1 to C4, with C1 representing the upper left subunit (11). The tetramer reversibly dissociates into dimers (C1-C2 or C3-C4) and then into monomers (12-13). Matrix-bound monomers of FBPase are inactive, whereas matrix-bound dimers exhibit reduced activity compared to tetramer (14). Structurally distinct interfaces lie between subunits C1-C2 and C1-C4. Active sites of FBPase require residues from both subunits C1 and C2 (15). Conformational changes at the C1-C4 interface influence FBPase activity and determine the quaternary state of the tetramer (18).

AMP inhibits FBPase competitively with respect to Mg^{2+} and non-competitively with respect to Fru-1,6-P_2 (9). AMP binding sites are near each other at the C1-C4 interface (16). Ligation by AMP induces a transition from an active R- to inactive T-state (16). The C1-C2 dimer rotates 15 ° relative to the C3-C4 dimer and displaces catalytically essential loops 50-72 from active sites (17-18). (Conformations of loop 50-72 associated with active and

inhibited states of the enzyme are called “engaged” and “disengaged”, respectively). Two AMP-bound intermediate states (I_R and I_T) have been observed in crystal structures of mutant FBPases. Both intermediate states have engaged loops 50-72 and intermediate dimer-dimer rotations of 3 and 12 °, respectively for the I_R- and I_T-states (19-20). Fru-2,6-P_2 binds to the active site of FBPase and stabilizes a conformation comparable to that of AMP-bond complexes, including a 13 ° dimer-dimer rotation and a disengaged loop 50-72 (21). The dimer-dimer rotation induced by Fru-2,6-P_2 is necessary for AMP/Fru-2,6-P_2 synergism (22). A similar conformational change appears in the complex of FBPase with the nonphysiological inhibitor OC252 (23), which also inhibits synergistically with AMP.

Escherichia coli FBPase (eFBPase) shares significant similarities in sequence and structure with mammalian FBPase (24). Fru-2,6-P_2, however, is not present in bacteria. Instead, glucose 6-phosphate (Glc-6-P) and AMP are synergistic inhibitors of eFBPase (25). eFBPase in solution exists in equilibrium between dimer and tetramer. Dilution of eFBPase leads to the slow loss of activity, consistent with an equilibrium shift from tetramer to less active dimer (26). Anion activators, such as phosphoenolpyruvate (PEP) bind to an allosteric site at the C1-C4 interface to stabilize the more active tetramer of eFBPase (24, 26). The PEP binding loci in eFBPase map onto negatively-charged glutamate side chains of eukaryotic FBPases (residue 192 in porcine FBPase).

The cooperative binding of AMP to FBPase (9-10) requires AMP binding to one site on each of two C1-C2 type dimers of the tetramer (13). Point mutations at the C1-C4 interface decrease the affinity and the cooperativity in AMP binding, and in some cases, change the kinetic mechanism of inhibition (27-31). The relationship of AMP inhibition to changes in structure of mutant FBPases is unclear largely because of absent structural information. Evaluated here are mutant FBPases with known changes in AMP cooperativity and two new FBPase point mutations, Lys^{42}→Met and Thr^{39}→Ala. Such mutant FBPases either exist in solution as C1-C2 dimers or as tetramers. Representative mutant FBPases representing the stable tetramer (Arg^{22}→Met) and stable dimer (Glu^{192}→Gln) are crystallized in the absence and presence of AMP. AMP complexes of both mutant FBPases are comparable in conformation to the AMP complex of wild-type FBPase, whereas complexes

in the absence of AMP adopt conformations that differ significantly from that of wild-type FBPase. The product complexes of Glu^{192}→Gln and Arg^{22}→Met FBPases have 2 and 14° dimer-dimer rotations relative to the wild-type product complex. AMP binding sites of these complexes in the absence of AMP have conformations similar to those observed in complexes of FBPases with AMP bound. Conformational changes at the AMP site due to quaternary changes alone could be the basis for properties of AMP cooperativity and AMP/Fru-2,6-P_2 synergism. Moreover, results here indicate two mechanisms for loss of cooperativity in AMP inhibition: dissociation of tetramers into dimers with the concomitant loss of the C1-C4 interface and the dominance of a T-like quaternary state under R-state conditions.

Experimental procedures

Materials— Fru-1,6-P_2, $NADP^+$ and AMP were purchased from Sigma. Glucose-6-phophate dehydrogenase and phosphoglucose isomerase were from Roche Applied Sciences. FBPase-deficient *Escherichia coli* strain DF 657 came from the Genetic Stock Center at Yale University. Other chemicals were of reagent grade or equivalent.

Directed mutations of wild type FBPase— Nucleotide base changes used the Transformer™ site-directed mutagenesis kit (Clontech). Oligonucleotide primers for the following mutations were as previously reported: Arg^{22}→Met (27), Ile^{190}→Thr (28), Gly^{191}→Ala (28), Glu^{192}→Gln (31). Thr^{39}→Ala and Lys^{42}→Met used 5'-CTCGCTGTGC**G**CCGCGGTCAAG -3' and: 5'-CACCGCGGTCA**T**GGCCATCTC-3', respectively. (Nucleotide bases altered from wild-type are underlined in bold typeface). The mutation and the integrity of the construct were confirmed by sequencing the entire open reading frame as well as the promoter region. The DNA sequence service was provided by Iowa State University sequencing facility using the fluorescent dye-dideoxy terminator method.

Expression and Purification of Wild-type and mutated FBPases— Supernatant solutions of cell free extracts were loaded onto a Cibracon Blue-Sepharose column equilibrated with 20 mM Tris-HCl, pH 7.5, 5mM $MgCl_2$. The column was washed with 20 mM Tris-HCl, pH 7.5.

The protein was eluted with 5 mM AMP, 20 mM Tris-HCl, pH 7.5. The pH of eluted protein sample was adjusted to 8.5 before loading onto a DEAE-Sepharose column equilibrated with 20 mM Tris-HCl, pH 8.3. Purified enzyme was eluted with a NaCl gradient (0–0.5 M) in 10 mM Tris-HCl, pH 8.3, and then dialyzed extensively against 50 mM potassium phosphate, pH 7.5, (AMP removal) and then against 50 mM Hepes, pH 7.5, (phosphate removal), before further characterization. Purity and concentration of FBPase preparations were confirmed by SDS-polyacrylamide gel electrophoresis (32) and the Bradford assay (33), respectively.

Kinetics Experiments— FBPase assays couple Fru-6-P production to the conversion of NADP to NADPH using phosphoglucose isomerase and glucose-6-phosphate dehydrogenase (1). Specific activity measurements (Fru-1,6-P_2 saturating at 20 μM) monitored NADPH formation by absorbance at 340 nm on UV spectrometer. Other assays used the same coupling enzymes but monitored the fluorescence of NADPH with excitation and emission at 340 and 470 nm, respectively. Assays were done at 22 ℃ in 50 mM Hepes, pH 7.5, with EDTA and KCl at concentrations of 10 μM and 150 mM, respectively. Assays were initiated by the addition of FBPase except for those assays that measured FBPase activity over extended time. Grafit (34) was used in fitting data to models.

Analytical Ultracentrifugation— Sedimentation equilibrium experiments were performed at 4 ℃ using a Beckman XLA ultracentrifuge with an AN-60 rotor. Three sample concentrations (280 nm absorbance of 0.3, 0.5 and 0.7) of each FBPase (wild-type and mutant enzymes) were prepared in 50 mM Hepes, pH 7.5. Samples were subjected to rotational velocities of 15000, 18000 and 21000 rotations per minute until equilibrium. Absorbance data were recorded at 280 nm in triplicate for each sample at each rotational velocity. The program UltraScan (35) was employed in global fitting of the data.

Crystallization of Met^{22} and Gln^{192} FBPase— The method of hanging drops was used in the crystallization of Met^{22} and Gln^{192} FBPases. 2 μl of protein solution was mixed with 2μl of precipitant solution. Wells contained 500 μl of the precipitant solution. Crystals of the product complex of Met^{22} FBPase grew from a protein solution (10 mg/ml), Hepes (25 mM, pH 7.4), $MgCl_2$ (5 mM), and Fru-1,6-P_2 (5 mM) combined with a precipitant solution (Hepes 100 mM, pH 7.4), polyethylene glycol 3350 (8% w/v), glycerol (27% v/v), and *t*-butyl

alcohol (5% v/v). Crystals of the product complex of Gln^{192} FBPase grew from a protein solution (10 mg/ml), Hepes (25 mM, pH 7.4), $ZnCl_2$ (5 mM), and Fru-1,6-P_2 (5 mM) combined with a precipitant solution (Hepes 100 mM, pH 7.4), polyethylene glycol 3350 (8% w/v), glycerol (27% v/v), and *t*-butyl alcohol (5% v/v). Crystals of AMP complex grew from a solution of either Met^{22} or Gln^{192} FBPase (10 mg/ml), Hepes (25 mM, pH 7.4), $MgCl_2$ (5 mM), Fru-1,6-P_2 (5 mM), and AMP (5 mM) combined with a precipitant solution of Hepes (100 mM, pH 7.4), polyethylene glycol 3350 (12% w/v), glycerol (23% v/v), and *t*-butyl alcohol (5% v/v). Crystals were of equal dimensions (0.2–0.4 mm), growing in approximately 3 days at 20 ℃. Crystals can be transferred directly from droplet to liquid nitrogen as cryo-protectants were included in conditions of crystallization.

Data collection, structure determination, and refinement— Data were collected at Iowa State University from single crystals on a Rigaku R-AXIS IV++ rotating anode/image plate system using CuK_α radiation from an Osmic confocal optics system and a temperature of 110 K. Program D*trek (36) was used in reducing data.

Structures in this report were solved by molecular replacement, using the R-state (PDBID: 1CNQ) as the initial model for the product complex of Gln^{192} FBPase and the T-state (PDBID:1EYJ) as the initial model for the product complex of Met^{22} FBPase and the product-AMP complexes of both Gln^{192} and Met^{22} FBPases. Model refinement employed CNS (37) with force constants and parameters of stereochemistry from Engh and Huber (38). A cycle of refinement consisted of slow cooling from 1000 to 300 K in steps of 25 K followed by 100 cycles of conjugate gradient minimization, concluding with the refinement of individual thermal parameters. Restraints of 1.5 $Å^2$ on nearest neighbor and next-to-nearest neighbor main chain atoms, 2.0 $Å^2$ on nearest neighbor side chain atoms, and 2.5 $Å^2$ on next-to-nearest neighbor side chain atoms were employed in thermal parameter refinement. Waters were added to difference electron density of 2.5σ or higher until no significant decrease was evident in the R_{free} value. Allowable donor-acceptor distances separate all water molecules in the final models. The stereochemistry of the models was analyzed by the use of PROCHECK (39).

Results

Rationale— Several point mutations at the dimer-dimer (C1-C4) interface of FBPase eliminate cooperative binding of AMP: Arg^{22}→Met, Lys^{42}→Ala, Lys^{42}→Thr, Lys^{42}→Glu, Ile^{190}→Thr, Gly^{191}→Ala, and Glu^{192}→Gln (27-28, 30-31) (Figure 1). Sidechains of Lys^{42} and Glu^{192} from different dimers formed stable charge-charge interactions in all FBPase crystal structures. Moreover, inter-dimer polar interactions occur between Glu^{192}:OE1 and Thr^{39}:OG1 and between Lys^{42}:NZ and backbone carbonyls of Ile^{190} and Gly^{191}. The side-chain of Arg^{22} is within contact distance of backbone carbonyls of residues 108-110 in R-state FBPase and hydrogen bonded to the backbone carbonyl of Thr^{27} in T-state of FBPase. The mutations Thr^{27}→Ala causes loss of AMP inhibition (27). Although all mutations listed here eliminate the cooperative binding of AMP, they differ significantly in kinetic mechanisms of inhibition and in AMP binding affinity. AMP inhibits Thr^{42}, Thr^{190} and Ala^{191} FBPases non-competitively with respect to Mg^{2+} (28), whereas in Met^{22} and Glu^{42} FBPases, AMP is a competitive inhibitor with respect to Mg^{2+} (same as wild-type enzyme) (27-28). AMP inhibition of Glu^{42}, Thr^{42}, Thr^{190} and Ala^{191} FBPases is significantly weaker than wild-type enzyme, but in contrast around 5-times more potent for Met^{22} FBPase (27). Moreover, AMP inhibition of Ala^{42} and Gln^{192} FBPases is biphasic, causing potent but partial inhibition at low concentrations of AMP, and additional inhibition at concentrations above 5 mM (30-31). The mutations Arg^{22}→Met, Ile^{190}→Thr, Gly^{191}→Ala, and Glu^{192}→Gln, as well as two new point mutations Thr^{39}→Ala and Lys^{42}→Met, are the basis for probing the role of interactions at the C1-C4 interface.

Kinetics of wild-type and mutant FBPases— Parameters for Met^{22}, Thr^{190}, Ala^{191}, and Gln^{192} FBPase are in the literature (27-28, 30-31) and listed in Table I to facilitate comparisons to those determined here for Ala^{39} and Met^{42} FBPases. As the mechanism of AMP inhibition of Gln^{192} FBPase was not determined in previous work, the properties of Gln^{192} FBPase were re-examined here. All the assays are initialized with addition of FBPase. Most parameters (specific activity, K_m for Fru-1,6-P_2, K_a for Mg^{2+} and K_i for Fru-2,6-P_2) for Ala^{39}, Met^{42} and Gln^{192} FBPases are comparable to those of the wild-type enzyme (Table I). However, Ala^{39}, Met^{42} and Gln^{192} FBPases exhibit biphasic AMP inhibition, though with different plateau

activity (Figure 2, A). AMP inhibition curves for both wild-type and mutated FBPases come from fits of Equation 1, in which measured velocities were put on a basis relative to the velocity measured in the absence of AMP.

$$V_r = \frac{1-V_{plateau}}{1+\left(\frac{I}{IC_{high}}\right)^{n_{high}}} + \frac{V_{plateau}}{1+\left(\frac{I}{IC_{low}}\right)^{n_{low}}} \qquad \text{Equation 1}$$

where V_r, $V_{plateau}$, I, IC_{high}, n_{high}, IC_{low} and n_{low} indicate relative velocity, relative velocity at the plateau, AMP concentration, the concentration of AMP that causes 50% of the high affinity inhibition, the Hill coefficient for high affinity inhibition, the concentration of AMP that causes 50% of the low affinity inhibition and the Hill coefficient for the low affinity inhibition, respectively. For wild-type FBPase, the $V_{plateau}$ is set to zero during fitting. IC_{high} falls 4-fold for Ala^{39} FBPase relative to the wild-type enzyme, and Hill coefficient associate with AMP inhibition is 1.33. IC_{high} is approximately 10-times higher for Gln^{192} and Met^{42} FBPases than IC_{high} of wild-type FBPase, whereas IC_{low} is near 10 mM. For all three mutants, AMP inhibition is not cooperative and is linearly competitive with respect to Mg^{2+} at low AMP concentrations (Figure 2, B-D).

Time dependence of FBPase activity— eFBPase has twice the specific activity in enzyme-initialized assays than Mg^{2+}-initialized assays (26). Moreover, AMP binds to eFBPase with positive cooperativity in enzyme initialized assays, and with diminished cooperativity in Mg^{2+}-initialized assays. The activity of eFBPase decreases slowly with time upon dilution of the enzyme. The same methods were applied here to wild-type and mutant FBPases to probe tetramer stability. Enzymes were incubated in assay mixtures at 1000-fold dilution without metal cofactors, followed by the addition of 5 mM of $MgCl_2$ (Figure 3). For both wild-type and Met^{22} FBPases, activity was independent of incubation time. In contrast, the activities of Ala^{39}, Met^{42}, Thr^{190}, Ala^{191} and Gln^{192} FBPases dropped by 50% with incubation times up to 5 hours, a behavior comparable to that of eFBPase.

Native Gel Electrophoresis— Protein migration in non-denaturing polyacrylamide gel electrophoresis depends on molecular weight, net charge and shape, hence mobility does not always correlate with molecular size. Nonetheless, wild-type FBPase has the least mobility, whereas mutant FBPases that exhibited time-dependent changes in activity upon dilution had

the highest mobilities (Figure 4). Met^{22} FBPase exhibits a faster mobility than wild-type, but less than other mutant FBPases, a phenomenon perhaps due to a net increase in negative charge relative to the wild-type protein.

Sedimentation Equilibrium— Wild-type and mutant FBPases at monomer concentrations of 15.6 μM (A_{280}=0.3), 26.0 μM (A_{280}=0.5) and 36.5 μM (A_{280}=0.7) were subjected to three different rotational velocities as described in the methods section. Data were fit to single-component, monomer-dimer equilibrium and monomer-dimer-tetramer equilibrium models using the program UltraScan (35). The monomer-dimer-tetramer equilibrium model did not provide acceptable outcomes, so fitting results with only the single-component and monomer-dimer equilibrium models are in Table II. On the basis of the single-component model, wild-type and Met^{22} FBPases exhibited molecular weights of approximately 110 kDa, whereas other mutant FBPases have molecular weights ranging from 60-75 kDa. The molecular weight for wild-type enzyme compares favorably with the value of 122 ±4 kDa from dynamic light scattering (26). Molecular weights from the monomer-dimer equilibrium model are similar to those from the single-component model; however, K_d values for the monomer-dimer equilibrium were over 1 molar, indicating a protein concentration range used in sedimentation equilibrium experiments far from the real K_d value for the monomer-dimer equilibrium.

Crystal Structures of Gln^{192} FBPase (Protein Data Bank code 4H45 and 4GX6)— Crystals of the product complex of Gln^{192} FBPase belong to space group *I222* and are isomorphous to the canonical R-state (17). A single monomer of the tetramer is in the asymmetric unit. The model begins with residue 10 and ends at residue 335. Weak electron density covers residues 56-71. This region of the model also has elevated B-parameters. Statistics for data collection and refinement are in Table III.

The product complex of Gln^{192} FBPase approximates the wild-type R-state, with a dimer-dimer rotation of 2 ° (Table IV, Figure 6). The active site has one molecule each of Fru-6-P and P_i and two Zn^{2+} at sites 1 and 2. The R-state product complex of wild-type FBPase by comparison has Zn^{2+} at sites 1, 2 and 3 (17). Loop 50-72 is in its engaged conformation, although weak electron density for residues 56-71 is consistent with the

absence of Zn^{2+} at metal site 3. Asp^{68} coordinates metal cations at site 3 (18, 19) and structures in which that coordination is evident have strong electron density for the entire loop. Helix HI (residues 10-21) shifts approximately 0.5 Å towards the center of tetramer relative to helix HII (residues 28-50) (Figure 6, B). The hydrogen bond between Thr^{14} and Asn^{35}, however, remains intact (donor-acceptor distance of 2.6 Å). In the I_R-state (3 ° dimer-dimer rotation) of the AMP/product complex of Leu^{54} FBPase the hydrogen bond between Thr^{14} and Asn^{35} is lost at a donor-acceptor distance of 3.5 Å (19). The side-chain of Ile^{10} moves away from its R-state hydrophobic contact surface, as observed in the AMP/product complex of Leu^{54} FBPase in its I_R quaternary state (3 ° dimer-dimer rotation). The side chain of Gln^{192} shifts 0.5 Å away from its R-state binding partners Lys^{42} and Thr^{39} (Figure 6, C.) to donor-acceptor distances of 3.0 (Lys^{42}:NZ to Gln^{192}:OD1) and 3.5 Å (Thr39:OG1 to Gln192:OD1). The corresponding distances are 2.9 and 2.7 Å in R-state and 2.7 and 3.7 Å in I_R-state. The contact between Arg^{22} and the backbone carbonyl of 108 is gone at a donor-acceptor distance of 5.3 Å.

Crystals of the AMP/product complex of Gln^{192} FBPase are isomorphous to those of wild-type FBPase in the canonical T-state (18), being in space group $P2_12_12$ with an asymmetric unit of a C1-C2 dimer. The model for Gln^{192} FBPase AMP goes from residue 9 to 335, with weak electron density for residues 61-71. The AMP/product complex of Gln^{192} FBPase is similar to that of wild-type FBPase (T-state, disengaged loop, with tetramer RMSD 0.32 Å). The presence of AMP was confirmed by its strong electron density. Detailed description of T-state will not be covered here.

Crystal Structures of Met^{22} FBPase (Protein Data Bank code 4GX3 and 4GX4)— Crystals of the product complex and AMP/product complex of Met^{22} FBPase are in space group $P2_12_12$ and isomorphous to crystals of the canonical T-state (18). A C1-C2 dimer is in the asymmetric unit for both complexes. Models start from residue 9 and end at residue 335. Electron density for residues 61-71 in the dynamic loop is weak, consistent with high values for B-parameters. Statistics for data collection and refinement are in Table III.

The product complex of Met^{22} FBPase (AMP absent) is in the T-state with a 14 ° dimer-dimer rotation and a disengaged loop 50-72. One Fru-6-P molecule, two Mg^{2+}

(occupying sites 1 and 2), and one P_i molecule are in the active site. Strong electron density covers the side chain of Met^{22} and P_i at the 5'-phosphoryl locus of the AMP pocket (Figure 5). The shearing translocation of helices H1 and H2 observed in the product complex of Gln^{192} FBPase is evident in the product complex of Met^{22} FBPase. Moreover, the hydrogen bond between Thr^{14} and Asn^{35} is broken (donor-acceptor distance of 6.4 Å). As loop 50-72 is disengaged, the hydrophobic interactions of Ile^{10} in the R-state are not only perturbed but are replaced altogether by hydrophobic interactions with disengaged loop 50-72 that evidently stabilize the T-state (19).

The AMP/product complex of Met^{22} FBPase has strong electron density covering allosterically bound AMP and the side chain of Met^{22}. The active site has one each of Fru-6-P and Pi, bound as products, with metal cations (Mg^{2+}) occupying sites 1 and 2. AMP/product complexes of wild-type FBPase have metal ions (Zn^{2+} or Mg^{2+}) at site 1 only (18); however, Leu^{54} FBPase has Mg^{2+} at sites 1 and 2 in its T-state, AMP/product complex (19). Root-mean-square deviations in Cα coordinates after superposition (Table IV and Figure 5) indicate a quaternary state for Met^{22} FBPase that closely approximates the canonical T-state irrespective of AMP concentration. A detailed description of T-state FBPase is elsewhere in the literature (18) and is not the focus of this report.

Survey of conformational changes in AMP pockets— AMP pockets in product complexes of Met^{22} and Gln^{192} FBPase mimic the AMP bound conformation. In fact, other FBPase complexes exhibit movement in helices H1 and H2 in the absence of bound AMP (Figure 7). AMP binding site inhibitors A37 and R15, which come from drug screening efforts and have substantially different binding modes that do not involve the carbonyl of Val^{17} and the side chain of Thr^{31}, cause similar global and local conformational changes as does AMP (Figure 7, D and E) (46-47). OC252 also comes from a drug screening effort and binds to the center of the FBPase tetramer (23). Ligation of OC252 causes a 12 ° dimer-dimer rotation and helix movement at AMP binding site (23). Fru-2,6-P_2 binds to the active site of FBPase and induces 13 ° and 2 ° dimer-dimer rotations in wild-type and His^{45}/Arg^{46}/Tyr^{186} FBPases, respectively (21-22). Fru-2,6-P_2 complexes of FBPase show again the same helix movements at the AMP binding site. Helix movements in the AMP pocket then are linked to

dimer-dimer rotations, whether they are caused directly by the binding of AMP or through the action of ligands elsewhere.

Discussion

Mammalian and yeast FBPases are stable homotetramers (26, 40-43); however, mutations on Thr^{39}, Lys^{42}, Ile^{190}, Gly^{191} or Glu^{192}, residues at or near the C1-C4 interface (Figure 1), similarly reduce the stability of the tetramer. Such mutant FBPases migrate with higher mobility than the wild-type enzyme on non-denaturing polyacrylamide gel electrophoresis. Equilibrium analytical ultracentrifugation indicated a mass half that expected for the tetramer. Dilution of concentrated solutions of mutant FBPases resulted in a slow 50% loss of activity, similar to the behavior of eFBPase in the absence of anion activators (24-26). Monomer forms of FBPase are inactive whereas dimers of FBPase have reduced activity when associated with a sepharose matrix (14). FBPase subunit exchange happens at both the dimer (C1-C2) and monomer level (12-13, 44), with the exchange of C1-C2 dimers preceding monomer exchange. These observations taken together support a common mechanism for the loss of AMP cooperativity, the dissociation of the tetramer into C1-C2 dimers due to point mutations at the C1-C4 interface.

The data here link tetramer stability to AMP cooperativity; however, loss of tetramer stability does not cause loss of AMP inhibition. In fact, IC_{high} for AMP increases only from 5- to 15-fold, for Ala^{39}, Met^{42} and Gln^{192} FBPases, however, AMP inhibition is clearly biphasic for these mutant enzymes, even as potent AMP inhibition remains competitive with Mg^{2+} (Figure 2). Kantrowitz and co-workers argue that biphasic inhibition of Ala^{42} FBPase by AMP is due to an active T-state (30). Given that biphasic kinetics occurs in enzymes that are not or may not be tetramers (AMP inhibition of Ala^{42} FBPase is not cooperative), one cannot characterize such systems as either R- or T-state. The observation of tetramers in crystal structures of Ala^{42} FBPase (30) and Gln^{192} FBPase (present work) may just be a consequence of the high concentration of protein used in crystallization experiments. On the other hand, biphasic inhibition of $Ile^{10}\rightarrow$Asp FBPase is cooperative (Hill coefficient of 2),

and the resulting crystal structures are FBPase tetramers, one of which is an AMP-bound tetramer in an intermediate state I_T with an engaged dynamic loop (45). The later suggest biphasic AMP inhibition can also be a property of the tetramer. AMP inhibition is more than a thousand-fold weaker than that of the wild-type enzyme and becomes non-competitive with respect to Mg^{2+} for Thr^{190} and Gly^{191} FBPases (28). Thr^{190} and Gly^{191} FBPases lack AMP cooperativity and are dimers, but do not exhibit biphasic AMP inhibition. The absence of such inhibition, however, may be a consequence of almost a complete loss of AMP inhibition.

That the loss of the C1-C4 interaction causes the loss of AMP cooperativity is no great surprise. Hybrid mutant FBPases exhibit no cooperativity when AMP binds to the same C1-C2 dimer, but exhibit cooperativity when AMP binds to one subunit each of the C1-C2 and C3-C4 dimers (13). The mechanism of AMP cooperativity arises putatively from interactions at the C1-C4 (equivalent to C2-C3) subunit interface (19). The base of AMP inserts between helices H1 and H2 of the C1 subunit and forms hydrogen bonds with the backbone carbonyl of Val^{17} (helix H1) and the side chain of Thr^{31} (helix H2). Helices H1 and H2 undergo a shear causing the loss of a hydrogen bond across the C1-C4 interface between Thr^{39} (helix H2, subunit C1) and Glu^{192} (subunit C4). The loss of the C1-C4 hydrogen bond facilitates the binding of a second molecule of AMP to subunit C4, which in turn disrupts the symmetry-related hydrogen bond between Thr^{39} (helix H2, subunit C4) and Glu^{192} (subunit C1). Evidently, movement in helices H1 and H2 does not require AMP binding. The rotation of dimer pairs in the absence of AMP in the product complexes of Met^{22} and Gln^{192} FBPases causes helix movement (Figure 7), albeit the effect is more certain in the case of Met^{22} FBPase which exhibits a 14 ° dimer-dimer rotation as opposed to Gln^{192} FBPase, which exhibits but a 2 ° rotation. Helix movement due to subunit-pair rotation should enhance the binding of AMP, and indeed, although AMP cooperativity is absent in Met^{22} FBPase, AMP binding affinity increases around 5-fold relative to the wild-type enzyme (27). Moreover, the complexes of Ser^{45}→His/Thr^{46}→Arg/Leu^{186}→Tyr FBPase and wild-type FBPase with Fru-2,6-P_2 exhibit 2 ° and 12 ° dimer-dimer rotations, respectively, and movement of helices H1 and H2 (21,22). Any mechanism that causes a dimer-dimer rotation perhaps as little as 2 ° could transform the AMP pocket from a low affinity R-state conformation to a high affinity T-state conformation.

The loss of AMP cooperativity in Met^{22} FBPase clearly is by a mechanism altogether different from the other mutant FBPases examined here. Met^{22} FBPase is a tetramer on the basis of time-independent kinetics upon dilution, with mobility nearly equal to the of the wild-type enzyme on non-denaturing polyacrylamide gel electrophoresis, and a molecular weight identical to that of the wild-type tetramer on the basis of analytical equilibrium ultracentrifugation. The molecular weight of approximately 110 kDa is substantially less than the expected weight of 148 kDa; however, the non-globular shape of the tetramer could well be responsible for the deviation from expected mass. The loss of AMP cooperativity is probably due to a tetramer locked in a T-like state, which already has maximal affinity for AMP. On the other hand, Mg^{2+} binds to Met^{22} FBPase with Hill coefficient greater than 2, indicating the incorporation of more than two Mg^{2+} molecules. Two Mg^{2+} molecules exist in both product complexes and AMP/product complexes of Met^{22} FBPase, in contrast to three metal cations in product complexes of wild-type FBPase and one metal cation in AMP/product complexes of wild-type FBPase. The cooperativity may derive from binding of Mg^{2+} to different subunits, where Mg^{2+} cooperatively drives T- to R-state transition of Met^{22} FBPase. Similar phenomena was observed in substrate binding: Fru-1,6-P_2 binding curve changed from hyperbolic to sigmoidal with addition of Fru-2,6-P_2, implying a cooperative transition from Fru-2,6-P_2 bound state (close to T-state) to substrate bound state (R-state) (5).

But why does methionine at position 22 overwhelmingly favor the T-state? In the wild-type enzyme, Arg^{22} is in position to interact with backbone carbonyls 108-110 of the neighboring subunit. The side-chain of Arg^{22} is poorly ordered, however, indicating either weak interactions, or multiple interactions that stabilize more than one conformation of the side-chain. In contrast Arg^{22} hydrogen bonds with the backbone carbonyl of Thr^{27} and is well-ordered in the T-state. If anything, Arg^{22} seems to have a greater stabilizing effect on the T-state rather than the R-state. Met^{22} adopts a different conformation from Arg^{22} in the T-state, allowing the side-chain to become less solvent-exposed. Hence, the increase in entropy due to the release of water molecules from the hydrophobic surface of Met^{22} in its T-state conformation may outweigh the loss of the hydrogen bond between the guanidine group of Arg^{22} and backbone carbonyl 27.

The observation of conformational changes in the AMP pocket due to dimer-dimer rotation (Figure 7) suggests that if any rotation were to occur in the absence of AMP, then AMP cooperativity will decrease or vanish. Indeed, the product complex of Met^{22} FBPase has a 14 ° dimer-dimer rotation and has no AMP cooperativity. Fru-2,6-P_2 enhances AMP binding by 8- and 2-fold for wild-type and $His^{45}/Arg^{46}/Tyr^{186}$ FBPase, respectively, (consistent with the 12 and 2 ° dimer-dimer rotations) and both wild-type and $His^{45}/Arg^{46}/Tyr^{186}$ FBPases in the presence of Fru-2,6-P_2 are without AMP cooperativity (21-22). OC252 binds cooperatively to FBPase and inhibits synergistically with AMP or Fru-2,6-P_2 (23). The presence of either AMP or Fru-2,6-P_2 decreases OC252 cooperativity, although the effect of OC252 on AMP cooperativity is unknown. The OC252/product complex of wild-type FBPase exhibits a 12 ° rotation. The structural and inhibition data consistently point to the AMP binding site with sheared helices as having high affinity and that of the canonical R-state as having low affinity. Cooperativity in AMP inhibition can come about from as little as a 2 ° dimer-dimer rotation.

FBPase is a target for the development of drugs in the treatment of diabetes Type II (23,46,47,49-53). A possible strategy for inhibiting multi-subunit enzymes is the disruption of quaternary structure, and in the case of mammalian FBPase the most vulnerable interface is between subunit C1 and C4. On the basis of results here, however, the properties of a drug-bound C1-C2 dimer are uncertain. A drug-stabilized dimer may have appreciable activity (up to 50% of the wild-type tetramer) and be 10-fold (or more) less susceptible to AMP inhibition. Inhibition by Fru-2,6-P_2, however, seems unabated in mutant dimers, although AMP/Fru-2,6-P_2 synergism is not likely a property of such dimers. Given the time and expense associated with the development of any drug, the search for molecules that promote the dissociation of the tetramer may not be rewarding. On the other hand, Met^{22} FBPase clearly demonstrates that a small change in FBPase tips the balance of quaternary states in favor of a form that is 10-fold move sensitive to AMP inhibition. In fact, eukaryotic organisms may have taken advantage of this attribute in the evolution of Fru-2,6-P_2, which independently stabilizes a T-like conformational state of FBPase that enhances AMP inhibition some 8-fold.

Table I. Parameters from kinetics experiments using wild-type and mutant FBPases.

FBPase type	Specific activity mg^{-1} s^{-1}	K_M Fru-1,6-P_2 (μM)	Hill-coef. Mg^{2+}	K_a-Mg^{2+} $(mM)^2$	IC_{high}[a]	n_{high}[a]	IC_{low}[a] (mM)	n_{low}[a]	K_i Fru-2,6-P_2 (μM)	Ref
Wild-type	25	1.47(7)	0.81(2)	1.71(7)	2.57(5)	2.25(9)	NA	NA	0.14(1)	
Ala^{39}	16	0.78(8)	1.18(5)	2.1(2)	9.4(4)	1.33(7)	10(4)	0.9(4)	0.068(6)	
Met^{42}	11	1.6(1)	1.94(7)	1.7(1)	30(4)	1.1(1)	15.2(6)	1.25(6)	0.13(3)	
Gln^{192}	13	0.87(8)	1.69(7)	1.7(1)	31(8)	0.9(1)	18(1)	1.4(1)	0.072(5)	
Met^{22}	70	2.5(1)	2.44(3)	0.3(1)	0.68(5)[b]	1.2(1)	NA	NA	0.16(3)	27
Thr^{190}	35	1.8(2)	1.6(1)	4.4(2)	10(1)[c]	1	NA	NA	0.03(0)	28
Ala^{191}	35	0.84(7)	1.5(1)	10.7(9)	15(4)[c]	1	NA	NA	0.03(0)	28

[a] Parameters are from Equation 1 in the results section. The concentrations of Mg^{2+} in AMP inhibition assays are 5 mM for wild-type, Ala^{39}, Met^{42}, and Gln^{192} FBPases, 2 mM for Met^{22} FBPase, and 12 mM for Thr^{190} and Ala^{191} FBPases. The unit for IC_{high} is μM for wild-type, Ala^{39}, Met^{42}, Gln^{192}, Met^{22} FBPases and mM for Thr^{190} and Ala^{191} FBPase.

[b] AMP is competitive inhibitor with respect to Mg^{2+} and noncompetitive inhibitor with respect to Fru-1,6-P_2, same as wild-type FBPase. In ref 27, the reported K_i (K_i = 3.0(5) μM; corresponding value for wild-type FBPase is 21(6) μM^2) was derived from AMP inhibition at varying Fru-1,6-P_2 concentration, with the presence of 5 mM Mg^{2+}. The Hill coefficient for AMP inhibition is 1.The IC_{50} for AMP inhibition was re-examined here.

[c] For both Thr^{190} and Ala^{191} FBPases, AMP inhibitions are noncompetitive with respect to Mg^{2+} and noncompetitive with respect to Fru-1,6-P_2.

Table II. Results of sedimentation equilibrium experiments using wild-type and mutant FBPases[a]

Protein	Single component, ideal		Monomer-dimer equilibrium		
	M.W.	*S.D.*[b]	*M.W.*	K_d (M)	*S.D.*[b]
Wild-type	112100	0.009	113900	2.718	0.01
Met^{22}	116300	0.006	118700	2.72	0.005
Ala^{39}	75250	0.006	71610	9.939	0.005
Met^{42}	68080	0.004	67490	31.84	0.004
Thr^{190}	60770	0.004	60750	2.719	0.004
Ala^{191}	71030	0.005	67370	8.058	0.005
Gln^{192}	60340	0.005	59860	44.67	0.005

[a] The results were derived from global fitting of all data with software Ultrascan

[b] Standard derivation of the global fitting

Table III. Statistics of data collection and refinement for mutant FBPase.

Enzyme/complex type[a]	Met^{22} FBPase/ products, Mg^{2+}	Met^{22} FBPase/ products, Mg^{2+}, AMP	Gln^{192} FBPase/ products, Zn^{2+}	Gln^{192} FBPase/ products, Mg^{2+}, AMP
Space group [a]	$P2_12_12$	$P2_12_12$	I222	$P2_12_12$
Resolution limit (Å)	2.25	2.50	3.00	2.50
Number of measurements	110,910	100,552	26,740	91,023
Number of unique reflections	32,141	27,370	7,665	25,867
Completeness of data (%):				
Overall	85.2	95.6	97.3	92,3
Last shell/range (Å)	69.2/2.33-2.25	96.3/2.59-2.50	99.9/3.11-3.00	94.1/2.59-2.50
R_{sym} [b]				
Overall	0.073	0.139	0.129	0.143
Last shell/range (Å)	0.299/2.33-2.25	0.427/2.59-2.50	0.426/3.11-3.00	0.331/2.59-2.50
Reflections in refinement	30,514	25,977	7,304	24,546
Number of atoms	5,412	5,358	2574	5,346
Number of solvent sites	370	280	58	266
R_{factor} [c]	0.207	0.206	0.208	0.204
R_{free} [d]	0.264	0.262	0.294	0.261
Mean B protein ($Å^2$)	24.9	31.0	50.3	27.9
Mean B AMP ($Å^2$)	-	30.2	-	25.7
Root mean square deviations:				
Bond lengths (Å)	0.020	0.018	0.016	0.017
Bond angles (degrees)	1.8	1.9	1.6	1.8

[a] Unit cell lengths (*a*, *b*, *c*) in Å for product and AMP complexes of Met^{22} and Gln^{192} FBPase are (59.249, 165.012, 79.135), (60.776, 166.535, 79.209), (53.996, 83.621, 166.220) and (59.923, 165.341, 79.112), respectively. Unit cell angles (α, β, γ) are 90° for space groups I222 and $P2_12_12$.

[b] $R_{sym} = \Sigma_j\Sigma_i \mid I_{ij} - \langle I_j \rangle \mid / \Sigma_i\Sigma_j I_{ij}$, where *i* runs over multiple observations of the same intensity, and *j* runs over all crystallographically unique intensities.

[c] $R_{factor} = \Sigma \parallel F_{obs} \mid - \mid F_{calc} \parallel / \Sigma \mid F_{obs} \mid$, where $\mid F_{obs} \mid > 0$.

[d] R_{free} based upon 10% of the data randomly culled and not used in the refinement.

Table IV. Root mean square deviations (Å) in the superposition of selected Cα atoms of Met^{22} and Gln^{192} structures against canonical R and T-state FBPases[a]

FBPase type/complex	R-state (PDB ID 1CNQ)			T-state (PDB ID 1EYJ)		
	Monomer	Dimer	Tetramer	Monomer	Dimer	Tetramer
Met^{22}/products, Mg^{2+}	0.66	0.74	4.80	0.27	0.30	0.38
Met^{22} products, Mg^{2+}, AMP	0.70	0.78	4.86	0.22	0.24	0.27
Gln^{192}/products, Zn^{2+}	0.39	0.45	0.64	0.59	0.74	4.64
Gln^{192}/products, Mg^{2+}, AMP	0.67	0.75	4.8	0.29	0.25	0.32

[a] Cα atoms of residues 10-50 and 72-330 were used in the alignment.

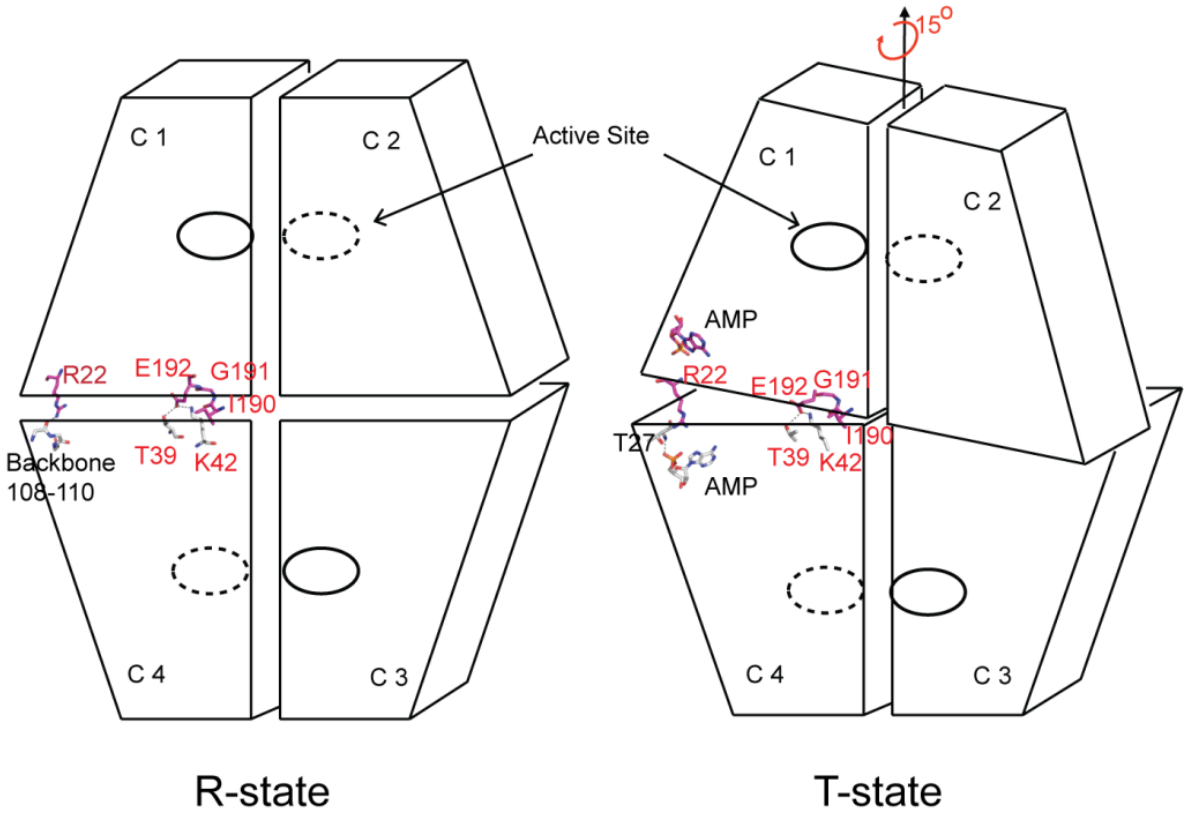

Figure 1. Dimer-dimer interface in R- and T-state of FBPase. Schemes of R- and T-states of FBPase were present with labeled subunits and active site. FBPase was homo-tetramer with D2-symmetry. C1-C4 interface and C2-C3 interface were symmetrically identical and only key residues at C1-C4 interface was shown in sticks. The interaction between Glu^{192} and Lys^{42} was present in both R- and T-state of FBPase whereas Arg^{22} changed its interacting partner during R- to T-state transition.

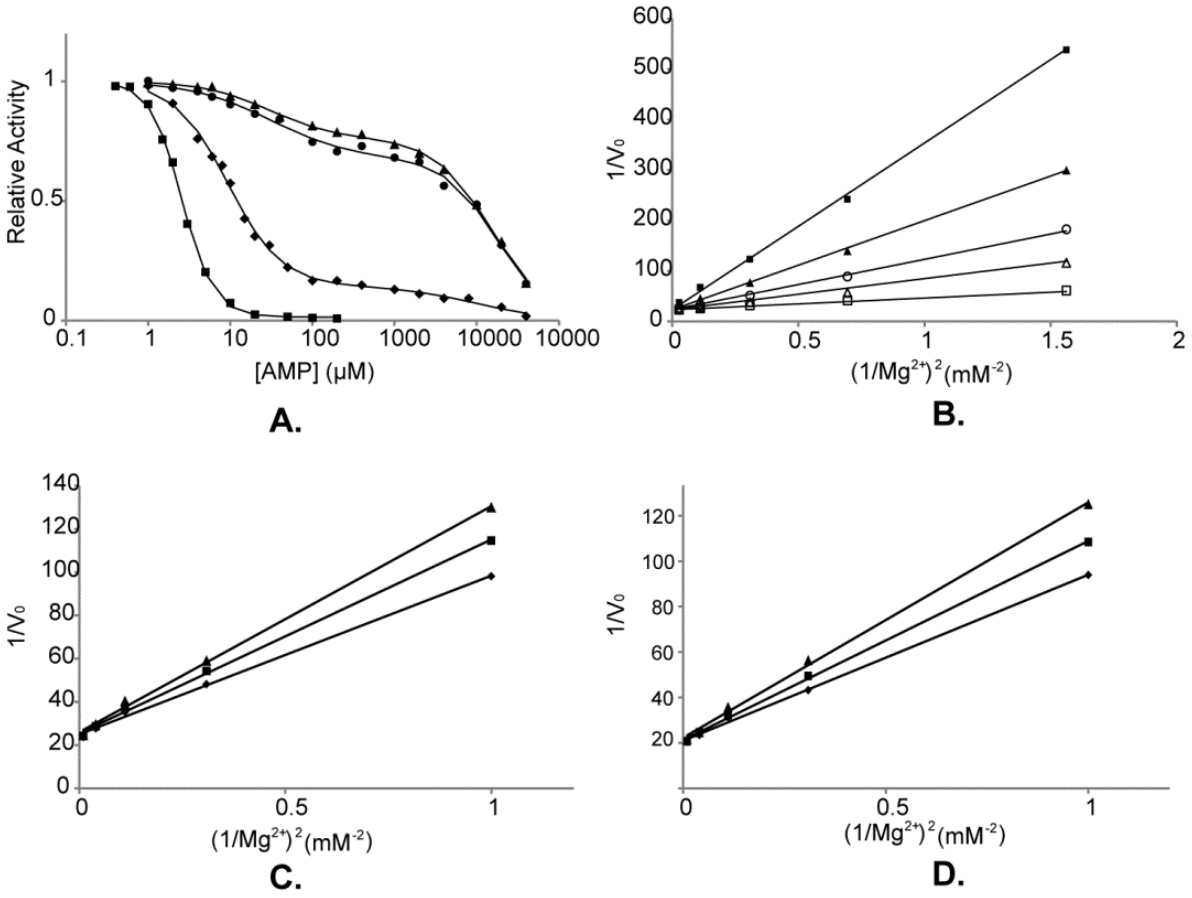

Figure 2. AMP inhibition of Ala[39], Met[42], and Gln[192] FBPase. A. AMP titrations are of wild-type (■), Ala39 (◆), Met42 (●), and Gln192 (▲) FBPase in saturating Fru-1,6-P_2 (20 μM) and Mg^{2+} (5-10 mM). AMP inhibition *versus* Mg^{2+} concentration for Ala[39] (*panel B*), Met[42] (*panel C*), and Gln[192] (*panel D*). AMP concentrations are 0 (□), 2 (Δ), 4 (○),8 (▲), and 16 μM (■) for Ala[39] FBPase and 0 (◆),3 (■), and 10 μM (▲) for Met[42] and Gln[192] FBPases.

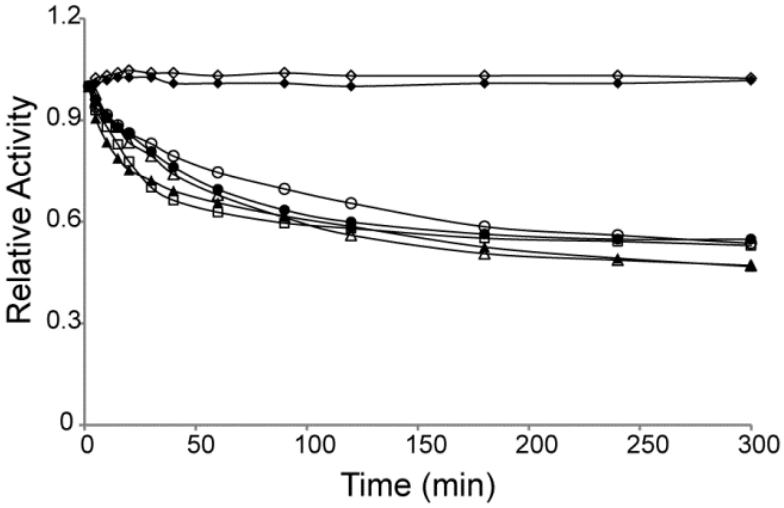

Figure 3. Non-denaturing polyacrylamide gel electrophoresis of wild-type and mutant FBPases. 20 μg of pure protein was loaded in each lane. The names of the protein are labeled above each band.

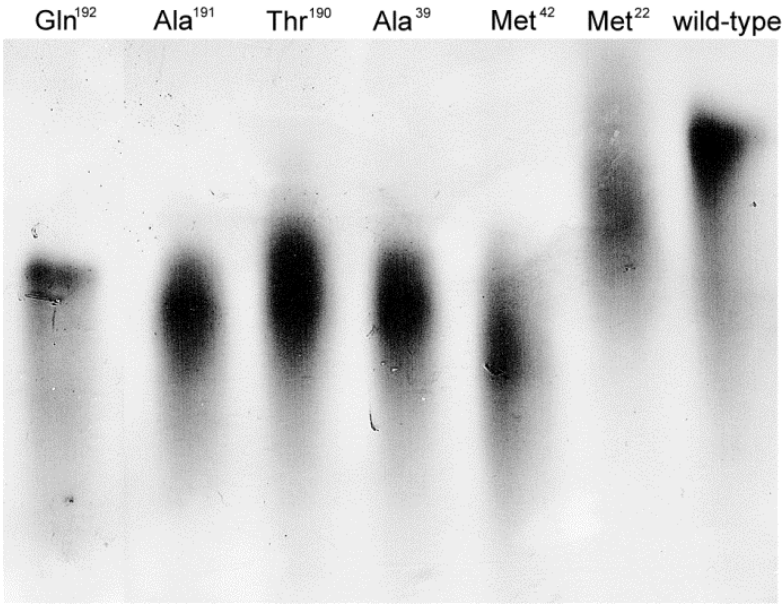

Figure 4. Time Dependent Inactivition of Mutated FBPase. Wild-type (◊) and Met^{22} (◆) FBPase retained activities upon dilution whereas Ala^{39} (▲), Met^{42} (●), Thr^{190} (○), Ala^{191} (Δ), and Gln^{192} (□) FBPase exhibited partial loss of activities within five hours upon dilution.

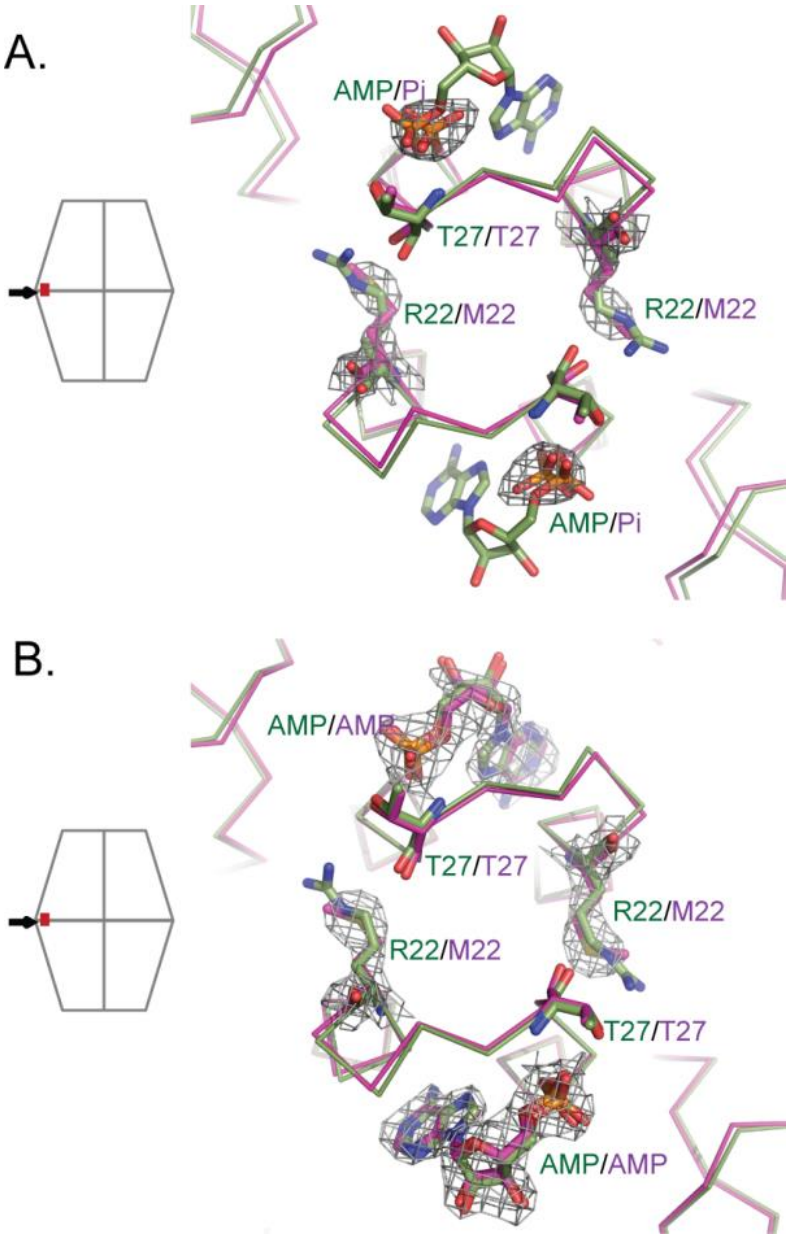

Figure 5. AMP binding sites in product and AMP complexes of Met^{22} FBPase. AMP binding sites of Met^{22} FBPase (magenta) from its product complex (*panel A*) and its AMP/product complex (*panel B*) were aligned to wild-type FBPase T-state (dark green). Electron densities of P_i, AMP and/or Met^{22} from Met^{22} FBPase are contoured at 1.5σ. AMP, P_i and residues 22 and 27 are shown as stick models. Pictures were prepared with pymol (54).

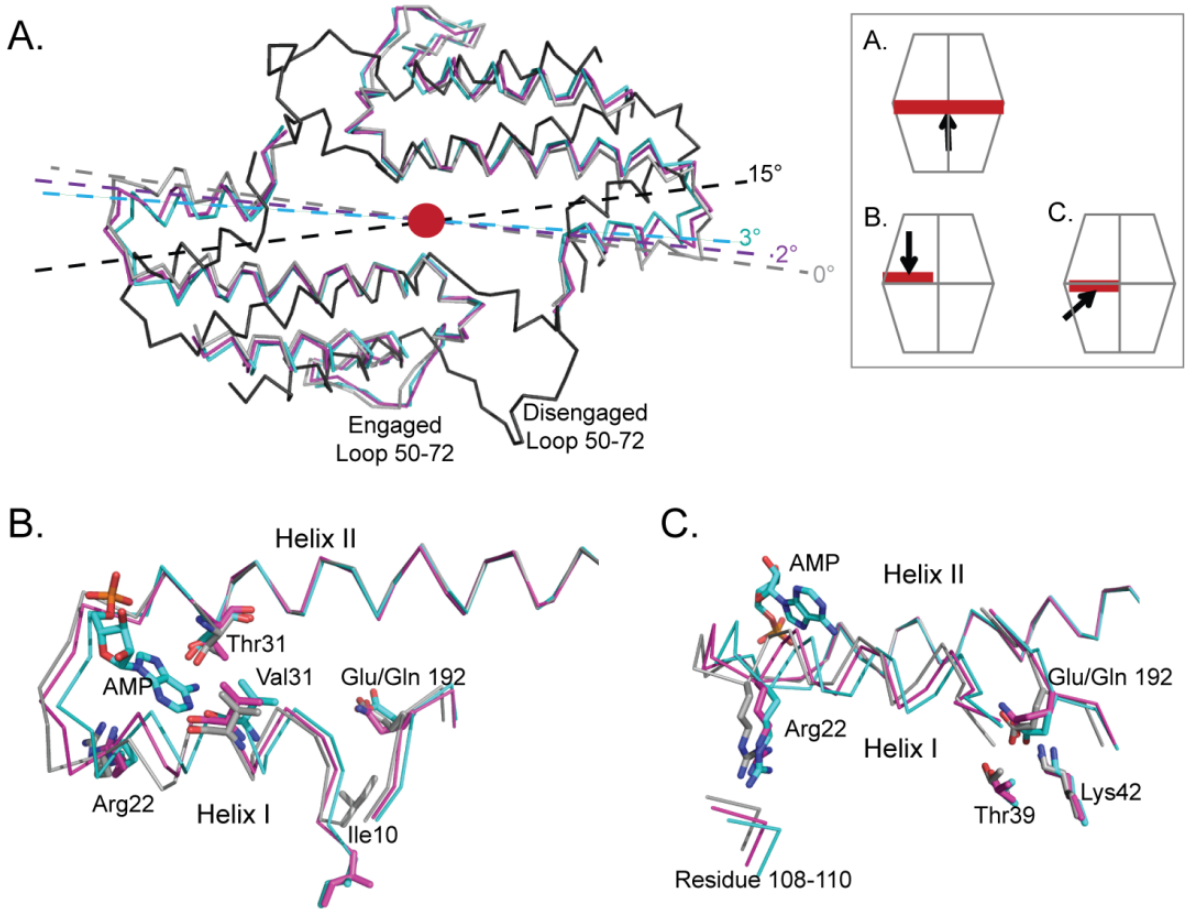

Figure 6. Structural alignment of the product complex of Gln^{192} FBPase with R-state and I_R-state of FBPase. Dimer-dimer rotations in the product complex of Gln^{192} FBPase (magenta), I_R-state (cyan) and T-state (black) is illustrated by residues 10-90 from the C1-C2 dimer (*panel A*). Residues 10-90 of all four subunits of each protein are superimposed on the R-state (*grey*). Helix H2 of the AMP binding site of Gln^{192} FBPase (*magenta*) is superimposed on R- (*grey*) and I_R-state (*cyan*) FBPases (*panel B*). Residues involved in AMP binding and C1-C4 subunit interactions using helix H2 to align structures of Gln^{192}, R- and I_R-state FBPases (*grey*,*cyan*, and *magenta*, respectively. Viewing directions and regions given by the associated FBPase icons in the upper right of the illustration. Pictures were prepared with pymol (54).

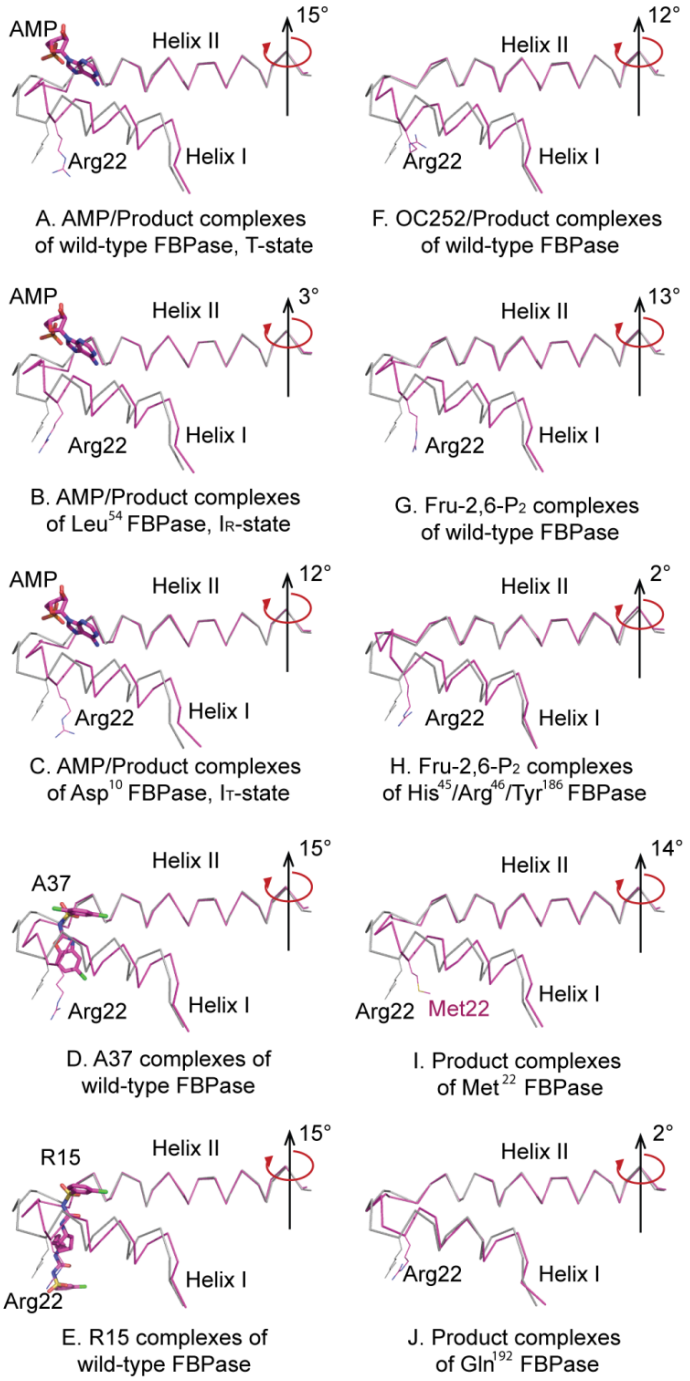

Figure 7. Survey of AMP binding sites in FBPases differing by mutations an conditions of ligation. T-state (A, PDB ID: 1EYJ), I_R-state (B, PDB ID: 1YYZ), I_T-state (C, PDB ID: 2F3D), Ala^{37} FBPase complex (D, PDB ID: 2FHY), Arg^{15} FBPase (E, PDB ID: 2JJK), OC252-bound FBPase (F, PDB ID: 1Q9D), Fru-2,6-P_2-bound FBPase (G, PDB ID: 2QVV), Fru-2,6-P_2-bound $His^{45}/Arg^{46}/Tyr^{186}$ FBPase complex (H, PDB ID: 4GWU), Met^{22} FBPase (I), and Gln^{192} FBPase complex (J) are colored magenta and aligned to R-state FBPase (PDB ID: 1CNQ) using helix H2. Dimer-dimer rotations for each complex are on right side of each panel. Viewing direction and region is that of Figure 5, panel B.

Reference

1. Benkovic, S. J., and de Maine, M. M. (1982) Mechanism of action of fructose 1,6-bisphosphatase. Adv. Enzymol. Relat. Areas Mol. Biol. 53, 45–82

2. Tejwani, G. A. (1983) Regulation of fructose-bisphosphatase activity. Adv. Enzymol. Relat. Areas Mol. Biol. 54, 121–194

3. Taketa, K., and Pogell, B. M. (1965) Allosteric inhibition of rat liver fructose 1,6-bisphosphatase by adenosine 5’-monophosphate. J. Biol. Chem. 240, 651–662

4. Pilkis, S. J., El-Maghrabi, Pilkis, J., and Claus, T. (1981) Inhibition of fructose-1,6-bisphosphatase by fructose 2,6-bisphosphate. J. Biol. Chem. 256, 3619–3622

5. Van Schaftingen, E., and Hers, H.-G. (1981) Inhibition of fructose-1,6-bisphosphatase by fructose 2,6-biphosphate. Proc. Natl. Acad. Sci. U. S. A. 78, 2861–2863

6. Pilkis S. J., El-Maghrabi, Pilkis, J., Claus, T. H., and Cumming D. A. (1981) Fructose 2,6-bisphosphate. A new activator of phosphofructokinase. J. Biol. Chem. 256, 3171–3174

7. Van Schaftingen, E., Jett, M.-F., Hue, L., and Hers, H.-G. (1981) Control of liver 6-phosphofructokinase by fructose 2,6-bisphosphate and other effectors. Proc. Natl.Acad. Sci. U. S. A. 78, 3483–3486

8. Uyeda, K., Furuya, E., and Luby, L. J. (1981) The effect of natural and synthetic D-fructose 2,6-bisphosphate on the regulatory kinetic properties of liver and muscle phosphofructokinase. J. Biol. Chem. 256, 8394–8399

9. Stone, S. R., and Fromm, H. J. (1980) Studies on the mechanism of adenosine 5’-monophosphate inhibition of borvine liver fructose 1,6-bisphosphatase. Biochemistry 19, 620–625

10. Nimmo, H. G., and Tipton, K. F. (1975) The effect of pH on the kinetics of beef-liver fructose bisphosphatase. Eur. J. Biochem. 58, 567–574

11. Ke, H., Thorpe, C. M., Seaton, B. A., Marcus, F., and Lipscomb, W. N. (1989) Molecular structure of fructose-1,6-bisphosphate at 2.8-Å resolution. Proc. Natl. Acad. Sci. U.S.A. 86, 1475-1479

12. Nelson, S. W., Honzatko, R. B., and Fromm, H. J. (2001) Spontaneous subunit exchange in porcine liver fructose-1,6-bisphosphatase. FEBS. Lett. 492, 254-258

13. Nelson, S. W, Honzatko, R. B., and Fromm, H. J. (2002) Hybrid tetramers of porcine liver fructose-1,6-bisphosphatase reveal multiple pathways of allosteric inhibition. J. Biol. Chem. 277, 15539-15545

14. Grazi, E., Magri, E., and Traniello, S. (1973) Active subunits of rabbit liver fructose diphosphatase. Biochem. Biophys. Res. Commun. 54, 1321-1325

15. Giroux, E., Williams, M. K., and Kantrowitz, E. R. (1994) Shared active sites of ructose-1,6-bisphosphatase. Arginine 243 mediates substrate binding and fructose 2,6-bisphosphate inhibition. J. Biol. Chem. 269, 31404-31409

16. Ke, H. M., Zhang, Y. P., and Lipscomb, W. N. (1990) Crystal structure of fructose-1,6-bisphosphatase complexed with fructose 6-phosphate, AMP, and magnesium. Proc. Natl. Acad. Sci. U.S.A. 87, 5243-5247

17. Choe, J. Y., Poland, B. W., Fromm, H. J., and Honzatko, R. B. (1998) Role of a dynamic loop in cation activation and allosteric regulation of recombinant porcine fructose-1,6-bisphosphatase.Biochemistry 37, 11441-11450

18. Choe, J. Y., Fromm, H. J., and Honzatko, R. B. (2000) Crystal structures of fructose 1,6-bisphosphatase: mechanism of catalysis and allosteric inhibition revealed in product complexes. Biochemistry 39, 8565-8574

19. Iancu, C. V., Mukund, S., Fromm, H. J., and Honzatko, R. B. (2005) R-state AMP complex reveals initial steps of the quaternary transition of fructose-1,6-bisphosphatase. J. Biol. Chem. 280, 19737-19745

20. Gao, Y., Iancu, C. V., Mukund, S., Choe, J. Y., and Honzatko, R. B. Mechanism of displacement of catalytically essential loop from the active site of fructose-1,6-bisphosphatase. To be submitted.

21. Hines, J. K., Chen, X., Nix, J. C., Fromm, H. J., and Honzatko, R. B. (2007) Structures of mammalian and bacterial fructose-1,6-bisphosphatase reveal the basis for synergism in AMP/fructose 2,6-bisphosphate inhibition. J. Biol. Chem. 282, 36121–36131

22. Gao, Y., and Honzatko, R. B. Hydrophobic Central Cavity in Fructose-1,6-bisphosphatase is Essential for the Synergism in AMP/Fructose 2,6-bisphosphate Inhibition. To be submitted.

23. Choe, J. Y., Nelson, S. W., Arienti, K. L., Axe, F. U., Collins, T. L., Jones, T. K., Kimmich, R. D., Newman, M. J., Norvell, K., Ripka, W. C., Romano, S. J., Short, K. M., Slee, D. H., Fromm, H. J., and Honzatko, R. B. (2003) Inhibition of fructose-1,6-bisphosphatase by a new class of allosteric effectors. J. Biol. Chem. 278, 51176-51183

24. Hines, J. K., Fromm, H. J., and Honzatko, R. B. (2006) Novel allosteric activation site in Escherichia coli fructose-1,6-bisphosphatase. J. Biol. Chem. 281, 18386–18393

25. Hines, J. K., Fromm, H. J., and Honzatko, R. B. (2007) Structures of activated fructose-1,6-bisphosphatase from Escherichia coli. Coordinate regulation of bacterial metabolism and the conservation of the R-state. J. Biol. Chem. 282, 11696–11704

26. Hines, J. K., Kruesel, C. E., Fromm, H. J., and Honzatko, R. B. (2007) Structures of inhibited fructose-1,6-bisphosphatase from Escherichia coli: distinct allosteric inhibition sites for AMP and glucose 6-phosphate and the characterization of a gluconeogenic switch. J. Biol. Chem. 282, 24697–24706

27. Shyur, L.-F., Aleshin, A. E., Honzatko, R. B. and Fromm, H. J. (1996) Site-directed mutagenesis of residues at subunit interfaces of porcine fructose-1,6-bisphosphatase. J. Biol. Chem. 271, 3005-3010

28. Shyur, L.-F., Aleshin, A. E., Honzatko, R. B. and Fromm, H. J. (1996) Biochemical properties of mutant and wild-type fructose-1,6-bisphosphatases are consistent with the coupling of intra- and intersubunit conformational changes in the T- and R-state transition. J. Biol. Chem. 271, 33301-33307

29. Shyur, L. F., Aleshin, A. E., Fromm, H. J. (1996) A study of subunit interface residues of fructose-1,6-bisphosphatase by site-directed mutagenesis: effects on AMP and Mg2+ affinities. Biochemistry 35, 7492-7498

30. Lu, G., Stec, B., Giroux, E. L., and Kantrowitz, E. R. (1996) Evidence for an active T-state pig kidney fructose 1,6-bisphosphatase: interface residue Lys-42 is important for allosteric inhibition and AMP cooperativity. Protein Sci. 5, 2333-2342

31. Lu, G., Giroux, E. L., and Kantrowitz, E. R. (1997) Importance of the dimer-dimer interface for allosteric signal transduction and AMP cooperativity of pig kidney fructose-1,6-bisphosphatase. Site-specific mutagenesis studies of Glu-192 and Asp-187 residues on the 190's loop. J. Biol. Chem. 272, 5076-5081

32. Laemmli, U. K. (1970) Cleavage of structural proteins during the assembly of the head of bacteriophage T4. Nature 227, 680-685

33. Bradford, M. M. (1976) A rapid sensitive method for the quantitation of microgram quantities of protein utilizing the principle of protein-dye binding. Anal. Biochem. 72, 248-252

34. Leatherbarrow, R.J. (2009) GraFit Version 7, Erithacus Software Ltd., Horley, U.K.

35. Demeler, B. (2005) UltraScan A Comprehensive Data Analysis Software Package for Analytical Ultracentrifugation Experiments. Modern Analytical Ultracentrifugation: Techniques and Methods. (D. J. Scott, S.E. Harding and A.J. Rowe. Eds.) Royal Society of Chemistry (UK), 210-229

36. Pflugraph, J. W. (1999) The finer things in X-ray diffraction data collection. Acta Crystallogr. D. 55, 1718-1725

37. Brünger, A. T., Adams, P. D., Clore, G. M., DeLano, W. L., Gros, P., Grosse-Kunstleve, R. W., Jiang, J.-S., Kuszewski, J., Nilges, M., Pannu, M. S., Read, R. J., Rice, L. M., Simonson, T., Warren, G. L. (1998) Crystallography & NMR system: A new software suite for macromolecular structure determination. Acta Crystallogr. D 54, 905-921

38. Engh, R. A., and Huber, R. (1991) Accurate bond and angle parameters for X-ray protein structure refinement. Acta Crystallogr. A. 47, 392-400

39. Laskowski, R. A., Mac Arthur, M. W., Moss, D. S., and Thornton, J. M. (1993) PROCHECK: a program to check the stereochemical quality of protein structures. J. Appl. Cryst. 26, 283-291

40. Mendicino, J., Kratowich, N., and Oliver, R. M. (1972) Role of enzyme-enzyme interactions in the regulation of gluconeogenesis. Properties and subunit structure of fructose 1,6-diphosphatase from wine kidney. J. Biol. Chem. 247, 6643-6650

41. Van Tonder, A., Terblanche, S. E., and Oelofsen, W. (1985) Isolation and partial characterization of rat muscle fructose bisphosphatas. Biochim. Biophys. Acta. 831, 186-191

42. Kolb, H. J. (1975) Sedimentation behavior of fructose 1,6-bisphosphatase in crude tissue extracts of the rabbit and the rat. Arch. Biochem. Biophys. 170, 710-715

43. Rittenhouse, J., Harrsch, P. B., and Marcus, F. (1984) A re-evaluation of the molecular weight of yeast (Saccharomyces cerevisiae) fructose-1,6-bisphosphatase. Biochem. Biophys. Res. Commun. 120, 467-463

44. Zhou, Y. Ph. D. dissertation

45. Nelson, S. W., Kurbanov, F. T., Honzatko, R. B., and Fromm, H. J. (2001) The N-terminal segment of recombinant porcine fructose-1,6-bisphosphatase participates in the allosteric regulation of catalysis. J. Biol. Chem. 276, 6119–6124

46. von Geldern, T. W., Lai, C., Gum, R. J., Daly, M., Sun, C., Fry, E. H., and Abad-Zapatero, C. (2006) Benzoxazole benzenesulfonamides are novel allosteric inhibitors of

fructose-1,6-bisphosphatase with a distinct binding mode. Bioorg. Med. Chem. Lett. 16, 1811-1815

47. Hebeisen, P., Kuhn, B., Kohler, P., Gubler, M., Huber, W., Kitas, E., Schott, B., Benz, J., Joseph, C., and Ruf, A. (2008) Allosteric FBPase inhibitors gain 10(5) times in potency when simultaneously binding two neighboring AMP sites. Bioorg. Med. Chem. Lett. 18, 4708-4712

48. Gao, Y. and Honzatko. Water Structure of the Central Hydrophobic Cavity of Mammalian Fructose 1,6-bisphosphatase: a Potential Thermodynamic Determinant of Allowed Quaternary States. To be submitted.

49. Wright, S. W., Carlo, A. A., Carty, M. D., Danley, D. E., Hageman, D. L., Karam, G. A., Levy, C. B., Mansour, M. N., Mathiowetz, A. M., McClure L. D., Nestor, N. B., McPherson, R. K., Pandit, J., Pustilnik, L. R., Schulte, G. K., Soeller, W. C., Treadway, J. L., Wang, I.-K., and Bauer, P. H. (2002) Anilinoquizoline inhibitors of fructose 1,6-bisphosphatase bind at a novel allosteric site: synthesis, in vitro characterization, and X-ray crystallography. J. Med. Chem. 45, 3865-3877

50. Erion, M. D., van Poelje, P. D., Dang, Q., Kasibhatla, S. R., Potter, S. C., Reddy, M. R., Reddy, K. R., Jiang, T., and Lipscomb, W. N. (2005) MB06322 (CS-917): A potent and selective inhibitor of fructose 1,6-bisphosphatase for controlling gluconeogenesis in type 2 diabetes. Proc. Natl.Acad. Sci. U. S. A. 102, 7970–7975

51. Rudnitskaya, A., Huynh, K., Török, B., and Stieglitz, K. (2009) Novel heteroaromatic organofluorine inhibitors of fructose-1,6-bisphosphatase. J. Med. Chem. 52, 878-882

52. Kitas, E., Mohr, P., Kuhn, B., Hebeisen, P., Wessel, H. P., Haap, W., Ruf, A., Benz, J., Joseph, C., Huber, W., Sanchez, R. A., Paehler, A., Benardeau, A., Gubler, M., Schott, B., and Tozzo, E. (2010) Sulfonylureido thiazoles as fructose-1,6-bisphosphatase inhibitors for the treatment of type-2 diabete. Bioorg. Med. Chem. Lett. 20, 594-599

53. Hebeisen, P., Haap, W., Kuhn, B., Mohr, P., Wessel, H. P., Zutter, U., Kirchner, S., Ruf, A., Benz, J., Joseph, C., Alvarez-Sánchez, R., Gubler, M., Schott, B., Benardeau, A., Tozzo, E., and Kitas, E. (2011) Orally active aminopyridines as inhibitors of tetrameric fructose-1,6-bisphosphatase. Bioorg. Med. Chem. Lett. 21, 3237-3242

54. The PyMOL Molecular Graphics System, Version 1.5.0.4 Schrödinger, LLC.

CHAPTER VI. FUNCTIONAL IMPORTANCE OF SUBUNIT-PAIR ROTATION IN THE REGULATION OF TETRAMERIC MAMMALIAN FRUCTOSE-1,6-BISPHOSPHATASE

A paper to be submitted to *Biochemistry*

Yang Gao and Richard B. Honzatko

Roy J. Carver Department of Biochemistry, Biophysics, and Molecular Biology,

Iowa State University, Ames, IA 50011

Abstract

Fructose-1,6-bisphosphate (FBPase) is a homo-tetrameric enzyme that governs gluconeogenesis. In eukaryotic organisms, AMP inhibits FBPase allosterically and cooperatively, whereas fructose 2,6-bisphosphate (Fru-2,6-P_2) is an active site inhibitor. AMP and Fru-2,6-P_2 cause similar conformational changes in FBPase: AMP drives a 15 ° subunit-pair rotation, transforming FBPase from an active R-state to an inactive T-state; Fru-2,6-P_2 causes a 13 ° rotation. Mutant forms of FBPase, which have different inhibitory properties, from partial AMP inhibition to a loss of AMP cooperativity, exhibit a range of intermediate levels of subunit-pair rotations. Mutations of Met^{18}, located at the subunit-pair interface, were pursued in order to further test models that subunit-pair rotation accounts for the properties of AMP inhibition of wild-type and mutant FBPases. The Met^{18}→Lys mutation resulted in FBPase dimers that crystallized as tetramers with no subunit-pair rotation in the presence of AMP and no sensitivity toward AMP in inhibitory assays. The Met^{18}→Trp mutation resulted in FBPase tetramers that have subunit-pair rotations of 4 ° and 13 ° in the absence and presence of AMP, respectively. Trp^{18} FBPase exhibits partial AMP inhibition, no cooperativity in AMP inhibition and significantly reduced AMP/Fru-2,6-P_2 binding synergism. The properties of Trp^{18} FBPase indicate that AMP cooperativity is linked to subunit-pair rotation and that full AMP inhibition requires full subunit-pair rotation.

.

Introduction

Fructose-1, 6-bisphosphate (D-fructose-1, 6-bisphosphate 1-phosphohydrolase; EC 3. 1. 3; FBPase) governs a key regulatory step in gluconeogenesis, hydrolyzing fructose-1,6-bisphosphate (Fru-1,6-P_2) to fructose 6-phosphate (Fru-6-P) and inorganic phosphate (1-2). A futile cycle is formed by FBPase and Fructose-6-phosphate-1-kinase (PFK-1), the counterpart of FBPase in glycolysis (3). Fructose 2,6-bisphosphate (Fru-2,6-P_2) and AMP are inhibitors for FBPase and activators of PFK-1 (3-9). Glucagon release in response to starvation leads to the phosphorylation of the bifunctional liver enzyme fructose-6-phosphate-2-kinase/fructose-2,6-bisphosphatase (PFK-2/FBPase-2), which in turn activates phosphatase activity toward Fru-2,6-P_2; whereas in the fed state, insulin reverses the effect of glucagon, leading to elevated levels of Fru-2,6-P_2 (10-13). The presence of Fru-2,6-P_2 enhances AMP inhibition up to 10-fold, a property called AMP/Fru-2,6-P_2 synergism (8-9). Thus, even though AMP concentration is relatively constant *in vivo*, varying concentrations of Fru-2,6-P_2 to cause AMP to be a dynamic regulator FBPase activity (14).

Porcine liver FBPase is homotetramer existing in at least two quaternary states, R and T. Product complexes of FBPase with divalent metals as Mg^{2+}, Mn^{2+} or Zn^{2+} structurally define the active R-state (15-16). AMP complexes of FBPase (with product and divalent metals) define the inactive T-state (17-18). The tetramer is an approximate square-planar assembly of subunits. The upper subunit pair rotates 15 °relative to lower subunit pair and an important dynamic loop (residue 50-72) moves from active site (engaged conformation) to an alternative conformation (the disengaged conformation) during the R- to T-state transition (16,18). AMP cooperatively binds to allosteric sites some 28 Å away from the nearest active site and proximal to the subunit-pair interface. The kinetic mechanism of inhibition by AMP is non-competitive with respect to substrate and competitive with respect to Mg^{2+}(19). In the R-state, loop 50-72 (engaged conformation) stabilizes two of three metal cations bound to the active site (16). The binding of AMP drives subunit-pair rotation, the consequence of which is the destabilization of the engaged conformation of loop 50-72. The AMP-induced displacement of loop 50-72 to its disengaged conformation leaves one divalent metal in the active site (18). Introduction of proline into hinge of the dynamic loop reduces activity and

AMP inhibition of FBPase (20). Molecular dynamics simulation of the R- to T-state transition pathway implies that the subunit-pair rotation precedes loop displacement (21). Experimentally, mutations that destabilize T-state lead to identification of two AMP-bound intermediate states (I_R-state and I_T-state), which have engaged dynamic loops and dimer-dimer rotations of 3 and 11 °, respectively (21-22).

Fru-2,6-P_2 is a competitive inhibitor with respect to Fru-1,6-P_2 (5-6). Although bound to the active site, Fru-2,6-P_2 induces a13 ° subunit-pair rotation with disengaged loops similar to effect of AMP (15 ° rotation, disengaged loops) (23). The similar end-states induced independently by AMP and Fru-2,6-P_2 is the structural basis of AMP/Fru-2,6-P_2 synergism (23). Mutations that reduce AMP/Fru-2,6-P_2 synergism also reduce Fru-2,6-P_2 subunit pair-rotation (24). For *Escherichia coli* FBPase (eFBPase), a structural homolog of porcine liver FBPase, has no AMP/Fru-2,6-P_2 synergism and no Fru-2,6-P_2-induced subunit-pair rotation (23).

Mutant FBPases that have different mechanisms of AMP inhibition fall into two groups, which are distinguished by their oligomeric states (29). Mutant FBPases that exist as dimers in solution lack cooperativity in AMP inhibition, and exhibit wide range of sensitivity toward AMP, and in some instances exhibit partial inhibition at saturating levels of AMP (29). A second group consistent with FBPase tetramers but with different subunit pair rotations exhibit reduced AMP cooperativity (29), or partial AMP inhibition (21). Mutations on Met^{18} provide further tests of the two structural determinants for AMP inhibition. The mutation of Met^{18}→Lys causes dissociation of the tetramer. AMP induces subunit-pair separation instead subunit-pair rotation. The resulting enzyme is insensitive to AMP, and thus lacks AMP cooperativity, yet conforms to the model proposed for AMP properties of FBPase dimers. Met^{18}→Trp FBPase is a stable tetramer that lacks AMP cooperativity and exhibits partial inhibition by AMP. Trp^{18} FBPase evidently cannot be in either the R- or T-state, having instead subunit-pair rotations of 4 ° and 13 ° in the presence and absence of AMP, respectively. Properties of Trp^{18} FBPase are consistent with AMP cooperativity originating from an R-state tetramer with little or no subunit-pair rotation, and full AMP inhibition requiring full subunit-pair rotation to the canonical T-state. Moreover, Trp^{18} FBPase could

serve as a useful target in screening for inhibitors of FBPase that act synergistically with AMP and Fru-2,6-P_2.

Experimental procedures

Materials— Fru-1,6-P_2, $NADP^+$ and AMP were purchased from Sigma. Fru-2,6-P_2 was produced by the method of Van Schaftingen and Hers (25). Glucose-6-phophate dehydrogenase and phosphoglucose isomerase came from Roche Applied Sciences. FBPase-deficient *E.* coli strain DF 657 was from the Genetic Stock Center at Yale University. Other chemicals were of reagent grade or equivalent.

Mutagenesis of wild-type FBPase— All mutations were accomplished by specific base changes utilizing the Transformer^{TM} site-directed mutagenesis kit (Clontech). Mutagenic primers were as follows: Met^{18}→Lys, 5'-ACCCGCTTCGTCA**A**GGAGGAGGGCAG-3'; Met^{18}→Trp, 5'- ACCCGCTTCGTC**TG**GGAGGAGGGCAG-3' (altered bases are underlined and in bold typeface). Constructs were confirmed by sequencing the promoter region and the entire open reading frame. The Iowa State University sequencing facility provided DNA sequences using the fluorescent dye-dideoxy terminator method.

Expression and purification of wild-type and mutant FBPases— Supernatant solutions of cell free extracts were loaded onto a Cibracon Blue-Sepharose column previously equilibrated with 20 mM Tris-HCl, pH 7.5, 5mM $MgCl_2$. The column was washed with 20 mM Tris-HCl, pH 7.5. Enzyme was eluted with a gradient of 0-1 M of sodium chloride in 20 mM Tris-HCl, pH 7.5, then dialyzed against 20 mM Tris-HCl, pH 8.5, before loading onto a DEAE-Sepharose column equilibrated with 20 mM Tris-HCl, pH 8.3. Purified enzyme was eluted with a sodium chloride gradient (0–0.5 M) in 20 mM Tris-HCl, pH 8.3, and then dialyzed extensively against 50 mM Hepes, pH 7.4, for kinetic investigations and for crystallization experiments. Purity and protein concentrations of FBPase preparations were confirmed by sodium dodecylsulfate-polyacrylamide gel electrophoresis (SDS-PAGE) (26) and the Bradford assay (27), respectively.

Kinetic experiments— Phosphoglucose isomerase and glucose-6-phosphate dehydrogenase are coupling enzymes in assays for FBPase activity (1). The formation of NADPH was monitored by absorbance at 340 nm on UV spectrometer for specific activity measurement and by its fluorescence emission at 470 nm using an excitation wavelength of 340 nm for all other assays. Assays were performed at 22 ℃ in 50 mM Hepes, pH 7.5, contained EDTA and KCl at concentrations of 10 μM and 150 mM, respectively, and were initialized by the addition of enzyme. Kinetics data were fit to models with Grafit (28).

Sedimentation equilibrium— Protocols for sedimentation equilibrium experiments are in reference 29. Three protein concentrations (OD280 = 0.3, 0.5 and 0.7) of wild-type and mutant FBPases were centrifuged to equilibrium at 15000, 18000 and 21000 rpm and 4 ℃, using a Beckman XLA ultracentrifuge with an AN-60 rotor. Data were to single component and two-component equilibrium models using the program UltraScan (30).

Crystallization of mutant FBPase— The method of hanging drops was used in the crystallization of FBPase. Droplets on cover slips with 2 μl of protein solution mixed with 2 μl of precipitant solution were suspended over wells containing 500 μl of the precipitant solution. Crystals of product complex grew from a protein solution of FBPase (10 mg/ml), Hepes (25 mM, pH 7.4), $MgCl_2$ (5 mM), and Fru-1,6-P_2 (5 mM)) combined with a precipitant solution of Hepes (100 mM, pH 7.4), polyethylene glycol 3350 (8% (w/v)), glycerol (27% (v/v)), and *t*-butyl alcohol (5% (v/v))). Crystals of the AMP/product complex grew from a protein solution of FBPase (10 mg/ml), Hepes (25 mM, pH 7.4), $MgCl_2$ (5 mM), Fru-1,6-P_2 (5 mM), and AMP (5 mM) combined with a precipitant solution of Hepes (100 mM, pH 7.4), polyethylene glycol 3350 (12% (w/v)), glycerol (23% (v/v)), and *t*-butyl alcohol (5% (v/v)). Crystals were of equal dimensions (0.2– 0.4 mm), growing in approximately 3 days at 20 ℃. Crystals can be transferred directly from droplet to liquid nitrogen as cryo-protectants were included in conditions of crystallization.

Data collection, structure determination and refinement— Data were collected at Iowa State University from single crystals on a Rigaku R-AXIS IV++ rotating anode/image plate system using CuK_α radiation from an Osmic confocal optics system and a temperature of 110 K. Program D*trek (31) was used in data reduction.

Product and AMP/product complexes of Lys^{18} FBPase and the product complex of Trp^{18} FBPase are isomorphous to R-state FBPase whereas the AMP/product complex of Trp^{18} FBPase is isomorphous to T-state FBPase. Structures were solved by molecular replacement with R-state FBPase (PDBID: 1CNQ) and T-state FBPase (PDBID:1EYJ) as initial models. The resulting models underwent refinement using CNS (32) with force constants and parameters of stereochemistry from Engh and Huber (33). A cycle of refinement consisted of slow cooling from 1000 to 300 K in steps of 25 K followed by 100 cycles of conjugate gradient minimization and concluded by the refinement of individual thermal parameters. Xtalview (34) and Coot (35) were used in manually adjustments to structures. Waters were added to difference electron density of 2.5σ or better until no significant decrease was evident in the R_{free} value. Stereochemistry of the models was examined by the use of PROCHECK (36).

Results

Rationale for position 18 mutations— Met^{18} is at the C1-C4 interface of FBPase (Figure 1). In the T-state, side chains of Met^{18} from subunits C1 and C4 pack mutually, whereas in the R-state the side chains are apart. The mutation of Met^{18} to lysine should eliminate the T-state simply because two positively charged residues would occupy hydrophobic space filled by side-chains of methionine. The mutation of Met^{18} to rigid tryptophan should significantly limit subunit-pair rotation, favoring intermediate conformational states for the tetramer.

Kinetics experiments— FBPases that exhibit a dimer-tetramer equilibrium such as eFBPase or specific mutants of porcine FBPase also show a decline in activity over several hours upon dilution (29,37). Lys^{18} FBPase exhibit similar behavior (data not shown), indicating an unstable tetramer. Initializing assays with enzyme (as opposed to incubation of enzyme with reagents and initiation with metal cofactor) eliminates the effects of dilution as only the first few minutes of the linear progression curve determines the initial velocity. Kinetic parameters from enzyme-initiated assays are in Table I.

Lys^{18} and Trp^{18} FBPass retain approximately 60% and 30% of wild-type activity, respectively, with K_m for Fru-1,6-P_2 unchanged. Mg^{2+} activates wild-type and many mutant FBPases with positive cooperativity modeled empirically by Equation 1:

$$v/V_m = \frac{1}{1+(\frac{A_{0.5}}{A})^n} \qquad \text{(Equation 1)}$$

Where v, V_m , A, $A_{0.5}$ and n are velocity, maximum velocity, Mg^{2+} concentration, Mg^{2+} concentration that gives 50% activation and Hill coefficient for Mg^{2+} binding, respectively. The cooperative binding of Mg^{2+} in wild-type (n=1.7) and Lys^{18} (n=1.9) FBPase disappears in Trp^{18} FBPase (n=1.2). The Michaelis-Menten constant for Mg^{2+} (K_a-Mg^{2+} in Table 1) employs Equation 2 in fitting initial velocity at different at different concentrations of Fru-1,6-P_2 and Mg^{2+}:

$$v/V_m = \frac{A^n \cdot B}{A^2 \cdot B + K_a \cdot B + K_b \cdot A^n + K_{ia} \cdot K_b} \qquad \text{(Equation 2)}$$

Where v, V_m, A, B, K_a, K_b, and K_{ia} represent initial velocity, maximum velocity, concentration of free Mg^{2+}, concentration of free Fru-1,6-P_2, the Michaelis-Menten constant for Mg^{2+}, the Michaelis-Menten constant for Fru-1,6-P_2, and the dissociation constant for Mg^{2+} from the enzyme-metal complex, respectively. n is set to 2 for both wild-type and Lys^{18} FBPase and to unity for Trp^{18} FBPase. K_a for Mg^{2+} decreases around 4- and 7-fold for Lys^{18} and Trp^{18} FBPases, respectively, relative to wild-type FBPase. Reduced Mg^{2+} affinity has also been observed in Arg^{15}→Ala and Glu^{19}→Gln FBPases (38).

AMP inhibition of Lys^{18} FBPase is essentially absent up to 10 mM (Figure 2). In contrast, AMP is a potent inhibitor of Trp^{18} FBPase. The AMP inhibition curve is a fit of Equation 3:

$$v/V_m = \frac{1-V_{plateu}}{1+(\frac{I}{I_{0.5}})^n} + V_{plateu} \qquad \text{(Equation 3)}$$

where v, V_m , $V_{plateau}$, I, $I_{0.5}$ and n are velocity, maximum velocity, relative velocity at saturating levels of AMP, AMP concentration, AMP concentration that gives 50% activity

and Hill coefficient for AMP binding, respectively. AMP binds to wild-type FBPase with positive cooperativity but to Trp^{18} FBPase with no cooperativity.

AMP inhibition is competitive with respect to Mg^{2+}. K_i for AMP comes from fits using Equation 4:

$$v/V_m = \frac{A^{n_a}}{A^{n_a} + K_a \cdot (1 + \frac{I^{n_i}}{K_i})} \qquad \text{(Equation 4)}$$

where v is the velocity, V_M is the maximum velocity, A is the concentration of Mg^{2+}, I is the concentration of AMP, K_a is the Michaelis constant for Mg^{2+}, and K_i is the dissociation constant for AMP from the enzyme-inhibitor complex, n_a and n_i are Hill coefficients for $Mg^{2+}$and AMP, respectively. n_a and n_i are set to 2 for wild-type FBPase and unity for Trp^{18} FBPase. For Lys^{18} FBPase is not inhibited by AMP.

Concentrations of 10 mM Mg^{2+} and 20 μM Fru-1,6-P_2 were employed in the determination of Fru-2,6-P_2/AMP synergism. AMP titrations were carried out using six fixed concentrations of Fru-1,6-P_2 (0, 0.1, 0.3, 1, 3, and 10 μM, respectively) (Figure 3). Equation 3 is fit to data each series of constant concentration of Fru-1,6-P_2. For wild-type FBPase, $I_{0.5}$ for AMP inhibition decreases significantly as Fru-2,6-P_2 concentration increases, indicating strong Fru-2,6-P_2/AMP synergism; on the other hand, Trp^{18} FBPase showed only marginal change. The $I_{0.5}$ at different Fru-2,6-P_2 concentration can be fit to Equation 5 (28):

$$I_{0.5} = I_{0.5}^{high} + \frac{I_{0.5}^{low} - I_{0.5}^{high}}{1 + \frac{I_b}{\alpha_b}} \qquad \text{(Equation 5)}$$

In the equation above, $I_{0.5}$ is the AMP concentration that causes 50% inhibition, $I_{0.5}^{high}$ is the AMP concentration that causes 50% inhibition in the presence of an infinite concentration of Fru-2,6-P_2, $I_{0.5}^{low}$ is the AMP concentration that causes 50% inhibition in the absence of Fru-2,6-P_2, I_b is the concentration of Fru-2,6-P_2, α_b is the concentration of Fru-2,6-P_2 that produce 50% of maximal synergism. The value of ($I_{0.5}^{low}/I_{0.5}^{high}$) is a measure of Fru-2,6-P_2/AMP synergism. For wild-type FBPase, AMP inhibition is enhanced 7.6 fold by Fru-2,6-P_2, whereas for Trp^{18} FBPase, the $I_{0.5}^{low}/I_{0.5}^{high}$ values is 1.6.

Sedimentation Equilibrium— Fitting results of sedimentation equilibrium data with single-component and dimer-tetramer equilibrium models were reported in Table II. Wild-type and Trp^{18} FBPase show molecular weights of approximately 110 kDa, whereas Lys^{18} FBPase has a molecular weight of 64 kDa, approximately half of wild-type value. A similar molecular weight has been obtained for wild-type FBPase through dynamic light scattering (37). Molecular weights of all three FBPases from the dimer-tetramer equilibrium model are close to those from the single-component model. K_d values from dimer-tetramer equilibrium model were over 1 M, which indicates the real K_d value for the dissociation of the tetramer into dimers is out of the concentration range used in sedimentation equilibrium experiments.

Crystal Structures of product and AMP/product complexex of Lys^{18} FBPase (Protein Data Bank code 4GWW and 4GWY)— Crystals of product and AMP/product complexes of Lys^{18} FBPase belong to space group *I222*, and are isomorphous to those of the canonical R-state (16). A monomer exists in the asymmetric unit. Models include residues 6-335 and 10-335 for product and AMP/product complexes of Lys^{18} FBPase, respectively. High B-parameters and weak electron density are associated with residues 54-70 of the dynamic loops in both complexes. Statistics of data collection and refinement are in Table III.

The product complex of Lys^{18} FBPase is in the R-state. The root-mean-squared deviation between Lys^{18} and wild-type R-states is approximately 0.4 Å, indicating no significant differences in global conformations. One Fru-6-P and P_i, and two metal cations (Mg^{2+} at sites 1 and 2) bind to the active site. The NZ atom of Lys^{18} is 3.3 Å away from the backbone carbonyl of Ser^{87} of an adjacent subunit (C1-C4 interaction). The structure is in other ways comparable to the canonical R-state, which is described in detail elsewhere (16).

The AMP/product complex of Lys^{18} FBPase appears to be an R-like tetramer (subunit-pair rotation of 0 °) with loops 50-72 in engaged conformations; however, subunit-pairs C1-C2 and C3-C4 are separated by approximately 1 Å relative to the canonical R-state (Figure 4). AMP binds to allosteric sites with Fru-6-P and P_i and three metal cations (Mg^{2+} at sites 1, 2 and 3) at the active site. The base of AMP hydrogen bonds with the side chain of Thr^{31} and the backbone carbonyl of Val^{17}, inducing conformational changes (Figure 5) comparable to those in other R-like complexes in the absence and presence of bound AMP

(22, 29): Helix H1 shifts towards and helix H2 away from the center of the tetramer and the side chain of Ile^{10} moves away from its interaction with Ile^{190}. Lys^{18} undergoes a conformational change that allows it to avoid a collision with the side chain of Ser^{87} from a symmetry related subunit. The separation of subunit pairs weakens C1-C4 interactions normally observed in stable tetramers. Backbone carbonyls of residues 108-110 are no longer within donor-acceptor distance of Arg^{22} and that between Thr^{39} and Glu^{192} increases by 0.6 Å. Similar changes occur in the I_R-state of the AMP/product complex of Leu^{54} FBPase; however, those changes are due to a 3 ° subunit-pair rotation rather than to the separation of subunit pairs without rotations as observed here.

Crystal Structures of Product Complex and AMP complex of Trp^{18} FBPase (Protein Data Bank code 4GWX, 4GWZ)— Crystals of the product complex of Trp^{18} FBPase are in space group *I222* (*a* = 53.422 Å; *b* = 82.646 Å; *c* = 165.423 Å), isomorphous to those of the canonical R-state (16). Crystals of the AMP/product complex of Trp^{18} FBPase are in space group $P2_12_12$ (*a* = 59.776 Å; *b* = 166.064 Å; *c* = 79.871 Å), isomorphous to those of the canonical T-state (18). Both models start from residue 9 and end at residue 335. Statistics for data collection and refinement are in Table III.

Three metal cations (Mg^{2+} at sites 1, 2 and 3), Fru-6-P and P_i are at the active site of the Trp^{18} FBPase product complex. Loop 50-72 is ordered and in its engaged conformation. As has been observed in the Fru-2,6-P_2 complex of His^{45}/Arg^{46}/Tyr^{186} FBPase (24), the AMP binding site in product complex adopts conformational changes observed typically in the presence of bound AMP (Figure 6). The C-terminal end of helix H1 shifts towards the center of the tetramer, and the side-chain of Ile^{10} leaves its hydrophobic contact with Ile^{190}.

The AMP/product complex of Trp^{18} FBPase has Fru-6-P and Pi at the active site with 2 metal cations (Mg^{2+} at site 1 and 2), as well as strong electron density covering a molecule of AMP at the allosteric site. Loop 50-72 is in its disengaged conformation with residues 62-72 disordered (weak electron density and high thermal parameters).

The quaternary structures of Trp^{18} FBPase with and without AMP differ by subunit-pair rotations that are considerable less than those of the wild-type enzyme (Figure 7). In the

absence of AMP, the product complex of Trp^{18} FBPase has a subunit-pair rotation of 4 ° and in the AMP/product complex a 13 ° of subunit-pair rotation. The corresponding values are 0 ° and 15 ° for wild-type FBPase. The restricted subunit-pair rotation observed for Trp^{18} FBPase is only in part due to steric constraints introduced by the rigid fused ring of the indole (Figure 6). Assuming no only rigid-body motion, a subunit-pair rotation of 0 ° puts that side chain of Trp^{18} 3.3 Å away from main-chain atoms of Ser^{88}, and a subunit-pair rotation of 15° puts that side chain 3.1 Å from the Cα atom of Gly^{28}. Unlike the wild-type side chain of Met^{18}, which falls into the steric well defined by helices H2 and H3 (R-state) or the well defined by helices H1 and H2 (T-state), the side chain of Trp^{18} remains in the steric well defined by helices H2 and H3, and evidently cannot transition into the well defined by helices H1 and H2. Instead, the χ^1 torsion angle of Trp^{18} may be the basis for two quaternary states. The R-like state (subunit-pair rotation of 4°) has a χ^1 angle of –63 °, whereas in the T-like state (subunit-pair rotation of 13°) the χ^1 torsion angle is –176 °. Hence, the two energy-minimum χ^1 angles of Trp^{18} define the two quaternary states of Trp^{18} FBPase.

Discussion

Several mutant forms of porcine FBPase without AMP cooperativity are in the literature (29, 37-41). Most are subunit-pair dimers in solution, and hence lose AMP cooperativity by the loss of C1-C4 interactions (29). Arg^{22}→Met FBPase, however, is a tetramer in solution without cooperativity and is in a T-like quaternary state in the absence of AMP (29). Presumably, cooperativity is absent in Met^{22} FBPase because a single molecule of AMP locks the tetramer into an inactive conformation. Hence, mutant FBPases fall into two groups (solution dimers and tetramers), which require different models to account for the properties of AMP inhibition.

The model for AMP cooperativity exhibited by the tetramer comes from the kinetics of hybrid tetramers (51) and the structure of an AMP-ligated R-like complex of Ala^{54}→Leu FBPase (22). AMP ligation of hybrid tetramers with functional pockets in one of two subunit-pairs of the tetramer (for instance subunits C1 and C2) is non-cooperative, whereas

the binding of one molecule of AMP to each of two subunit-pairs is cooperative. The AMP/product complex of Leu^{54} FBPase (I_R-state, 3° subunit-pair rotation) putatively captures the effect of AMP binding to the R-state; however, are observed conformational changes due to the binding of AMP or the 3° subunit-pair rotation? Trp^{18} FBPase is a tetramer in solution (Table II). Its product complex exhibits a 4° subunit-pair rotation in the absence of AMP. The displacement of Ile^{10} from the surface of Ile^{190} is evident; however, hydrogen bonds critical to the proposed mechanism of cooperativity are intact (Thr^{39} retains its hydrogen bond with Glu^{192} across the C1-C4 interface and Asn^{35} retains its hydrogen bond with Thr^{14}). Hence, a 4° subunit-pair rotation alone does not cause conformational change in the AMP pocket. Such changes must come with the binding of AMP.

If AMP pockets of the product complex of Trp^{18} FBPase are similar to those of wild-type R-state, then why has the K_i for AMP increased by 10-fold (Table I)? As in the wild-type enzyme, the binding of AMP must shear helices H1 and H2 and consequently disrupts hydrogen bonds between Asn^{35} and Thr^{14} and between Thr^{39} and Glu^{192} (the latter reforms after transition to the T-state). Additionally for Trp^{18} FBPase, χ^1 of Trp^{18} must undergo a 120° rotation, which requires more AMP binding energy relative to the wild-type system, hence the increase in K_i. Moreover, Trp^{18} FBPase with AMP only harbors 13 degree subunit-pair rotation, 2 degree away from the optimal AMP binding conformation observed in wild-type enzyme.

AMP is a non-cooperative inhibitor of Trp^{18} FBPase if the binding of a single molecule of AMP triggers the R- to T-state transition (the proposed model for the absence of AMP cooperativity for Arg^{22}→Met FBPase). A single molecule of AMP maximally inhibits the mutant enzyme, so that the binding of additional molecules of AMP has no effect on reaction velocity. The absence of cooperativity in the inhibition of wild-type FBPase by Fru-2,6-P_2 is subject to a similar explanation. If a single molecule of Fru-2,6-P_2 puts the wild-type tetramer into a T-like state, then the cooperative binding of additional molecules of Fru-2,6-P_2 has no influence on activity. The appearance of cooperativity in substrate-saturation curves in the presence of low levels of Fru-2,6-P_2 (6) infers that an Fru-2,6-P_2-stabilized T-state can be driven back into the R-state by the binding of one or more molecules of Fru-1,6-

P_2. The unoccupied active sites will necessarily have a higher affinity for substrate, hence the observed sigmoidicity in substrate-binding curves.

The model for partial AMP inhibition of Ile^{10}→Asp FBPase applies to Trp^{18} FBPase. Both enzymes are tetramers (Asp^{10} FBPase retains a wild-type Hill coefficient for AMP inhibition of two). Subunit-pair rotation in the tetramer correlates with AMP inhibition (24). Hence, the observed subunit-pair rotation of 13° in the AMP/product complex of Trp^{18} FBPase is the basis for 10% activity in the presence of saturating levels of AMP. Full inhibition by AMP in the tetramer requires full subunit-pair rotation (15°) as has been observed in the kinetics and structures of Arg^{22}→Met FBPase (29).

Solution dimers represent the other subgroup of FBPase mutants, of which Lys^{18} FBPase is evidently a member (Table II). Loss of the C1-C4 interface abolishes cooperativity (29); however, levels of AMP inhibition vary widely, being absent (Lys^{18} FBPase), or biphasic (Gln^{192} and Ala^{39} FBPases). Perhaps the simplest model to account for these observations is one of a reversible dimer-tetramer equilibrium in which AMP stabilizes an inactive T-state tetamer (Scheme I):

$$\begin{array}{ccc} P & \overset{+S}{\leftrightarrow} & PS \rightarrow \text{products} \\ {\scriptstyle +I}\updownarrow & & {\scriptstyle +I}\updownarrow \\ PI & \overset{+S}{\leftrightarrow} & PIS \rightarrow \text{products} \\ {\scriptstyle +I}\updownarrow & & {\scriptstyle +I}\updownarrow \\ P_2I_2 & \overset{+S}{\leftrightarrow} & P_2I_2S_2 \end{array}$$

Scheme I

AMP arrests subunit exchange (51), indicating a stabilizing effect on the tetramer. Lys^{18} FBPase differs from other mutant dimers in that it cannot form a stable T-state tetramer. In the T-state, side chains of Lys^{18} from subunits C1 and C4 would be in contact and buried at a hydrophobic interface (Figure 1). Other dimers (for instance, Gln^{192} and Ala^{39} FBPases) bind AMP, presumably without inhibition, and form inactive T-state tetramers. Velocity as a function of AMP concentration for the model (Figure 2, 29) depends on the constant governing the equilibrium between AMP-bound dimers and tetramers. Partial activity is

determined by the fraction of AMP-bound dimers in the presence of saturating AMP, and the Hill coefficient for AMP inhibition is unity.

Mg^{2+} cooperativity in Trp^{18} FBPase has fallen to near unity, but that of Lys^{18} FBPase is unchanged from the wild-type enzyme (Table 1). Mg^{2+} cooperativity is a property of the FBPase monomer, and is due putatively to the coupled binding of Mg^{2+} to metal sites 2 and 3 (42). Hence, undiminished Mg^{2+} cooperativity for a solution dimer (such as Lys^{18} FBPase) comes as no surprise; however, the loss of Mg^{2+} cooperativity in Trp^{18} FBPase (a tetramer) is noteworthy. The deletion of 7 and 10 residues from the N-terminus of FBPase reduces Mg^{2+} cooperativity and increases the K_a for Mg^{2+} by 20-fold. Mutations of $Asp^{2}\rightarrow$Ala, $Phe^{6}\rightarrow$Trp, $Asp^{7}\rightarrow$Ala and $Asn^{9}\rightarrow$Ala modestly elevate the K_a for Mg^{2+} and depress the Hill coefficient for Mg^{2+} (52). Residues 1 to9 of FBPase have weak electron density R-state structures (and electron density altogether absent in the T-state), but Asn^{9} hydrogen bonds with $Arg^{15}$and may indirectly stabilize the engaged conformation of loop 50-72 (52). The likely consequence of a destabilized engaged conformation for loop 50-72 is weak binding of Mg^{2+} at site 3, causing an increase in the K_a for Mg^{2+}, reduced cooperativity and decreased activity. As Trp^{18} FBPase cannot reach the canonical R-state (its product complex has a 4° subunit-pair rotation), its engaged loop 50-72 may be destabilized with the resulting impact on the properties of Mg^{2+} activation of catalysis.

FBPase is a drug target for type II diabetes (44). To date, most drug development efforts have focused on the AMP binding site (45-50); however, there is an inherent weakness in targeting the AMP site. Firstly, the AMP binding site is hydrophilic and hydrophilic inhibitors pass through membranes with difficulty. Secondly, adenine nucleotides pervade metabolism as regulators and substrates, necessitating the incorporation of specific attributes that are unique to the AMP pocket of FBPase. The cavity occupied by Met^{18} in the T-state could be a good target for drug development. Indeed, some inhibitors of FBPase occupy the Met^{18} pocket and the adenine pocket of T-state complexes of FBPase (46). In such complexes, Met^{18} remains in the well between helices H2 and H3 to create space for planar hydrophobic moieties from a pair of inhibitor molecules (Figure 8). The T-like state of Trp^{18} FBPase leaves a comparable void also by remaining in the well defined by helices

H2 and H3. Trp^{18} (the only tryptophan in this mutant form of FBPase) provides a reporter group for the binding of ligands to the Met^{18} pocket, which offers a simple fluorescence-based assay for screening ligands. Any ligand that occupies this cavity should in principle inhibit FBPase synergistically with AMP and Fru-2,6-P_2.

Table I. Kinetic parameters for wild-type and mutant FBPases.

FBPase	Specific Activity	K_M Fru-1,6-P_2	Hill Mg^{2+}	K_a Mg^{2+}	Hill AMP	K_i AMP	K_i Fru-2,6-P_2
	Units/mg/s	μM		mM[2 a]		μM[2 b]	μM
Wild-type	25	1.47 ±0.07	1.7 ±0.1	0.70 ±0.05	2.2 ±0.1	0.76 ±0.08	0.14 ±0.01
Lys^{18}	16	1.2 ±0.1	1.9 ±0.1	3.3 ±0.7	N.D.[c]	N.D.	0.15 ±0.03
Trp^{18}	7.5	1.2 ±0.2	1.2 ±0.1	5.1 ±0.4	1.05 ±0.09	8.2 ±0.5	0.079 ±0.005

[a] K_a for Mg^{2+} for Trp^{18} FBPase is in unit mM

[b] K_i for AMP for Trp^{18} FBPase is in unit μM

[c] Not determined

Table II. Sedimentation equilibrium data fitting for wild-type and mutated FBPase

Protein	Single component, ideal		Monomer-dimer equilibrium		
	M.W.	*S.D.*[b]	*M.W.*	K_d (M)	*S.D.*[b]
Wild-Type	112100	0.009	113900	2.718	0.01
Lys^{18}	64270	0.006	64270	2.718	0.006
Trp^{18}	114100	0.007	114100	2.718	0.007

[a] The results were derived from global fitting of all data with software Ultrascan
[b] Standard derivation of the global fitting

Table III. Statistics of data collection and refinement for Lys[18] and Trp[18] FBPase.

Crystalline complex[a]	Product Complex of Trp[18]	AMP/Product Complex of Trp[18]	Product Complex of Lys[18]	AMP/Product Complex of Lys[18]
Space group	*I222*	*P2$_1$2$_1$2*	*I222*	*I222*
Resolution limit (Å)	2.34	2.60	3.00	3.00
Number of measurements	56,218	89,544	21,589	26,433
Number of unique reflections	15,914	24,685	7,145	7139
Completeness of data (%):				
Overall	99.4	97.8	93.1	91.5
Last shell/resolution-range (Å)	99.9/2.43-2.35	99.6/2.69-2.60	96.6/3.11-3.00	94.3/3.11-3.00
R_{sym}[b]				
Overall	0.094	0.086	0.169	0.137
Last shell/resolution-range (Å)	0.313/2.43-2.35	0.338/2.69-2.60	0.488/3.11-3.00	0.401/3.11-3.00
Number of reflections in refinement	15,112	23,377	6,810	6,811
Number of atoms	2,670	5261	2589	2,614
Number of solvent sites	139	166	38	75
R_{factor}[c]	0.204	0.205	0.223	0.210
R_{free}[d]	0.254	0.275	0.292	0.267
Mean B (Å^2) overall/protein	32.7	37.0	63.6	43.0
Mean B (Å^2) for AMP	-	39.1	-	62.4
Root mean square deviations:				
Bond lengths (Å)	0.021	0.017	0.015	0.016
Bond angles (°)	1.6	1.8	1.5	1.6

[a] Unit cell lengths (*a*, *b*, *c*) in Å for product and AMP/product complexes of Trp[18] and Lys[18] FBPase are (53.971, 83.272, 165.772), (59.776, 166.064, 79.871), (53.433, 82.646, 165.423) and (53.261, 82.571, 168.885), respectively. Unit cell angles (α, β, γ) are 90° for space groups *I222* and *P2$_1$2$_1$2*.

[b] $R_{sym} = \Sigma_j\Sigma_i \mid I_{ij} - \langle I_j \rangle \mid / \Sigma_i\Sigma_j I_{ij}$, where *i* runs over multiple observations of the same intensity, and *j* runs over all crystallographically unique intensities.

[c] $R_{factor} = \Sigma \parallel F_{obs} \mid - \mid F_{calc} \parallel / \Sigma \mid F_{obs} \mid$, where $\mid F_{obs} \mid > 0$.

[d] R_{free} based upon 10% of the data randomly culled and not used in the refinement.

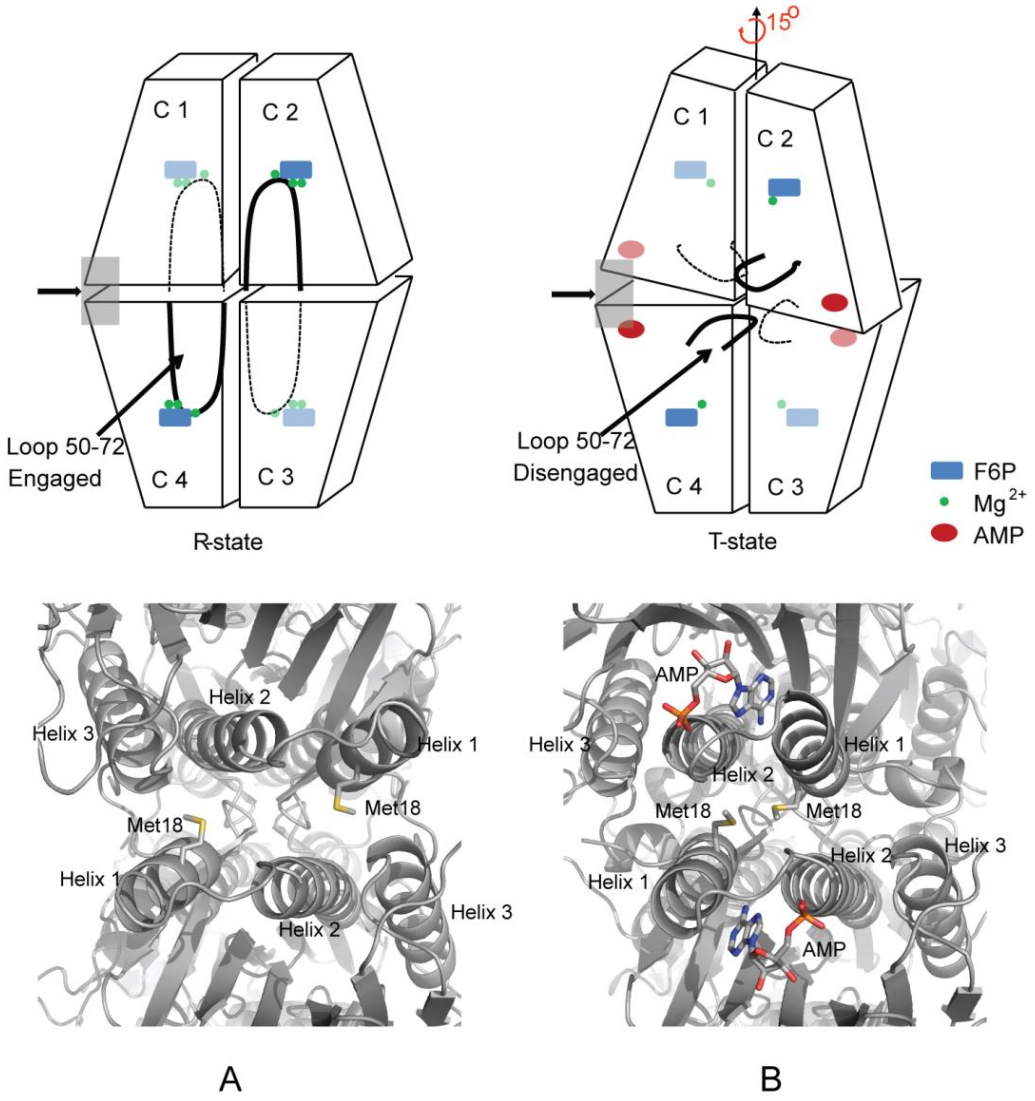

Figure 1. R- and T-states of FBPase. Cartoon representation of R-state (upper left) and T-state (upper right) defines the subunit-pair rotation which has subunits C1 and C2 move as a rigid body relative to subunits C3 and C4. Bold lines and dark colors represent structural elements and ligands binding to the front face of the tetramer. Thin lines and pastel colors represent structural elements and ligands on the back face of the tetramer. Shaded regions with arrows represent regions and viewing directions, respectively, for the panels below. In the R-state (lower left), Met^{18} (stick representation) occupies the well between helices H2 and H3, whereas in the T-state (lower right), Met^{18} is in contact with its symmetry partner and occupies the well between helices H1 and H2.

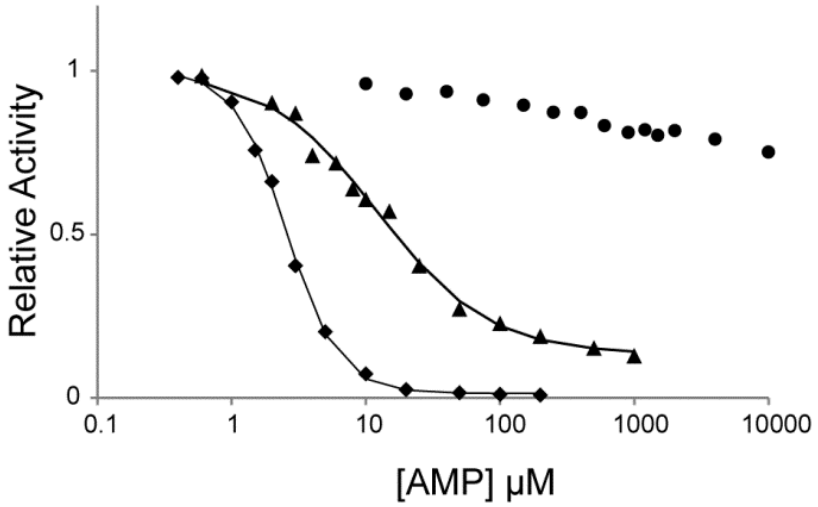

Figure 2. AMP inhibition of wild-type and mutant FBPases. Relative velocity as a function of AMP concentrations for wild-type (◆), Trp^{18} (▲) and Lys^{18} (●) FBPases were shown. Curves come from fits of equation 3 for wild-type and Trp^{18} FBPase.

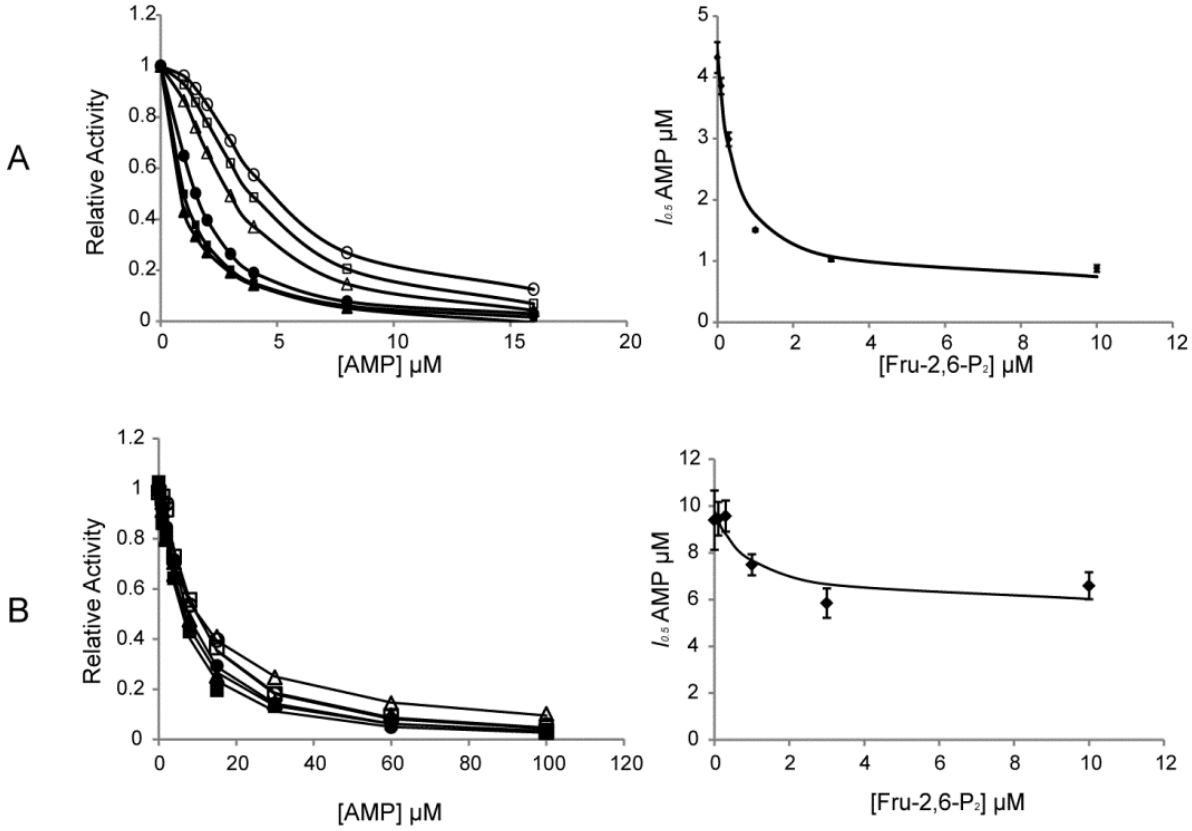

Figure 3. Fru-2,6-P_2/AMP synergism for wild type and Trp[18] FBPase. A and B represent data from wild type and Trp[18] FBPase, respectively. AMP titration curve (left panels) at different Fru-2,6-P_2 concentrations: 0 (○), 0.1 (□), 0.3 (△), 1 (●), 3 (■), and 10 μM (▲). The $I_{0.5}$ values determined from AMP titrations are plotted against Fru-2,6-P_2 concentrations (right panels).

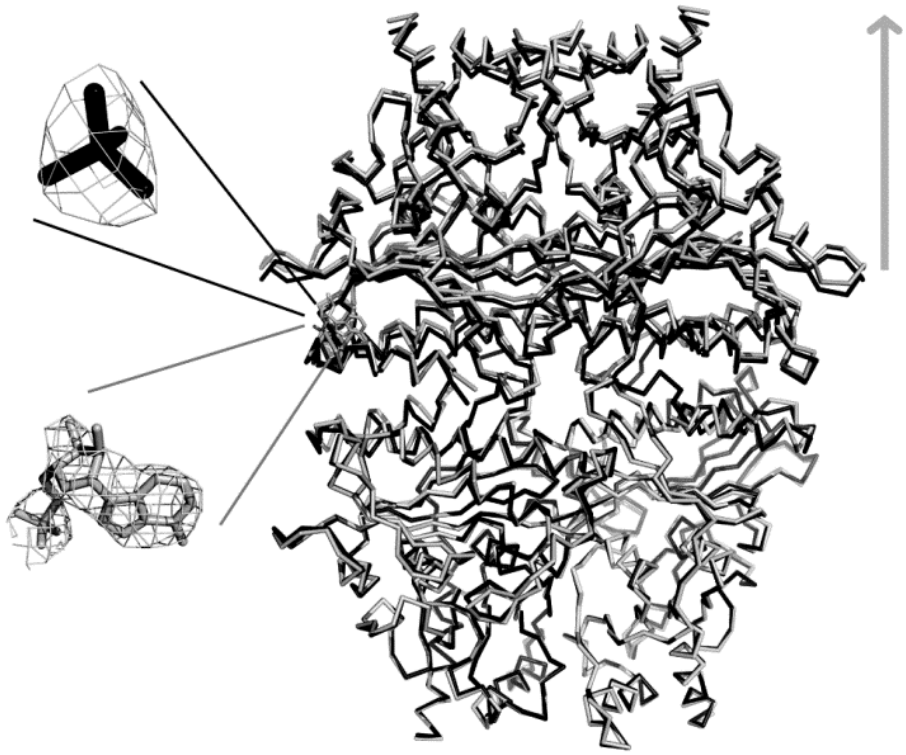

Figure 4. Crystal structure of product and AMP/product complexes of Lys[18] FBPase. Lower dimer of the product (black) and AMP/product (grey) complexes of Lys[18] FBPase are aligned to reveal the dimer-dimer separation the latter complex. Ligands at the AMP site are depicted with associated electron densities.

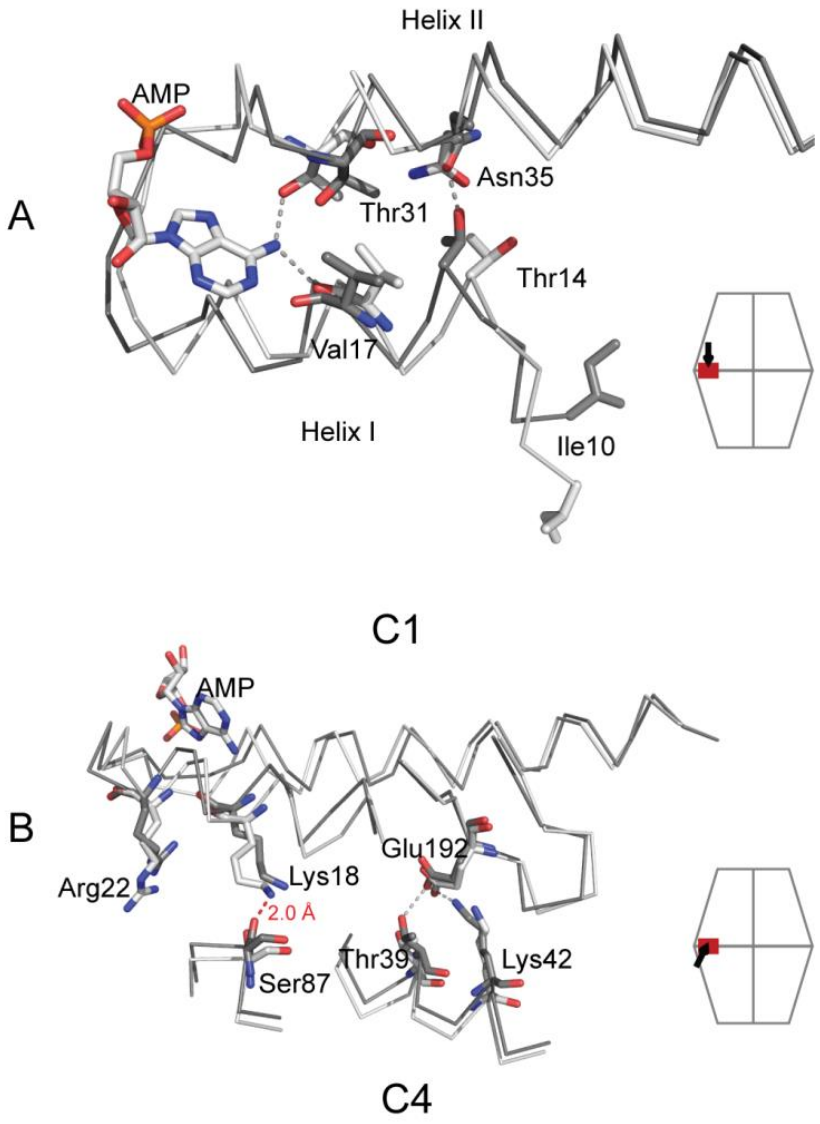

Figure 5. Conformational change at AMP binding site upon AMP ligation of Lys[18] FBPase. Subunit C1 of product (dark grey) and AMP/product complexes (light grey) of Lys[18] FBPase are aligned with top- (A) and side- (B) views of the AMP binding site presented. Selected residues are in stick-model representation. Grey dotted lines indicate donor-acceptor bonds, whereas red dotted lines in B indicate the potential conflict between Lys[18] and Ser[87] in the absence of the 1 Å dimer-dimer separation.

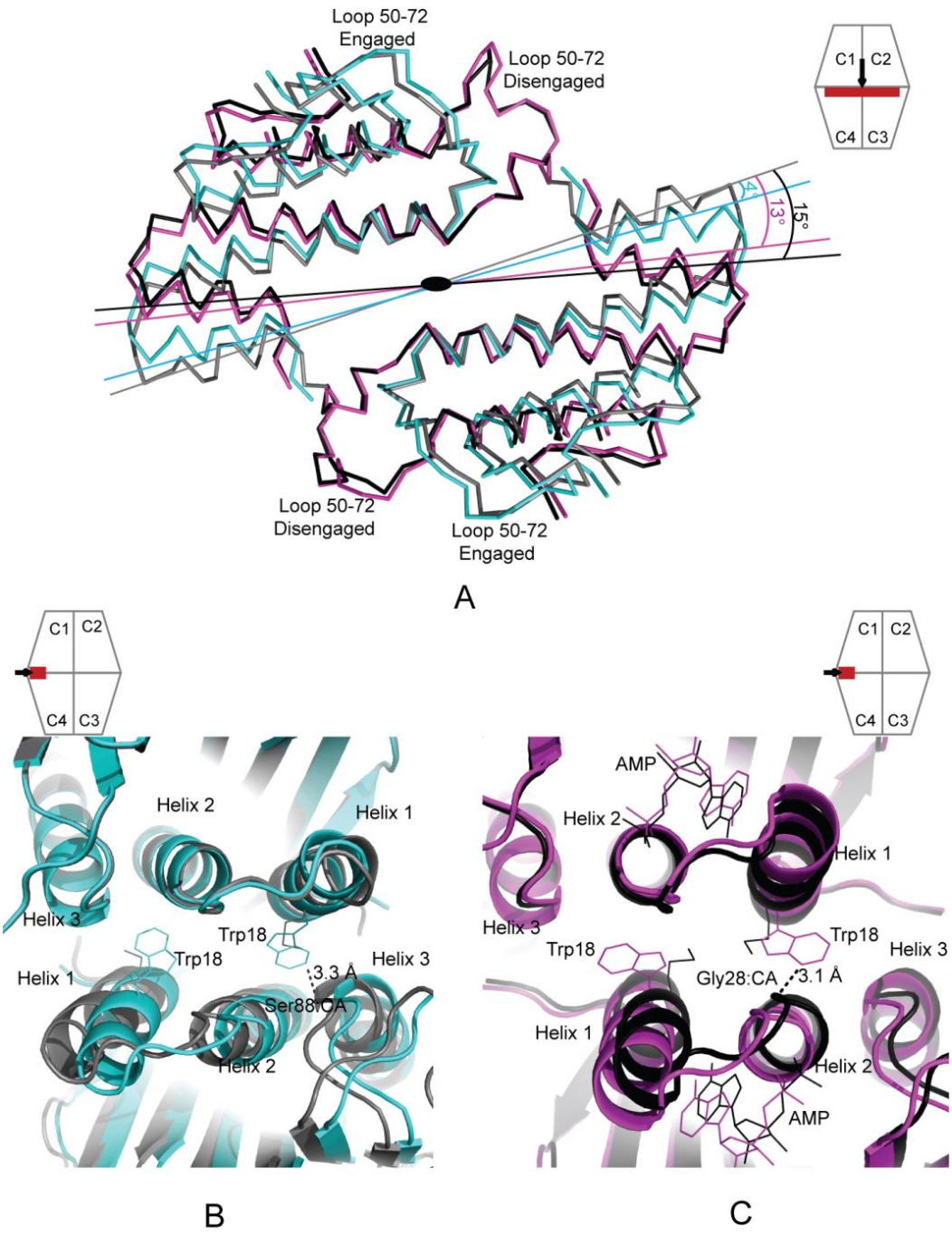

Figure 6. Global conformational changes of Trp^{18} FBPase. A. lower dimers of wild-type product complex (grey), wild-type AMP/product complex (black), Trp^{18} product complex (magenta) and Trp^{18} AMP complex (cyan) are aligned and the first 90 residues of the upper dimer of each structure are shown. Dimer-dimer rotations and the rotational axis are indicated in the figure. B. Side-view of the alignment of the product complex of wild-type (grey) and Trp^{18} (magenta) FBPase is shown. The potential conflict between sidechain of Trp^{18} and Ser^{88} is indicated by a dotted line. C. Side-view of the alignment of AMP/product complex of wild-type (black) and Trp^{18} (cyan) FBPase is shown. The potential conflict between sidechain of Trp^{18} and Gly^{28} is indicated by a dotted line.

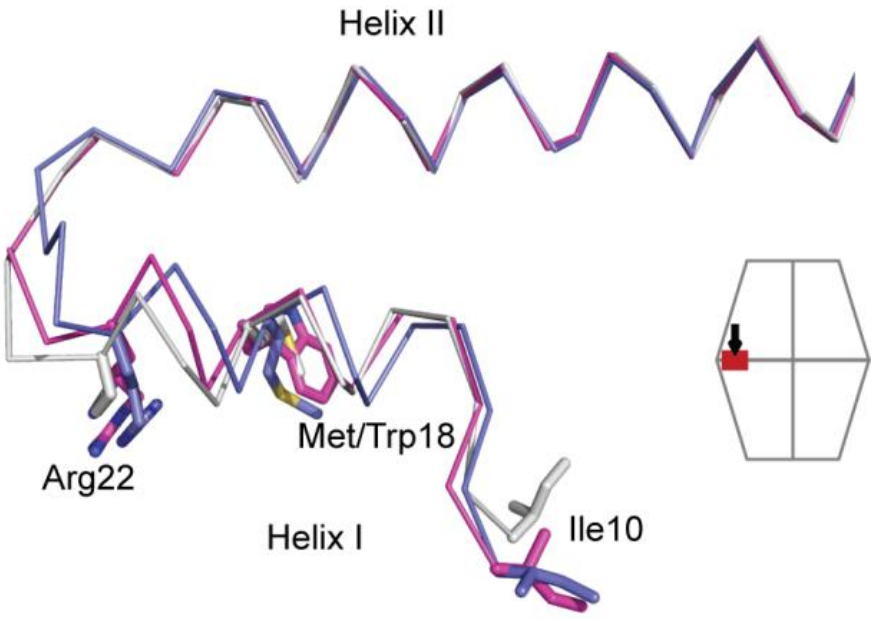

Figure 7. Structure alignment of first two helixes of wild-type product complex (grey), Trp[18] product complex (magenta) and His[45]/Arg[46]/Tyr[186] Fru-2,6-P_2 complex (cyan). Helix 2 from all complexes is aligned to reveal the relative change between Helix 1 and Helix 2.

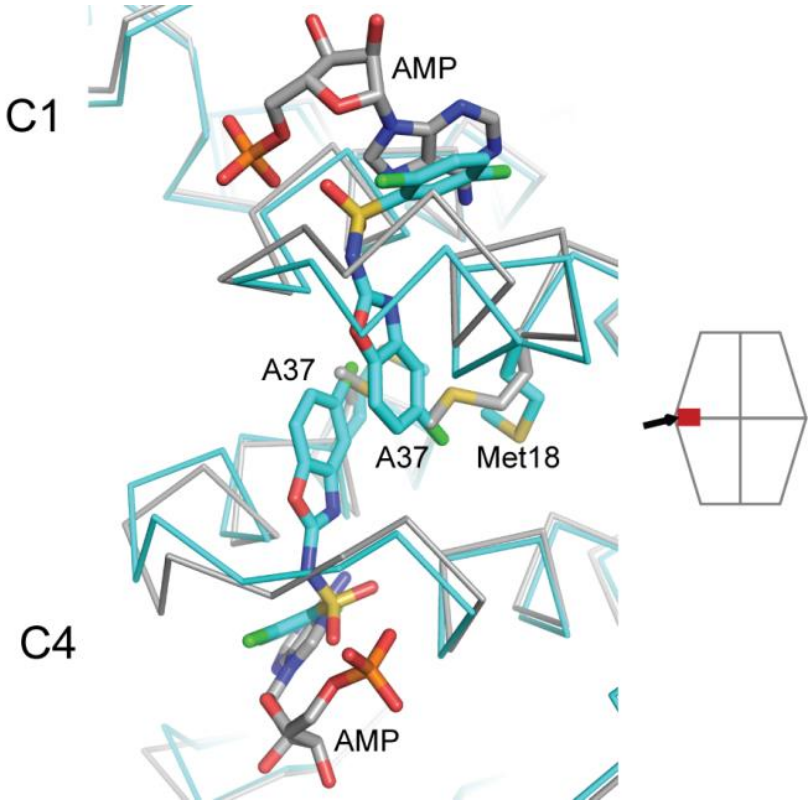

Figure 8. Met[18] cavity in T-state of FBPase. T-state FBPase with AMP (PDB ID: 1EYJ) (grey) and A37 (PDB ID: 2FHY) (cyan) are aligned. A37 is an AMP binding site effector that spans both the AMP binding site and the Met[18] cavity. Binding modes of AMP and A37 are illustrated by stick representations.

Reference

1. Benkovic, S. J., and de Maine, M. M. (1982) Mechanism of action of fructose 1,6-bisphosphatase. Adv. Enzymol. Relat. Areas Mol. Biol. 53, 45–82

2. Tejwani, G. A. (1983) Regulation of fructose-bisphosphatase activity. Adv. Enzymol. Relat. Areas Mol. Biol. 54, 121–194

3. Blangy, D., Buc, H. & Monod, J. (1968) Kinetics of the allosteric interactions of phosphofructokinase from Escherichia coli. J. Mol. Biol. 31, 13-35

4. Taketa, K., and Pogell, B. M. (1965) Allosteric inhibition of rat liver fructose 1,6-bisphosphatase by adenosine 5'-monophosphate. J. Biol. Chem. 240, 651–662

5. Pilkis, S. J., El-Maghrabi, Pilkis, J., and Claus, T. (1981) Inhibition of fructose-1,6-bisphosphatase by fructose 2,6-bisphosphate. J. Biol. Chem. 256, 3619–3622

6. Van Schaftingen, E., and Hers, H.-G. (1981) Inhibition of fructose-1,6-bisphosphatase by fructose 2,6-biphosphate. Proc. Natl. Acad. Sci. U. S. A. 78, 2861–2863

7. Pilkis S. J., El-Maghrabi, Pilkis, J., Claus, T. H., and Cumming D. A. (1981) Fructose 2,6-bisphosphate. A new activator of phosphofructokinase. J. Biol. Chem. 256, 3171–3174

8. Van Schaftingen, E., Jett, M.-F., Hue, L., and Hers, H.-G. (1981) Control of liver 6-phosphofructokinase by fructose 2,6-bisphosphate and other effectors. Proc. Natl.Acad. Sci. U. S. A. 78, 3483–3486

9. Uyeda, K., Furuya, E., and Luby, L. J. (1981) The effect of natural and synthetic D-fructose 2,6-bisphosphate on the regulatory kinetic properties of liver and muscle phosphofructokinase. J. Biol. Chem. 256, 8394–8399

10. Pilkis, S. J., el-Maghrabi, M. R., and Claus, T. H. (1988) Hormonal regulation of hepatic gluconeogenesis and glycolysis. Annu. Rev. Biochem. 57, 755-783

11. Christophe, J. (1995) Glucagon receptors: from genetic structure and expression to effector coupling and biological responses. Biochim. Biophys. Acta. 1241, 45-57

12. Pilkis, S. J., Claus, T. H., Kurland, I. J., and Lange, A. J. (1995) 6-Phosphofructo-2-kinase/fructose-2,6-bisphosphatase: a metabolic signaling enzyme. Annu. Rev. Biochem. 64, 799-835

13. Okar, D. A., Manzano, A., Navarro-Sabate, A., Riera, L., Bartrons, R., and Lange, A. J. (2001) PFK-2/FBPase-2: maker and breaker of the essential biofactor fructose-2,6-bisphosphate. Trends Biochem. Sci. 26, 30-35

14. Okar, D. A., and Lange, A. J. (1999) Fructose-2,6-bisphosphate and control of carbohydrate metabolism in eukaryotes. Biofactors 10, 1–14

15. Ke, H., Thorpe, C. M., Seaton, B. A., Marcus, F., and Lipscomb, W. N. (1989) Molecular structure of fructose-1,6-bisphosphatase at 2.8-Å resolution. Proc. Natl. Acad. Sci. U.S.A. 86, 1475-1479

16. Choe, J. Y., Poland, B. W., Fromm, H. J., and Honzatko, R. B. (1998) Role of a dynamic loop in cation activation and allosteric regulation of recombinant porcine fructose-1,6-bisphosphatase.Biochemistry 37, 11441-11450

17. Ke, H. M., Zhang, Y. P., and Lipscomb, W. N. (1990) Crystal structure of fructose-1,6-bisphosphatase complexed with fructose 6-phosphate, AMP, and magnesium. Proc. Natl. Acad. Sci. U.S.A. 87, 5243-5247

18. Choe, J. Y., Fromm, H. J., and Honzatko, R. B. (2000) Crystal structures of fructose 1,6-bisphosphatase: mechanism of catalysis and allosteric inhibition revealed in product complexes. Biochemistry 39, 8565-8574

19. Stone, S. R., and Fromm, H. J. (1980) Studies on the mechanism of adenosine 5'-monophosphate inhibition of borvine liver fructose 1,6-bisphosphatase. Biochemistry 19, 620–625

20. Nelson, S. W., Choe, J. Y., Honzatko, R. B., and Fromm, H. J. (2000) Mutations in the hinge of a dynamic loop broadly influence functional properties of fructose-1,6-bisphosphatase. J. Biol. Chem. 275, 29986-29992

21. Gao, Y., Iancu, C. V., Mukund, S., Choe, J. Y., and Honzatko, R. B. Mechanism of displacement of catalytically essential loop from the active site of fructose-1,6-bisphosphatase. To be submitted.

22. Iancu, C. V., Mukund, S., Fromm, H. J., and Honzatko, R. B. (2005) R-state AMP complex reveals initial steps of the quaternary transition of fructose-1,6-bisphosphatase. J. Biol. Chem. 280, 19737-19745

23. Hines, J. K., Chen, X., Nix, J. C., Fromm, H. J., and Honzatko, R. B. (2007) Structures of mammalian and bacterial fructose-1,6-bisphosphatase reveal the basis for synergism in AMP/fructose 2,6-bisphosphate inhibition. J. Biol. Chem. 282, 36121–36131

24. Gao, Y., and Honzatko, R. B. Hydrophobic Central Cavity in Fructose-1,6-bisphosphatase is Essential for the Synergism in AMP/Fructose 2,6-bisphosphate Inhibition. To be submitted.

25. Van Schaftingen, E., and Hers, H-G. (1981) Formation of fructose 2,6-bisphosphate from fructose 1,6-bisphosphate by intramolecular cyclisation followed by alkaline hydrolysis. Eur. J. Biochem. 117, 319-323

26. Laemmli, U. K. (1970) Cleavage of structural proteins during the assembly of the head of bacteriophage T4. Nature 227, 680-685

27. Bradford, M. M. (1976) A rapid sensitive method for the quantitation of microgram quantities of protein utilizing the principle of protein-dye binding. Anal. Biochem. 72, 248-252

28. Leatherbarrow, R.J. (2009) GraFit Version 7, Erithacus Software Ltd., Horley, U.K.

29. Gao, Y, and Honzatko, R. B. Dimer-dimer Interface in Porcine Liver Fructose-1,6-bisphosphatase is Essential in Cooperative Binding of AMP. To be submitted.

30. Demeler, B. (2005) UltraScan A Comprehensive Data Analysis Software Package for Analytical Ultracentrifugation Experiments. Modern Analytical Ultracentrifugation: Techniques and Methods. (D. J. Scott, S.E. Harding and A.J. Rowe. Eds.) Royal Society of Chemistry (UK), 210-229

31. Pflugraph, J. W. (1999) The finer things in X-ray diffraction data collection. Acta Crystallogr. D. 55, 1718-1725

32. Brünger, A. T., Adams, P. D., Clore, G. M., DeLano, W. L., Gros, P., Grosse-Kunstleve, R. W., Jiang, J.-S., Kuszewski, J., Nilges, M., Pannu, M. S., Read, R. J., Rice, L. M., Simonson, T., Warren, G. L. (1998) Crystallography & NMR system: A new software suite for macromolecular structure determination. Acta Crystallogr. D 54, 905-921

33. Engh, R. A., and Huber, R. (1991) Accurate bond and angle parameters for X-ray protein structure refinement. Acta Crystallogr. A. 47, 392-400

34. McRee, D. E. (1998) XtalView/Xfit—A versatile program for manipulating atomic coordinates and electron density. J. Struct. Biol. 125, 156-165

35. Emsley, P. and Cowtan, K. (2004)Coot: model building tools for molecular graphics. Acta Cryst. D. 60, 2126-2132

36. Laskowski, R. A., Mac Arthur, M. W., Moss, D. S., and Thornton, J. M. (1993) PROCHECK: a program to check the stereochemical quality of protein structures. J. Appl. Cryst. 26, 283-291

37. Hines, J. K., Fromm, H. J., and Honzatko, R. B. (2007) Structures of activated fructose-1,6-bisphosphatase from Escherichia coli. Coordinate regulation of bacterial metabolism and the conservation of the R-state. J. Biol. Chem. 282, 11696–11704

38. Shyur, L.-F., Aleshin, A. E., Honzatko, R. B. and Fromm, H. J. (1996) Site-directed mutagenesis of residues at subunit interfaces of porcine fructose-1,6-bisphosphatase. J. Biol. Chem. 271, 3005-3010

39. Shyur, L.-F., Aleshin, A. E., Honzatko, R. B. and Fromm, H. J. (1996) Biochemical properties of mutant and wild-type fructose-1,6-bisphosphatases are consistent with the coupling of intra- and intersubunit conformational changes in the T- and R-state transition. J. Biol. Chem. 271, 33301-33307

40. Lu, G., Stec, B., Giroux, E. L., and Kantrowitz, E. R. (1996) Evidence for an active T-state pig kidney fructose 1,6-bisphosphatase: interface residue Lys-42 is important for allosteric inhibition and AMP cooperativity. Protein Sci. 5, 2333-2342

41. Lu, G., Giroux, E. L., and Kantrowitz, E. R. (1997) Importance of the dimer-dimer interface for allosteric signal transduction and AMP cooperativity of pig kidney fructose-1,6-bisphosphatase. Site-specific mutagenesis studies of Glu-192 and Asp-187 residues on the 190's loop. J. Biol. Chem. 272, 5076-5081

42. Nelson, S. W., Honzatko, R. B., and Fromm, H. J. (2004) Origin of cooperativity in the activation of fructose-1,6-bisphosphatase by Mg2+. J. Biol. Chem. 279, 18481-18487

43. Kurbanov, F. T., Choe, J.-Y., Honzatko, R. B., and Fromm, H. J. (1998) Directed mutations in the poorly defined region of porcine liver fructose-1,6-bisphosphatase significantly affect catalysis and the mechanism of AMP inhibition. J. Biol.Chem. 273, 17511–17516

44. Moller, D. E. (2001) New drug targets for type 2 diabetes and the metabolic syndrome. Nature 414, 821-827

45. Erion, M. D., van Poelje, P. D., Dang, Q., Kasibhatla, S. R., Potter, S. C., Reddy, M. R., Reddy, K. R., Jiang, T., and Lipscomb, W. N. (2005) MB06322 (CS-917): A potent and selective inhibitor of fructose 1,6-bisphosphatase for controlling gluconeogenesis in type 2 diabetes. Proc. Natl.Acad. Sci. U. S. A. 102, 7970–7975

46. von Geldern, T. W., Lai, C., Gum, R. J., Daly, M., Sun, C., Fry, E. H., and Abad-Zapatero, C. (2006) Benzoxazole benzenesulfonamides are novel allosteric inhibitors of fructose-1,6-bisphosphatase with a distinct binding mode. Bioorg. Med. Chem. Lett. 16, 1811-1815

47. Hebeisen, P., Kuhn, B., Kohler, P., Gubler, M., Huber, W., Kitas, E., Schott, B., Benz, J., Joseph, C., and Ruf, A. (2008) Allosteric FBPase inhibitors gain 105 times in potency when simultaneously binding two neighboring AMP sites. Bioorg. Med. Chem. Lett. 18, 4708-4712

48. Rudnitskaya, A., Huynh, K., Török, B., and Stieglitz, K. (2009) Novel heteroaromatic organofluorine inhibitors of fructose-1,6-bisphosphatase. J. Med. Chem. 52, 878-882

49. Kitas, E., Mohr, P., Kuhn, B., Hebeisen, P., Wessel, H. P., Haap, W., Ruf, A., Benz, J., Joseph, C., Huber, W., Sanchez, R. A., Paehler, A., Benardeau, A., Gubler, M., Schott, B., and Tozzo, E. (2010) Sulfonylureido thiazoles as fructose-1,6-bisphosphatase inhibitors for the treatment of type-2 diabete. Bioorg. Med. Chem. Lett. 20, 594-599

50. Hebeisen, P., Haap, W., Kuhn, B., Mohr, P., Wessel, H. P., Zutter, U., Kirchner, S., Ruf, A., Benz, J., Joseph, C., Alvarez-Sánchez, R., Gubler, M., Schott, B., Benardeau, A., Tozzo, E., and Kitas, E. (2011) Orally active aminopyridines as inhibitors of tetrameric fructose-1,6-bisphosphatase. Bioorg. Med. Chem. Lett. 21, 3237-3242

51. Nelson, S. W, Honzatko, R. B., and Fromm, H. J. (2002) Hybrid tetramers of porcine liver fructose-1,6-bisphosphatase reveal multiple pathways of allosteric inhibition. J. Biol. Chem. 277, 15539-15545

52. Nelson, S. W., Kurbanov, F., Honzatko, R. B. and Fromm, H, J. (2001) The N-terminal segment of recombinant porcine fructose-1,6-bisphosphatase participates in the allosteric regulation of catalysis. J. Biol. Chem. 276, 6119-6124

CHAPTER VII. FRUCTOSE-1,6-BISPHOSPHATASE FROM FROM *Leptospira interrogans*: A PREDICTION OF ALLOSTERIC REGULATION LEADS TO A POSSIBLE EVOLUTIONARY PRECURSOR OF AMP/FRUCTOSE-2,6-BISPHOSPHATE SYNERGISM IN EUKARYOTIC ORGANISMS

A paper to be submitted to *Biochemistry*

Yang Gao, Lu Shen, and Richard B. Honzatko

Roy J. Carver Department of Biochemistry, Biophysics, and Molecular Biology,

Iowa State University, Ames, IA 50011

Abstract

Fructose-1, 6-bisphosphatase (FBPase) is a key regulatory enzyme in gluconeogenesis. Porcine liver FBPase is a model for eukaryotic FBPases, being an active tetramer subject to inhibition by AMP and fructose 2,6-bisphosphate (Fru-2,6-P_2). In contrast, *Escherichia coli* FBPase, a model FBPase for many bacterial systems, is subject to feed-forward activation by phosphoenolpyruvate (PEP) and synergistic inhibition by AMP and glucose 6-phosphate (Glc-6-P). To the best of our knowledge Fru-2,6-P_2 is present in eukaryotic organisms, but in no bacterial system. The dissimilarity in regulation of *E. coli* and porcine FBPases begs the question: What is the starting point in evolution for Fru-2,6-P_2 inhibition and AMP/Fruc-2,6-P_2 synergism of eukaryotic FBPases? FBPase from the bacterium *Leptospira interrogans* is one of a select group with key residues characteristic of eukaryotic FBPases. Experiments here verify *L. interrogans* FBPase as a stable tetramer with cooperative AMP inhibition and AMP/Fru-2,6-P_2 synergism, regulatory properties common to eukaryotic FBPases. *L. interrogans*, however, lacks genes associated with Fru-2,6-P_2 biosynthesis. Instead on the basis of tryptophan fluorescence, the product of the FBPase reaction (Fru-6-P) binds synergistically with AMP to *L. interrogans* FBPase. AMP/Fru-6-P synergism in a bacterial FBPase suggests an ancient mode of regulation that

may have been the basis in evolution for Fru-2,6-P_2 inhibition and AMP/Fru-2,6-P_2 synergism in eukaryotic systems.

Introduction

Fructose-1,6-bisphosphatase (D-fructose-1, 6-bisphosphate 1-phosphohydrolase; EC 3. 1. 3; FBPase) is a key regulatory enzyme in gluconeogenesis. With divalent cations (Mg^{2+}, Mn^{2+}, or Zn^{2+}) as cofactors, FBPase catalyzes the hydrolysis of fructose 1,6-bisphosphate (Fru-1,6-P_2) to fructose 6-phosphate (Fru-6-P) and phosphate (Pi) (1, 2).

Regulatory mechanisms of Type-1 FBPases vary widely with organism. Fructose 2,6-bisphosphate (Fru-2,6-P_2) and AMP inhibit FBPases from eukaryotic organisms (4-6). AMP binds with positive cooperativity to an allosteric site on a stable tetramer (4). Fru-2,6-P_2 not only competes with substrate for the active site but also enhances AMP inhibition by several fold, a property named AMP/Fru-2,6-P_2 synergism (5, 6). AMP/Fru-2,6-P_2 synergism is evident in plant cytosolic FBPase and yeast FBPase (7-8), as well as mammalian organisms (1). AMP concentration *in vi*vo is relatively constant, but fluctuating levels of Fru-2,6-P_2, determined by the hormonal and nutritional status of the organism (9), insure that both AMP and Fru-2,6-P_2 are dynamic inhibitors. In eukaryotic organisms, FBPase and fructose-6-phosphate-1-kinase (PFK-1) from glycolysis define a futile cycle (3). In order to avoid the uncontrolled consumption of ATP in that cycle and maintain glucose hemostasis, FBPase activity is regulated coordinately with that of PFK-1. Hence, Fru-2,6-P_2 is an allosteric activator of PFK-1 (3, 10-12).

Other mechanisms of FBPase regulation differ substantially from that of eukaryotic systems. FBPase from the chloroplast is insensitive to AMP (13). The activity of chloroplast FBPase is controlled indirectly by light through a redox signaling pathway (14-15). Bacterial systems lack Fru-2,6-P_2 (16). *Escherichia coli* FBPase (hereafter *e*FBPase) uses glucose 6-phosphate (Glc-6-P) and AMP as synergistic inhibitors (17). Moreover, anions such as sulfate, phosphoenolpyruvate (PEP) or citrate antagonize Glc-6-P/AMP inhibition and activate *e*FBPase (18, 19).

Porcine liver FBPase (*p*FBPase) is a model system for FBPases from eukaryotic organisms. *p*FBPase is a stable homotetramer that adopts at least two quaternary states, an active R-state and an inactive T-state (20, 21). *p*FBPase with bound product and divalent cations (Mg^{2+}, Mn^{2+}, or Zn^{2+}) defines the R-state (20). AMP and/or Fru-2,6-P_2 drive the R- to T-state transition of *p*FBPase. The AMP and AMP/Fru-2,6-P_2 complexes of *p*FBPase exhibit a subunit-pair rotation of 15 ° and that of Fru-2,6-P_2 a 13 ° rotation relative to the R-state (21-23). The subunit-pair rotation is in part responsible for the displacement of an essential loop (loop 50-72) from its engaged conformation, which stabilizes the binding of substrate and three divalent cations at the active site. Upon displacement, loop 50-72 acquires its disengaged conformation, re-positioning catalytically essential residues some 30 Å away from the active site. The similar end-state caused by AMP and Fru-2,6-P_2 individually is the putative basis for AMP/Fru-2,6-P_2 synergism (23). Moreover, the central cavity of the *p*FBPase tetramer and the stable cluster of water molecules in that cavity, are factors in defining the quaternary state (24). The mutation of Ser^{45}→His in *p*FBPase fills the cavity and eliminates AMP/Fru-2,6-P_2 synergism as well as Fru-2,6-P_2 induced subunit-pair rotation (25).

*e*FBPase is similar in sequence (40% identical) and structure (same fold) to *p*FBPase (18). AMP is a potent inhibitor of *e*FBPase and the binding of AMP drives a subunit-pair rotation similar to that observed in *p*FBPase (17); however, an important salt bridge in *p*FBPase (Lys^{42}–Glu^{192}) at the dimer-dimer interface is missing in *e*FBPase (Lys^{34}–Val^{186}). As a consequence, *e*FBPase is in dimer-tetramer equilibrium, with the tetramer form more active (18). Anion activators, such as PEP or citrate stabilize the tetramer by binding to the dimer-dimer interface (19). Glc-6-P binds to an allosteric site at the C1-C2 interface and inhibits *e*FBPase synergistically with AMP (17). Although not present in *E. coli*, Fru-2,6-P_2 is a potent inhibitor of *e*FBPase; however, AMP/Fru-2,6-P_2 synergism is absent in *e*FBPase. Structurally, *e*FBPase lacks the large central cavity (histidine is at the position corresponding to Ser^{45} in *p*FBPase) and Fru-2,6-P_2 does not cause a subunit-pair rotation (23).

The full scope and evolution of FBPase regulatory mechanisms is the focus of the investigation here. How Fru-2,6-P_2 came to be a regulator of all known eukaryotic FBPases,

when there is no instance of Fru-2,6-P_2 in non-eukaryotic organisms, is a mystery. The dissimilarity in the regulation of *e*FBPase and *p*FBPase argues against one being a direct evolutionary precursor of the other. Sequence analysis of Type-1 FBPases, however, indicates FBPases from *Leptospira* should have the regulatory properties of porcine and other eukaryotic FBPases (25). *Leptospira interrogans* FBPase (herafter, *l*FBPase) has most of the key residues for AMP inhibition, AMP/Fru-2,6-P_2 synergism, central cavity formation and tetramer stability, but lacks residues for anion activation and Glc-6-P inhibition. Given the current status of our knowledge of allosteric regulation in FBPases, we predict *l*FBPase to have AMP/Fru-2,6-P_2 synergism even though *L. interrogans* lacks the genes associated with Fru-2,6-P_2 biosynthesis. Presented here are the properties of *l*FBPase, which as predicted, are similar to those of *p*FBPase. In addition, as *l*FBPase has a single, naturally-occuring tryptophan at the active site, we find for the first time in an FBPase the existence of AMP/Fru-6-P synergism. Results here indicate that the existence of AMP/Fru-6-P synergism in a primordial FBPase may have enabled the evolution of AMP/Fru-2,6-P_2 synergism in eukaryotic organisms.

Experimental procedures

Materials— Fru-1,6-P_2, $NADP^+$ and AMP came from Sigma. Fru-2,6-P_2 was produced according by published protocols (26). Glucose-6-phosphate dehydrogenase and phosphoglucose isomerase were purchased from Roche Applied Sciences. The FBPase-deficient *E. coli* strain DF 657 was from the Genetic Stock Center at Yale University. Other chemicals were of reagent grade or equivalent.

Cloning, Expression and Purification of lFBPase— *l*FBPase (UniProt ID: Q8F421) was synthesized and cloned into pET24b plasmid by Genscript (http://www.genscript.com/). The integrity of the construct was confirmed by sequencing the promoter region and the entire open reading frame. Iowa State University sequencing facility provided DNA sequencing services with the fluorescent dye-dideoxy terminator method. *E. coli* strain DF 657 was used for expression of *l*FBPase. The cell culture of *E. coli* DF657 transformed with the *l*FBPase

plasmid grew to A_{600} of 1.0, at which time transcription was induced by the addition of isopropyl-β-D-thiogalactopyranoside (IPTG, final concentration 1 mM). The culture was maintained (with shaking, 37 ℃) for an additional 16 hrs before harvesting. The supernatant component of the cell free extract was subject to ammonium sulfate fractionation. The 30-50% ammonium sulfate fraction was collected and dialyzed thoroughly in 20 mM Tris, pH 8.0, before loading onto a DEAE-sepharose column. Purified enzyme was eluted with a NaCl gradient (0–0.5 M) in 20 mM Tris-HCl, pH 8.0. Enzyme was dialyzed extensively against 50 mM Hepes, pH 7.4, prior to kinetics studies. Purity and protein concentrations of FBPase preparations were confirmed by sodium dodecylsulfate-polyacrylamide gel electrophoresis (SDS-PAGE) (27) and by Bradford assay (28), respectively.

Sedimentation Equilibrium— Sedimentation equilibrium experiments followed published protocols (29). *l*FBPase with three protein concentrations (OD280 = 0.3, 0.5 and 0.7) was sedimented to equilibrium at angular speeds 15000, 18000 and 21000 rpm. Equilibrium data were fit with the program UltraScan (30).

Kinetic Experiments— Phosphoglucose isomerase and glucose-6-phosphate dehydrogenase were used as coupling enzymes in assays of FBPase activity (1). For specific activity measurements, reduction of NADP to NADPH was monitored by absorbance at 340 nm on UV spectrometer. Other assays used the same coupling enzymes but monitored the formation of NADPH by its fluorescence emission at 470 nm using an excitation wavelength of 340 nm. Assays were performed at 22 ℃ in 50 mM Hepes, pH 7.5. 300 mM KCl was added in the assays for *p*FBPase but not for *l*FBPase. Assay solutions contained EDTA at a concentration of 10 μM. Enzyme initialized assay and Mg^{2+} initialized assay were both performed for AMP inhibition of *p*FBPase, which gave undistinguishable results, unlike *e*FBPase (19). All kinetics data reported were results from enzyme initialized assays except anion activation experiment, which used Mg^{2+} initialized assay. Data for AMP inhibition with respect to Mg^{2+} and Fru-2,6-P_2 inhibition with respect to Fru-1,6-P_2 were fit to several models and results from best fit were reported. Data fitting was carried out with software Grafit (31).

Fluorescence experiment—Fluorescence measurements were made at room temperature using a 1-cm^2 quartz cuvette on aSLM Amico 8000 fluorometer. The excitation wavelength was 295 nm, and emission scans were integrated from 310 to 370 nm. Fluorescence scans (repeat of 3 scans for each data point) were performed after additions of small volumes of ligand to 2 mL of a 2 μM *l*FBPase solution. The total concentration of added titrant did not exceed 1% of the initial volume. Data fitting was carried out using protocols in the literature (32).

Results

Sequence Alignment— Sequence alignments of *l*FBPase, *p*FBPase and *e*FBPase reveal identities of 40–48% in pairwise combinations. Active site residues are conserved for the most part among the three FBPases. Asp^{121}, Gly^{122}, Ser^{123}, Asn^{212}, Asn^{215}, Arg^{243}, Tyr^{244}, Leu^{248}, Tyr^{264}, Lys^{274}, and Arg^{276} (*p*FBPase numerology and type) form hydrogen-bonds with products (Fru-6-P and Pi) in the R-state of *p*FBPase (20). Among these, only Tyr^{215} and Met^{248} differ (becoming asparagine and leucine, respectively) in both *e*FBPase and *p*FBPase. Divalent metal cations (Mg^{2+}, Mn^{2+}, or Zn^{2+}) are essential co-factors for FBPase and three metal cations are required for each subunit for catalysis by *p*FBPase. Metal binding residues are conserved (Glu^{97}, Glu^{98}, Asp^{118}, Asp^{121}, and Glu^{280}) except for Asp^{68} of pFBPase which is glutamate in *e*FBPase and *l*FBPase. Conservation of active site residues indicates a similar mechanism of catalysis for *l*FBPase, *e*FBPase and *p*FBPase.

Although *l*FBPase shares higher identity with *e*FBPase (48%) than with *p*FBPase (41%), the key residues for regulation in *l*FBPase are more similar to those in *p*FBPase than *e*FBPase. All three FBPases have signature residues for an AMP binding site (Figure 1); however, *e*FBPase has two allosteric binding sites, one for the anion activation between subunits at the C1-C4 interface and one for Glc-6-P inhibition between subunits at the C1-C2 interface (17, 19). These binding sites are not present in *p*FBPase, and signature residues are not present in the *l*FBPase sequence. In contrast, position 45 (*p*FBPase numerology) is serine in *l*FBPase and *p*FBPase and histidine in *e*FBPase. The small side chain (serine) in *p*FBPase

and *l*FBPase indicates a central cavity and the property of AMP/Fru-2,6-P_2 synergism for *l*FBPase even though the genes associated with Fru-2,6-P_2 synthesis are not present in this bacterial system. The salt link between Lys^{42} and Glu^{192} in *p*FBPase is essential for tetramer stability (29). The salt link is absent in *e*FBPase but present in *l*FBPase. Key residues in the sequence of *l*FBPase indicate regulatory/structural properties similar to those of *p*FBPase, which include AMP inhibition, AMP/Fru-2,6-P_2 synergism, and a stable tetramer with a central cavity.

Expression and purification of LiFBPase— Expression and isolation procedures described in the methods section provide *l*FBPase with at least 95% purity as confirmed by sodium dodecylsulfate-polyacrylamide gel electrophoresis (data not shown).

Sedimentation Equilibrium— Sedimentation equilibrium data are fit to single component and dimer-tetramer equilibrium models with UltraScan (Table 2). Regardless of model, *p*FBPase and *l*FBPase give similar apparent molecular weights in sedimentation equilibrium experiments, 111.9 and 112.1 kDa for *l*FBPase and *p*FBPase, respectively. The determined molecular weights are less than the calculated weight of 140 kDa for the tetramer.

Enzyme activity—Parameters from the reaction kinetics of *l*FBPase and *p*FBPase are in Table 1. K^+ is an activator for *p*FBPase at low concentration (1-2, 33) but an inhibitor for *l*FBPase. So KCl is only presented in the assays for *p*FBPase. *l*FBPase catalyzes the hydrolysis of Fru-1,6-P_2 with specific activity and K_m values comparable to those of *p*FBPase. Mg^{2+} is an essential cofactor, but unlike *p*FBPase, Mg^{2+} activation is not cooperative in *l*FBPase catalysis (Hill coefficient of 0.77±0.08 compared to that of *p*FBPase of 1.7±0.1). The dependence of initial velocity on concentrations of Fru-1,6-P_2 and Mg^{2+} is given by Equation 1:

$$v = \frac{V_m . A^n . B}{A^n . B + K_a . B + K_b . A^n + K_{ia} . K_b} \quad \text{(Equation 1)}$$

where V_m, A, B, K_a, K_b, K_{ia} , n represent the maximum velocity of the reaction, the concentration of free Mg^{2+}, the concentration of free Fru-1,6-P_2, the Michaelis-Menten constant for Mg^{2+}, the Michaelis-Menten constant for Fru-1,6-P_2, the dissociation constant

for Mg^{2+}, and the Hill coefficient for Mg^{2+}, respectively. *n* is set to 2 for *p*FBPase and unity for *l*FBPase. Plots of reciprocal velocity versus reciprocal substrate concentration are consistent with a Random Bi Bi or Steady-State Ordered mechanism (Figure 2), both of which are consistent with Equation 1. Comparable values for K_a and K_{ia} for Mg^{2+} (K_a= 1.3±0.1 μM versus K_{ia}= 2.7±0.6 μM) implies no synergism in the binding of substrate and metal cofactor, which is consistent with the Random Bi Bi mechanism. That Random Bi Bi mechanism has been demonstrated unequivocally for *p*FBPase by inhibition assays (34).

AMP inhibition— AMP inhibits *l*FBPase with high affinity. The $I_{0.5}$ and Hill coefficient for AMP inhibition are determined by titration of AMP in the presence of a saturating concentration of substrate (20 μM) and Mg^{2+} (5 mM). Data was fit to Equation 2,

$$v = \frac{V_{\mathrm{m}}}{1+(\frac{I}{I_{0.5}})^n} \qquad \text{(Equation 2)}$$

where *v*, V_m, *I*, $I_{0.5}$ and *n* are velocity, maximum velocity, AMP concentration, AMP concentration that gives 50% activity and the Hill coefficient for AMP, respectively. AMP inhibition for *l*FBPase is cooperative, with a Hill coefficient close to 2. AMP is a competitive inhibitor with respect to Mg^{2+} (K_i = 0.58±0.05 μM, Figure 3) and an non-competitive inhibitor with respect to Fru-1,6-P_2 (K_i = K_{is} =0.83±0.05 μM). AMP inhibition is comparable to that of *p*FBPase.

Fru-2,6-P_2 inhibition— Although not present in bacteria system, Fru-2,6-P_2 is a highly potent inhibitor for *l*FBPase. $I_{0.5}$ for Fru-2,6-P_2 inhibition in the presence of saturating substrate (20 μM) and Mg^{2+} (5 mM) is 0.33±0.02 μM, with a Hill coefficient 1.05±0.08. The inhibition of Fru-2,6-P_2 is competitive with respect to substrate (Figure 4).

Effect of anions and Glc-6-P—Anion activators such as PEP or citrate activate *e*FBPase by promoting tetramer formation (19). To test the effect of PEP on *l*FBPase, Mg^{2+} initialized assays were used. PEP activation is not present for *l*FBPase. Instead, milli-molar level PEP causes moderate inhibition. Assays of Glc-6-P inhibition follow the published protocol for *e*FBPase (18). Glc-6-P inhibition becomes evident only at milli-molar level, which is around

50-times weaker than Glc-6-P inhibition in *e*FBPase. Similar level of Glc-6-P inhibition has also been observed for *p*FBPase.

AMP/Fru-2,6-P_2 synergism—AMP/Fru-2,6-P_2 synergism is indicated by the level of AMP inhibition in the absence and presence of Fru-2,6-P_2. Inhibition curves are fit to Equation 2. The AMP inhibition is enhanced by ~2 fold in the presence of small amounts of Fru-2,6-P_2 ([Fru-2,6-P_2] = $I_{0.5}$ =0.33 μM). Vice versa Fru-2,6-P_2 inhibition is enhanced twofold in the presence of a small amount of AMP ([AMP] = $I_{0.5}$ =1.8 μM). Moreover, the Hill coefficient for AMP inhibition drops from 2.2 to close to unity upon the addition of Fru-2,6-P_2. Similar phenomena have been observed in both wild-type *p*FBPase and mutant *p*FBPases with reduced AMP/Fru-2,6-P_2 synergism (23, 25).

Steady-state Tryptophan Fluorescence of lFBPase— *l*FBPase has but one tryptophan (Trp^{219}). Assuming a structure for *l*FBPase similar to that of *e*FBPase and *p*FBPase, Trp^{219} is near the common binding sites for the 6-phosphoryl groups of substrate, product and Fru-2,6-P_2. Steady-state fluorescence emission from Trp^{219} increases as levels of substrate, product or Fru-2,6-P_2 increase (Figure 6A), whereas increasing concentrations of AMP cause little change. Substrate, product, Fru-2,6-P_2, and AMP have no effect on the fluorescence emission of 100 μM tryptophan in the absence of *l*FBPase. The fluorescence change caused by Fru-6-P, Fru-1,6-P_2, or Fru-2,6-P_2 is arguably the result of a change in the local environment Trp^{219} due to the binding of 6-phosphore group at the active site. Indeed, at saturating concentrations, the three active-site ligands induce nearly identical changes in fluorescence emission. Data from titrations of 6-phosphoryl ligands carried out in the presence and absence of AMP are fit to Equation 3:

$$\frac{\Delta F}{F_0} = \left(\frac{\Delta F_{max}}{F_0}\right).\frac{L}{K_d+L} \qquad \text{(Equation 3)}$$

where ΔF is the change in fluorescence caused upon addition of ligand L, F_0 is the fluorescence in the absence of ligand, and K_d is the dissociation constant. AMP does not affect the binding of Fru-1,6-P_2 (Table 3). In contrast, a small amount of AMP ([AMP] = $I_{0.5}$ = 1.8 μM) can enhance binding of Fru-2,6-P_2 by approximately twofold, consistent with data from kinetics experiments. AMP has a similar synergistic effect on the binding of Fru-6-P.

Discussion

The sequence of *l*FBPase was identified by homology analysis of the genome sequence of *Leptospira interrogans* (35). The experimental characterization of *l*FBPase here confirms the assignment. *l*FBPase exhibits a K_m for Fru-1,6-P_2 and a specific activity comparable to that of *p*FBPase and *e*FBPase. The reaction catalyzed by *l*FBPase requires Mg^{2+} as an essential co-factor. Unlike the cooperative binding of Mg^{2+} to *p*FBPase, however, the binding of Mg^{2+} to *l*FBPase is non-cooperative. This alteration in property may be due to the change in residue type from aspartate to glutamate at position 68 (*p*FBPase numerology). All other Mg^{2+} binding residues are identical among *l*FBPase, *p*FBPase and *e*FBPase. The mutation Asp^{68}→Glu in *p*FBPase reduces Mg^{2+} cooperativity (36), and *l*FBPase and *e*FBPase have no Mg^{2+} cooperativity (37).

On the basis of sequence similarity, *l*FBPase should be a stable tetramer, similar to *p*FBPase and dissimilar to *e*FBPase, the latter existing as an equilibrium mixture of dimers and tetramers. Salt links (Lys^{42}–Glu^{192}) between subunit-pairs of the *p*FBPase tetramer are essential for tetramer stability. The mutation of Glu^{192} to glutamine disrupts the wild-type tetramer of *p*FBPase and creates a stable dimer with diminished activity (29). *l*FBPase has the signature salt-links of *p*FBPase, and consistent with hypothesis, behaves identically (within experimental uncertainty) to *p*FBPase in sedimentation equilibrium. In contrast, *e*FBPase exists as a fully active tetramer in equilibrium with a less active dimer (19). Dilution of *e*FBPase results in a slow loss of activity, which is not observed for either *p*FBPase or *l*FBPase.

By hypothesis based on sequence similarity, AMP should inhibit *l*FBPase with cooperativity, and indeed this is confirmed here by experiment. AMP cooperativity for *e*FBPase is weak or absent in enzyme initialized assays and Mg^{2+} initialized assays, respectively (19). Studies of *p*FBPase indicate that AMP cooperativity derives from nucleotide binding to each subunit-pair (C1-C2 and C3-C4) of the tetramer (38). Disruption of the *p*FBPase tetramer causes a loss of cooperativity in AMP inhibition (29). Hence the presence of AMP cooperativity in the inhibition of *l*FBPase is another manifestation of tetramer stability.

The large cavity at the center of the *p*FBPase tetramer is another attribute that distinguishes *p*FBPase from *e*FBPase (25). That cavity is responsible for AMP/Fru-2,6-P_2 synergism in *p*FBPase and is largely filled by the side chains of His^{45} from each of four subunits of *e*FBPase. *l*FBPase has serine at the position 45, the same residue type as in *p*FBPase. Both kinetics and equilibrium binding experiments involving *l*FBPase reveal AMP/Fru-2,6-P_2 synergism, again consistent with hypothesis derived from sequence comparisons. Predictions of tetramer stability, cooperative inhibition by AMP, and AMP/Fru-2,6-P2 synergism for *l*FBPase have been confirmed by experiment.

AMP/Fru-6-P binding synergism for *l*FBPase, observed by monitoring tryptophan fluorescence, has been missed in past studies of FBPase presumably because of assay design. FBPase activity is measured by coupling the formation of NADPH to that of Fru-6-P. Hence, concentrations of Fru-6-P are not subject to controlled variation in kinetics as would be necessary to detect AMP/Fru-6-P synergism.

AMP/Fru-6-P binding synergism arguably represents an evolutionary prelude to AMP/Fru-2,6-P_2 synergism observed in eukaryotic organisms. Properties of *l*FBPase then are not unlike those anticipated for a direct evolutionary precursor of eukaryotic FBPase. At some point in evolution, the primordial FBPase may have existed as an equilibrium mixture of dimers and tertramers (Figure 7). This primordial FBPase may have been subject to AMP inhibition, perhaps without cooperativity, and feedback inhibition by Fru-6-P. One pathway of evolution stabilizes the tetramer through the creation of an anion-activation site. Over time, this form of FBPase acquires a site for Glc-6-P inhibition which acts synergistically with AMP, in short becoming the present-day *e*FBPase. An alternative pathway of evolution also led to a stable FBPase tetramer through the formation of Glu^{192}–Lys^{42} salt-links. As this form of the tetramer is stable and at all times fully active, a robust mechanism of inhibition would presumably co-evolve with activation. Mutation of position 45 from histidine to serine would create a nascent central cavity in the primordial enzyme without an effect on activity. The introduction of the Glu^{192}–Lys^{42} salt link in a Ser^{45} ancestral FBPase would create a stable tetramer with a central cavity. The central cavity would enable AMP/Fru-6-P synergism that would in turn be the counterpoint to enhanced activity of a stable tertamer.

Over time, some organism found survival advantage by replacing Fru-6-P with Fru-2,6-P_2 as a dynamic regulator. Crystal structures of Fru-2,6-P_2 bound to *p*FBPase clearly show that all atoms except those of the 2-phosphoryl group occupy the positions of corresponding atoms of Fru-6-P (23). Hence, Fru-2,6-P_2 can be regarded as a high-affinity form of the product Fru-6-P.

L. interrogans is a pathogenic bacterium with a metabolism strikingly different from that of mammals (35). *L. interrogans* lacks hexokinase and cannot capture and directly use glucose from exogenous sources (35, 39). Instead, lipid is the principal energy source for *L. interrogans*. Enzymes of gluconeogenesis are present, however (35). The apparent role of gluconeogenesis in *L. interrogans* is the generation of Fru-6-P exclusively as a precursor for sugar-nucleotide biosynthesis. As a gene coding for glucose 6-phosphate dehydrogenase is absent in *L. interrogans* (35), Fru-6-P must enter the non-oxidative pentose phosphate pathway in order to produce ribose 5-phosphate. The conversion of Fru-1,6-P_2 into Fru-6-P in *L. interrogans* then represents the first committed step in ribose 5-phosphate biosynthesis. Enzymes that govern the first committed step of metabolic pathways (in this instance *l*FBPase) are often subject to feedback regulation. Moreover, high levels of Fru-6-P should inhibit only *l*FBPase due to absence of glycolysis. Feedback regulation of *l*FBPase by AMP/Fru-6-P synergism then seems a reasonable strategy of regulation. When nucleotides are in demand, the concentrations of AMP and Fru-6-P (the latter being in equilibrium with the pool of ribose 5-phosphate) should be low and non-inhibitory; however, a surplus of nucleotides, and by inference ribose 5-phosphate, should cause levels of Fru-6-P to rise. Even if the concentration of AMP is constant under these conditions, AMP becomes inhibitory concomitantly with rising levels of Fru-6-P because of the property of AMP/Fru-6-P synergism.

Leptospira is the causative agent of Leptospirosis, a disease of global concern. Infection in human causes renal and hepatic damage, and in some instances sudden and fatal hemoptysis (35, 39). Infections in livestock and domestic animals can expose individuals to *Leptospira* infections through sanitary waste or contaminated drinking water. Little information is known about the metabolism of *L. interrogans* by direct experimentation.

Given the current status of our knowledge, one could regard FBPase from *Leptospira* as a potential target in the development of agents of anti-microbial growth.

Table 1. Parameters from the kinetics of wild-type and mutant FBPases.

Uncertainties in the last significant digit are in parentheses.

FBPase	Specific activity [a] Units mg^{-1} s^{-1}	K_m-Fru-1,6-P_2 [b] (μM)	Mg^{2+} Hill-coef.[c]	K_a-Mg^{2+} [c] (mM^2)	AMP Hill-coef.[d]	K_i-AMP [d] (μM^2)	K_i-Fru-2,6-P_2 [e] (μM)
*p*FBPase	25	1.47(7)	1.7(1)	0.70(5)	2.2(1)	0.76(8)	0.14(1)
*l*FBPase	15	1.0(1)	0.77(8)	1.3(1)[f]	2.2(2)	0.58(5)	0.05(1)

[a] Specific activity is determined at saturated Fru-1,6-P_2 (20 μM) and Mg^{2+} (5mM) level. The reported results are average values of 5 repeats.

[b] K_M for Fru-1,6-P_2 is determined at saturated Mg^{2+} (5mM) level. The Fru-1,6-P_2 concentration varies from 0.3 to 20 μM.

[c] Hill coefficient for Mg^{2+} is determined by titrating 0.2 to 10 mM Mg^{2+} to assays that contain saturated level of Fru-1,6-P_2 (20 μM). The concentration ranges of Mg^{2+} and Fru-1,6-P_2 in determination of K_a are 0.5 to 5 mM and 0.5 to 10 μM, respectively.

[d] Hill coefficient for AMP is determined by titrating 0.1 to 100 μM AMP to assays that contain saturated level of Fru-1,6-P_2 (20 μM) and Mg^{2+} (5 mM). The concentration of Mg^{2+} varies from 0.5 to 5 mM and the concentration ranges of AMP are 0 to 5 μM for determination of K_i-AMP.

[e] Assays contain Mg^{2+} (5mM). The concentration of Fru-1,6-P_2 varies from 0.5 to 10 μM and the concentration ranges of Fru-2,6-P_2 are 0 to 0.5 μM.

[f] K_a-Mg^{2+} for *l*FBPase has units of mM

Table 2. Fitting results of sedimentation equilibrium data for *l*FBPase and *p*FBPase [a].

Protein	Single component, ideal		Monomer-dimer equilibrium		
	M.W.[b]	*S.D.*[c]	*M.W.*	K_d (M)	*S.D.*[c]
*p*FBPase	112100	0.009147	113900	2.718	0.010514
*l*FBPase	111900	0.006866	112100	2.718	0.00597

[a] The results were derived from global fitting of all data with software Ultrascan
[b] Molecular weight in Dalton
[c] Standard derivation of the global fitting

Table 3. Effect of AMP on the binding of ligands to the active site.

Standard deviation in last significant figure is given parenthetically.

Ligand	K_d (AMP = 0), μM	K_d (AMP = 1.8 μM), μM
Fru-1,6-P_2	0.77(9)	0.73(5)
Fru-2,6-P_2	0.32(7)	0.17(2)
Fru-6-P	105(9)	50(7)

A

```
                          14        --  27  31          42 45                    68
S. scrofa      TDQAAFDTNI VTLTRFVMEE GRK-ARGTGE MTQLLNSLCT AVKAISTAVR KAGIAH-LYG IAGSTNVTGD   68
L. interrogans   MSVHPTQT LSLSQYLIEE QLKLPQATGD FTALMSHLVY AAKIVSREVR KAGLLENILG ATETVNVQGE   68
E. coli                M KTLGEFIVEK QHEFSHATGE LTALLSAIKL GAKIIHRDIN KAGLVD-ILG ASGAENVQGE   60
                                88          97 98          112 113 118  123
S. scrofa      QVKKLDVLSN DLVINVLKSS FATCVLVSEE DKNAI-IVEP EKRGKYVVCF DPLDGSSNID CLVSIGTIFG  137
L. interrogans TQMKLDEYAD KVFNHTLTRS GHLCILGSEE HEETVPVPNG YKIGKYTIAI DPLDGSSNID ANVSIGTIFS  138
E. coli        VQQKLDLFAN EKLKAALKAR DIVAGIASEE EDEIV-VFEG CEHAKYVVLM DPLDGSSNID VNVSVGTIFS  129
                                                                    192
S. scrofa      IYRKNST--D EPSEKDALQP GRNLVAAGYA LYGSATMLVL AMVNGVNCFM LDPAIGEFIL VDRDVKIKKK  205
L. interrogans VHLRKSPAGT PGTLSDLLQQ GSGQRAAGYV LYGSSTMLIL CTGKGVSGFT LDPSCGEFIL SHPDMQIPET  208
E. coli        IYRRVTPVGT PVTEEDFLQP GNKQVAAGYV VYGSSTMLVY TTGCGVHAFT YDPSLGVFCL CQERMRFPEK  199
               212 215 216       228 230       243 244 248             264
S. scrofa      GSIYSINEGY AKEFDPAITE YIQR-KKFPP DNSAPYGARY VGSMVADVHR TLVYGGIFMY PA---NKKSP  271
L. interrogans GGIYSINEGN YNYWSDEVKN YIRDIKSIEG G-RKPQSGRY IGSLVADFHR NLLKGGIFLY PNDTKSTKYP  277
E. coli        GKTYSINEGN YIKFPNGVKK YIKFCQEEDK STNRPYTSRY IGSLVADFHR NLLKGGIYLY PS---TASHP  266
               274 276 280
S. scrofa      KGKLRLLYEC NPMAYVMEKA GGLA-TTGKE AVLDIVPTDI HQRAPIILGS PEDVTELLEI YQKHAAK     337
L. interrogans NGKLRLLYEA APMAFIAEQA GGMAVTVYGE RILDLTPKEL HERTTLVVGS KKEVEHFLKF APKKS      342
E. coli        DGKLRLLYEC NPMAFLAEQA GGKA-SDGKE RILDIIPETL HQRRSFFVGN DHMVEDVERF IREFPDA     332
```

B

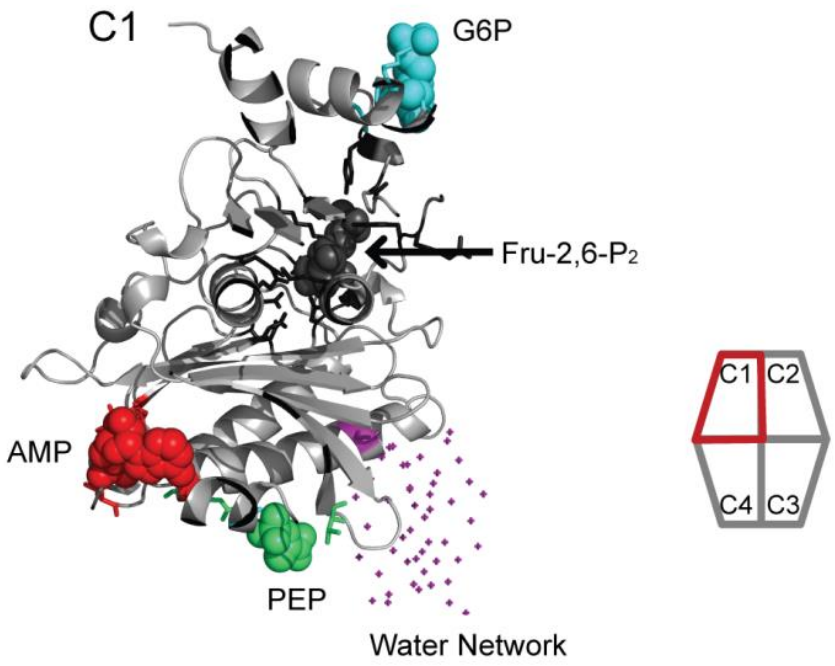

Figure 1. Key residues of FBPase catalysis and regulation. A. Sequence alignment of *l*FBPase, *p*FBPase and *e*FBPase reveals residues for product binding and metal coordination (black), AMP inhibition (red), tetramer formation (yellow), central cavity (purple), anion activation (purple) and Glc-6-P inhibition (blue). B. FBPase subunit with bound Fru-2,6-P_2 (black, from PDB ID: 2QVU), AMP (red, from PDB ID: 1EYJ), Glc-6-P (blue, from PDB ID: 2Q8M), phosphoenolpyruvate (green, from PDB ID: 2OX3), and ordered water molecules in central cavity (purple, from PDB ID: 1YYZ), all shown in sphere representations. Only subunit C1 of FBPase tetramer (right corner) is presented. The figure is prepared by Pymol (40).

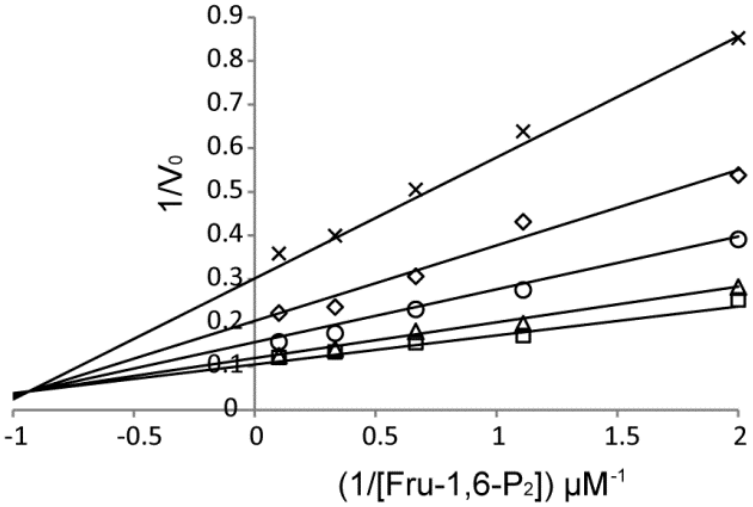

Figure 2. Activation of *l*FBPase by Mg^{2+}. Plots of reciprocal velocity against 1/[Fru-1,6-P_2] with fixed free Mg^{2+} concentrations of 0.5 (□), 0.9 (△), 1.5 (○), 3 (◊) and 5 mM (x) are shown. Lines in the figure are calculated based on Equation 2 in the results section.

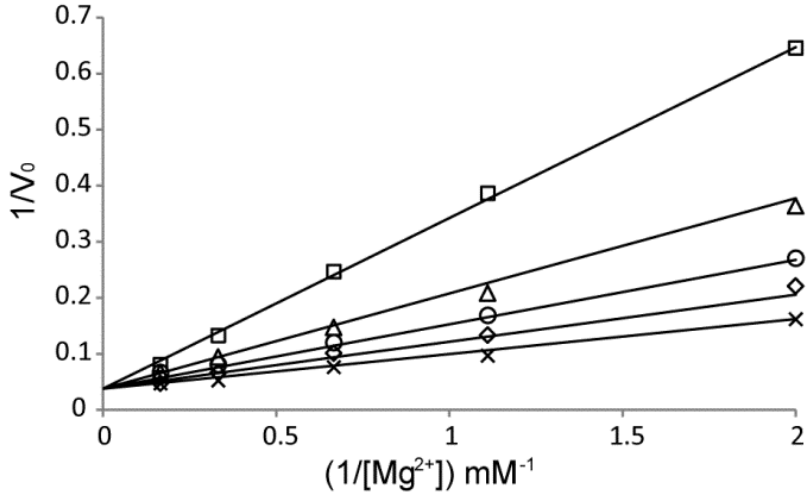

Figure 3. AMP inhibition of *l*FBPase. Reciprocal velocities are plotted against $1/[Mg^{2+}]$ at fixed AMP concentrations of 0 (x), 0.45 (◊), 0.7 (○), 1 (△) and 1.5 μM (□).

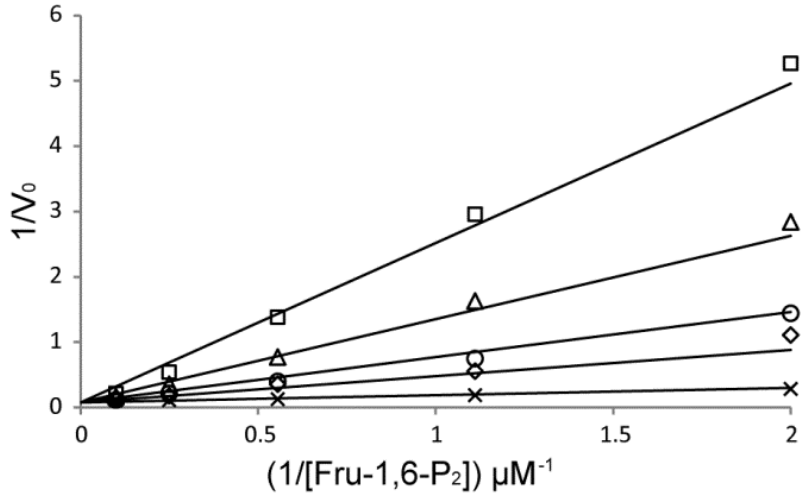

Figure 4. Fru-2,6-P_2 inhibition of *l*FBPase. Reciprocal velocities plotted against 1/[Fru-1,6-P_2] at fixed Fru-2,6-P_2 concentrations of 0 (x), 0.05 (◊), 0.1 (○), 0.2 (△) and 0.4 µM (□).

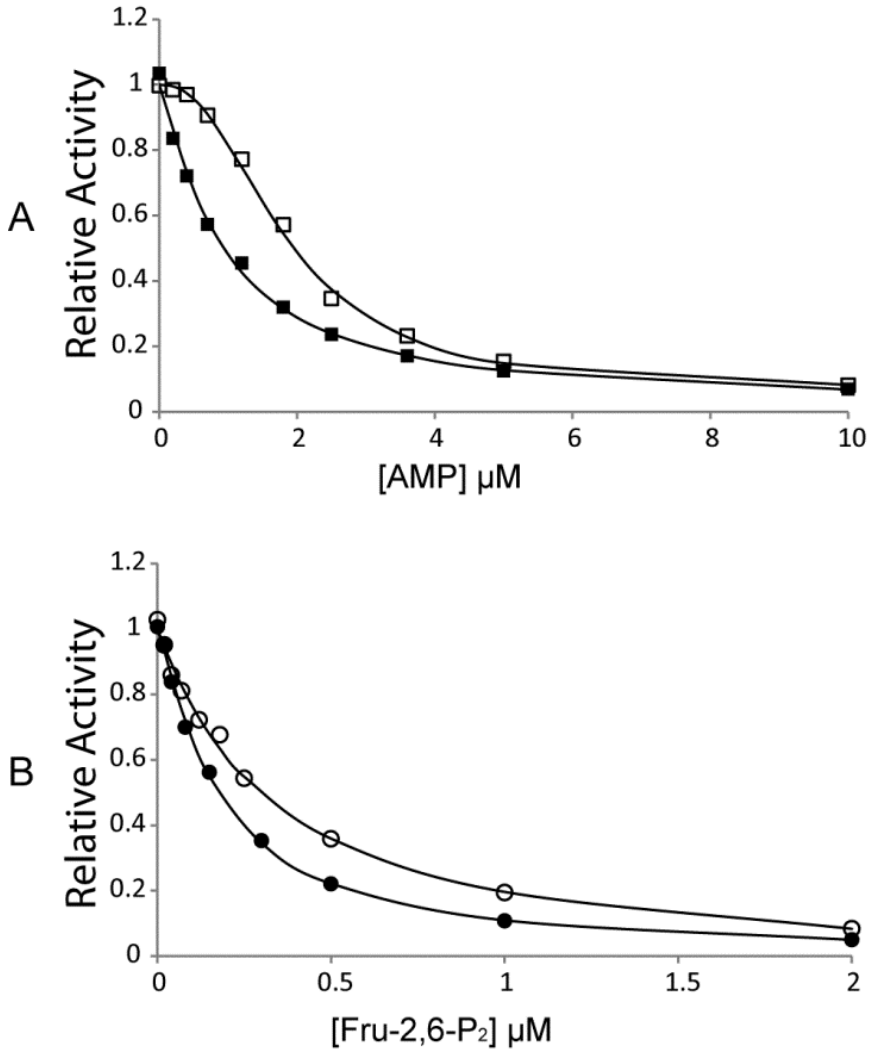

Figure5. Determination of AMP/Fru-2,6-P_2 synergism by kinetics. A. AMP inhibition in the absence (□) and presence (■) of Fru-2,6-P_2 ([Fru-2,6-P_2] = $I_{0.5}$-Fru-2,6-P_2 = 0.33 µM). B. Fru-2,6-P_2 inhibition in the absence (○) and presence (●) of AMP ([AMP] = $I_{0.5}$-AMP = 1.8 µM). All assays are carried out with saturating Fru-1,6-P_2 (20 µM) and Mg^{2+} (5 mM).

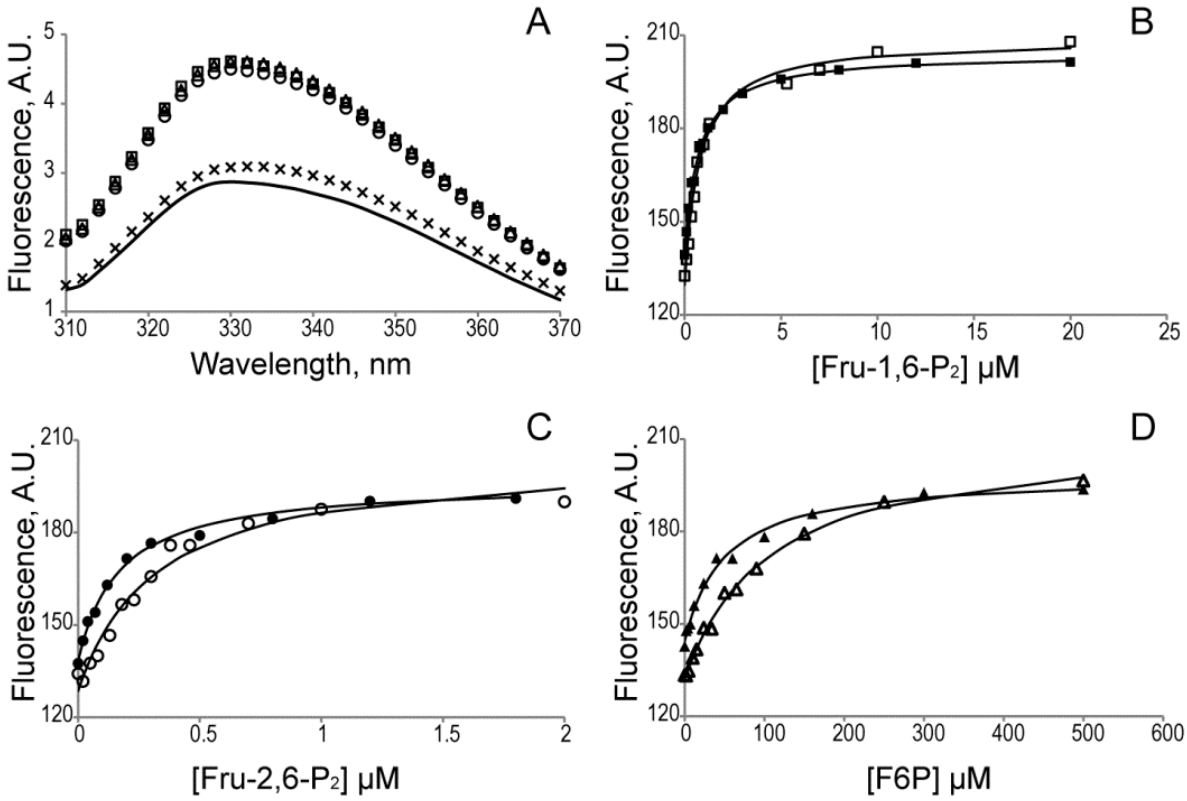

Figure 6. Ligand binding to the active site as revealed by fluorescence emission from tryptophan. A. Saturating levels of Fru-1,6-P_2 (20 μM, □), Fru-2,6-P_2 (10 μM, ○), or Fru-6-P (500 μM, △) significantly increase Trp^{219} fluorescence emission whereas AMP (10 μM, x) causes little changes relative to baseline (solid curve). Titrations for Fru-1,6-P_2 (panel B), Fru-2,6-P_2 (panel C), and Fru-6-P (panel D) performed in the absence (open symbols) and presence (filled symbols) of AMP ([AMP] = $I_{0.5}$-AMP = 1.8 μM) reveal binding synergism between AMP and only Fru-6-P and Fru-2,6-P_2. Each titration data point represents integration of the Trp^{219} emission spectrum from 310-370 nm.

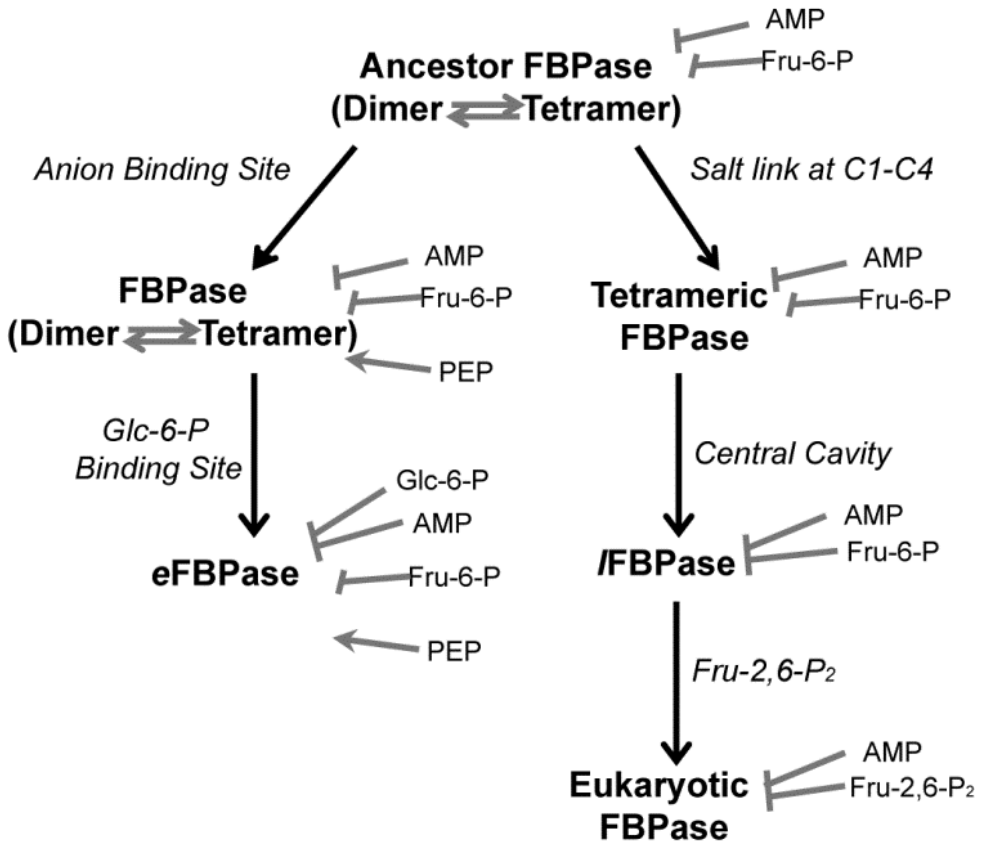

Figure 7. Proposed evolution of the regulatory properties of FBPases. Different mechanisms of tetramer stabilization (anion activation and salt-link formation) led *E. coli*-like and eukaryotic mechanisms of regulation.

Reference

1. Benkovic, S. J., and de Maine, M. M. (1982) Mechanism of action of fructose 1,6-bisphosphatase. Adv. Enzymol. Relat. Areas Mol. Biol. 53, 45–82

2. Tejwani, G. A. (1983) Regulation of fructose-bisphosphatase activity. Adv. Enzymol. Relat. Areas Mol. Biol. 54, 121–194

3. Blangy, D., Buc, H. & Monod, J. (1968) Kinetics of the allosteric interactions of phosphofructokinase from Escherichia coli. J. Mol. Biol. 31, 13-35.

4. Taketa, K., and Pogell, B. M. (1965) Allosteric inhibition of rat liver fructose 1,6-bisphosphatase by adenosine 5'-monophosphate. J. Biol. Chem. 240, 651–662

5. Pilkis, S. J., El-Maghrabi, Pilkis, J., and Claus, T. (1981) Inhibition of fructose-1,6-bisphosphatase by fructose 2,6-bisphosphate. J. Biol. Chem. 256, 3619–3622

6. Van Schaftingen, E., and Hers, H.-G. (1981) Inhibition of fructose-1,6-bisphosphatase by fructose 2,6-biphosphate. Proc. Natl. Acad. Sci. U. S. A. 78, 2861–2863

7. Kruger, N. J., and Beevers, H. (1984) Effect of fructose 2,6-bisphosphate on the kinetic properties of cytoplasmic fructose 1,6-bosphosphatase from germinating castor bean endosperm. Plant Physiol. 76, 49-54

8. Noda, T., Hoffschulte, H., Holzer, H. (1984) Characterization of fructose 1,6-bisphosphatase from baker's yeast. J. Biol. Chem. 259, 7191-7197

9. Okar, D. A., and Lange, A. J. (1999) Fructose-2,6-bisphosphate and control of carbohydrate metabolism in eukaryotes. Biofactors 10, 1–14

10. Pilkis S. J., El-Maghrabi, Pilkis, J., Claus, T. H., and Cumming D. A. (1981) Fructose 2,6-bisphosphate. A new activator of phosphofructokinase. J. Biol. Chem. 256, 3171–3174

11. Van Schaftingen, E., Jett, M.-F., Hue, L., and Hers, H.-G. (1981) Control of liver 6-phosphofructokinase by fructose 2,6-bisphosphate and other effectors. Proc. Natl.Acad. Sci. U. S. A. 78, 3483–3486

12. Uyeda, K., Furuya, E., and Luby, L. J. (1981) The effect of natural and synthetic D-fructose 2,6-bisphosphate on the regulatory kinetic properties of liver and muscle phosphofructokinase. J. Biol. Chem. 256, 8394–8399

13. Preiss, J., Biggs, M. L., Greenberg, E. (1967) The effect of magnesium ion concentration on the pH optimum of the spinach leaf alkaline fructose diphosphatase. J. Biol. Chem. 242, 2292-2294

14. Buchanan, B. B., and Wolosiuk, R. A. (1976) Photosynthetic regulatory protein found in animal and bacterial cells Nature 264, 669-670

15. Buchanan, B. B. (1980) Role of light in the regulation of chloroplast enzymes. Annu. Rev. Plant Physiol. 31, 341-374

16. Michels, P. A., and Ridgen, D. J. (2006) Evolutionary analysis of fructose 2,6-bisphosphate metabolism. IUBMB Life 58, 133-141

17. Hines, J. K., Kruesel, C. E., Fromm, H. J., and Honzatko, R. B. (2007) Structures of inhibited fructose-1,6-bisphosphatase from Escherichia coli: distinct allosteric inhibition sites for AMP and glucose 6-phosphate and the characterization of a gluconeogenic switch. J. Biol. Chem. 282, 24697–24706

18. Hines, J. K., Fromm, H. J., and Honzatko, R. B. (2006) Novel allosteric activation site in Escherichia coli fructose-1,6-bisphosphatase. J. Biol. Chem. 281, 18386–18393

19. Hines, J. K., Fromm, H. J., and Honzatko, R. B. (2007) Structures of activated fructose-1,6-bisphosphatase from Escherichia coli. Coordinate regulation of bacterial metabolism and the conservation of the R-state. J. Biol. Chem. 282, 11696–11704

20. Choe, J. Y., Poland, B. W., Fromm, H. J., and Honzatko, R. B. (1998) Role of a dynamic loop in cation activation and allosteric regulation of recombinant porcine fructose-1,6-bisphosphatase.Biochemistry 37, 11441-11450

21. Choe, J. Y., Fromm, H. J., and Honzatko, R. B. (2000) Crystal structures of fructose 1,6-bisphosphatase: mechanism of catalysis and allosteric inhibition revealed in product complexes. Biochemistry 39, 8565-8574

22. Xue, Y., Huang, S., Liang, J., Zhang, Y., and Lipscomb, W. N. (1994) Crystal structure of fructose-1,6-bisphosphatase complexed with fructose 2,6-bisphosphate, AMP, and Zn2+ at 2.0-Å resolution: aspects of synergism between inhibitors. Proc. Natl. Acad. Sci. U.S.A. 91, 12482-12486

23. Hines, J. K., Chen, X., Nix, J. C., Fromm, H. J., and Honzatko, R. B. (2007) Structures of mammalian and bacterial fructose-1,6-bisphosphatase reveal the basis for synergism in AMP/fructose 2,6-bisphosphate inhibition. J. Biol. Chem. 282, 36121–36131

24. Gao, Y., and Honzatko, R. H. Water structure of the central hydrophobic cavity of mammalian fructose 1,6-bisphosphatase: a potential thermodynamic determinant of allowed quaternary states. In preparation.

25. Gao, Y., and Honzatko, R. B. Hydrophobic Central Cavity in Fructose-1,6-bisphosphatase is Essential for the Synergism in AMP/Fructose 2,6-bisphosphate Inhibition. To be submitted.

26. Van Schaftingen, E., and Hers, H-G. (1981) Formation of fructose 2,6-bisphosphate from fructose 1,6-bisphosphate by intramolecular cyclisation followed by alkaline hydrolysis. Eur. J. Biochem. 117, 319-323

27. Laemmli, U. K. (1970) Cleavage of structural proteins during the assembly of the head of bacteriophage T4. Nature 227, 680-685

28. Bradford, M. M. (1976) A rapid sensitive method for the quantitation of microgram quantities of protein utilizing the principle of protein-dye binding. Anal. Biochem. 72, 248-252

29. Gao, Y, and Honzatko, R. B. Dimer-dimer Interface in Porcine Liver Fructose-1,6-bisphosphatase is Essential in Cooperative Binding of AMP. To be submitted.

30. Demeler, B. (2005) UltraScan A Comprehensive Data Analysis Software Package for Analytical Ultracentrifugation Experiments. Modern Analytical Ultracentrifugation: Techniques and Methods. (D. J. Scott, S.E. Harding and A.J. Rowe. Eds.) Royal Society of Chemistry (UK), 210-229

31. Leatherbarrow, R.J. (2009) GraFit Version 7, Erithacus Software Ltd., Horley, U.K.

32. Nelson, S. W., Choe, J-Y., Iancu, C. V., Honzatko, R. B., and Fromm, H. J. (2000) Tryptophan fluorescence reveals the conformational state of a dynamic loop in recombinant porcine fructose-1,6-bisphosphatase. Biochemistry 39, 11100-11106

33. Zhang, R., Villeret, V., Lipscomb, W. N., and Fromm, H. J. (1996) Kinetics and mechanisms of activation and inhibition of porcine liver fructose-1,6-bisphosphatase by monovalent cations. Biochemistry 35, 3038-3043

34. Nelson, S. W., Honzatko, R. B., and Fromm, H. J. (2004) Origin of cooperativity in the activation of fructose-1,6-bisphosphatase by Mg2+. J. Biol. Chem. 279, 18481-18487

35. Ren, S., Fu, G., Jiang, X., Zeng, R., Miao, Y., Xu, H., Zhang, Y., Xiong, H., Lu, G., Lu, L., Jiang, H., Jia, J., Tu, Y., Jiang, J., Gu, W., Zhang, Y., Cai, Z., Sheng, H., Yin, H., Zhang, Y., Zhu, G., Wan, M., Huang, H., Qian, Z., Wang, S., Ma, W., Yao, Z., Shen, Y.,

Qiang, B., Xia, Q., Guo, X., Danchin, A., Firons, I. S., Somerville, R. L., Wen, Y., Shi, M., Chen, Z., Xu, J., Zhao, G. (2003) Unique physiological and pathogenic features of Leptospira interrogans revealed by whole-genome sequencing. Nature 422, 888-893

36. Kurbanov, F. T., Choe, J., Honzatko, R. B., and Fromm, H. J. (1998) Directed mutation in the poorly defined region of porcine liver fructose-1,6-bisphosphatase significantly affect catalysis and the mechanism of AMP inhibition. J. Biol. Chem. 273, 17511-17516

37. Kelley-Loughnane, N., Biolsi, S. A., Gibson, K. M., Lu, G., Hehir, M. J., Phelan, P., Kantrowitz, E. R. (2002) Purification, kinetic studies, and homology model of Escherichia coli fructose-1,6-bisphosphatase. Biochim. Biophys. Acta 1594, 6-16

38. Nelson, S. W, Honzatko, R. B., and Fromm, H. J. (2002) Hybrid tetramers of porcine liver fructose-1,6-bisphosphatase reveal multiple pathways of allosteric inhibition. J. Biol. Chem. 277, 15539-15545

39. Faine, S., Adler, B., Bolin, C. & Perolat, P. Leptospira and Leptospirosis (Medisci, Melbourne, 1999).

40. The PyMOL Molecular Graphics System, Version 1.5.0.4 Schrödinger, LLC.

CHAPTER VIII. GENERAL CONCLUSION

Mammalian FBPase exists as a stable tetramer in solution, with two distinct subunit interfaces (C1-C2 and C1-C4) and one large hydrophobic cavity at the center. All the potent regulatory sites identified to date locate on/nearby subunit interface or central cavity and communicate with active site and with each other allosterically. My dissertation work illucidated how key structural features of FBPase, including stable tetramer, subunit pair rotation within tetramer and central cavity, determine proper regulation of mammalian FBPase.

Inspired by *E. coli* FBPase, which exists in dimer-tetramer equilibrium in solution, I have confirmed the key interaction at C1-C4 interface, the salt link Glu^{192}-Met^{42} (Chapter V). Point mutations on or surrounding the salt link led to the formation of FBPase dimmers (C1-C2 or C3-C4). Introduction of positive charge amino acid at position 18 also affected tetramer stability (Chapter VI). All mutant FBPases in dimer form are with diminished AMP cooperativity and exhibit a range of changes in AMP inhibition, from altered inhibitory mechanism, partial inhibition to totally loss of AMP inhibition. The result here indicated the importance of stable tetramer in AMP inhibition.

Tetrameric FBPase exists in at least two quaternary states, active R-state and inactive T-state, which are mainly distinguished by a 15 degree subunit-pair rotation (between C1-C2 dimer and C3-C4 dimer). Ligation of AMP nearby C1-C4 interface disrupts local hydrogen bonds and triggers subunit-pair rotation (Chapter II). Small subunit-pair rotation correlates to catalytic efficiency of FBPase: the more of rotation towards T-state, the less active of FBPase (Chapter III). Subunit-pair rotation close to T-state generates close contacts on loop 50-72 and drives the displacement of the essential catalytic loop 50-72 (Chapter II). Additionally, subunit-pair rotation governs AMP/Fru-2,6-P_2 synergism and AMP binding cooperativity in tetrameric FBPase: restraining Fru-2,6-P_2 induced subunit pair rotation reduces AMP/Fru-2,6-P_2 synergism (Chapter IV); subunit-pair rotation towards T-state eliminates AMP cooperativity (Chapter IV, V, VI).

The central cavity of FBPase is populated with ordered waters, verified by both crystallography and molecular dynamics simulation (Chapter III). The waters are most stable in I_R-state of Leu^{54} FBPase (3 degree subunit-pair rotation), and in I_T-state of Asp^{10} FBPase (12 degree subunit-pair rotation), both of which lie on the R- to T-state transition pathway. The extra stability of waters in intermediate states of FBPase would become an energy barrier that determines quaternary states of FBPase. Indeed, Leu^{54} FBPase in the presence of AMP exhibits different level of subunit-pair rotations in different solvent systems (Chapter III). The central cavity in *E. coli* FBPase is filled with large hydrophilic sidechains. The mimic of *E. coli* central cavity in mammalian FBPase reduces Fru-2,6-P_2 induced subunit-pair rotation and AMP/Fru-2,6-P_2 synergism (Chapter IV).

Our rich knowledge on allosteric regulation of porcine liver FBPase and FBPase from *Escherichia coli* allow us to predict the regulatory properties of all Type-I FBPases, for which sequence information is available. Subsequent expression of FBPase from a bacterial organism, predicted to have the regulatory properties of a eukaryotic FBPase, proved correct and established a basis for the evolution of regulatory properties for all Type-I FBPases (Chapter VII).

In summary, my dissertation largely illustrates the structural basis for allosteric regulation of mammalian FBPase: stable tetramer is prerequisite for AMP inhibition; subunit pair rotation mediate communication between AMP sites from different subunit and between AMP site and active site; the central cavity acts as a thermodynamic hinge for subunit-pair rotation. The work here also provides future directions for drug screening/design towards FBPase. Anything that induce subunit-pair rotation would be an inhibitor of FBPase and will work synergistically with physiological inhibitors AMP and Fru-2,6-P_2.

ACKNOWLEDGEMENTS

I would like to thank my major professor, Dr. Richard Honzatko, for his guidance and support. I really appreciate that he assigned me such an interesting project and gave me the freedom to try various ideas and techniques in my research. I would like to thank my current and previous committee members, Dr. Amy Andreotti, Dr. Mark Hargrove, Dr. Scott Nelson, Dr. Guang Song, Dr. Gaya Amarasinghe and Dr. Herbert Fromm for their advice and support. Many thanks go to my dear colleagues, Dr. Lu Shen and Muneaki Watanabi, for their constant help and encouragement throughout my Ph. D. period. Finally, I would like to thank my parents; the desire of making them proud has been a great motivation for me.